The Function of NOD2 in Antigen Presenting Cells

Dr. Philip James Allan

Submitted for examination towards the award of Doctor of Philosophy
in Biomedical Sciences

Green Templeton College
Trinity 2012

Human Immunology Unit
Weatherall Institute of Molecular Medicine
Oxford

and

Translational Gastroenterology Unit
Nuffield Dept. of Experimental Medicine
Oxford







Declaration of authorship

© Philip James Allan, University of Oxford, 2012

This thesis is the result of my own work, and includes nothing that is the result of work by others except where done in collaboration with others and is otherwise indicated in the text.

This thesis has not already been accepted, or is being concurrently submitted, by me or any other author, for any degree, diploma or other qualification in this University or elsewhere.

This thesis does not exceed 50 000 words, excluding bibliography, figure legends and appendices.

All trademarks used are acknowledged to be the property of the appropriate owner.

Acknowledgements

I would like to thank my supervisors, Alison Simmons and Fiona Powrie for their support, ideas and direction in enabling me to go through the process of this DPhil.

Thanks to all the members of the TGU and HIU labs, in particular Oliver Brain and John Baker for their introduction to NOD2, phosphoproteomics and the fun of DCs. Elham Khatamzas, Tica Pichulik, Al Leslie, Peter Simpson and latterly Ben Owens and Tessa Steevels have all provided much needed support and encouragement. Ben and Tessa in particular need thanks for direction over style and content.

I would like to thank all at the Medical Sciences Doctoral Training Centre and my sponsors Prof. Raj Thakker, Prof. Paul Klennerman, Prof. Peter Ratcliffe and Prof. Andrew McMichael. I would also like to thank my college advisor, Prof. Peter Friend.

This work was generously funded by The Wellcome Trust as part of their research grants for Clinical Training Fellowships within Oxford, and I am very grateful for their support.

To my parents, James and Jennifer, and my siblings, Virginia, Caroline and William, thank you for supporting me through this and providing words of encouragement and wisdom.

I would like to convey just how grateful I am to my ever-patient provider of tea, cakes and proofreading. Finally, to my delightful, ever supportive, most persevering, wife, Rachel, who has maintained her sense of humour and kept us going through the highs and lows of the last few years. Thank you for everything.

Gloria in Excelsis Deo

Index

Title page	i
Declaration of authorship	ii
Acknowledgements	iii
Contents	v
Contents of Figures	xv
Contents of Tables	xviii
Abbreviations	xx
Abstract	xxvii
Chapter 1: Introduction	1
Chapter 2: Materials and Methods	60
Chapter 3: Dissecting the NOD2 and NOD2/TLR2 signalling cascades	90
Chapter 4: LCP1, SHP1 and HMGB1: novel downstream mediators of NOD2/TLR2 signalling	118
Chapter 5: Assessing the function of DAPK1 in the NOD2/TLR2 signalling cascade	154
Chapter 6: Discussion and Conclusion	176
Bibliography	182
Appendix	208
Papers published during DPhil	212

Contents

1. Introduction **1**

1.1. Inflammatory Bowel Disease and Crohn's Disease **1**

1.1.1. Epidemiology and Genetics 1

1.1.2. Current treatments of CD 3

1.1.3. Aetiology and pathogenesis of CD 4

1.1.3.1. Genetic predisposition to CD 4
1.1.3.1.1. Linkage and association studies in CD 4
1.1.3.1.2. Genome Wide Association Studies (GWAS) in CD 5

1.1.3.2. The Microbiota and its role in CD 9
1.1.3.2.1. The microbiota's role in CD defined by antibiotics 12

1.1.4. Mucosal barrier function to prevent inflammation in the gut 14

1.1.4.1. Mucus barrier and epithelial defence 14

1.1.4.2. The impact of the underlying stroma 16

1.1.4.3. Paneth Cells: guardians of the crypt 18

1.1.4.4. The role of the adaptive immune system in gut inflammation 19

1.1.5. Innate immunity and Crohn's Disease 23

1.1.5.1. Dendritic Cells 23
1.1.5.1.1. Bacterial handling and antigen presentation 25

1.1.5.2. Pattern Recognition Receptors 26
1.1.5.2.1. Toll-like Receptors 26
1.1.5.2.2. NOD-like Receptors 27

1.1.6. Nucleotide Oligomerisation Domain 2 (NOD2) 30

1.1.6.1. The protein and its function 30

1.1.6.2. Negative regulation of NOD2 31

1.1.6.3. NOD2 interacts with RIP2, a signalling adaptor molecule, causing downstream signalling effects 31

1.1.6.4. The role of NOD2 in Crohn's Disease 34

1.1.6.5. Other roles of NOD2 34

1.1.7. TLR2 and its role within innate immunity 37

1.1.7.1. The TLR2 protein 37

1.1.7.2. Mechanism of action of TLR2 37

1.1.8. PRR crosstalk 39

1.1.9. Autophagy and its role in innate immunity 42

1.2. Proteomics and phospho-proteomics 47

1.2.1. MASCOT score 49

1.2.2. Post-translational modifications 49

1.3. An introduction to the main proteins identified through the proteomic study of the function of NOD2 in APCs 51

1.3.1. L-plastin or LCP-1 51

1.3.2. Phospho-tyrosine protein non-receptor 6 (PTPN6) or Src-homology domain 2-containing protein tyrosine phosphatase 1(SHP1) 53

1.3.3. High Mobility Group B1 (HMGB1) 55

1.3.4. Death Associated Protein Kinase (DAPK1) 56

1.3.4.1. DAPK1 induction, structure and phosphorylation 56

1.3.4.2. DAPK1 and autophagy 56

1.3.4.3. Endocytosis and the role for DAPK1 57

1.3.5. HSP27 58

1.3.6. MAPK/ERK Kinase 1 (MEK1) 60

1.4. Conclusion and Aims of Thesis 61

2. Methods and Materials **62**

2.1. Tissue culture **62**

2.1.1. Preparation of primary human immature monocyte-derived dendritic cell (DC) preparation 62

2.1.2. Preparation of primary human monocyte derived macrophages 63

2.1.3. Harvesting DCs and macrophages 64

2.2. Stimulation of DCs and macrophages **65**

2.2.1. Gene expression stimulation and immunoblotting 65

2.2.2. Stimulation of DCs to investigate phosphorylation cascades 65

2.2.3. Stimulation of DCs for confocal experiments 66

2.2.4. Bacterial culture 67

2.2.5. Antigen presentation and proliferation assays 67

2.2.6. Bacterial handling assays 68

2.2.7. Confocal microscopy 68

2.2.8. Flow cytometry 70

2.2.8.1. Live-Dead staining 70

2.2.8.2. PhosFlow (BD Biosciences) 70

2.2.9. Dendritic cell transfection 71

2.2.10. Small molecule inhibitors 71

2.3. Deoxyribose nucleic acid (DNA) and Ribose nucleic acid (RNA) methods **72**

2.3.1. Isolating DNA from buffy coats and whole blood samples 72

2.3.2. Quantifying DNA and ensuring quality 72

2.3.3. Genotyping of CD-associated polymorphisms 72

2.3.4. PCR product purification 74

2.3.5. Agarose gel electrophoresis 74

2.3.6. RNA extraction 75

2.3.7. Reverse transcriptase quantitative PCR (qPCR) 75

2.4. Protein analysis and preparation for mass spectrometry 77

2.4.1. Cell lysis 77

2.4.2. Protein separation by electrophoresis 78

2.4.3. Immunoblotting or western blotting 78

2.4.4. Native protein assessment 79

2.4.5. Phosphoprotein purification 79

2.4.6. Protein desalting using methanol chloroform precipitation and other methods 81

2.4.7. Tandem Mass Tagging (TMT) Labelling 81

2.4.8. Sep-Pak purification 83

2.4.9. OFFGEL isoelectric protein and peptide separation 83

2.4.10. Mass spectrometry 84

2.4.11. ELISAs and Cytometric bead assays 84

2.5. Materials, Solutions and Chemicals used 87

2.5.1. Nucleic Acid analysis 87

2.5.1.1. Tris Borate EDTA (TBE) 87

2.5.1.2. Agarose gel 87

2.5.1.3. Gel Red (Biotium) 87

2.5.2. Lysis Buffers and Solutions 87

2.5.2.1. NP40 87

2.5.2.2. Triton X114 87

2.5.2.3. Sodium Fluoride (NaF) 87
2.5.2.4. Activated Sodium Orthovanadoate 87
2.5.2.5. EDTA 87
2.5.3. Immunoblotting 88
2.5.3.1. TBS Tween 88
2.5.3.2. Blocking Buffer 88
2.5.3.3. Precast SDS-PAGE Gels (Invitrogen) 88
2.5.3.4. Other products used 88
2.5.4. Tissue Culture 88
2.5.4.1. R10 88
2.5.4.2. Macrophage R1 88
2.5.4.3. MACS Buffer 88
2.5.4.4. Leucocyte separation solution 89
2.5.5. Microbiological media 89
2.5.5.1. Leuers Broth 89
2.5.5.2. LB Agar 89
2.5.5.3. Gentamicin 89
2.5.6. Confocal and Flow Cytometry 89
2.5.6.1. PBA 89
2.5.6.2. ToPro (Invitrogen) 89
2.5.6.3. Pepstatin 89
2.5.6.4. E64d 89
2.5.6.5. Lysotracker-Red (Invitrogen) 89
2.5.6.6. PFA 90
2.5.6.7. Triton X-100 90

2.5.6.8. Vectashield (Vector Laboratories) 90

2.5.7. OFFGEL Fractionation 90

2.5.7.1. Protein OFFGEL Stock Solution (1.25X)(Agilent) 90

2.5.7.2. Peptide OFFGEL Stock Solution (1.25X) (Agilent) 90

2.5.8. Mass spectrometry 90

2.5.8.1. Buffer A 90

2.5.8.2. Buffer B 90

2.5.9. ELISA and cytometric bead assays 91

3. Dissecting the NOD2 and NOD2/TLR2 signalling cascades 92

3.1. Introduction 92

3.2. Results 93

3.2.1. Schema of approach 93

3.2.2. Preparation of NOD2 stimulated samples for mass spectrometry 95

3.2.3. Verification of some targets does not concur with mass spectrometry data 96

3.2.4. Targets validated and in agreement with MS 98

3.2.5. OFFGEL fractionation has the potential to reveal post-translational modifications, such as phosphorylation 100

3.2.6. Investigating NOD2/TLR2 crosstalk by MS 101

3.2.7. Verification of proteins identified as differentially phosphorylated on NOD2/TLR2 stimulation 105

3.2.8. LCP1 and DAPK1 verified in NOD2/TLR2 crosstalk signalling cascade 107

3.2.9. The determination of whether the verification targets are involved in TLR signalling cascade and not NOD2 signalling cascade 109

3.2.10. Starvation-induced autophagy does not involve differential phosphorylation of LCP1, MEK1 or HSP27 112

3.2.11. Quantification of signalling intermediates from NOD2/TLR2 signalling cascades 113

3.3. Discussion 114

3.4. Conclusion 119

4. LCP1, SHP1 and HMGB1: novel downstream mediators of NOD2/TLR2 signalling 120

4.1. Overall Introduction 120

4.2. L-plastin or Lymphocyte Cytosolic Protein 1 (LCP1) 121

4.2.1. Introduction 121

4.2.2. LCP1 Results 122

4.2.2.1. LCP1 is part of the PRR signalling cascades 122

4.2.2.2. Silencing LCP1 to enable investigation of function 125

4.2.2.3. LCP1 knockdown reduces phagocytosis but does not alter downstream bacterial killing in DCs 126

4.2.2.4. LCP1 increases MCP1 release from DCs on MDP stimulation 128

4.2.2.5. LCP1 does not affect DC survival or maturation 130

4.2.3. LCP1 Discussion 132

4.2.3.1. LCP1 phosphorylation and effective silence by siRNA 132

4.2.3.2. LCP1 is important for phagocytosis but not bacterial persistence 132

4.2.3.3. LCP1 and cytokine production 134

4.2.3.4. LCP1 did not alter integrin expression 135

4.2.4. LCP1 Conclusion 136

4.3. Src homology domain 2-containing protein tyrosine phosphatase 1 (SHP1) or Protein Tyrosine Phosphatase Non-receptor 6 (PTPN6) 137

4.3.1. Introduction 137

4.3.2. SHP1 Results 138

4.3.2.1. SHP1 is phosphorylated on MDP stimulation 138

4.3.2.2. Silencing of SHP1 by siRNA 138

4.3.2.3. Loss of SHP1 alters signalling via p44/42 MAPK 140

4.3.2.4. Loss of SHP1 increases secretion of MIP1β or CCL4 142

4.3.2.5. Loss of SHP1 does not impact DC survival or maturation 144

4.3.3. SHP1 Discussion 145

4.3.3.1. SHP1 and its role in NOD2 signalling 145

4.3.3.2. SHP1 and cytokine production 145

4.3.3.3. Cell migration and control by SHP1 146

4.3.3.4. SHP1 determines phagocytic potential 146

4.3.4. SHP1 Conclusion 148

4.4. High Mobility Group Protein B1 (HMGB1) 149

4.4.1. Introduction 149

4.4.2. HMGB1 Results 150

4.4.2.1. HMGB1 is dephosphorylated on MDP stimulation of DCs 150

4.4.2.2. Transcription of HMGB1 is unaffected by PRR stimulation 150

4.4.2.3. HMGB1 can be silenced in DCs 152

4.4.2.4. HMGB1 is localised to the nucleus 152

4.4.2.5. HMGB1 and CCR7 surface expression 152

4.4.3. HMGB1 Discussion 153

4.4.4. HMGB1 Conclusion 154

4.5. Overall Discussion and Conclusion 155

5. Assessing the function of DAPK1 in the NOD2/TLR2 signalling cascade 156

5.1. Introduction 156

5.2. Results 157

5.2.1. Verification of DAPK1 in NOD2/TLR2 signalling cascade 157

5.2.2. Silencing DAPK1 effectively 161

5.2.3. DAPK1 associates with MHC II-loading compartment and this is not under the control of NOD2 162

5.2.4. Levels of CLIP-loaded immature HLA-DR and mature HLA-DR are not affected by DAPK1 protein silencing 164

5.2.5. Loss of DAPK1 does not impact on cell survival or activation in DCs 167

5.2.6. DAPK1 silencing does not interfere with cytokine production 169

5.2.7. DAPK1 and the immunological synapse 170

5.2.8. DAPK1 and Autophagy induction 170

5.3. Discussion 172

5.3.1. DAPK1 forms part of the NOD2/TLR2 signalling cascade 173

5.3.2. DAPK1 is not degraded on initial PRR stimulation 173

5.3.3. DAPK1 and MHC II loading 174

5.3.4. Silencing DAPK to assess function 175

5.4. Conclusion 177

6. Discussion and Conclusion **178**

6.1. Investigating the NOD2 signalling cascade **178**

6.2. The role of LCP1 in the NOD2 signalling cascade **179**

6.3. The role of SHP1 in the NOD2 signalling cascade **180**

6.4. The role of DAPK1 in the NOD2 signalling cascade **181**

6.5. Other proteins identified **182**

6.6. Conclusion **184**

7. Bibliography **185**

8. Appendix **211**

8.1. Mass spectrometry data tables **211**

8.2. Gentamicin killing assay **218**

9. Papers published during DPhil **219**

Contents of Figures

Figure 1	A cartoon representing the NLR family and their constitutive domains	28
Figure 2	Cartoon of NOD2 stimulation and subsequent induction of signalling pathways through known intermediates p38 and p44/42 MAPK	33
Figure 3	Cartoon summarising Activation or Initiation and Elongation steps of autophagosome formation	44
Figure 4	Cartoon demonstrating the main mechanism of autophagy in both starvation and immune scenarios	45
Figure 5	Preparation of immature DCs	64
Figure 6	Cartoon of bacterial killing assay	68
Figure 7	Analysis of the three common NOD2 polymorphisms associated with CD	74
Figure 8	Cartoon of phosphoprotein protocol	80
Figure 9	Tandem mass tagging methodology	82
Figure 10	Demonstration of different methods of determining intermediates in the NOD2 signalling cascade	94
Figure 11	Immunoblot of proteins identified by MS but with no identifiable change in phosphorylation status between unstimulated or stimulated conditions	97
Figure 12	Immunoblot of proteins found to be differentially phosphorylated on NOD2 stimulation with its ligand MDP	98
Figure 13	Immunoblot of OFFGEL fractionation phospho-enriched eluate	99
Figure 14	Selection of 6 biological replicates for MS analysis and 5 rejected replicates	102
Figure 15	Graph showing linearization of the 126/127 ratios	102
Figure 16	Immunoblot to verify potential proteins differentially phosphorylated on NOD2/TLR2 crosstalk	106

Figure 17 Immunoblot of verified proteins differentially phosphorylated on dual stimulation of DCs 107

Figure 18 A panel of PRR ligands differentially phosphorylate proteins in the NOD2/TLR2 signalling cascade but not on starvation 110

Figure 19 Correlation of phosphorylation of p44 MAPK and MEK1 expressed as a ratio of phosphorylation in dual stimulated cells compared to unstimulated 111

Figure 20 An overview of the interaction of proteins involved in NOD2/TLR2 signalling 118

Figure 21 Assessment of LCP1 phosphorylation by a panel of PRR ligands 123

Figure 22 LCP1 is effectively silenced at mRNA and protein level by siRNA targeting LCP1 125

Figure 23 Assessment of the role of LCP1 in phagocytosis and bacterial persistence 127

Figure 24 Assessment of the role of LCP1 on cytokine secretion 129

Figure 25 Assessment of the role of LCP1 in cell survival, maturation and MHC II loading/HLA-DR expression in DCs 131

Figure 26 Investigation of SHP1 phosphorylation by MDP and knockdown of SHP1 using siRNA 139

Figure 27 Effect of SHP1 knockdown on MDP-mediated MAPK and NF-κB activation 141

Figure 28 Comparison of phosphorylation of known intermediates ERK1/2, NF-κB or p38 MAPK using Phosflow technique demonstrating loss of signalling in SHP1 knockdown cells 141

Figure 29 Effect of SHP1 on MIP1β (CCL4) and IL-12p40 but not TNFα or IL-10 secretion in MDP stimulated cells 143

Figure 30 Assessment of SHP1 function in survival, maturation or MHC II loading/HLA-DR expression in DCs 144

Figure 31 HMGB1 phosphorylation status is dependent on NOD2

stimulation by its ligand MDP, but its mRNA transcription level is not 151

Figure 32 Verification of DAPK1 phosphorylation by immunoblot in phospho-eluate in dual stimulated DCs 159

Figure 33 Phosphorylated DAPK1 at serine 308 (p-DAPK(ser308)) demonstrating Phosflow technique 160

Figure 34 Demonstration of DAPK1 reduction by siRNA measured by quantitative PCR (qPCR) and immunoblot 161

Figure 35 Assessment of DAPK1 localisation with HLA-DM in the MHC Class II loading compartment 163

Figure 36 Optimisation of CerCLIP and HLA-DR staining for flow cytometry 165

Figure 37 Assessment of the effect of DAPK1 on MHC Class II cell surface expression 166

Figure 38 Effect of DAPK1 on cell death and DC maturation 168

Figure 39 Assessment of DAPK1 in IL-1β secretion 169

Appendix Figure

Figure 1 Gentamicin killing assay 218

Contents of Tables

Table 1	Crohn's disease risk loci ranked according to Odds Ratio contributed by risk allele.	7
Table 2	siRNAs used	71
Table 3	Primers for routine genotyping of buffy coat and donor samples	73
Table 4	Components and quantities for genotyping PCR	73
Table 5	Genotyping PCR cycle conditions	73
Table 6	Taqman RT PCR reagents	76
Table 7	Primary antibodies used	85
Table 8	Secondary antibodies used	86
Table 9	Flow Cytometry antibodies used	86
Table 10	Selection of proteins identified by MS with their MASCOT score, fraction and whether preferentially phosphorylated or dephosphorylated	97
Table 11	Details of proteins verified positively by immunoblot, with their MASCOT score, fraction identified in and whether phosphorylated or dephosphorylated.	99
Table 12	Proteins that are differentially phosphorylated on both MDP stimulation alone and dual MDP and PAM stimulation for 30 minutes	104
Table 13	Induction of phosphorylation of key intermediates in the NOD2/TLR2 signalling cascade	107
Table 14	Mean Log_{10} [ratio] compared to unstimulated with SD, SEM, and ratio t-test for MEK1	113
Table 15	Mean Log_{10} [ratio] compared to unstimulated with SD, SEM,and ratio t-test for HSP27	113
Table 16	Mean of Log_{10} [ratio], SD, SEM, 95% confidence interval and ratio t-test p value for LCP1 phosphorylation at tyr28 after PRR triggering	123
Table 17	Comparison of mean, SD, SEM and unpaired t-test for NS and LCP1 silenced cells infected with bacteria at different time points	127

Appendix Tables

Table 1 Proteins identified by MS on single stimulation of DCs with MDP 211

Table 2 Not significantly phosphorylated or dephosphorylated proteins on either MDP alone or MDP/PAM stimulated DCs 212

Table 3 Significantly phosphorylated (left group) and dephosphorylated (right group) proteins identified by MS from MDP/PAM stimulated DCs but were not found on MDP alone 213

Table 4 Non-significantly dephosphorylated (top set) and phosphorylated (bottom set) proteins identified by MS from MDP/PAM stimulated DCs but were not found on MDP alone 217

Abbreviations

AAMP	Angio-associated migratory cell protein
AIEC	Adherent invasive *Escherichia coli*
AMPK	5'-Adenosine monophosphate-activated protein kinase
5-ASA	5-Aminosalicylic acid
APC	Antigen presenting cell
ASC	Apoptosis-associated speck-like protein containing a CARD
ASCA	Anti-*Saccharomyces cerevisiae* antibodies
ATG16L1	Autophagy-related protein 16 L1
ATP	Adenosine triphosphate
BAFF	B cell activation factor of the TNF family
BIR	Baclovirus inhibitor of apoptosis protein (IAP) repeat
BLIMP	B lymphocyte induced maturation protein
BMDCs	Bone marrow derived dendritic cells
BMDMs	Bone marrow derived macrophages
BSA	Bovine serum albumin
CARD	Caspase activation and recruitment domain
CCR	C-C chemokine receptor
CD	Crohn's Disease
CD4+	Cluster of differentiation 4+ (T cells)
CEACAM	Carcinoembryonic antigen-related cell adhesion molecule
Cfr	C-fragment
CFU	Colony forming unit
CHAPS	3-[(3-cholamidopropyl)dimethylammonio]-1-propanesulfonate
CHIP	Carboxy terminus of HSP70 interacting protein
ChIP-seq	Chromatin immunoprecipitation DNA sequencing
CLIP	Class II-associated invariant chain peptide
CSFE	Carboxyfluorescein succinimidyl ester
cSMAC	Central SMAC
CTLA-4	Cytotoxic T lymphocyte protein 4
CIITA	MHC Class II transcription activator
DAMP	Danger associated molecular pattern
DAPK	Death associated protein kinase
DC	Dendritic cell
Delta Ct	Change in cycle number in RT-qPCR
DIP1	DAPK interacting protein 1
DMSO	Dimethyl sulphoxide
DNA	Deoxyribose nucleic acid
DRAK	DAP kinase related apoptosis inducing protein kinase
DSS	Dextran Sodium Sulphate
EBSS	Earles' balanced salt solution
E. coli	*Escherichia coli*
E-cadherin	Epithelial cadherin

ECL	Enhanced chemiluminescence
EDTA	Ethylenediaminetetraacetic acid
EEF2	Eukaryotic elongation factor 2
EGFR	Epidermal growth factor receptor
ELISA	Enzyme-linked immunosorbent assay
EOS	Early onset sarcoidosis
ERK	Extracellular receptor – mediated kinase
ESI	Electrospray ionisation
EXOC8	Exocyst complex component 8
FAK	Focal adhesion kinase
FCS	Fetal calf serum
FIP200	FAK-interacting protein 200
FITC	Fluorescein isothiocyanate
FLA	Flagellin
FoxP3	Forkhead box P3
FS1007insC	Frameshift 1007 insertion C
GALT	Gut associated lymphoid tissue
GAPDH	Glyceraldehyde 3-phosphate dehydrogenase
GDI1	Guanosine diphosphate dissociation inhibitor 1
GFP	Green fluorescent protein
GI	Gastrointestinal
GM-CSF	Granulocyte/macrophage-colony stimulating factor
GNB2L1	Guanine nucleotide-binding protein subunit beta-2-like 1
GPCR	G-protein coupled receptor complexes
GTP	Guanine triphosphate
GvHD	Graft versus Host Disease
GWAS	Genome Wide Association Studies
HapMap	International Haplotype Map resource
HBS	Hepes Buffered Saline
HCT	High capacity ion trap
HD5	Human defensin 5
HEK293	Human Embryonic Kidney 293 cell line
Hep3B cells	Hepatoma 3B cell line
HET-E	Incompatibility protein from *Podospora anserine*
HIV	Human Immunodeficiency virus
HLA	Human Leucocyte Antigen
HMGB1	High-Mobility Group protein B1
HRP	Horseradish peroxidase
HSP	Heat shock protein
HT29	Human colon adenocarcinoma cell line
Hr	Hour
IAP	Inhibitor of apoptosis protein
IBD	Inflammatory Bowel Disease
ICAM	Intracellular adhesion molecule
ICE	IL-1β converting enzyme

IFN	Interferon
IGF	Insulin-like growth factor
IGFBP	IGF binding protein
IKK	Inhibitor of NF-κB Kinase
IL	Interleukin
IL-23R	Interleukin-23 receptor
Ig	Immunoglobulin
INSR	Insulin receptor
IP	Immunoprecipitation
IPAF	ICE-like-protease-activating factor
IPEX	Inflammatory condition characterised by immune dysregulation, polyendocrinopathy, enteropathy and is X-linked
IRAK	IL-1 receptor associated kinase
IRF	Interferon regulatory factor
IRGM	Immune related GTPase family protein M
IT	Ion trap
ITCH	E3 ubiquitin-protein ligase Itchy homolog
ITIM	Immune receptor tyrosine based inhibitory motif
iTRAQ	Isotope-tagged amine-reactive agents
JAMA	Journal American Medical Association
JNK	c-Jun N-terminal kinase
KLH20	Keitch-like protein homologue 20
LAG-3	Lymphocyte activation gene 3
LAMP	Lysosome-associated membrane glycoprotein
LAR	Leucocyte common antigen-related protein
LB	Leuer's broth
LC	Liquid chromatography
LC/MS	Liquid chromatography/ mass spectrometry
LCP1	Plastin-2 or Lymphocyte cytosolic protein 1
LDS	Lithium dodecyl sulfate
LFA-1	Lymphocyte function associated antigen 1
LOD	Logarithm of Odds
LPS	Lipopolysaccharide
LRR	Leucine-rich repeat
LRRFIP	LRR flightless-interacting protein
LRRK	LRR serine/threonine-protein kinase
Lymphoprep	Sodium diatrizoate / polysaccharide solution
Mac-1	Macrophage-1 antigen
MAL	MyD88 adaptor-like protein
MALDI	Matrix-associated laser desorption/ionisation
MALP-2	Lipoproteins/macrophage activating lipopeptide 2
MAPK	Mitogen activated protein kinase
MAP3K	Mitogen activated protein kinase kinase kinase
M-CSF	Macrophage – colony stimulating factor
MDDC	Monocyte-derived dendritic cell

MDM	Monocyte-Derived Macrophage
MDP	Muramyl Dipeptide
MEK	MAPK/ERK kinase 1
Meso-DAP	gamma-D-glutamyl-meso diaminopimelic acid
MFI	Mean fluorescence index
MHC	Major histocompatibility complex
miR	micro RNA
MK	p38-MAPKAP
MKK	MAPK kinase
mL	Millilitre
MLC	Myosin light chain 2
MLCK	Myosin light chain kinase
MLH	mutL homologue 1
mM	Millimole
MMP	Matrix metalloproteinase
MOI	Multiplicity of Infection
MIP1β	Macrophage inhibitory protein 1β
mRNA	Messenger RNA
MRP	Myeloid related protein 8
MS	Mass Spectrometry
MS/MS	Tandem mass spectrometry
MST	Macrophage stimulatory protein
MTB	Mycobacterium Tuberculosis
mTOR	mammalian target of rapamycin
mTORC1	mTOR complex 1
MUC19	Mucin-19
MyD88	Myeloid differentiation primary response gene 88
NaCl	Sodium chloride
NACHT	NAIP, CIITA, HET-E, TP1
NAIP	Neuronal apoptosis inhibitory protein
NALP	NACHT, LRR and Pyrin domain containing protein
N-Cadherin	Neuronal cadherin
NDFIP1	Nedd 4 family interacting protein 1
NEMO	NF-κB essential modulator
NF-κB	Nuclear Factor kappa B
NLR	NOD-like Receptor
NOD	NACHT oligomerisation domain
NOD2	Nucleotide-binding Oligomerisation Domain containing protein 2
NOTCH	Neurogenic locus notch homolog
NS	Non-sense
Omp C	*E. coli* outer membrane protein C
ORMDL3	ORM1-like protein 3
2D-PAGE	2 dimensional polyacrylamide gel electrophoresis
PAM	Pam3CysK4, Synthetic triacylated lipoprotein – TLR2 ligand
PAMP	Pathogen associated molecular patterns
PBA	PBS containing BSA

PBMC	Peripheral blood mononuclear cells
PBS	Phosphate buffered saline
PCR	Polymerase chain reaction
PE	Phycoerythrin
PGE4	Prostaglandin E4
PGN	Peptidoglycan
PI(3)K	Phosphatidylinositol 3-kinase
PIN1	Peptidyl-prolyl cis-trans isomerase NIMA-interacting 1
Beta-PIX	AKA Rho guanine nucleotide exchange factor 7
PKC	Protein kinase C
PMA	Phorbol 12-myristate 13-acetate
PP2A	Protein phosphatase 2A
PRR	Pattern Recognition Receptor
PSMB10	Proteasome subunit β10
pSMAC	Peripheral SMAC
PTGER4	Prostaglandin E2 receptor EP4 subtype
PTP	Protein tyrosine phosphatase
PTPN	Protein tyrosine phosphatase non-receptor
PYD	Pyrin domain
qPCR	quantitative PCR
RA	Rheumatoid Arthritis
RAGE	Receptor for advanced glycation end products
RANKL	Receptor activator of NF-κB ligand
RAW 264.7	Murine macrophage cell line
Rheb	Ras homologue enriched in brain
RIPK/RIP	Receptor-Interacting Protein Kinase
ROCK	Rho – associated kinase
RORγ	RAR-related orphan receptor γ
ROS	Reactive oxygen species
RNA	Ribonucleic Acid
RSK	Receptor Ser / Thr kinase
RT	Reverse transcriptase
RT	Room temperature
SAMHDI	SAM-domain and HD-domain containing protein 1
SBP	Spontaneous bacterial peritonitis
SD	Standard Deviation
SDS-PAGE	Sodium dodecyl sulphate-polyacrylamide gel electrophoresis
SEM	Standard error of the mean
Ser	Serine
siRNA	small interfering RiboNucleic Acid
SH3BP1	SH3-domain binding protein 1
SHP-1	src-homology domain 2-containing protein tyrosine phosphatase-1
SILAC	Stable isotope labelling of amino acids in culture
SLE	Systemic lupus erythematosus
SMAC	Supramolecular activation complex
SOCS	Suppressor of cytokine signalling

SNP	Single Nucleotide Polymorphism
STAT3	Signal transducer and activator of transcription 3
Syk	Spleen tyrosine kinase
S6K	Ribosomal S6 kinase
T1D	Type 1 Diabetes mellitus
TAB	TAK1 binding protein
TAK	TGFβ activating kinase
TB	Tuberculosis
TBE	Tris borate EDTA
TBS	Tris buffered solution
TCR	T cell receptor
TEAB	Triethylammonium bicarbonate
TCEP	Tris(2-carboxyethyl)phosphine
TGFB1	Transforming Growth Factor Beta1
TGN	Transgolgi
T_H17	CD4+ T Helper 17 Cell
THP1	Monocyte cell line
Thr	Threonine
TIMP	Tissue inhibitor of metalloproteinases
TIR	Toll / IL-1 receptor
TLR	Toll-like receptor
TMT	Tandem mass tagging
TNF	Tumour necrosis factor
TNFAIP3	TNF alpha induced protein 3
TNFR	TNF receptor
TNFSF	Tumour necrosis factor super-family
TOF	Time-of-flight
TP	Telomerase – associated protein
TRAF	TNF receptor associated factor
Tregs	Regulatory T cells
TREX	Three prime repair exonuclease
TRIF	TIR-domain containing adaptor-inducing IFNβ
TRIKA	TRAF6 – regulated IKK activator 1
TSC	Tuberous sclerosis protein
Tyr	Tyrosine
UC	Ulcerative Colitis
UEV1A	Ubiquitin-conjugating enzyme E2 variant 1A
ULK	Unc-51-like kinase
UPR	Unfolded protein response
UK	United Kingdom
VASP	Vasodilator-stimulated phosphoprotein
VDJ gene	Variable, diverse and joining gene
VEGF	Vascular epithelial growth factor
VIP	Vasoactive intestinal protein
WASP	Wiscott-Aldrich syndrome protein

WB	Western Blot
WCL	Whole cell lysate
WT	Wild type
XBPI	X-box binding protein 1
XIAP	X-linked IAP
Y	Tyrosine
ZIPK	Zipper-interacting kinase
ZO	Zona occludens

Abstract

Crohn's disease (CD), a chronic inflammatory condition of the gut affecting 1:1000 of western populations, is thought to arise from a dysregulated immune response in a genetically susceptible individual. Polymorphisms in the ligand recognition domain of an intracellular pattern recognition receptor (PRR), NOD2, remain the strongest genetic risk factor for the development of CD. NOD2 directs autophagy in human DCs to facilitate bacterial destruction and antigen presentation; the CD-variant-NOD2 shows defects in this pathway. Recent work in the laboratory has demonstrated NOD2 signals to control expression induction of microRNA-29, which is impaired in cells from CD patients expressing CD NOD2-variants, and among other immunoregulatory effects, microRNA-29 suppresses IL-12p40/IL-23. Thus NOD2 directs key anti-microbe and immunoregulatory functions whose breakdown in the presence of CD-variant-NOD2 could act as a trigger for inflammation in this disease.

In comparison with other PRRs, relatively little is understood of the hardwiring of NOD2 signalling, the mechanism of NOD2-mediated autophagy induction, the means by which NOD2 recruits a signalling platform within the cytosol and the mechanism of synergy with other PRRs and the inflammasome. In this work I used quantitative proteomics to map the NOD2 signalling cascade and its cross-talk with TLR2, demonstrating novel mediators: LCP1, a plastin, reduced phagocytosis of bacteria but did not alter bacterial killing, and aided control of the release of MCP1 and may be involved in IL-12p40 release. SHP1, a phospho-tyrosine phosphatase, is required for the propagation of signalling cascades via p38, p44/42 MAPK and NF-κB. It

controls release of MIP1β and IL-12p40. HMGB1, an alarmin, is dephosphorylated on NOD2 stimulation and would result in changes to cellular location of HMGB1. Lastly, DAPK1, a serine/threonine kinase, is associated with HLA-DM loading compartment on NOD2 triggering, but does not alter CLIP levels on the surface of the cells. Thus, defining the hard wiring of NOD2 signalling in healthy donors, in comparison with CD donors expressing variant NOD2, is important to define targets amenable to drug design within this pathway.

1. Introduction

1.1. Inflammatory Bowel Disease and Crohn's Disease

1.1.1. Epidemiology and Genetics

The first descriptions of inflammation of the gastrointestinal (GI) tract that are consistent with current definitions of inflammatory bowel disease (IBD), consisting of Ulcerative Colitis (UC) and Crohn's Disease (CD), emerged in the early 18th Century [1]. Subsequently, Kennedy Dalziel, a Glasgow surgeon, described a chronic intestinal ileitis and made the first connection with the gut microflora by suggesting that it resembled Johne's bovine mycobacterial intestinal disease [2]. However, it was a case series of 14 patients at the Mount Sinai Hospital published in the Journal of the American Medical Association (JAMA) in 1932 that finally led to the term "Crohn's Disease" being coined [3].

Since then CD has increased in both incidence and prevalence. The latest epidemiological study to define CD incidence and prevalence worldwide [4] describes an incidence of CD at 10.6 (per 100 000 person-years) in the United Kingdom (UK) in 1991 [5]. In other westernised countries over the last 20 years the incidence has been equally high, such as 17.4 in Australia [6] and 20.2 in Canada [7]. Comparatively, the prevalence (per 100 000) was 319 in Canada [7], 343 in Australia [6], 322 in Sicily [8] and 300 in the UK [9]. Current estimates of 1:1000 prevalence of CD in Western Europe may therefore be underestimating the problem, and thus may be closer to 3:1000 or 1:300. In contrast, developing countries around the world have a far

lower incidence and prevalence of CD. This has started to change over the last ten years and within India, China, and across southeast Asia, there is an increase in CD. This may be due to a number of factors including increased diagnostic capabilities, a reducing incidence of masking conditions, such as infectious diarrhoea and tuberculosis (TB), and as yet unknown environmental factors. These may include a more westernised diet and migration [10] [11] [12].

Understanding the underlying aetiology of a condition that, until the early 20th century, was rarely seen and now affects many people in the UK, is a matter of medical urgency, if not economic urgency with rising admission rates [13] and costs of treatment [14]. To put the underlying aetiology and gut mucosal immunology in context, a brief overview of treatment strategies for CD will be discussed first, particularly with the need for novel therapeutic targets to alleviate the suffering of CD patients.

1.1.2. Current treatments of CD

Treatment of CD utilises a multi-disciplinary approach to managing the complex physical, nutritional, and psychological needs of patients. 5-aminosalicylic acid (5-ASA), the mainstay of treatment for UC, has limited benefit in CD [15] [16] [17]. Acute presentations of inflammation in CD are managed with corticosteroids and antibiotics. In order to maintain remission of CD and prevent onset of stricturing or fibrostenotic disease, immunomodulators are used, such as thiopurines (azathioprine and 6-mercaptopurine) or methotrexate and finally anti-Tumour Necrosis Factor-α (TNFα) agents, such as Infliximab or Adalimumab. Anti-TNFα agents are successful in maintaining remission in a proportion of CD patients, however in our cohort up to 15 % show primary non-response and 40 % experience secondary non-response, which compares favourably with published data [18] [19].

Surgery remains an important treatment strategy for CD patients with 42-71 % having a single resection by 10 years [20] [21], 44 % will go on to have disease recurrence at 10 years after resection [20] and an estimated 31-39 % will have a second operation within 10 years of the first [22] [23]. In general the behaviour of CD remains relatively constant despite intervention [24] and recurrence is higher in penetrating CD rather than non-penetrating [24].

1.1.3. Aetiology and pathogenesis of CD

Whilst the aetiology of CD remains unknown, it is currently hypothesised that the pathogenesis results from a dysregulated immune response to gut microflora in a genetically predisposed individual [25]. These three main aspects will be covered in turn starting with genetics, through the microflora to the dysregulated immune response.

1.1.3.1. Genetic predisposition to CD

Genetic predisposition towards CD was first documented with familial clustering [3]. More recent population based studies have further clarified the familial risk from 6.7 % to 29.4 % [26] [27]. Among family groups it has been noted that there is an increased risk in Ashkenazi Jews with a lifetime risk of 7.8 % compared to 5.2 % in non-Jews [28] [29] [30]. Asian migrants have an increased risk when born in the UK compared to their compatriots who remained in Asia, which then brings in the aspect of environment on a genetic predisposition [31] [32]. Further family studies in twins have demonstrated there is approximately a 45 % chance of developing CD in a monozygotic twin if the other already has CD [33] [34].

1.1.3.1.1. Linkage and association studies in CD

Initial attempts at understanding the heritability of CD revolved around using family cohort studies, looking at relative pairs, where microsatellite markers (tri- and tetra-nucleotide repeats) were studied. Greater than 50 % allelic sharing of a microsatellite area suggests a disease-associated gene present in that area. A

logarithm of odds (LOD) score is used to ensure significance is greater than chance [35]. Once linkage is suggested, association studies are carried out to determine the frequency of a site in cases compared to controls; controls from the same family remove uncontrolled variability of unrelated individuals. A meta-analysis of 10 such studies confirmed genes in IBD1 locus as contributing to small intestinal CD [36] [37]. Linkage studies first revealed the strongest associated susceptibility gene for CD determined to date, that of Nucleotide-binding Oligomerisation Domain containing protein 2 (NOD2) [38] [39] [40]. This was found following observations establishing the IBD1 locus as a risk region [41] [42] and part of the wider linkage studies that defined linkage to nine loci named IBD1-9 on chromosomes 1 (IBD7), 3 (IBD9), 5 (IBD5), 6 (IBD3), 12 (IBD2), 14 (IBD4), 16 (IBD1, IBD8) and 19 (IBD6).

1.1.3.1.2. Genome Wide Association Studies (GWAS) in CD

Genome Wide Association Studies (GWAS) take a hypothesis free approach to finding single nucleotide polymorphisms (SNPs) in cases compared to controls. This required large cohorts of well-characterised patients, known as cases, and controls without the disease to achieve statistical significance. In GWAS, genomic deoxyribose nucleic acid (DNA) is hybridised to an array of many thousands of oligonucleotides representing SNPs that cover the whole genome. The SNP identity is largely determined from the International Haplotype Map resource (HapMap) [43] that correlates key genomic variation from four populations.

The unbiased nature of the results has confirmed known genetic polymorphisms, but has also revealed new and previously unrelated genes that are involved in the

pathogenesis of CD. The first GWAS in CD was carried out in Japan and implicated polymorphisms of the gene TNF superfamily receptor 15 (TNFSF15), which is part of the tumour necrosis factor super-family, in the pathogenesis of CD in Japanese patients [44]. This was further confirmed in UK patients but with a significantly lower p value [45].

Now over 90 genes have been identified from GWAS studies that have an association with IBD, and some of these genes overlap with other diseases. Table 1 summarises the key results for CD adapted from a recent meta-analysis of such studies [46]. The risk attributable to a SNP is reported as an odds ratio (OR), that is a ratio of those carrying the SNP with CD compared to those who have the SNP in the control population. A number of key points are notable from this recent meta-analysis: firstly, that the top six risk SNPs are from both the adaptive and innate immune system. For the adaptive, the interleukin-23 receptor (IL-23R) G allele has the highest OR at 2.66, followed by the innate genes mucin-19 (MUC19) (OR 1.74), leucine-rich repeat (LRR) serine/threonine-protein kinase 2 (LRRK2) (OR 1.74), NOD2 (OR 1.53), immune-related guanine triphosphate (GTP)ase family protein M (IRGM) (OR 1.37) and autophagy-related protein 16 L1 (ATG16L1) (OR 1.34). Secondly, a great deal have a low OR, and whilst for each individual patient a genetic polymorphism may play a part in the pathogenesis of CD, as a population the overall risk is low.

GWAS has not only been used in CD but across many different inflammatory conditions, such as UC [47], multiple sclerosis [48] [49] [50], type 1 diabetes mellitus (T1D) [50] [51], and rheumatoid arthritis (RA) [50] [52]. Indeed, GWAS studies have identified a

Chr.	Risk allele	Allele frequency in controls	P value meta-analysis	OR (95% CI)	Association reported with other phenotypes	Positional candidate genes of interest
1p31	G	0.932	1.00 × 10−64	2.66 (2.36–3.00)	UC, AS, Ps, PBC, GC, BD	IL23R
12q12	A	0.025	6.17 × 10−21	1.74 (1.55–1.95)	PD, leprosy	MUC19, LRRK2
16q12	G	0.260	3.98 × 10−69	1.53 (1.46–1.60)	Leprosy, atopy, Blau, GvHD	NOD2
5q33	G	0.088	7.76 × 10−19	1.37 (1.28–1.47)	TB	IRGM
2q37	A	0.529	6.76 × 10−41	1.34 (1.29–1.40)	UC	ATG16L1
5p13	C	0.606	7.08 × 10−36	1.33 (1.27–1.39)	MS	PTGER4
1p13	G	0.907	4.47 × 10−9	1.26 (1.17–1.37)	T1D, RAa, SLE, Ps, Vitiligoa, AITD	PTPN22
18p11	G	0.153	1.29 × 10−14	1.25 (1.18–1.32)	T1D, coeliac	PTPN2
5q31	T	0.422	1.41 × 10−20	1.23 (1.18–1.28)	Ps, fibrinogen, asthma, TB, UC	SLC22A4, SLC22A5, IRF1, IL3
10q21	G	0.538	4.37 × 10−22	1.23 (1.18–1.29)	BC	ZNF365
8q24	T	0.865	2.29 × 10−6	1.23 (1.17–1.30)		
14q35	T	0.119	1.29 × 10−8	1.23 (1.16–1.31)		GALC, GPR65
22q13	C	0.830	1.70 × 10−10	1.23 (1.17–1.29)		MAP3K7IP1
1q24	T	0.246	1.51 × 10−15	1.22 (1.16–1.28)	HepC, SLE, SSc, T2D	TNFSF18, TNFSF4, FASLG
3p21	A	0.297	6.17 × 10−17	1.22 (1.16–1.27)	UC	MST1, GPX1, BSN
10q24	T	0.492	2.29 × 10−20	1.22 (1.17–1.27)	UC	NKX2-3
9q32	C	0.682	1.00 × 10−15	1.21 (1.15–1.27)	UC, leprosy, SpA	TNFSF15, TNFSF8
17q12	A	0.723	1.70 × 10−13	1.20 (1.14–1.26)	HIV resistance	CCL2, CCL7
6p21	C	0.209	3.98 × 10−11	1.19 (1.13–1.25)	Multiple including UC	LTA, HLA-DQA2, TNF, LST1, LTB
2q12c	G	0.231	1.58 × 10−12	1.19 (1.14–1.26)	Coeliac, asthma, T1D, HSV	IL18RAP, IL12RL2, IL18R1, IL1RL1
10q21	C	0.774	1.41 × 10−7	1.19 (1.13–1.25)	AD	UBE2D1
10q22	G	0.669	2.00 × 10−10	1.19 (1.15–1.23)	Coeliac, MS, vitiligo, BC	ZMIZ1
5q33	A	0.332	5.37 × 10−14	1.18 (1.13–1.24)	Ps, SLE, malaria, asthma	IL12B
9p24	C	0.349	1.00 × 10−13	1.18 (1.13–1.23)	UC, MPD	JAK2
21q22	G	0.391	2.09 × 10−14	1.18 (1.13–1.23)	Coeliac, UC	ICOSLG
9q34c	T	0.411	4.37 × 10−19	1.18 (1.13–1.22)	UC, AS	CARD9, SNAPC4
6p22	C	0.784	1.41 × 10−8	1.17 (1.11–1.23)	T2D, Ps, UC	CDKAL1
6q27	C	0.522	2.51 × 10−12	1.17 (1.12–1.22)	RA, Graves	CCR6
8q24	A	0.609	1.51 × 10−12	1.17 (1.12–1.23)		
11q13	T	0.389	5.62 × 10−13	1.17 (1.12–1.22)	Atopya	C11orf30
13q14	G	0.245	1.41 × 10−10	1.17 (1.12–1.23)	Leprosy	C13orf31
19p13	G	0.247	8.13 × 10−12	1.16 (1.10–1.21)		GPX4, SBNO2
21q21	C	0.579	9.33 × 10−12	1.16 (1.11–1.21)	UC	
1q23	A	0.801	6.17 × 10−7	1.15 (1.09–1.21)	SLE, RA	CD244, ITLN1
10p11	G	0.315	1.10 × 10−9	1.15 (1.10–1.20)	UC	CREM
17q21	A	0.756	2.51 × 10−8	1.15 (1.10–1.21)	MSa, obesity, HIES	MLX, STAT3
2p23	T	0.418	1.10 × 10−4	1.15 (1.10–1.21)	CRP, glucose, TGs	GCKR
1q32	C	0.726	1.58 × 10−7	1.14 (1.08–1.19)	UC, coeliac, MS	C1orf106, KIF21B
7p12	T	0.690	1.20 × 10−8	1.14 (1.09–1.20)	AD, SLE, MCV, ALL	IKZF1, ZPBP, FIGNL1
17q21	A	0.458	1.51 × 10−9	1.14 (1.09–1.19)	Asthma, UC, PBC, T1D, RA, WBC	GSMDL, ZPBP2, ORMDL3, IKZF3
2p21	T	0.129	7.70 × 10−8	1.14 (1.09–1.20)	T2D, PC	THADA
2p16	T	0.420	6.61 × 10−9	1.14 (1.09–1.19)	RA, UC, coeliac	C2orf74, REL
6q21	G	0.301	4.37 × 10−8	1.13 (1.07–1.18)	SLE, RA	PRDM1
1q22	A	0.250	1.29 × 10−9	1.13 (1.06–1.19)	T2D, asthma, PD	SCAMP3, MUC1
1q32	T	0.157	8.32 × 10−9	1.12 (1.07–1.17)	T1D, UC, SLE, BD, HepC	IL10, IL19
2q37	T	0.187	4.57 × 10−9	1.12 (1.07–1.18)	CLL	SP140
5q13	A	0.600	2.00 × 10−6	1.12 (1.07–1.17)		
15q22	T	0.233	1.41 × 10−13	1.12 (1.07–1.16)	CAD, T2D	SMAD3
19p13	G	0.084	9.20 × 10−10	1.12 (1.06–1.19)	T1D, SLE, MS, HIES	TYK2, ICAM1, ICAM3
20q13	G	0.709	2.51 × 10−12	1.12 (1.06–1.18)	Glioma	RTEL1, TNFRSF6B, SLC2A4RG
10p15	C	0.852	8.51 × 10−6	1.11 (1.05–1.16)	MS, T1D, vitiligo, RA, AA, asthma, AITD	IL2RA
6p25	T	0.639	6.16 × 10−7	1.10 (1.05–1.16)		
6q25	G	0.393	1.41 × 10−7	1.10 (1.05–1.14)	RA, coeliac, T1Dd	TAGAP
11q13	A	0.626	3.38 × 10−7	1.10 (1.05–1.16)	AA	PRDX5, ESRRA
13q14	G	0.346	2.00 × 10—6	1.10 (1.05–1.15)	BMD, RA	TNFSF11
22q11	T	0.203	6.31 × 10−13	1.10 (1.06–1.15)	RA, coeliac, SLE, MCV	YDJC
3p24	A	0.322	8.20 × 10−7	1.08 (1.03–1.13)		
5q35	T	0.571	5.25 × 10−8	1.08 (1.04–1.12)		CPEB4
11q12	C	0.341	7.24 × 10−8	1.08 (1.04–1.12)	CAD, dyslipidemia	FADS1
22q12	C	0.471	5.70 × 10−9	1.08 (1.04–1.13)	IBD, T1D	MTMR3
6q15	G	0.658	3.63 × 10−6	1.07 (1.03–1.11)	T1D, coeliac	BACH2
14q24	G	0.584	2.00 × 10−7	1.07 (1.11–1.04)	Coeliac, T1D	ZFP36L1
16p11	G	0.386	1.10 × 10−10	1.07 (1.03–1.12)	T1D, obesity, asthma, CRC, SLE, RA, IBD	IL27, SH2B1, EIF3C, LAT, CD19
19q13	A	0.487	8.60 × 10−10	1.07 (1.04–1.11)	B12, norovirus, HP	FUT2, RASIP1
2p23	G	0.326	1.41 × 10−8	1.06 (1.03–1.10)		DNMT3A
2q33	A	0.473	1.82 × 10−7	1.06 (1.02–1.11)	CAD	PLCL1
5q31	C	0.796	1.10 × 10−9	1.06 (1.02–1.11)		NDFIP1
19q13	T	0.612	2.69 × 10−7	1.06 (1.02–1.11)		
1p36	A	0.190	2.69 × 10−10	1.05 (1.01–1.10)	Coeliac	VAMP3
5q15	C	0.409	4.47 × 10−11	1.05 (1.02–1.09)	AS, PD, T1D, PET	ERAP2, LRAP
1q31	G	0.302	4.90 × 10−9	1.04 (1.00–1.09)	Asthma	DENND1B

Table 1 Crohn's disease risk loci ranked according to Odds Ratio contributed by risk allele (adapted from Franke *et al* [46]) Key: AA=alopecia areata, AD=Alzheimer's disease, AITD=autoimmune thyroid disease, ALL=acute lymphocytic leukaemia, AS=ankylosing spondylitis, BC=breast cancer, BD=Behcet's disease, BMD=bone mineral density, B12=serum vitamin B12 levels, CAD=coronary artery disease, Chr.=chromosome, CLL=chronic lymphocytic leukaemia, CRC=colorectal cancer, CRP=C-reactive protein, GC=gastric cancer, GvHD=graft versus host disease, HepC=hepatitis C susceptibility, HIES=hyper immunoglobulin E syndrome, HP=*Helicobacter pylori*, HSV=human simplex virus, MCV=mean corpuscular volume, MPD=myeloproliferative disease, MS=multiple sclerosis, PBC=primary biliary cirrhosis, PC=prostate cancer, PD=Parkinson's disease, Ps=psoriasis, RA=rheumatoid arthritis, SLE=systemic lupus erythematosis, Spa=spondyloarthritis, SSc=systemic sclerosis, TB=tuberculosis, TGs=triglycerides, T1D=diabetes mellitus type 1, T2D=diabetes mellitus type 2, UC=ulcerative colitis, WBC=white blood cell count.

number of genes that are implicated across a number of different inflammatory conditions, such as IL-2 and IL-21 associated with coeliac disease, multiple sclerosis, RA and T1D [53] [54] and others, as can be seen in Table 1 above. However, the most exciting part of GWAS was the discovery of polymorphisms within genes that were not traditionally thought to be part of the pathogenesis of either CD or other inflammatory conditions. Of particular note in CD were innate cellular processes, such as autophagy [50] [55] [56], or control of the adaptive immune response by the IL-23 receptor [47].

Unfortunately GWAS does not always provide clear answers, as some polymorphisms may occur in stretches of DNA that encode a number of different genes, or conversely in gene deserts, such as on chromosome 5p13 [50] [57] [58] where variants appear to modulate expression of a prostaglandin, prostaglandin E2 receptor EP4 subtype (PTGER4) [58]. Another useful feature of GWAS has been to highlight genetic risk factors shared across different diseases. For example, a locus on chromosome 3p21 for the gene macrophage stimulatory protein 1 (MST1) in CD, being also associated with mutL homologue 1 (MLH1) in UC [59], three prime repair exonuclease 1 (TREX1) in systemic lupus erythematosis (SLE) [60] and C-C chemokine receptor 2 (CCR2) in T1D [61]. This suggests that either there are common pathways involved in the aetiopathogenesis of inflammatory conditions, or the polymorphism detected is a surrogate marker for the actual genetic influence in the surrounding DNA.

Finally, whilst GWAS are powered to characterise polymorphisms with at least 1 % frequency, rare frequency alleles are ignored. Other methodology is therefore

employed to improve understanding of the genetic heritability: Family pedigrees lends towards fine mapping of specific genetic areas; Exome sequencing is better at identifying rare variants from the final splicing; and Whole Genome sequencing is useful for identifying modifier loci. These latter techniques are being used in the current UK IBD Genetics Consortium looking at the genetics of adverse drug reactions (www.ibdresearch.co.uk, accessed April 2012).

An individual's genetics plays a large role within the pathogenesis of CD, but this is balanced by the role of the gut microflora, which will be discussed next.

1.1.3.2. The Microbiota and its role in CD

Evidence for a contribution of the intestinal microbiota in developing colitis was originally postulated by clinical observations that diversion of the faecal stream away from an affected part of the gut, using an ileostomy, resulted in an improvement in symptoms [62] [63]. In addition, antibiotics have been part of the treatment strategy for CD for some time [64]. Other evidence for a contribution of the microbiota derives from animal models of colitis where the presence of specific microbes induces inflammation, such as *Citrobacter rodentium* [65], *Brachyspira (Serpulina) hyodysenteriae* [66], *Helicobacter hepaticus* [67], and *Cryptosporidium parvum* [68]. Furthermore, large-scale genetic studies have implicated the innate immune system in the pathogenesis of CD [50]. The presence of NOD2 CD-risk polymorphisms is associated with gut dysbiosis, which is indirectly suggestive of a role for the commensal microflora in disease [69].

To investigate the gut microflora in more depth, next-generation sequencing techniques have been employed to characterise the intestinal microbiota in both murine models and humans, with estimates of approximately 1 800 genera and 15 000-36 000 species in the GI tract [70]. The low levels of bacteria in the upper GI tract, 10^3, increase to 10^{11-12} per millilitre (mL) of luminal contents in the caecum and give a total estimated number of bacteria of 10^{13} [14] [71], contributing 100 times more genes than that found in the human genome [72]. Intestinal bacteria provide a variety of beneficial functions for their host including energy provision [73], intestinal epithelial function [74] [75] [76] [77], and immune response [78] [79] [80] [81].

There is mounting evidence for a dysbiosis occurring in CD using next-generation sequencing techniques. Reduced anaerobic bacterial populations have been observed in children with IBD [82]. In adults with IBD, studies have found reduced *Firmicute* populations [83] or reduced *Bacteroidetes* and *Lachnospiraceae* species but increased *Actinobacteria* and *Proteobacteria* populations [70]. A difference between luminal flora and that observed at the mucosal surface has been detected [84] [85], yet similar bacterial species are observed in areas of inflammation and normal mucosa within the same individual [84]. One study found greater diversity in healthy individuals compared to those with IBD, but healthy monozygotic twins showed a closer similarity of profile compared to twins with IBD. Indeed, twins who both had IBD had a more similar profile than twins where only one of the twins had IBD. In particular, it was noted in these cases that there was altered *Bacteroides* species within their luminal microbiota [86]. Treatment with Rifaximin, which is a non-systemically absorbed rifamycin-based antibiotic that blocks ribonucleic acid (RNA) polymerase, as a novel treatment strategy for CD, was associated with an increase in

potentially therapeutic *Bifidobacterium*, *Faecalibacterium prausnitzii (F. prausnitzii)*, and *Atopobium* [87]. *F. prausnitzii* is of particular interest, as many different groups around the world have consistently reported a dysbiosis of this particular bacterium, whereby low counts are associated with active CD compared to UC and healthy controls, including in twin studies [88 89 90 91 92 93].

Debate continues as to whether a single causative bacterial species is involved in the pathogenesis of CD, including *Mycobacterium avium* subspecies *paratuberculosis* [94 95] and an increased frequency of adherent invasive *Escherichia coli* (*E. coli*, AIEC) in the mucosal samples of some CD patients [96 97]. These AIEC survive in macrophages and induce TNFα but not IL-1β [98] and need aberrant expression of carcinoembryonic antigen-related cell adhesion molecule 6 (CEACAM6) to facilitate their colonisation of the gut. Once colonised, they cause an increase in claudin-2 expression at the surface of the epithelial cells resulting in increased gut permeability and facilitated translocation of the AIEC beyond the epithelium [99].

Mucosal immunoglobulin (Ig) secretion, in the form of IgA, by B cells and plasma cells residing in Peyer's patches aids protection against microorganisms. It results from presentation of commensal bacteria by dendritic cells (DCs), typically in a T cell independent manner, but secretion is enhanced with T cell co-activation [78 79]. Whilst serological immunoglobulin markers to microbial antigens are associated with disease severity [100], these do not necessarily implicate any particular aetiological cause and may have occurred in response to surgery, perforating disease or strictures. These antibodies have specificity towards microbial products such as anti-*Saccharomyces cerevisiae* antibodies (ASCA) that targets oligomannan,

or anti-*E. coli* outer membrane protein C (anti-OmpC) or anti-CD-related bacterial sequence that targets *Pseudomonas fluorescens* [100]. In addition, antibody and cluster of differentiation 4 ($CD4^+$) T cell responses to flagellin (FLA), a protein in the bacterial tail, can be found in CD patients [101].

1.1.3.2.1. The microbiota's role in CD defined by antibiotics

Antibiotics are used empirically to treat systemic symptoms, such as fever for presumptive bacteraemia, and in penetrating disease, such as for abscesses from small perforations or fistulas. However, others have used antibiotic therapy in the clinical treatment of patients [64]. The mechanism of effect is not clear, but may modulate gut flora [15], and both metronidazole [15] and quinolones have been show to modulate the immune system [102]. The link to mycobacterium has been at the centre of a number of studies, but a lack of long term prevention of relapse prevents widespread use [103]. Meta-analyses have been carried out on the treatment of CD with both anti-mycobacterial [104] and broad-spectrum antibiotics. One analysis was in favour of CD treatment with antibiotics [105] and another analysis suggested there was no statistical benefit [106]. Thus, the role of antibiotics to positively modulate the gut flora to aid treatment of CD remains out of reach currently, and using antibiotics may not alter the long-term prognosis of CD. However their use to treat sepsis in an acute admission or bacterial overgrowth in outpatients, remains important.

Defining the gut microflora will continue to challenge, and the balance between commensals and pathogenic bacteria may play a role in the pathogenesis of CD. The different defence mechanisms erected by the gut mucosa and immune system to

prevent systemic infection and hold the commensal microflora in check will now be discussed.

1.1.4. Mucosal barrier function to prevent inflammation in the gut

The gut mucosa provides a barrier between the microbiota and the internal host cells that likely prevent excessive activation of the immune system in the face of 10^9 microbes mL^{-1} in the terminal ileum [71]. The mechanisms that the mucosa employs to maintain control on these microbes and hold them in a constant symbiotic relationship, providing them with the niche environment yet utilise nutrients that are produced, will now be discussed with reference to what distorts that balance in CD.

1.1.4.1. Mucus barrier and epithelial defence

Mucin lines the mucosal surface and in the colon has a double layered effect with the inner layer, at 50-200 micro-metre (μM) thick, being sterile [107]. Interestingly, whilst mucus in other parts of the body, such as the lung and cervix, is different between individuals, the mucus *O*-glycan structure in the colon is relatively conserved across individuals, irrespective of their underlying human leucocyte antigen (HLA) genotype and it is hypothesised that this may be necessary to provide an environment suitable for commensal bacteria [108]. There is evidence for dysregulated goblet cell homeostasis in IBD with a depletion in UC and an increase in CD [109] [110]. In a MUC2 knockout mouse, mucus deficiency results in bacteria having access to the crypts and causing colitis [107]. Reduced MUC1 messenger RNA (mRNA) expression has been observed in the inflamed ileum from CD patients compared to healthy controls, and that MUC3, 4, and 5B were reduced in the uninflamed ileum from CD patients compared to healthy controls [111].

Intestinal epithelial cells are held together by the apical junction complex, made up of tight junctions, adherent junctions and desmosomes. Tight junctions contain proteins such as occludins, claudins and zona occludens (ZO) proteins, and adherent junctions contain proteins such as epithelial cadherin (E-cadherin) and catenins [112]. It is the apical junction complex that maintains polarity of the epithelial cells and integrity of the barrier, which can then be affected by inflammation causing increased leakiness due to upregulation of claudin-2 [113]. Gut permeability can be further reduced by a repeated structure of phosphate, or polyphosphate known as Poly P, obtained from a luminal commensal *Lactobacillus brevis*. This causes β1 integrin-mediated activation of the p38 mitogen activated protein kinase (MAPK) pathway in association with the induction of heat-shock protein 27 (HSP27) [77] resulting in improved survival in mice exposed to dextran sodium sulphate (DSS). The adaptive immune system further enhances luminal integrity by RAR-related orphan receptor γ (RORγ)-expressing epithelial T cells that express the aryl hydrocarbon receptors and provide IL-22 to enable epithelial integrity [114] [115].

Epithelial cell survival is maintained by the phosphorylation of focal adhesion kinase (FAK) in response to stress by integrins [116]. However, as the epithelium is in a continual state of rejuvenation, the coordinated response to epithelial cell death requires claudins, E-Cadherin, F-actin, myosin II, Rho-associated kinase (ROCK) and myosin light chain kinase (MLCK) to protect the stromal layer beneath the epithelium from coming into contact with luminal contents, particularly bacteria [117]. However, if the stromal cells were exposed to microorganisms, these cells express major histocompatibility complex II (MHC II) and can present microbial peptides to T cells [118].

1.1.4.2. The impact of the underlying stroma

Underlying the intestinal epithelium is the stroma comprising fibroblasts, a collagen matrix and immune cells. The exposure of the stroma to intestinal contents is normally prevented by coordinated mechanisms [117]. The immune cells present include monocytes, macrophages, DCs for the innate immune system and T and B cells for the adaptive, and they usually congregate at Peyer's patches in the ileum or other gut-associated lymphoid tissue (GALT).

Fibrosis and stenosis becomes commoner than inflammation as part of the natural history of CD, and in 10 years 53 % will have penetrating or stricturing disease [119]. Stricturing CD is particularly more common in terminal ileal disease and a feature of NOD2 polymorphisms [120]. Wound repair within the intestine follows a typical process of inflammation, new tissue formation and remodelling [121]. The second stage of wound healing, or inflammatory stage, is characterised by fibroblast migration into the wound, secretion of collagen, and is followed by contraction of the wound surface and disordered remodelling that takes a process of weeks to months and perhaps explains why strictures are the late complications of CD.

A number of factors work in concert to promote fibrosis. Fibroblasts produce chemokines and cytokines in response to different stimuli, including IL-6, IL-8, macrophage-colony stimulating factor (M-CSF) and granulocyte/macrophage-colony stimulating factor (GM-CSF). The ability to produce these chemokines and cytokines does not differ between stimulated cells from uninflamed or inflamed mucosa [122]. Mucosal damage also causes the release of growth factors. In a

paediatric population basic fibroblast growth factor [123] and vascular epithelial growth factor (VEGF) [124] were found to correlate with disease activity, which was replicated in an adult population [125]. VEGF reduces epithelial cell proliferation but increases cellular migration and healing at a wound site in epithelial cells, in a transforming growth factor β1 (TGFβ1)-dependent manner [126]. Furthermore, VEGF induces chemotaxis of monocytes [127].

Wound restitution requires coordinated arrival of monocytes and migration of intestinal fibroblasts, which is enhanced in intestinal fibroblasts that exhibit increased levels of neuronal cadherin (N-cadherin) in response to TGFβ1 [128]. However, reduced migration has also been noted in IBD colonic fibroblasts as a result of decreased FAK phosphorylation caused by interferon-γ (IFNγ) and TNFα [129]. Adhesion molecules, such as intracellular adhesion molecule 1 (ICAM-1) are increased in IBD patients, in particular in CD. Higher ICAM-1 expression in CD patients is associated with less ICAM-1 responsiveness to IL-1β compared to controls, suggesting that ICAM-1 expression is induced in response to inflammation [130]. However, the ICAM-1 expression can be reduced by vasoactive intestinal peptide (VIP), which acts on nuclear factor-κB (NF-κB) [131]. Interestingly, VIP levels are decreased in the intestines of CD patients [132].

During the matrix deposition phase, collagen is laid down by fibroblasts under the control of insulin-like growth factor 1 (IGF1). IGF1 stimulation of rat intestinal smooth muscle cells increased the expression of both procollagen α1 and IGF1's carrier protein insulin-like growth factor binding protein 5 (IGFBP5) [133]. Expression of IGF1 and IGFBP5 are increased in inflamed CD intestine [134]. Regulation of collagen

production by mothers against decapentaplegic homologue 3 (SMAD3) phosphorylation, originally observed post myocardial infarction [135], occurs secondarily to increased levels of IGFBP3 in strictures [136]. Collagen production is also dependent on TGFβ in an extracellular receptor-mediated kinase (ERK1/2 or p44/42 MAPK)- and protein kinase C (PKC)-dependent manner [137]. The action of TGFβ is negatively regulated by endoglin, a TGFβ receptor, which binds TGFβ and prevents it stimulating through its usual receptor. Loss of endoglin results in increased phosphorylation of SMAD3 and increased collagen contraction [138].

One mechanism postulated to influence the formation of strictures is inhibition of matrix metalloproteinase (MMP) by tissue inhibitor of metalloproteinases 1 (TIMP1). TIMP1 has an increased expression in CD compared to UC and controls and this is dependent on TGFβ1 or 2 but not TGFβ3. The physiological relevance of this is unclear, as TIMP1 expression did not appear to alter levels of MMP1, 2, or 3 [139]. The authors speculated that the higher expression of TIMP1 would inhibit MMPs and so increase occurrence of stricture formation.

1.1.4.3. Paneth Cells: guardians of the crypt

At the base of the crypts interwoven with stem cells are Paneth cells, which do not move up the crypt unlike other epithelial cells. Paneth cells are present in the terminal ileum [140] but are markedly absent from the colon except in cases of IBD, known as Paneth cell metaplasia [141]. Paneth cells have anti-microbial granules that contain components such as lysozyme [142], phospholipase A_2 [143] and small peptides. One antimicrobial peptide family is the cryptdins or defensins [144], of which a

number have been identified, including α-defensins, particularly Human Defensin 5 (HD5) and HD6 [145] and β-defensins [146]. Paneth cells express NOD2 [147], which is detected near the anti-microbial granules in the cytosol [140]. Production of defensins are reduced in patients with CD, particularly in those expressing NOD2 polymorphisms associated with CD, such that there is a 3-fold reduction in HD5 production compared to healthy controls and a 9-fold reduction in those with the frame-shift 1007 insertion C (FS1007insC) mutation [148]. However, whilst there is a reduction in HD6 in CD patients compared to healthy controls, this was unrelated to NOD2 mutations [148]. Crypt secretion of defensins has also been reduced in murine NOD2 knockout mice [149]. Over-production of defensins can also cause inflammation of the gut as observed in patients with ankylosing spondylitis [150].

1.1.4.4. The role of the adaptive immune system in gut inflammation

If the innate immune system is able to broadly recognise microbes through pathogen associated molecular patterns (PAMP) recognition by pattern recognition receptors (PRR), it is then the presentation of microbial peptides to activate or anergise highly specific adaptive immune cells that results in inflammation in IBD. There are a number of different T cell subsets in the mucosa, such as regulatory T cells (T_{regs}), characterised by expression of Forkhead box P3 (FoxP3) with secretion of anti-inflammatory cytokines IL-10 [151] and TGFβ, and pro-inflammatory T cells, such as T_H1, T_H2 and T_H17. T_H1 subsets are characterised by the secretion of pro-inflammatory cytokines, such as TNFα and IFNγ; T_H2 by secretion of IL-4, IL-5, Il-6 and IL-13; and T_H17 by IL-17. In CD, increased T_H1 and T_H17 responses are observed while in UC T_H2 responses are increased. In immune conditions where

T_{regs} are deficient, such as seen in IPEX (an inflammatory condition characterised by immune dysregulation, polyendocrinopathy, enteropathy, and is X-linked [152 153]) or Wiscott-Aldrich syndrome protein (WASP) deficiency [154], intestinal inflammation occurs.

It is not merely the proportions of the T cell populations, but the activation of diverse subgroups by a variety of stimulations from antigen presenting cells (APCs), cytokines, microbes and metabolites that determine the final T cell balance and phenotype. For example, in the presence of abundant TGFβ, and even more so in the presence of retinoic acid, naïve $CD4^+$ T cells develop into T_{regs}, which is dependent on B lymphocyte induced maturation protein (BLIMP) and interferon regulatory factor 4 (IRF4) [155]. T_{regs} require priming by mucosal $CD103^+$ DCs in a manner dependent on TGFβ and retinoic acid [156]. The survival of T_{regs} is further dependent on NOD2 [157]. IBD can develop in patients with SNPs in the protein Nedd 4 family interacting protein 1 (NDFIP1), which has been shown to regulate E3 ubiquitin-protein ligase Itchy homolog (ITCH) [158]. ITCH has further been demonstrated to regulate TNFα induced protein 3 (TNFAIP3), known as A20 [159], and patients lacking ITCH have been shown to develop an enteropathy due to infiltration of inflammatory cells, which from mouse models is thought to be due to a lack of T_{regs} [160 161].

Intriguingly, whilst T_{regs} develop in the presence of TGFβ, T_H17 cells also develop in the presence of TGFβ together with pro-inflammatory cytokines such as IL-6 [162]. However, T_H17 cells can also develop in the absence of TGFβ but in the presence of pro-inflammatory cytokines such as IL-23, Il-6 and IL-17 [163] suggesting redundancy

of TGFβ. In addition, γδ T cells have the ability to drive a T_H17 phenotype and cause experimental colitis [164] but this can be overcome by the addition of T_{regs} [165]. Furthermore, T_{regs} can promote the development of T_H17 subsets, which is dependent on low levels of IL-2 [166].

The importance of the IL-23-T_H17 axis has further been demonstrated with the discovery of the protective IL-23R polymorphisms [167] [168]. Healthy individuals, who are heterozygote for the protective R381Q allele, were demonstrated to have a reduction of signal transducer and activator of transcription 3 (STAT3) phosphorylation and IL-17A secretion, despite normal amounts of IL-17A mRNA, in IL-23 stimulated T_H17 cells, which perhaps explains the mechanism of protection [169].

B cell biology maintains mucosal immunity by the production of immunoglobulins including IgA. The presence of antibodies to FLA [101] and *Saccharomyces cerevisiae* [100] demonstrate functional B cell reactivity in IBD. Whilst there are case reports of patients with IgA deficiency having inflammation of the gut, a recent GWAS study into IgA deficiency has discovered similarities with IBD. Among the genes reported were ORM1-like protein 3 (ORMDL3) and protein tyrosine phosphatase non-receptor 22 (PTPN22) associated with CD and Rel associated with UC [170]. In a murine model of CD, some B cell subsets can block T_{regs} resulting in worsening ileitis [171]. However, in a T cell receptor (TCR) knockout mouse model a B cell subset that is characterised by CD1c upregulation acts in an anti-inflammatory way through secretion of IL-10 [172]. Finally, B cells also act as an APC, taking up antigen through the B cell receptor and trafficking it to MHC II to present to T cells [173].

The adaptive immune system, therefore, plays a pivotal role in the pathogenesis of CD as the effector arm to the commensal microbial antigens presented by the innate immune system. The role of the innate immune system in the pathogenesis of CD will now be discussed.

1.1.5. Innate immunity and Crohn's Disease

The innate immune system provides a rapid response to invading or sensed microorganisms. Cells of the innate immune system, such as DCs or macrophages contain a number of PRRs and these respond in a stereotypical manner to PAMPs, which are conserved structural motifs on microorganisms, such as peptides or sugars on the surface of bacteria. The role of different PRRs will be discussed later in this section. The intestinal epithelium expresses innate immune receptors, which in conjunction with innate immune cells, such as DCs and macrophages, continually sample the intestinal microbiota to provide information to the adaptive immune system [25].

The innate immune system had, until the first GWA studies were carried out, been largely ignored in the pathogenesis of CD. In the hypothesis-free analyses of GWAS a number of different innate immune functions were highlighted including PRR signalling, through, both already identified NOD2 but also Toll-like receptor 4 (TLR4), autophagy induction with ATG16L1 [55 174] and IRGM [175], prostaglandin (PG) signalling with PGE4, reactive oxygen species (ROS) production with neutrophil cytosol factor 4 (NCF4) and finally MST1. In contrast in the adaptive immune response, SNPs in the IL-23 receptor and PTPN2, a negative regulator of T cell receptor signalling [50] have been identified and implicated in the pathogenesis of CD.

1.1.5.1. Dendritic Cells

DCs are professional APCs that were discovered in the early 1970s by Ralph Steinman [176]. Their appearance was reported to be unlike any other leucocyte,

having a, "…stellate appearance with continually extending and retracting dendrites…" (Copyright (2007) Wiley. Used with permission from (Steinman RM, Dendritic Cells: Understanding Immunogenicity, European Journal of Immunology, Wiley) [177]. DCs are part of the large family of myeloid derived phagocytic cells that includes monocytes, terminally differentiated macrophages and DCs. Within the macrophage and DC groups are further subsets of cells defined anatomically, genetically and phenotypically. Some authors define DC subsets on where they are located, such as resident versus migratory, being a pre-DC or a mature DC, whether the host is in a steady state or inflammatory state and finally whether the DC is immature or activated [178]. Others do not recognise that DCs exist and suggest they are a continuum with macrophages and form part of a mononuclear phagocytic system [179].

Circulating monocytes constitute 10 % of peripheral leucocytes, are formed from a common myeloid progenitor that is shared with granulocytes and are non-dividing cells [180] [181]. Monocytes, DCs and macrophages develop from a common macrophage/DC precursor that separates into a precursor that is fated towards classical DCs and plasmacytoid DCs or into a precursor that is fated towards monocyte-derived DCs or macrophages [182].

The main defining feature of a DC is its ability to profoundly stimulate naïve T cells [183]. 'Immature' DCs are readily cultured from monocytes stimulated with GM-CSF and IL-4 and are then matured by cytokines, such as TNFα [184], or by PRR stimulation, such as lipopolysaccharide (LPS) [185]. In contrast, macrophages are usually cultured by stimulation with M-CSF or GM-CSF alone or with autologous

serum. Indeed removal of IL-4 from cultured monocyte-derived DCs can change them into cells with a typical macrophage appearance. This would suggest a significant level of plasticity within the monocyte family to be able to be cultured into a cell resembling a different member.

One of the other main defining functions of DCs is to endocytose material, whether dead or dying cells or microorganisms. The endocytic potential is dependent on the maturity of the cell [186]. DCs are able to endocytose by phagocytosis, under the control of the Rho-GTPase cell division control 42 homologue (Cdc42) [186], by macropinocytosis, under the control of Rac [187] and by clathrin-lined pits [188]. Once material has been endocytosed it can be processed ready to be presented to other cells, such as T or B cells, to activate or anergise the adaptive immune system.

1.1.5.1.1. Bacterial handling and antigen presentation

DCs handle bacteria through phagocytosis and degradation in phagolysosomes and, through presentation of bacterial peptides, activate T cells. It has been previously shown that the process of antigen presentation may utilise autophagy (see section 1.1.9), which is constitutively active in APCs providing both extracellular and intracellular proteins to the MHC II loading compartment [189] and that mutation in both NOD2 and ATG16L1 prevent adequate presentation of bacterial antigens [190].

Up to 20 % of protein peptides presented on MHC II may be intracellular proteins in origin [191], though it may be as high as 85 % [192]. This is thought to occur due to autophagy trafficking intracellular proteins to the MHC II loading compartment,

particularly in times of increased autophagy function [193], either as a result of starvation or as bystander proteins in handling intracellular pathogens.

1.1.5.2. Pattern Recognition Receptors

In order that the innate immune system could recognise microorganisms, a system of receptors had to be developed. Unlike the adaptive arm of the immune system, where variable, diverse and joining (VDJ) gene recombination and somatic hypermutation generate receptor diversity [194], the innate immune system has PRRs that recognise conserved PAMPs and result in stereotypical responses, such as cellular activation, maturation and pro-inflammatory cytokine production.

1.1.5.2.1. Toll-like Receptors

TLRs were the first innate immune PRR to be described and consist of a number of structurally similar proteins. These are membrane bound proteins that exist to sample extracellular proteins, such as TLR1, 2, 4, and 5 and some are intracellularly membrane bound sampling extracellular proteins in the endosome, such as TLR 3, 7, 8, and 9 [195]. The cytoplasmic tail of the TLRs is conserved across the family, and shares marked homology with the IL-1 receptor and is now termed the Toll/IL-1 Receptor (TIR). Unlike the IL-1 receptor that has an immunoglobulin extracellular domain, TLRs share, along with other PRRs, an LRR region as their extracellular and ligand-binding domain [196].

The TLRs recognise PAMPs and these differ according to the TLR. TLR1/2 is stimulated by a wide range of microbial PAMPs [197] including triacylated lipoprotein [198], whereas TLR2/6 is stimulated by diacylated lipoprotein in comparison [199]. TLR5

is triggered by FLA [200] and TLR4 by LPS [201]. Whilst viral DNA stimulates TLR3, other viral proteins further stimulate TLR7, TLR8 by single stranded RNA [202] and TLR9 by cytosine-phosphate-guanine (CpG) DNA [203]. The stimulation cascade that ensues from ligand binding is both dependent on myeloid differentiation primary response gene 88 (MyD88) [204] and independent of MyD88 [205]. The resulting cascade involves IL-1 receptor associated kinase (IRAK) [206], and TNF receptor associated factor 6 (TRAF6) [207].

1.1.5.2.2. NOD-like Receptors

Another major PRR family are the NOD-like Receptors (NLRs). These are proteins that contain three main domains, with a C-terminal LRR region that is the ligand binding domain, and an N-terminal protein-protein interaction or effector domain. This effector domain can be a pyrin domain (PYD), caspase activation and recruitment domain (CARD), or baclovirus inhibitor of apoptosis protein (IAP) repeat (BIR) domain. The central NACHT oligomerisation domain (NOD) enables self-oligomerisation during activation and NACHT is an abbreviation for a domain conserved in neuronal apoptosis inhibitory protein (NAIP), MHC Class II transcription activator (CIITA), incompatibility protein from *Podospora anserine* (HET-E) and telomerase-associated protein 1 (TP1) [208]. NLRs are further divided into subfamilies: the members of the NACHT, LRR-containing, PYD-containing proteins (or NALPs); the members of the NODs and CIITA; and the IL-1β converting enzyme (ICE)-like-protease-activating factor (IPAF) and the BIR-containing NAIP, which was the founder protein of the IAP family [209]. See Figure 1 for cartoon representation of NLRs [210].

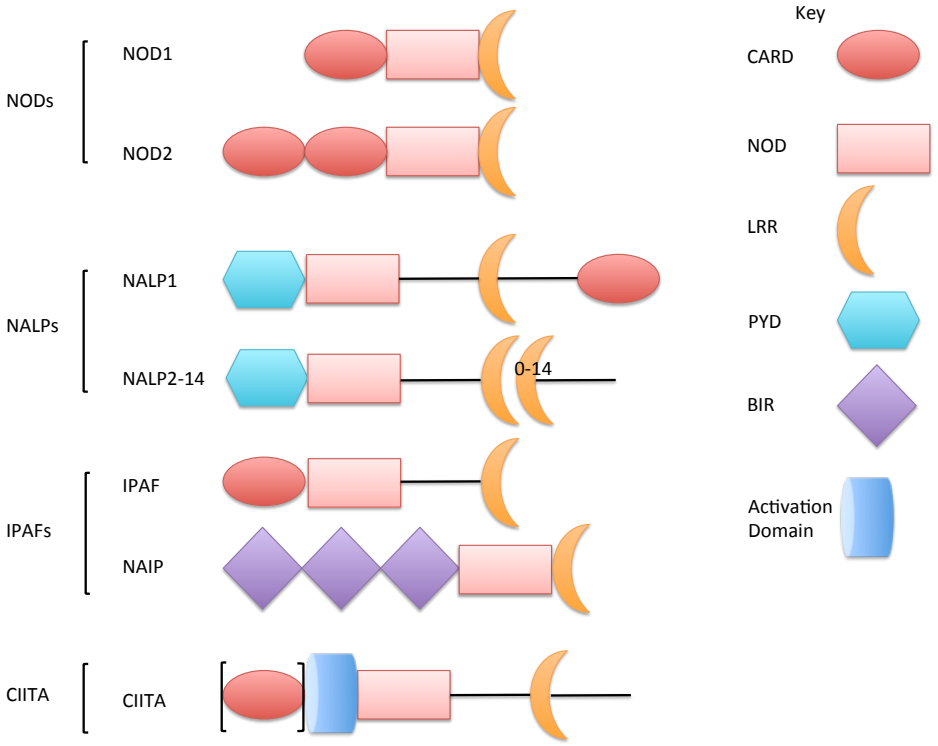


Figure 1: A cartoon representing the NLR family and their constitutive domains (adapted from Chamaillard *et al* [210]). The bracket around CIITA is because the CARD domain is only seen in the subtype of CIITA found in DCs. See main text for abbreviations.

The NODs consist of NOD1 and NOD2. These contain a similar structure but NOD1 has CARD4 as its effector domain, rather than the two CARD15 domains seen in NOD2, and binds γ-D-glutamyl-*meso*-diaminopimelic acid (*meso*-DAP) found in the breakdown product of peptidoglycan from Gram-negative and some Gram-positive bacteria. NOD1 is ubiquitously expressed and stimulation results in activation of NF-κB via TRAF2 and TRAF5 [211]. NOD2 will be discussed later in section 1.1.6.

The other main group within the NLR family are the proteins that constitute the inflammasome, which are typically NALPs. The inflammasome is part of the innate immune system that recognises danger associated molecular patterns (DAMPs)

released by injured cells, such as products of oxidative stress, and foreign particles, such as silica or uric acid crystals [212]. The inflammasome consists of an LRR and effector domains as described above, which can be a PYD, CARD, or BIR domain. The NALPs may associate with the scaffolding adaptor apoptosis-associated speck-like protein containing a CARD (ASC), and then, together with caspase-1, on activation form pentameric or septameric structures [213]. Following activation of the inflammasome, caspase-1 priming then enables cleavage of pro-IL-1β, pro-IL-18 and pro-IL-33 into mature active forms that constitute part of the pro-inflammatory response. It is clear that mature IL-1β release requires two signals: a priming signal via TLRs or NLRs such as NOD2, and then an activating signal, such as provided by adenosine triphosphate (ATP). Interestingly, this IL-1β processing is lost when stimulating cells that express a NOD2 polymorphism associated with CD, such as FS1007insC [214]. It is known that muramyl dipeptide (MDP) mediated activation of the inflammasome occurs in both NALP1 and NALP3 inflammasomes and may require NOD2 [215-218]. Recently there has been evidence for a reciprocal relationship between autophagy and inflammasome activity, in that when autophagy is inhibited, inflammasome activity is increased [219-222].

1.1.6. Nucleotide Oligomerisation Domain 2 (NOD2)

1.1.6.1. The protein and its function

NOD2, a PRR, is found in monocyte-derived cells, such as monocyte-derived DC and monocyte-derived macrophages, and intestinal epithelial cells, such as Paneth Cells [147] and myofibroblasts [223]. As detailed above, structurally NOD2 contains an LRR domain, a NOD domain and two CARD domains. Polymorphisms associated with NOD2 are centred on the LRR domain, whereas polymorphisms associated with Blau syndrome are in the NOD domain.

NOD2 is activated by MDP [224,225], which is a breakdown product of peptidoglycan found on the cell wall of gram-negative and gram-positive bacteria. It is unclear how and where NOD2 interacts with its ligand MDP, whether in cytosol, phagosomes, endosomes or autophagosomes, but MDP is thought to enter the cytosol through clathrin-coated pits [226] and in a dynamin-dependent, caveosome-independent mechanism that requires a pH 5.5-6 [227]. Once in proximity, MDP interacts with the LRR of NOD2 causing conformational change that includes oligomerisation and recruitment of receptor-interacting serine/threonine protein kinase 2 (RIPK2 or receptor-interacting protein 2 (RIP2)) to the CARD domain of NOD2. The association of the CARD of RIPK2 and the CARD of NOD2 [228] results in the initiation of a signalling cascade through known intermediates such as p38 MAPK [229,230] and p44/42 MAPK (or ERK1/2) [231]. The resulting cascade activates NF-κB and enables nuclear translocation of NF-κB, pro-inflammatory gene transcription and a pro-inflammatory phenotype for the APC: up-regulation of MHC II and co-receptors for the activation of $CD4^+$ T cells, production of chemotactic signals, DAMPs, and pro-

inflammatory cytokines. NOD2 stimulation also induces autophagy [184] and in the face of invading bacteria recruits ATG16L1 to the cell membrane in a RIPK2-independent manner [232]. Polymorphisms in the LRR result in a loss of signalling [224] and loss of autophagy induction [190] [232].

1.1.6.2. Negative regulation of NOD2

When stimulation of NOD2 by MDP directs NOD2 to localise to membrane structures, NOD2 interacts with its negative regulator, Erbin [233] [234], which is dependent on Rac1 and Rho guanine nucleotide exchange factor 7 (ARHGEF7 or β-PIX) [235]. Other negative regulators of NOD2 function exist: Angio-associated migratory cell protein (AAMP) affects the CARD domain of NOD2 resulting in a reduction in NF-κB activation [236]; an inhibitory splice variant isoform of NOD2 (NOD2-S) binds the CARD domain preventing oligomerisation on MDP stimulation and subsequent NF-κB activation [237] and upstream open reading frame alternative exon splice variants that control mRNA translation [238]; and lastly Centaurin β1 binds NOD2 and prevents activation of NF-κB, though this seems most likely to be in epithelial/stromal cells rather than monocytes/DCs [239].

1.1.6.3. NOD2 interacts with RIP2, a signalling adaptor molecule, causing downstream signalling effects

RIPK2 or RIP2 is a serine/threonine kinase that is NOD2's adaptor molecule that through interaction with NOD2's CARD domains mediates the majority of NOD2 signals, though as mentioned above not all [232]. Loss of RIP2, in $RIP2^{-/-}$ cells, demonstrate loss of p38, c-Jun N-terminal kinase (JNK) and inhibitor of NF-κB

kinase (IKKα/β) phosphorylation and lack of proteasomal degradation of IκBα on NOD2 stimulation [240] [241]. RIP2 is inducibly phosphorylated at tyrosine 474 by NOD2 and the kinase activity of RIP2 can be inhibited by off-target effects of epidermal growth factor receptor (EGFR) inhibitors [242]. RIP2 is lysine 63 (K63)-polyubiquitinated at Lysine 208 [243] and further work has determined that this occurs by cIAP1 and cIAP2 acting as E3-ubiquitin ligases [241] in conjunction with Ubc13 and Ver1a acting as E2-ubiquitin ligases [244]. cIAPs are part of the potent family of inhibitors of cell death, which also includes X-linked IAP (XIAP). In TNF receptor 1 (TNFR1) signalling RIP1 is K63 polyubiquitinated by Ubc13, Ver1a, cIAP1 and cIAP2 to enable interaction with TGFβ-activating kinase 1 (TAK1). This in turn activates NF-κB and causes cell survival [245]. ITCH can also ubiquitinate RIP2 and reduce its function, but it is unclear whether this is K63 or K48 ubiquitination. In RIP1 physiology, when the K63 ubiquitin is changed to K48 it marks RIP1 for proteasomal degradation [246] and this maybe how ITCH is functioning. A20, which removes K63 ubiquitin chains, rapidly deubiquitinises RIP2 [243] [247] and may alter it from K63 to K48 so marking it for proteasomal degradation.

The poly-ubiquitination of RIP2 was suggested to occur by the TRAF6 [244] but this has not been replicated [245]. Instead ubiquitination of RIP2 is suggested to occur by cIAP1 and cIAP2, independent of the CARD domain of RIP2 [241]. The phosphorylation of RIP2 on NOD2 stimulation causes ubiquitination of NF-κB essential modulator (NEMO) at lysine 285 by K63 ubiquitin chains [228]. The ubiquitination of RIP2, and likely NEMO, provides the scaffold to allow TAK1 to bind the LRR region of NOD2 so propagating NOD2 signalling via RIP2 to activate NF-κB [248]. In the absence of RIP2, NOD2 then has a reciprocal inhibitory effect on TAK1 and TAK1-induced NF-κB

activation. This inhibitory effect is reduced if there is a frame-shift polymorphism of the LRR region of NOD2 [248]. TAK1 activation results in phosphorylation of IκB-related kinase and dual specificity MAPK kinase 6 (MKK6), which results in activation of NF-κB and JNK-p38 pathways [249]. TAK1 is necessary for IL-1β [249 250 251], TNFα [250], IL-18 [252], receptor activator of NF-κB ligand (RANKL) [253] and TGFβ-mediated activation of NF-κB [254]. Thus TAK1 may be a common mediator both of PRR stimulation, such as through TLRs and NOD2, and of inflammatory cytokines.

RIP2 also associates with CARD9 [255]. The association of CARD9 with RIP2 is involved in cytokine production via the activation of JNK and ERK pathways, but is not involved in the activation of NF-κB. CARD9 has been shown to be involved in spleen tyrosine kinase (Syk)-induced C-type lectin signalling [256], and therefore questions remain whether C-type lectin signalling is required for NOD2 signalling, or whether Syk is required.

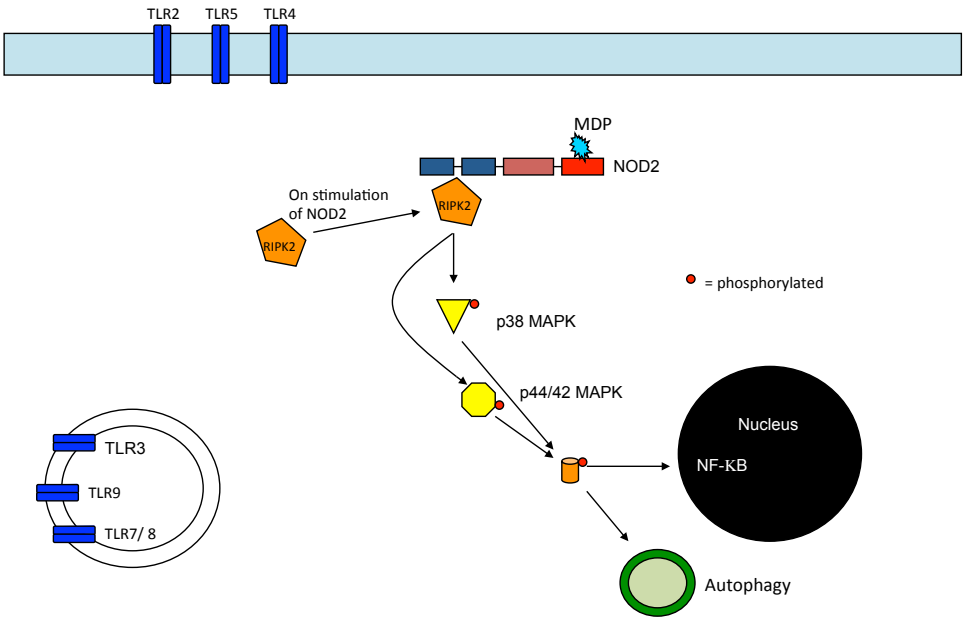


Figure 2: Cartoon of NOD2 stimulation and subsequent induction of signalling pathways through known intermediates p38 and p44/42 MAPK.

1.1.6.4. The role of NOD2 in Crohn's Disease

NOD2 is one of the strongest CD susceptibility genes described to date [38] [40] [50] [257]. Three main SNPs have been identified that are associated with CD: R702W, G908R and FS1007insC [38]. These account for 81 % of the total CD-associated risk alleles in NOD2 [258]. These SNPs lie in the LRR, or ligand-binding domain of NOD2 [38]. New alleles have been identified [168] and some minor alleles are associated with Ashkenazi Jews [259].

A large study of 15 countries data found that in healthy Caucasian populations 7.3 % carried a single mutation in NOD2 (R702W 4.3 %, G908R 1.2 %, FS1007insC 2.3 %) and of those 0.17 % were homozygous for a CD-susceptibility allele, and 0.34 % were compound heterozygotes [260]. This was corroborated by a Danish cohort followed for 31 years, with simple heterozygotes 11 %, homozygotes 0.15 % and compound heterozygotes 0.23 % of the population [261]. Polymorphisms in NOD2 predispose to CD in Caucasian individuals. Whilst simple heterozygotes are carried by African-Americans [262], there is no increased risk of NOD2 mutations among African-Americans or those of Hispanic descent [263]. Furthermore, Japanese patients do not have NOD2 polymorphisms associated with CD [264] [265], nor do Chinese [266], Indian [267], Korean [268] [269], Malaysian [270], Turkish [271] or Tunisian patients [272].

1.1.6.5. Other roles of NOD2

NOD2 has been linked to other clinical conditions aside from CD, for example in Graft versus Host Disease (GvHD). Here, T cell activation to recipient minor and major HLA alleles leads to a significant pro-inflammatory cytokine response, with

symptoms typically being diarrhoea and mucositis. Whilst the impact of HLA is clearly important, CD-associated NOD2 polymorphisms also reduce the efficacy of transplant. As a result there is increased mortality, where 1 year transplant-related mortality in unrelated donor-recipient pairs is 20 % and is further increased to 49% in those with a SNP in both donor and recipient [273]. In all bar one donor-recipient pair, the SNPs were simple heterozygote SNPs not homozygous or compound heterozygotes.

Simple heterozygote polymorphisms in NOD2 increase mortality not only in GvHD but in other conditions, such as decompensated liver disease through an increased incidence of spontaneous bacterial peritonitis (SBP) [274] [275], which has also been noted in polymorphisms of other PRRs such as TLR2 [276]. Furthermore, the presence of CD-associated NOD2 polymorphisms in children undergoing combined bowel and liver transplantation resulted in a greater chance of rejection, sepsis and death [277] [278]. However, whilst no effect of NOD2 SNPs were seen in renal transplant recipients from a cardiovascular/atherosclerotic endpoint [279], there was an increased rate of death among those patients expressing CD-associated NOD2 polymorphisms despite better graft survival rates [280].

NOD2 polymorphisms have recently been associated with leprosy, a chronic granulomatous infection caused by *Mycobacterium leprae*, though the SNPs differ to those observed in CD [281] [282]. TB, caused by *Mycobacterium tuberculosis* (MTB), was not associated with CD-associated NOD2 polymorphisms in Ghanaian [283] or South African [284] cohorts, but other polymorphisms have been associated with susceptibility in African-Caribbean TB patients in the United States of America [285].

NOD2 polymorphisms are also found in Blau syndrome, an autosomal dominant chronic granulomatous inflammatory condition affecting the joints, with cystic symmetrical small joint arthritis of the fingers, wrists, elbows and ankles; the skin, with an erythematous papular eruption and butterfly facial distribution; and the eyes, with an anterior chamber iritis [286] [287]. Three polymorphisms in CARD15/NOD2 were observed in four different families: L469F, R334Q and R334W [288]. Unlike CD, Blau-associated NOD2 polymorphisms are noted in both France [288] and Japan [289]. Further polymorphisms have since been discovered [290].

Early onset sarcoidosis (EOS) shares a similar clinical phenotype with Blau syndrome, characterised by juvenile-onset systemic granulomatous syndrome affecting skin, joints and eyes. One of the Blau-associated NOD2 polymorphisms, R334W, was replicated in cases of EOS, but a further five novel polymorphisms were also discovered [291], and a sixth associated with cardiac infiltration [292]. Previous investigation of patients with adult sarcoidosis had revealed no association with CD-associated NOD2 polymorphisms [293] [294] nor was the iritis associated with sarcoidosis a manifestation of NOD2 polymorphisms [295].

1.1.7. TLR2 and its role within innate immunity

PRRs often cross-talk, as seen below in section 1.1.8, and NOD2 and TLR2 are known to synergise, that is the effect of their dual stimulation is greater than the sum of the stimulation of each PRR individually. The role of TLR2 in innate immunity will therefore be discussed.

1.1.7.1. The TLR2 protein

TLR2 is found on the extracellular surface and its crystal structure in conjunction with TLR1 on stimulation with triacylated lipoprotein in the form of PAM_3CSK_4 (PAM) has been solved [296]. TLR1 and TLR2 fold in an M-shape to bring their TIR in close enough proximity to facilitate dimerisation and initiate signalling.

1.1.7.2. Mechanism of action of TLR2

TLR2, like the other members of the TLR family, has a LRR extracellular domain and a TIR that then enables it to signal via a number of adaptor molecules. TLR2 dimerises with TLR1 on exposure to triacylated lipoproteins [198] [296] and with TLR6 on recognition of diacylated lipoproteins/macrophage activating lipopeptide (MALP-2) [199] [297]. The latter is dependent on CD36 [298].

The main adapter molecules for TLR2 are MyD88 and MyD88 adaptor-like (MAL). MyD88 is required for p38, JNK and NF-κB activation [299]. On dimerisation of TLR2, with either TLR1 or TLR6, MyD88 and MAL are recruited. MAL is phosphorylated by Bruton's tyrosine kinase (BTK) [300] and negatively regulated by suppressor of

cytokine signalling 1 (SOCS1) [301] enabling its degradation; furthermore, Caspase-1 also targets MAL degradation [302]. Having recruited MyD88 and MAL, IRAK4 recruits IRAK1 and phosphorylation of IRAK1 results in it being released from the complex to bind TRAF6, which is negatively regulated by IRAK-M [303]. TRAF6 binds two intermediates, TRAF6-regulated inhibitor of NF-κB kinase (IKK) activator 1 (TRIKA1) and TRIKA2. The TRIKA1 intermediate is an enzyme complex composed of dimers of ubiquitin-conjugating enzyme E2 variant 1A (UEV1A) and UBC13, and functionally acts as an ubiquitin-ligase that K63-polyubiquitinates IKK to activate it [304]. TRIKA2 is a complex of TAK1 binding protein (TAB1), TAB2 and TAK1, which in conjunction with TRIKA1 forms a complex that results in IκB degradation, IKKγ activation and NF-κB activation [249]. Whilst studies on TLR4 have demonstrated LRR flightless-interacting protein (LRRFIP1) and LRRFIP2 further potentiate the signalling process by competing with negative regulators of MyD88 this may not necessarily be the case for TLR2 [305]. In some instances TLR2 signalling requires β3-integrin [306].

1.1.8. PRR crosstalk

PRRs do not work in isolation when recognising bacterial PAMPs. This is important to determine how a cell, particularly an APC such as a DC, is activated and how the activation directs subsequent innate-adaptive immune system interaction. The combination of PRRs activated will be determined by where the microbial PAMPs were detected, for example extracellular versus intracellular versus both intracellular and extracellular PRRs working in concert. PRR cross-talk will occur at many different levels from affecting the mRNA and protein expression levels [307], to enhancing or inhibiting different cellular phenotypes via different pathways, such as through chemokine expression [308].

NOD2 and TLR2 sense different peptidoglycan breakdown products, MDP and PAM, and may explain why NOD2 and TLR2 in particular demonstrate cross-talk. However, cross-talk occurs not only between TLRs [307], but also between TLRs and NLRs [309] and between TLRs and the mannose receptor [310]. Furthermore, NLRs have been shown to cross-talk and when NOD2 and NALP3 are co-stimulated, synergistic gene expression changes are observed [311].

As a result of stimulation of PRRs, the intracellular signalling results in NF-κB activation and gene expression, such as cytokine release. Synergistic effects are observed on stimulation of TLRs and NOD receptors in both inflammatory, such as IL-6 or IL-8, and anti-inflammatory cytokine production, such as IL-10 [309]. Cytokine production is altered not only by which PRRs are stimulated, but also the order in which they are stimulated. Pre-treatment of human enterocyte cell line, HT29, with

peptidoglycan before stimulation with a TLR9 ligand abrogated IL-8 production [307]. The control of cytokine production, however, appears to be dependent on NF-κB, p38 and phosphatidylinositol 3-kinase (PI(3)K) for IL-12p40 expression, but NF-κB and PI(3)K for IL-6 expression [312].

PRR cross-talk is important in maturing DCs. DC maturation is negatively regulated by cytotoxic T lymphocyte protein 4 (CTLA-4) and TGFβ [313]. However, stimulation of PRRs, either in isolation or in concert, overcomes the negative regulation of DC maturation by CTLA-4 or TGFβ, and this process is dependent on neurogenic locus notch homolog 1 (NOTCH1)-PI(3)K signalling [313].

PRR synergy is not restricted to innate cells such as DCs but B cells also express PRRs and stimulation of NLRs with or without TLR ligands enhance both B cell proliferation and survival [314]. Furthermore, aside from immune cells, PRR cross-talk has also been shown to alter bone resorption and osteoclastogenesis [315].

Cross-talk between different PRRs has further been harnessed for novel therapeutic strategies. In influenza-induced pneumonia, either pre- or post-exposure to TLR2/6 and TLR9 ligands protect mice compared to placebo [316]. The addition of LPS onto nano-particles for the administration of a vaccine improves efficacy of the vaccine [317].

PRR cross-talk, therefore, provides the framework for a coordinated physiological response to microorganisms and ensures that the correct response occurs, whether

by controlling maturation or the nature and magnitude of the response, such as through cytokine release.

1.1.9. Autophagy and its role in innate immunity

Downstream of PRR activation, whether alone or in synergy, induction of autophagy occurs. What autophagy is and the importance of autophagy in the innate immune response will now be discussed.

Autophagy is a highly conserved process found in simple eukaryotic cells such as yeasts through to complex mammalian cells. Three types of autophagy exist: microautophagy, chaperone-mediated autophagy and lastly macroautophagy, which herewith will be called autophagy. Ubiquitin tags determine the selection of which intracellular organelles are destined for autophagy [318,319], and the ubiquitin proteasome (via p62, NBR1 and LC3 [320,321]) aid their clearance.

Autophagy, involves the formation of a double membrane vesicle around intracellular structures typically during times of stress or starvation where the reutilisation of amino acids are necessary for the continued survival of the cell. It also occurs in response to misfolded proteins or cytosolic pathogens, where stimulation of the immune pathways via TLRs [322] and, more recently, NOD2 [190] activates autophagy enabling the degradation and containment of intracellular pathogen infection. Our group demonstrated this by looking at the requirement of wildtype NOD2 for MDP-mediated autophagy induction, MHC II upregulation, antigen presentation and bacterial handling (*Salmonella enterica*) but these effects were defective in patients with variants of NOD2 associated with CD [190]. A simultaneous murine paper showed that both NOD2 and ATG16L1, another CD susceptibility gene, are vital for the recruitment of autophagic machinery to

phagosomes that have engulfed bacteria, again showing defects in NOD2 knockout cells [231]. Several CD susceptibility genes have previously been determined to have roles in the autophagy pathway including ATG16L1 [55 174], IRGM [175], LRRK2 [323], and X-box binding protein 1 (XBP1) [324]. This adds weight to the hypothesis that this pathway is dysregulated in CD.

Induction of autophagy is via three main steps of initiation, elongation of the isolation membrane and maturation of the autophagosome as it fuses with the lysosome, to form an autophagolysosome and finally, autophagolysosomes mature into residual bodies by ubiquitination [325]. In starvation the autophagosome is formed, in part by exocyst complex component 8 (EXOC8) [326].

Inhibition of autophagy occurs by mammalian target of rapamycin (mTOR) directly inhibiting the Unc-51-like kinase 1 (ULK1 or ATG1)-ATG13-FAK-interacting protein of 200kDa (FIP200) complex [327]. Activation of autophagy requires inhibition of mTOR and this occurs through the inhibition of its activator, Ras homolog enriched in brain (Rheb). The inactivation of Rheb occurs by dephosphorylation of tuberous sclerosis protein 2 (TSC2) facilitating the binding of TSC2 to TSC1 [328]. The phosphorylation of TSC2 is by the serine/threonine kinase death associated protein kinase 1 (DAPK1) [329]. The inhibition of mTOR by the simultaneous activation of 5'-adenosine monophosphate-activated protein kinase (AMPK) results in the dephosphorylation of ULK1 and subsequent re-phosphorylation of ULK1 at a different residue by AMPK to activate the ULK1-ATG13-FIP200 complex [330]. This complex interacts with ATG101 [327 331], which then, in an unspecified manner, causes activation of the PI(3)K and Beclin-ATG14-VSP34 complex, which coats the

elongation cup in PI(3) phosphate. Beclin1 can further be activated by high mobility group protein B1 (HMGB1) [332] and DAPK1 [333].

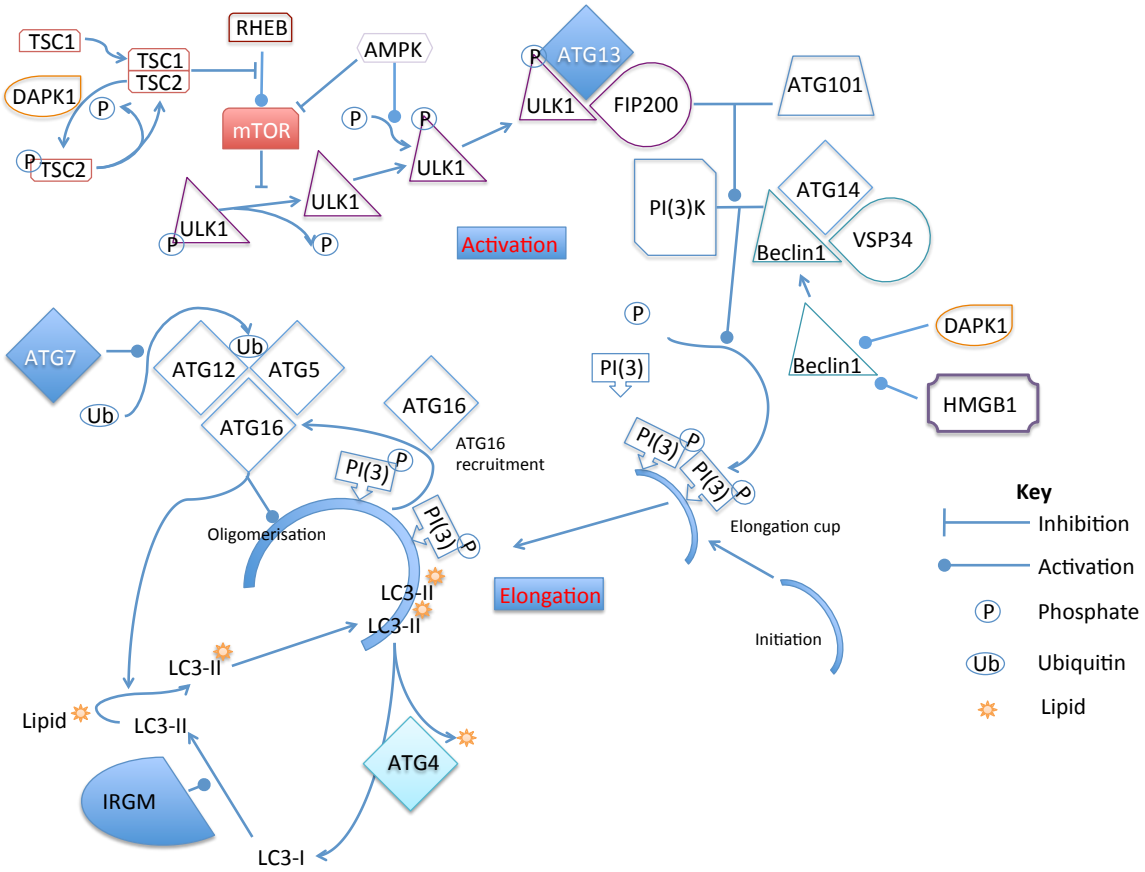


Figure 3: Cartoon summarising Activation or Initiation and Elongation steps of Autophagosome formation

Elongation of the autophagosome to surround the material within the autophagosome is reported to occur through two main mechanisms. Firstly the coating by PI(3) phosphate recruits ATG16 to the membrane [334], which is facilitated by the ubiquitination of ATG5 to ATG12 by ATG7 [335]. This triggers oligomerisation on the outside membrane of the growing autophagosome, and thus may determine the curvature of the autophagosome [336]. The second elongation mechanism is mediated by light chain 3 (LC3) (known as ATG8). LC3-I, a cytosolic protein, is

converted by IRGM to the active autophagy isoform, LC3-II [175,337]. The ATG16-ATG12-ATG5 complex is necessary for the lipidation of the LC3 molecule, which when conjugated to lipid (phosphatidylethanolamine), is recycled by the removal of the lipid by ATG4. LC3 is then re-lipidated to be further involved in the elongation of the autophagosome. Lysosome-associated membrane glycoprotein 1 (LAMP-1) and LAMP-2 are added to form a late autophagosome, which then fuses with lysosomes, where there is vesicle breakdown, and nutrient recycling [338].

Autophagy is involved in both adaptive and innate immune pathways. In the adaptive, ATG5 knockout mice have reduced peripheral T cell numbers and the inability to differentiate effectively into T_H1 or T_H2 phenotypes [339]. In the innate immune system LC3 is recruited directly to phagosomes [340] [341] and stimulation of PRRs such as TLRs and NLRs activate autophagy [190] [322]. Loss of inflammasome proteins IPAF and caspase-1 induce autophagy [221]. Autophagic vesicles provide peptide for the MHC II loading compartment enabling presentation of peptides to T cells [342]. More recently, use of autophagic cross presentation to MHC I is being investigated as a novel therapeutic strategy to treat tumours [343].

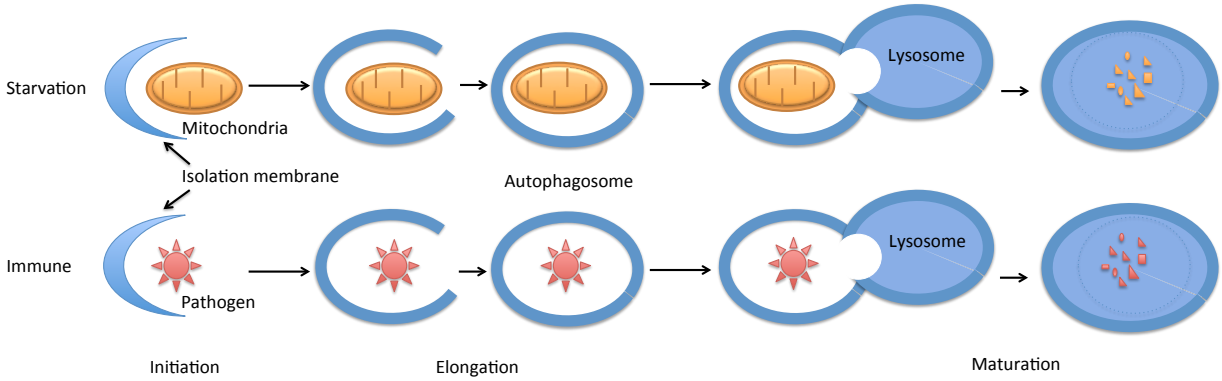


Figure 4: Cartoon demonstrating the main mechanism of autophagy in both starvation and immune scenarios (Adapted from Levine *et al* [338])

The importance of the innate and adaptive immune systems in the pathogenesis of CD has been highlighted, in particular the underlying genetic polymorphisms that contribute to a dysregulated immune response to commensal and pathogenic bacteria, the role of the gut microflora, the role of autophagy and of NOD2, the strongest CD-associated genetic susceptibility. The function of NOD2 within APCs is the subject of this thesis and this was carried out using a proteomic study. The remainder of the introduction will be concerned with proteomics and phospho-proteomics in particular and then a brief introduction to the main proteins identified through this project.

1.2. Proteomics and phospho-proteomics

This thesis is concerned with studying the function of NOD2, the strongest genetic susceptibility gene for CD. In order to investigate the role of a protein within its cellular environment requires the study of proteomics. Recent advances in proteomics have enabled detailed examination of cellular functions. Proteomic workflows typically involve sample selection, protein preparation, separation, identification and proteome-bioinformatics [344]. Proteomic studies use a number of different approaches: simple protein identification by weight and detection, analysis of multi-protein complexes by protein tagging or tandem affinity purification, chip arrays, and mass spectrometry (MS).

MS is core in proteomic studies for both protein separation, by chromatography, and protein identification. Typical platforms available include electrospray ionisation (ESI), matrix-assisted laser desorption/ionisation (MALDI), time-of-flight (TOF), liquid chromatography (LC), ion trap (IT), tandem mass spectrometry (MS/MS) or a combination of the above to derive detailed analysis, such as MALDI-IT-MS (Orbitrap), MALDI-TOF-MS, MALDI-MS/MS and LC-MS/MS [345].

Quantitative proteomics measures relative quantification of proteins within different experimental conditions. Traditional approaches of gel based 2-dimensional polyacrylamide gel electrophoresis (2D-PAGE), with inherent reproducibility issues, have been superseded by isotope-tagging or labelling techniques, such as Stable Isotope Labelling of Amino acids in Culture (SILAC [346]) or differentially weighted labels by isobaric tags for relative and absolute

quantification (iTRAQ [347]) and the isotope-free Tandem Mass Tagging (TMT [348]), and finally label-free techniques [349]. SILAC uses radio-labelled amino-acids to enter the cell and be incorporated into proteins, which takes time and often needs dividing cells to best utilise this approach. iTRAQ and TMT on the other hand are post-protein extraction and pre-MS methods of labelling and quantifying proteins.

MS platforms have enabled use of different proteomic approaches: Discovery, or shotgun, proteomics through directed proteomics to targeted or selected reaction monitoring proteomics. In discovery proteomics no prior knowledge of potential proteins is necessary, and this is then improved by directed proteomics, which assesses quantitative changes first and in a second MS run then sequences differential peptides found. Targeted proteomics provides a dynamic picture of how protein interactions change in time or space using selected reaction monitoring, where *a priori* selection of proteins is required [350].

Phospho-proteomics involves the detection of proteins differentially phosphorylated within cells, and often identified by MS. Along with standard proteomics and phospho-proteomics, analysis of the proteins identified is used to create networks of interacting proteins, which can either be in signalling cascades or curated interactions. The comparison of identified proteins between different conditions, such as pre- and post-stimulation or from different disease states, allows the addition to the network of other proteins known to interact with those identified, and in doing so opening up novel co-interactions, termed the "first neighbour" approach [351].

1.2.1. MASCOT score

A number of different scoring systems determine the quality of the data and identity of peptides recorded during proteomic experiments. One such score is the MASCOT score. The MASCOT score is assigned to a protein as a measurement of probability that the protein identified by the peptide produced by the mass spectrometer is indeed really present in the sample. A score greater than 35 is considered good, and above 70 is considered significant [352].

1.2.2. Post-translational modifications

After translation proteins undergo post-translational modifications to acquire specific functions, and it is estimated there are thousands of post-translational modifications and a few will be discussed briefly. Calcium flux, an early marker of signalling that occurs within seconds, can alter protein functionality [353] [354]. Potassium excess in the extracellular space switches off intracellular functions, such as inflammasome activation [355].

Phosphorylation by a kinase occurs rapidly, such as within 1 minute [356], and is balanced by a phosphatase removing phosphate groups. Phosphorylation kinetics is best modelled by hippocampal neurons where two different phosphorylation pathways of a single protein, cyclic-adenosine monophosphate (cAMP)-responsive element binding protein (CREB), occurs: one within 3 minutes causing activation of a calmodulin kinase (CaMK) pathway; the second a MAPK pathway that causes phosphorylation later to 60 minutes causing gene transcription [357].

Ubiquitination occurs in two key ways: Firstly, K48 poly-ubiquitination marking proteins for proteasomal degradation, a process intrinsic to MHC I peptide presentation [358] [359] and endocytosis [360]. Secondly, K63 poly-ubiquitination activates proteins, such as TRIKA1 activation of IKK [304]. Ubiquitination regulates proteins that have been activated, such as the removal of Tyk2 enabling IFN production, the direction of B-cell receptor-antigen complexes to the correct compartments [361], the regulation of MHC II expression on DCs [362] or the induction of tolerance in DCs [363]. Phosphorylated proteins may be targeted for ubiquitination and subsequent proteasomal degradation [364]. Autophagy occasionally requires ubiquitination of bacteria [365] [366] and the ubiquitin-activating enzyme E1 to mature the autophagolysosomes into residual bodies [325]. Ubiquitination is utilised by autophagic proteins themselves, as, ATG7, which is a ubiquitin-E1-like enzyme, is required to link ATG12 to ATG5 [335].

1.3. An introduction to the main proteins identified through the proteomic study of the function of NOD2 in APCs

The following proteins were identified within the study on the function of NOD2 in APCs. Before demonstrating their role within the NOD2/TLR2 signalling cascades, a brief overview of the structure and function is necessary.

1.3.1. L-plastin or LCP1

L-plastin or lymphocyte cytosolic protein 1 (LCP1) is found in leucocytes and forms part of the plastin family that are homologous to the fimbrin family. Fimbrins were originally identified in chicken intestinal microvilli [367] and were located in membrane ruffles and within the cytosol [368]. The two other proteins within the plastin family are plastin-1, or I-plastin, found mainly in intestinal epithelial cells and fibroblasts, and plastin-3 or T-plastin, found in many solid organs, such as kidney cells. Overexpression of LCP1 is associated with increased invasiveness of colorectal cancer cells [369] and in melanoma cells when phosphorylated [370], but phosphorylation confers resistance to TNFα-induced apoptosis in breast cancer cells [371].

Migration by immune cells requires phosphorylation of LCP1, as there is reduced GM-CSF-induced eosinophilic migration on inhibition of PKCβII, which phosphorylates LCP1 [372]. T cell migration has been shown to require LCP1 as $LCP1^{-/-}$ T cells fail to migrate as efficiently on stimulation [373]. In contrast, migration of neutrophils from $LCP1^{-/-}$ mice is not affected [374].

Integrins are surface proteins that are integral to APC function both in terms of adhesion [375] and signalling function [374]. Components of the signalling cascade that control integrin function have included Rho-GTPases, L-plastin [376] and Syk [374]. In T cells, LCP1 aids the formation of the immunological synapse [377] [378] in association with Talin and the integrin lymphocyte function associated antigen 1 (LFA-1, composed of CD11a/CD18), which forms the peripheral supramolecular activation complex (pSMAC) in a Calmodulin-dependent manner [377]. The inner or central SMAC (cSMAC) is composed of T cell receptor, CD3 and PKC [379].

LCP1 is an actin bundling protein that is expressed in monocytes with varied roles within intracellular functions including cytoskeletal changes, migration, cytokine production, integrin function, phagocytosis and respiratory burst. In T cells it is also involved in the immunological synapse. The integrin and cytoskeletal interface may also suggest that LCP1 is a scaffold protein.

1.3.2. Phospho-tyrosine protein non-receptor 6 (PTPN6) or Src-homology domain 2 containing protein tyrosine phosphatase 1 (SHP1)

SHP1 is a phosphatase that is expressed in haematopoietic cells, smooth muscle [380] and epithelial cells [381], and it is involved in multiple functions within leucocytes and epithelial cells, particularly regulation of immune receptor tyrosine-based inhibitory motifs (ITIMs) [382] [383]. Activation of SHP1 is through stimulation of tyrosine receptors, such as the insulin receptor (INSR) [384], CCR5 [385], TLR4 [386], and by CD4 stimulation [387]. Phosphorylation of SHP1 is dependent on c-Src [388].

A great deal of work done on SHP1 has been in regard to T cell signalling via the TCR and the role of inhibitory signals on the T cell side of the immune synapse. In the motheaten (me) or motheaten viable (mev) knockout mouse ($SHP1^{me/me}$ or $SHP1^{mev/mev}$) there is prolonged tyrosine phosphorylation of the TCR, subsequent T cell hyper-proliferation and an autoimmune phenotype [387]. However, in innate cells, loss of SHP1 alters signalling cascades involving intermediates such as JNK and p38 [389] and p44/42 MAPK [389] [390]. The resulting changes in phenotype include loss of cytokines IL-8 [391] [392], IL-1β [389] [393] and TNFα. However, TNFα is more controversial as some have found release to be independent of SHP1 [386] and others it is an SHP1-dependent manner [389] [390].

The role of SHP1 in other cellular functions has been studied including migration, phagocytosis and communication with the adaptive immune system. In SHP1 silenced macrophages, increased cellular stickiness and a reduction in migration were observed [394], but in bone marrow derived DCs (BMDCs) a 4-fold increase in cells migrated with SHP1 silencing than without [389]. Phagocytosis of an encapsulated

Streptococcus suis was observed to be increased in SHP1 silenced cells [356]. When DCs present antigen to T_{regs} the MHC II stimulation of T_{regs} causes crosslinking of the MHC II by Lymphocyte activation gene-3 (LAG-3) and results in an inhibitory signal in DCs that is dependent on SHP1 [395].

SHP1 is an important ITIM regulator and alters cellular phenotype through changes in signalling pathway intermediates. Furthermore, SHP1 is involved in phagocytosis, migration and bi-directional signalling with the adaptive immune system.

1.3.3. High Mobility Group B1 (HMGB1)

HMGB1 is an alarmin or DAMP whose release by necrotic cells, rather than apoptotic cells, induces inflammation [396]. Extracellular HMGB1 binds to receptor for advanced glycation end-products (RAGE) [397]. Downstream activation of NF-κB requires both RAGE and macrophage-1 antigen (Mac-1) [398]. Extracellular HMGB1 in vitro is able to elicit a pro-inflammatory response characterised by the release of IL-1β, IL-6, IL-8 and macrophage inflammatory protein-1β (MIP1β), but not IL-12 or IL-10 [399]. In vivo, serum TNFα was released on intraperitoneal HMGB1 stimulation for 6 hours [399].

HMGB1 release from the cytoplasm is calcium dependent and phosphorylation on a serine residue on LPS stimulation is mediated by PKC. However, PI(3)K inhibitors reduced secretion of HMGB1, as did JNK inhibitors, but not ERK, NF-κB or p38 inhibitors [400]. HMGB1 reduction by extracellular anti-HMGB1 antibodies was shown to reduce CCR7 expression [401] and, as a result, reduce DC migration in response to C-C chemokine ligand 19 (CCL19).

HMGB1 translocated out of the nucleus into the cytoplasm in response to starvation and ROS. In the cytoplasm, HMGB1 then associated with Beclin1, by causing the dissociation of Beclin1 from Bcl2, and so induced autophagy [402]. In concert with HSP27, HMGB1 is a critical regulator of mitochondrial function [332] and HMGB1-induced mitophagy and autophagy is carried out by HSP27 [332].

1.3.4. Death Associated Protein Kinase 1 (DAPK1)

1.3.4.1. DAPK1 induction, structure and phosphorylation

DAPK1 is a key immune regulator that was first discovered as a mediator of cell death [403]. It is part of a family of death domain kinases that includes DAPK1-related protein 1 (or DAPK2), Zipper-interacting kinase (ZIPK or DAPK3), DAP kinase related apoptosis inducing protein kinase 1 (DRAK1) and DRAK2 [404]. DAPK1 is induced by TGFβ [405].

DAPK1 has 5 main domains within the protein: a kinase, a calmodulin-binding domain, 8 ankyrin repeat domains, a cytoskeletal and a death domain. Activation of DAPK1's kinase domain requires the combined dephosphorylation of the autophosphorylation site, ser308, by PP2A [406] and dephosphorylation of ser289 to enable the binding of calmodulin [407], which together cause a conformational change allowing the kinase binding domain to open for kinase activity [408] [409] [410].

1.3.4.2. DAPK1 and autophagy

The role of DAPK1 in autophagy is controversial. DAPK1 prevents autophagy by phosphorylation of the tumour suppressor protein, TSC2, which then dissociates from TSC1. The dissociation prevents the TSC1/2 complex inhibiting mTOR complex 1 (mTORC1), a powerful inhibitor of autophagy when active. On activation of mTORC1, DAPK1 phosphorylates S6K (thr389) and S6, important ribosomal proteins and effectors of mTORC1 [329]. Conversely, DAPK1 can induce autophagy by

phosphorylating Beclin1 at thr119, causing the dissociation of Beclin-1 from BCL-X_L [333]. This replicates JNK's interaction with Bcl2 causing it to dissociate with Beclin1 in starvation-induced autophagy [411]. Yet, no link of DAPK1 in starvation-induced autophagy has been proven, and unpublished data suggests it is not [412]. DAPK1 also phosphorylates another member of the DAPK family, ZIPK, and this phosphorylation results in activation of autophagy by ZIPK.

1.3.4.3. Endocytosis and the role for DAPK1

Endocytosis is an important mechanism by which cells take up nutrients, molecules or, in the form of phagocytosis, bacteria. DAPK1 phosphorylation of Syntaxin-1 results in failure of synaptic vesicle docking [413]. Loss of DAPK1 expression results in the accumulation of early and late endosomes under the cell surface [414]. Further elucidation of the role of DAPK1 in this area is needed.

Thus, DAPK1 is a vital and pivotal ser/thr kinase that is both pro- and anti-apoptotic. It both activates and prevents autophagy, and is involved in endocytosis.

1.3.5. HSP27

HSP27 or HSPB1 is a chaperone protein in the heat shock family, whose transcription is regulated by HMGB1 [332]. In colonic mucosa TNFα and IFNγ cause a reduction in translation of HSP27 by eIF-2α, and perhaps increased removal of HSP27 [415]. Yet, for cells to produce IL-6 on stimulation by TNFα this requires HSP27 to facilitate it [416]. The prevention of apoptosis can also be mediated by HSP27 [417].

HSP27 forms part of the p38-MAPKAP kinase (MK)-HSP27 axis [418]. HSP27 phosphorylation occurs at three main phospho-serine sites: 15, 78 and 82. These are mediated by different MKs with MK2 and 3 being upstream of ser 15; MK2, MK3 and MK5 being the upstream kinase of ser78; but MK3+5 being upstream of ser82 [419]. Furthermore, the phosphorylation of HSP27 at ser78 is determined by cAMP/protein kinase A (PKA) activation signalling via MK5. However, in response to stress, phosphorylation is determined by MK2 downstream of p38 [419]. The phosphorylation of HSP27 at ser82 in colonic biopsies was increased in patients who responded to infliximab treatment compared to short responders or non-responders [420].

HSP27 has two other sites of phosphorylation: ser86, described alone, or in cooperation with phosphorylation at ser15. Firstly, ser86 was dephosphorylated by ROS created by the administration of DSS to cause colitis in mice [421]. Phosphorylation of HSP27 was shown to be involved in actin bundling [422]. Phosphorylation at ser15, 78 and 82 together reduce chaperone activity whereas mutations on their own of ser15 or ser78+ser82 do not [423]. HSP27 is important in

cytoskeletal changes, most likely mediated by phosphorylation of FAK [424] [425], in response to stress [426] [427], fluid phase pinocytosis [427] and VEGF-induced migration of fibroblasts through activation of p38 and subsequent phosphorylation of HSP27 by MK2/3 [428].

HSP27 has been implicated in autophagy as mutations at ser15 and ser86 caused loss of autophagy [332]. HSP27 prevented apoptosis and increased autophagy caused by the unfolded protein response (UPR) [429].

1.3.6. MAPK/ERK Kinase 1 (MEK1)

MAPK signalling cascades form three of the main cascades, that of ERK1/2, JNK and p38 MAPK. MEK1 is a universal signalling protein that is involved in the ERK pathway and results in activation of a number of different cellular pathways. Signals are transmitted from a receptor, such as a PRR, via small GTPases, such as Ras, or an adaptor molecule, to activate MAP4K. This activates MAPK kinase kinase (MAP3K), where it is transmitted to MAPKK or MEK1/2 [430]. MEK1/2 is one of a few dual specificity MAPKs that can activate, by phosphorylation, both of ERK's phosphorylation sites, thr202 and try204 [431].

In the adaptive immune system, MEK1 is phosphorylated downstream of CCR7 and the TCR [432]. In innate immunity, MEK1 has a variety of functions. MEK1 binds to β-arrestin and activates ERK2. The activation of ERK2 phosphorylates β-arrestin at ser412 and renders β-arrestin inactive [433]. The dephosphorylation of β-arrestin is required for β-arrestin-mediated endocytosis. Peptidyl-prolyl cis-trans isomerase NIMA-interacting 1 (PIN1) regulates MEK1 through direct interaction and this results in phosphorylation of MEK1 and downstream signals cause the increase in LC3 levels [434].

However, the activation of MEK1 is not always beneficial, as the action of IL-6 on gut epithelial cells activates MEK1 and increases claudin-2 expression. This leads to increased permeability of the gut epithelial tight junctions [435].

1.4. Conclusion and Aims of Thesis

Polymorphisms in the ligand recognition domain of NOD2 remain the strongest genetic risk factor for the development of CD. NOD2 directs autophagy in human DCs to facilitate bacterial destruction and antigen presentation; the CD-variant-NOD2 shows defects in this pathway. Work in the laboratory has demonstrated NOD2 signals to control expression of microRNA-29, which has important immunoregulatory effects including suppression of IL-12p40/IL-23. Induction of this microRNA is impaired in cells from CD patients expressing NOD2-variants associated with the disease. Thus, NOD2 directs key anti-microbial and immunoregulatory functions, whose breakdown, in the presence of CD-variant NOD2, could act as a trigger for inflammation in this disease.

In comparison with other PRRs, relatively little is understood of the hardwiring of NOD2 signalling, the mechanism of NOD2-mediated autophagy induction, the means by which NOD2 recruits a signalling platform within the cytosol and the mechanism of synergy with other PRRs and the inflammasome. In this work I will use quantitative proteomics to map the NOD2 signalling cascade and its cross-talk with TLR2. Defining the hard wiring of NOD2 signalling in healthy donors, in comparison with CD donors expressing variant NOD2, is important to define targets amenable to drug design within this pathway.

2. Materials and Methods

2.1. Tissue culture

All cells were cultured at 37 °C in incubators that were humidified and supplemented with 5 % Carbon Dioxide. Where cell lines were used, mycoplasma infection was routinely tested for and excluded.

2.1.1. Primary human immature monocyte-derived DC preparation

Buffy coats, the leucocyte and platelet rich component from whole blood, were transported from the National Blood Service (Bristol, UK) 24 hours after venesection through the Oxford Blood Service and then processed in our laboratory to extract primary human immature monocytes. These were then differentiated into immature monocyte-derived DCs. The buffy coat samples were from healthy donors and the immature monocytes were removed by the following protocol.

The buffy coat sample was diluted in an equal volume of RPMI-1640 medium (Sigma), and separated by centrifugation for 25 minutes at 931 g (2000 rpm), without a brake during deceleration, over a Sodium Diatrizoate/Polysaccharide solution (Lymphoprep, Axis-Shield). From the lymphoprep/medium interface, the mononuclear cell layer was harvested using Pasteur pipettes, and then washed three times in ice-cold RPMI-1640. Using anti-CD14 microbeads and MACS LS columns (Miltenyi Biotech, Bergisch Gladbach), $CD14^+$ monocytes were positively selected from the mononuclear cells according to the manufacturers protocol as follows: Leucocytes were resuspended in 4 mL of MACS buffer (500 ml Dulbecco's

Phosphate Buffered Saline (PBS, Sigma) supplemented with 2 mL 0.5 M ethylenediaminetetraacetic acid (EDTA) pH 8.0 and 2.5 g bovine serum albumin (BSA)), and incubated with 250 μL of CD14 MACS beads for 20 minutes at 4 °C with gentle swirling after 10 minutes. The suspension was washed in an additional 26 ml of MACS buffer to remove unbound excess beads, and the cells were resuspended in 5 mL of ice-cold MACS buffer. During this time, MACS LS columns and pre-separation filters (Miltenyi biotech) were primed with 5 mL of MACS buffer. Using gravity alone, the mononuclear cell suspension was then allowed to flow through the primed columns. The columns were washed three times with 3 mL ice-cold MACS buffer prior to recovery of the $CD14^+$ cells in a further 6 mL of MACS buffer. The recovered $CD14^+$ cells were washed once at 4 °C in ice-cold RPMI-1640 at 456 g (1400 rpm), and then plated for culture in R10 (RPMI-1640 supplemented with 10% heat-inactivated Fetal Calf Serum (FCS), Glutamine 2 mM, and Penicillin/Streptomycin 2mM (all from Sigma)). Mononuclear cells from an individual buffy coat were plated into 2x 20 cm sterile culture plates (Nunc), each with 25 mL of warm R10 supplemented with IL-4 and GM-CSF (Peprotech) at 40 ng mL^{-1}. All components of culture medium were sterile filtered. Each plate was supplemented with an additional 25 mL of warm R10 with IL-4 and GM-CSF at 20 ng mL^{-1} (final concentration) on day 3 of culture. Immature DCs were harvested for experiments after 3-5 days of culture. All dishes were checked for contamination and viability by light microscopy and Trypan blue staining prior to use.

2.1.2. Preparation of primary human monocyte derived macrophages

Monocyte derived macrophages were derived in the same manner as DCs, except 15-20 mL serum was retrieved from above the leucocyte interface layer (above the

Lymphoprep) before the cells were retrieved; it was heat inactivated (54 °C for 30 minutes), centrifuged and filtered. It was used with RPMI-1640, supplemented with glutamine and pen/strep, at 1 % concentration instead of FCS at 10 %. Cells were incubated at 37 °C, 5 % CO_2 for 5-7 days and were plated in 6-8 x 9 cm plates.

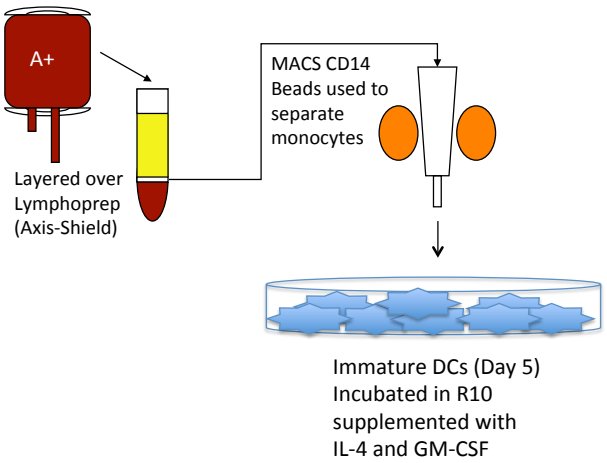


Figure 5: Preparation of immature DCs. Leucocyte separation on Lymphoprep (Axis-Shield) followed by 20 minute incubation with MACS CD14 beads (Miltenyi) to positively select CD14+ monocytes, which were then incubated in R10 supplemented with IL-4 and GM-CSF (Peprotech).

2.1.3. Harvesting DCs and macrophages

DCs were harvested by aspirating off the culture media, then gentle scraping of the cells whilst bathed in ice-cold PBS or RPMI-1640. The collected cells were washed twice in cold PBS or RPMI-1640, and counted before carrying out experiments. Unlike DCs, macrophages were more adherent. To ease harvesting, lidocaine 4 mg mL^{-1} and 0.5 mM EDTA in ice-cold PBS for 10 minutes at 4 °C enabled lifting of macrophages and with gentle scraping retained greater survival. These were then stimulated according to experiments defined in the text.

2.2. **Stimulation of DCs and macrophages**

2.2.1. Gene expression stimulation and immunoblotting

Immature DCs of known NOD2 genotype (that is homozygous wild type NOD2 were used, any found to have variants of NOD2 were not included in any study in this thesis) were harvested on Day 5 of culture as previously described (see 2.1.3), and were washed twice in 50 mL ice-cold RPMI-1640 (Sigma) or PBS. 3-10 million cells per condition were plated in 4 mL warm R10 in 6 well flat bottomed culture plates (Nunc) and stimulated with various concentrations of PRR ligands, such as MDP (Invivogen), PAM (Invivogen), FLA (Invivogen), LPS (Invivogen) or left unstimulated, for the required time interval at 37 °C as described in the text. At the end of the stimulation period, stimulation was ended by transferring cells onto ice and the addition of 4 mL of ice-cold sterile PBS to each well. Cells were then harvested, and washed three times with ice-cold sterile PBS in 15 mL falcons. Cells were then transferred to 1.5 mL eppendorfs on ice for lysis and RNA extraction using Qiagen RNeasy kits as described elsewhere. If the cell was to be lysed for immunoblotting by Western Blot, then the cells were lysed for immunoblotting as described elsewhere (2.4.1).

2.2.2. Stimulation of DCs to investigate phosphorylation cascades

On day 5 of culture, DCs were harvested and washed twice in ice-cold RPMI-1640 medium (Sigma). After washing, up to 55 million cells per condition were resuspended on ice (in 15 mL Falcon tubes) in 4 mL of R10 with or without PRR ligand MDP, PAM, FLA or LPS or starvation media (Earle's Balanced Salt Solution (EBSS, Sigma)), as indicated in the text, and transferred initially to a water bath for 2

minutes at 37 °C, then into an incubator. After 30 minutes of stimulation, immediate transfer onto ice and the addition of 10 mL of ice-cold Hepes Buffered Saline (HBS, Sigma) supplemented with 0.1 % Phosphatase inhibitor cocktail 1 or 3 (Sigma, 1:100) terminated experiments. Cells were washed once more in ice-cold HBS with phosphatase inhibitors, and then lysed with Phosphoprotein lysis buffer supplemented with 3-[(3-cholamidopropyl)dimethylammonio]-1-propanesulfonate (CHAPS) (25 μL mL^{-1}), protease inhibitors (1 per 5 mL, Complete Mini EDTA-free, Roche), and Benzonase (10 μL mL^{-1}) (All Qiagen), and Phosphatase inhibitor cocktail 1 or 3 (Sigma, 1:100) for 40 minutes at 4 °C. Lysates were then cleared of cellular debris by centrifugation, and phosphoproteins enriched using a Qiagen phosphoprotein purification kit (Qiagen). Enriched phosphoproteins were then immunoblotted or subjected to mass spectrometry (see 2.4.10).

2.2.3. Stimulation of DCs for confocal experiments

Immature DCs with wild type NOD2 genotype were harvested on day 5 of culture as previously described, and were washed twice in 50 mL ice-cold RPMI-1640 or PBS. DCs were seeded at 2 x 10^5 cells $well^{-1}$ onto 8-well Tissue Culture Slides (BD Biosciences) coated with poly-L/D-lysine. Cells were allowed to adhere for 30-60 minutes prior to stimulation in 180-400 μL R10. In autophagy experiments E64d and Pepstatin was used at 10 μg mL^{-1} to inhibit fusion of autophagosomes to lysosomes thus preventing degradation of autophagosomes for 10 minutes prior to stimulation. Starvation of cells with EBSS was used as a positive control for autophagy induction, where R10 was replaced by pre-warmed EBSS in the appropriate wells for the last 2 hours of stimulation. When lysosomes were required to be highlighted, Lysotracker-Red (Invitrogen) was added to the wells for the last 2

hours of stimulation, at a final concentration of 0.2 % (vol/vol). At the end of the stimulation period, cells were washed and stained for confocal microscopy as described in 2.2.7.

2.2.4. Bacterial culture

LB medium was made as described in 2.5.5.1, as per lab protocol, and was autoclaved at 15 psi for 20 minutes, and allowed to cool before use. LB agar was made using the same compounds for LB medium with the addition of Agar, as per 2.5.5.2, prior to autoclaving. Autoclaved agar was poured into 9 cm sterile Petri dishes (Nunc or BD Bioscience) either prior to solidifying post-autoclaving, or after melting by microwaving. *Salmonella typhimurium*-tagged with green fluorescent protein (GFP) were given by Professor David Holden. These were cultured to logarithmic phase in LB at 37 °C. GFP-*Salmonella* were estimated to be at 10^9 colony forming units (CFU) mL^{-1} when absorbance was 0.5 at 600 nM. Bacteria were usually used at a multiplicity of infection (MOI) of 25:1 DC.

2.2.5. Antigen presentation and proliferation assays

CD4-negative selection microbeads (Miltenyi Biotec) were used to isolate $CD4^+$ T cells, using a similar method as described for isolation of $CD14^+$ monocytes above. For tetanus toxin specific T cell proliferation assays, DCs were first co-cultured with beads coated with the C-fragment (Cfr) of tetanus toxin, made with Poly-link kit (Polyscience), for 2 hours at a MOI of 25:1. DCs were then washed extensively in RPMI-1640. Autologous $CD4^+$ T cells were stained with carboxyfluorescein succinimidyl ester (CSFE, Invitrogen) for 15 minutes at 37 °C at 10 μM, incubated for further 30 minutes in CSFE-free media and washed 3 times. The stained 10^3 –

10^5 T cells were then co-cultured 10:1 with DCs, pre-exposed to beads as above, for 7 days and staining assessed by flow cytometry.

2.2.6. Bacterial handling assays

For bacterial persistence assay, 1 x 10^5 DCs were exposed to GFP-*Salmonella* at an MOI of 25 for 1 hour in R10 at 37 °C. After 90 minutes, gentamicin was added at 50 μg mL^{-1} for the following 2 hours. Cells were lysed using 300 μL 1 % NP40 in PBS for 20-30 minutes, diluted to concentration of 1:100 or 1:1000 in LB and then 100 μL plated on duplicate plates directly onto the agar, and incubated overnight. Intracellular bacterial survival was assayed by mean CFU counted from 2 plates.

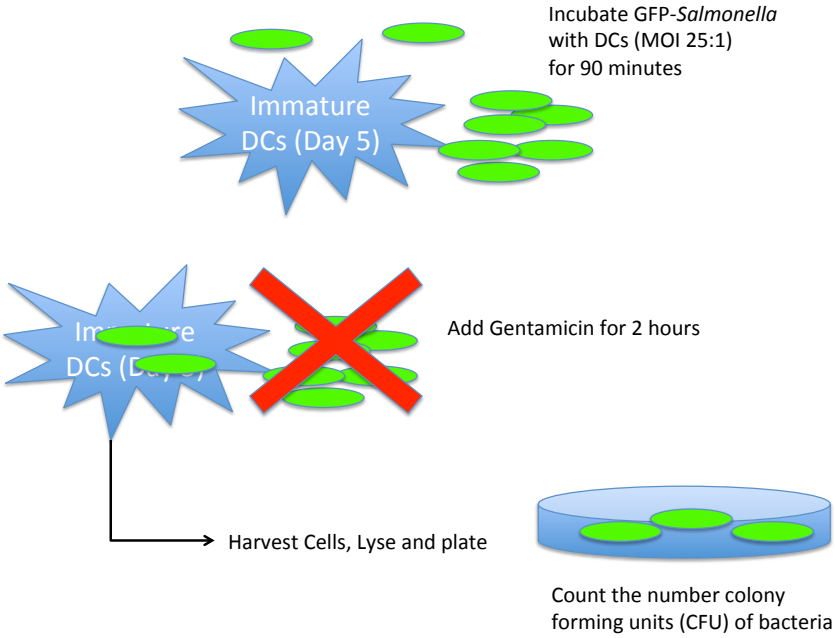


Figure 6: Cartoon of Bacterial Killing Assay. Immature DCs were incubated with GFP-Salmonella (MOI 25:1) for 90 minutes and then gentamicin was added at 50 μg ml-1 for a further 120 minutes before cells were harvested and lysed with 300 μL of 1 % NP40, plated and grown before counting CFU.

2.2.7. Confocal microscopy

To prepare the confocal slides, 200 μL of poly-L/D-lysine at a concentration of 10 μg

mL^{-1} (Sigma) was placed in the floor of each well for 10 minutes at room temperature (RT). This was aspirated off and replaced by 500 μL of 70-100 % ethanol and the slides were tilted to coat each wall in its entirety. After 2 minutes the ethanol was aspirated off and the wells allowed to air dry. Prior to stimulation, cells were harvested and divided into the 8 wells and allowed to rest for 30-120 minutes.

Following stimulation, cells were washed 3 x in warm PBS, fixed by incubation for 10 minutes at RT in 4 % (wt/vol) paraformaldehyde, washed in PBS 3 x, permeabilised with 0.1 % (vol/vol) Triton X-100 over 7 minutes and then washed 3 x with 1 % PBA (PBS containing 1 % (wt/vol) BSA (Sigma)). Cells were stained with primary antibody overnight at 4 °C or 1 hour at RT. Cells were washed 3 x with 1 % PBA, and stained with secondary antibody (AlexaFluor secondary antibodies, Invitrogen) for 1 hour at RT, avoiding exposure to light. Where nuclear staining with To-Pro (Invitrogen) was used, cells were washed 3 x with PBA after incubation with the secondary antibody, and To-Pro-3 nuclear stain added for 10 minutes at 0.05 % (vol/vol) in 1 % PBA at RT, maintaining avoidance of exposure to light. After staining, cells were washed extensively in 1 % PBA, then finally in PBS. The well walls were prised off the slides, which were then air dried in the dark and coverslips mounted using a DAPI-containing Vectashield (Vector Laboratories). A Radiance 2000 laser-scanning confocal microscope was used for confocal microscopy, followed by analysis with LaserSharp 2000 software (Bio-Rad). All images were acquired in sequential scanning mode.

2.2.8. Flow cytometry

Cells were harvested and washed twice in ice-cold PBS. The cells, as indicated in the text for number of cells per condition, were stained with live/dead stain in PBS (see 2.2.8.1) and then washed in ice-cold PBA. The supernatant was discarded, cells were resuspended by vortexing, and stained for (typically) 30 mins on ice with the appropriate antibody. Cells were then washed with 1 mL ice-cold PBA, and resuspended in 100 μL of PBS + 1 % paraformaldehyde. Samples were stored in the dark at 4 °C until analysed using a Cyan (Beckton Dickinson) or LSRII (BD Biosciences) flow cytometer. Data was analysed using FlowJo.

2.2.8.1. Live-Dead staining

Knowing which cellular population was alive required use of either Live-Dead stain (violet channel, Invitrogen), which had the advantage that it was fixable. However, using the live-dead stain (APC-Cy7, Invitrogen) required staining to occur in PBS.

2.2.8.2. PhosFlow (BD Biosciences)

PhosFlow staining required prestaining cells with a marker such as CD11c or HLA-DR and Live-Dead stain for 30 minutes on ice. Cells were washed and allowed to rest for no more than 15 minutes prior to stimulation. Immediately after stimulation, cells were fixed by applying an equal volume of Cytofix (BD Biosciences) and incubated for 15 minutes at 37 °C. Cells were washed in 0.1 % PBA then permeabilised using Permeabilisation Buffer IV (BD Biosciences) for 30 minutes at RT avoiding exposure to light. Cells were washed again in 0.1 % PBA and then stained for intracellular phospho-proteins for 45-60 minutes at RT avoiding exposure to light. Cells were washed once more in 0.1 % PBA and then resuspended in PBS before immediately analysing on a flow cytometer.

2.2.9. Dendritic cell transfection

Nuclear transfections were performed with Amaxa primary cell DC transfection reagent (Lonza) using an Amaxa nucleofector (Lonza), according to the manufacturer's instructions. 3 million immature DCs were resuspended in 100 μL of transfection reagent, mixed with 2.5 μL of 20 μM or 5 μL of 10 μM siRNA in a nucleofection cuvette and electroporated with program U-02. Cells were immediately transferred to culture dishes containing 3 mL warm R10, and incubated for 24 hours prior to use in experiments. All siRNAs were obtained from Qiagen or Dharmicon, and are shown in Table 2.

Protein	siRNA Code	Company	Catalogue Number	Target Sequence	Sense strand	Anti-sense strand
Non-Sense	AllStars Negatice Control	Qiagen	1027280	Proprietary		
DAPK1	Hs_DAPK1_5	Qiagen	S102223774	AAGCATGTAATGTTAATGTTA		
DAPK1	Hs_DAPK1_9	Qiagen	S103061471	CACGTCGATACCTTGAAATTT		
HMGB1	Hs_HMGB1_4	Qiagen	S102627842	5'-TCCTTTCATATAGTTAGCTAA-3'	5'-CUUUCAUAUAGUUAGCUAATT-3'	4'UUAGCUAACUAUAUGAAAGGA-3'
LCP1	Hs_LCP1_8	Qiagen	S104750333	5'-CAGAGTAAACAAACCGCCATA-3'	5'-GAGU8AAACAAACCGCCAUATT-3'	5'UAUGGCGGUUUGUUUACUCTG-3'
NOD2	Hs_CARD15_4	Qiagen	S100133056	5'CAACATGGCCGTGAACTTTAT-3'	5'ACAUGGCCGUGAACUUUAUTT-3'	5'-AUAAAGUUCACGGCCAUGUTG-3'
SHP1	Hs_PTPN6_5	Qiagen	S102658726			

Protein	siRNA Code	Company	Catalogue Number	Target Sequences
DAPK1	DAPK1 smartpool (1612)	Dharmicon	L-004417-00-0005	AUACUACAGUUGCUCAUUA
				AUACGAAGCCAGAUUGUUU
				GUUUGUCGCUCCUGAGAUA
				GAAUGGAGUUGGCGAUUUC

Table 2: siRNAs used. Top panel Qiagen siRNA, bottom panel Dharmicon siRNA.

2.2.10. Small molecule inhibitors

CP-380956 and E64d (Sigma) were diluted to 10 or 20 mg mL^{-1} (respectively) in sterile dimethyl sulphoxide (DMSO). They were stored as recommended by the manufacturer and used at either the concentration found by doing an inhibitory curve or at 10 μg mL^{-1}. Pepstatin A (Enzo Lifesciences) was diluted in 100 % alcohol to 20 mg mL^{-1} and used at 10 μg mL^{-1}.

2.3. **Deoxyribose Nucleic Acid (DNA) and Ribose Nucleic Acid (RNA) methods**

2.3.1. Isolating DNA from buffy coats and whole blood samples

Isolation of DNA by isopropanol precipitation using the FlexiGene DNA purification kit (Qiagen) was performed on buffy coat and whole blood samples; 1-2 mL of sample material was used. For 1 mL buffy coat was washed in buffer FG1, cells lysed using 1 mL protease-supplemented (10 μL) buffer FG2 at 65 °C for 10 minutes, and DNA precipitated with 2 mL isopropranol. The resulting pellet was washed in 70 % ethanol and resuspended in 400 μL buffer FG3 at 65 °C for 1 hour. DNA samples were stored at -80 °C until required.

2.3.2. Quantifying DNA and ensuring quality

Ultraviolet Light (UV) spectrophotometry (NanoDrop ND-1000 spectrophotometer, ThermoScientific) was used to assay DNA concentration, requiring 1.5 μL of sample. Sample purity was confirmed using the 260 nm/ 280 nm absorbance ratio.

2.3.3. Genotyping of CD-associated polymorphisms

Regions flanking the three major Crohn's-associated NOD2 mutations (FS1007insC, G908R and R702W) were amplified using PCR primers as shown in Table 3. Polymerase Chain Reaction (PCR) was performed using a PCR Taq core kit (Qiagen) that contained Taq DNA polymerase. This was done under the conditions described in Table 4 according to the manufacturer's instructions, but Magnesium Chloride was not added. The resulting PCR products were purified as described in 2.3.4. Sequencing of the PCR products was performed using the same primers described in

Table 3 at the WIMM core sequencing facility (University of Oxford) using an ABI sequencer. Genotypes were read manually from signal traces using 4Peaks software (by A. Griekspoor & Tom Groothuis, mekentosj.com), and examples are shown in Figure 7. For the work described in this thesis, all buffy coats used were homozygote wild type at the three major NOD2 mutations.

NOD2 SNP	5' primer	3' primer
RS2066844 (R702W)	5-GAA TTC CTT CAC ATC ACT TTC CAG T-3'	5'-GTC AAC TTG AGG TGC CCA ACA TT-3'
RS2066845 (G908R)	5'-CCC AGC TCC TCC CTC TTC-3'	5'-AAG TCT GTA ATG TAA AGC CAC-3'
RS2066847 (1007FSinsC)	5'-CTG AGC CTT TGT TGA TGA GC–3'	5'- TCT TCA ACC ACA TCC CCA TT–3'

Table 3: Primers for routine genotyping of buffy coat and donor samples

Component	Volume (µL)
Template DNA (200 ng/µL)	1
10x PCR buffer	2
10 mM dNTPs	0.5
Taq polymerase (5 U/µL)	0.2
Each primer (100 pM)	0.2
Nuclease-free water	15.9
Total reaction volume	20

Table 4: Components and quantities for genotyping PCR

Step	Temperature (Celcius)	Time (minutes)
Denaturation	95	5
35 cycles of:		
Denaturation	95	1
Annealing	62	1
Extension	72	1
Followed by:		
Final extension	72	10
Hold	4	

Table 5: Genotyping PCR cycle conditions

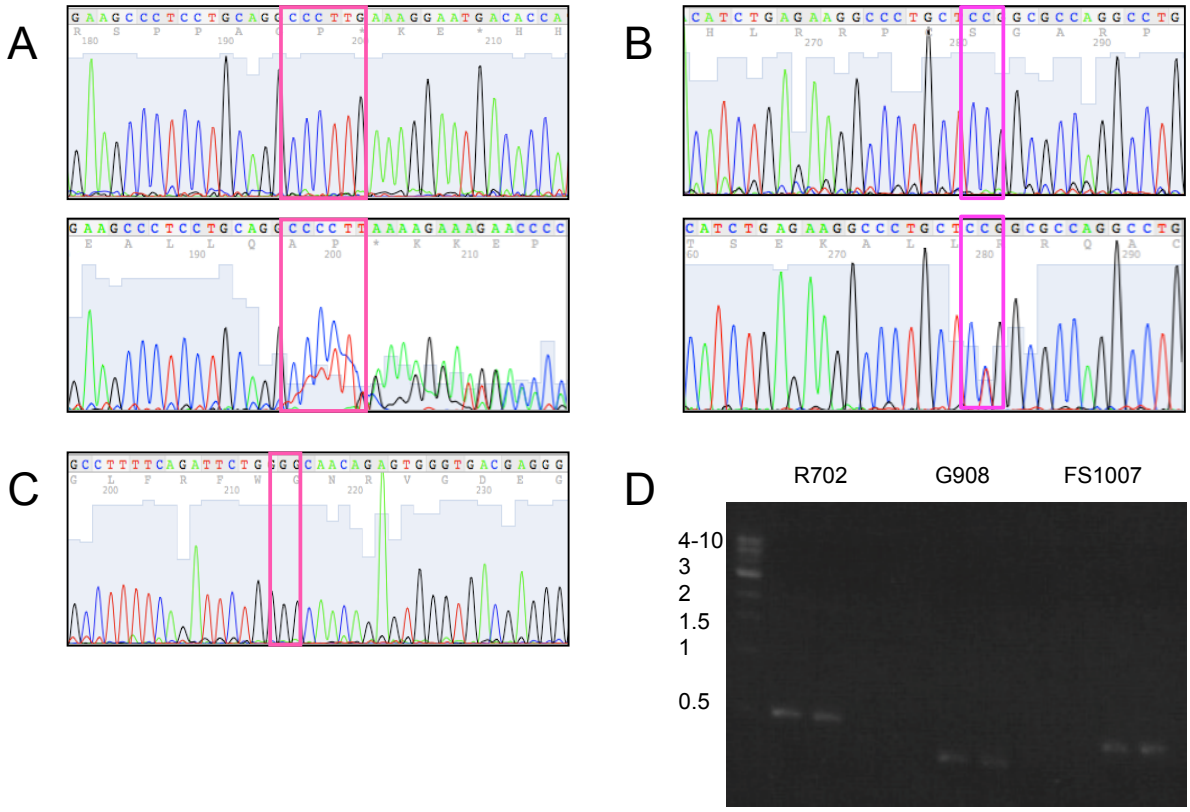


Figure 7: Analysis of the three common NOD2 polymorphisms associated with CD: regions of interest were amplified by PCR using primers for the 3 main genotyping SNPs, PCR products were purified, these underwent bi-directional sequencing, and finally analysis on 4Peaks software. A) Upper panel wild type (WT) NOD2 and lower panel heterozygous FS1007insC SNP with an extra C after the 3 Cs before the T. B) Upper panel demonstrates WT NOD2, but in R702W SNP there would be a T and in the lower panel heterozygote R702W is demonstrated. C) WT NOD2 has the highlighted G but the G908R SNP would have switched to a C. D) 0.01% Agarose gel showing the 3 different SNPs at ~0.5kBp

2.3.4. PCR product purification

PCR products for sequencing were purified using a QIAquick PCR purification kit (Qiagen) according to the manufacturer's instructions. Post-purification PCR product concentration was determined using UV spectrophotometry, and, periodically prior to sequencing, the presence of the expected product was checked by agarose gel electrophoresis, as described in 2.3.5.

2.3.5. Agarose gel electrophoresis

DNA samples were run on 50 mL volume 0.5 % agarose minigels containing 1.5 μL

Ethidium bromide/Gel Red (Biotium) in 1x TAE buffer at 50 V, and maximum current of 200 mA. DNA was observed using a UV transilluminator, and photographed using a digital camera.

2.3.6. RNA extraction

After stimulation, cell activation was stopped by ice-cold PBS; cells were harvested, and washed twice in ice-cold PBS. After washing, cells were lysed in buffer RLT (Qiagen) supplemented with β-Mercaptopurine (Sigma) using shear force by 15 bi-directional passes through a 21 G (green) needle. The RNA was extracted using an RNeasy Mini Kit (Qiagen), including shearing as above in buffer RLT, then wash in buffer RW1 followed by 2 wash steps of buffer RPE. RNA was eluted in 30 μL of RNAase-free water and concentration determined using UV spectrophotometry. Samples were stored at -20 °C until required for analysis by quantitative PCR, see section 2.3.7.

2.3.7. Reverse transcriptase quantitative PCR (qPCR)

The extraction of RNA from samples was through RNeasy mini kits (Qiagen) as before (see 2.3.6) and assayed by UV spectrophotometry. Up to 4 μg of RNA per sample was reverse transcribed with random hexamer primers and MultiScribe reverse transcriptase using a High Capacity RNA-to-cDNA kit (Applied Biosystems), following the manufacturer's standard protocols. Taqman primer pairs (Applied Biosystems) were obtained for the genes listed in Table 6, and were used in Real-Time PCR reactions using TaqMan Gene Expression Master Mix (Applied Biosystems). 45 ng of cDNA per sample was used in each experiment. Glyceraldehyde 3-phosphate dehydrogenase (GAPDH) was used as the internal

control for gene expression changes. Assays were run using a 7300 Real-Time PCR thermal cycler system (Applied Biosystems). In each experiment, fold changes were calculated using, as a marker of relative abundance, the change in cycle number (delta Ct) at which threshold fluorescence intensity was achieved for each test probe-set compared to the reference probe-set of GAPDH. This was calculated by subtracting test from GAPDH abundance, and mean difference calculated. The delta delta Ct was calculated by comparing delta Ct for each treatment to delta Ct for the control condition. The fold change was then calculated as 2 to the power of negative delta delta Ct.

Protein	Taqman Probe
GAPDH	Hs99999905_m1
DAPK1	Hs00234489_m1
LCP1	Hs00158701_m1
SHP-1	Hs00169359_m1
HMGB1	Hs01923466_g1
IL-1β	Hs01555410_m1

Table 6: Taqman RT PCR reagents

2.4. **Protein analysis and preparation for mass spectrometry**

2.4.1. Cell lysis

For standard immunoblotting and immunoprecipitation, cells were harvested, washed twice in ice-cold PBS, and then lysed for 30 minutes in NP-40 lysis buffer (1% Nonidet P40/ Igepal (Sigma), 450 mM NaCl, 50 mM Tris at pH 8.0, 5 mM EDTA) supplemented with protease inhibitors (1 mM NaF and Complete Mini protease inhibitors (Roche) 1 per 10 mL) and phosphatase inhibitor (either 1 mM activated Sodium Orthovanadate or phosphatase inhibitor cocktail 1 or cocktail 3 (Sigma) at 1:100 dilution).

For NOD2 and LC3/autophagosome immunoblotting described in the text, cells were harvested and washed as before, and lysed for 90 minutes in 2 % Triton X-114 supplemented with Roche Complete Mini protease inhibitors (Roche), 1 mM NaF and 1 mM activated Sodium Orthovanadate.

For phosphoprotein immunoblotting experiments described in the text, cells were harvested and washed in HBS rather than PBS to prevent dephosphorylation of phosphoproteins. Lysis was performed at 4 °C for 60 minutes using Qiagen Phosphoprotein lysis buffer (Phosphoprotein purification kit, Qiagen) supplemented with Phosphatase inhibitor cocktail 1 or 3 (Sigma), protease inhibitor (supplied by Qiagen or EDTA-free Complete mini protease inhibitor (Roche)), nuclease inhibitor (0.002 % Benzonase, Qiagen) and 0.25 % CHAPS.

In all experiments, cellular debris was removed from the lysates by centrifugation at

15.7 g (13000 rpm) in a bench-top centrifuge for 30 minutes at 4 °C. Where required protein concentrations of lysates were assayed and equalised using a Bradford assay (BioRad) according to the manufacturer's instructions.

2.4.2. Protein separation by electrophoresis

Protein samples, and concentration adjusted as necessary, were mixed 3:1 with 4x NuPAGE lithium dodecyl sulfate (LDS) elecrophoresis sample buffer (Invitrogen), and then heated to >90 °C for 5 minutes. Samples were returned to ice and pulse centrifuged prior to loading onto pre-cast NuPAGE 4-12 % or 10 % Bis-Tris gels (Invitrogen). Gels were run using NuPAGE MOPS or NuPAGE MES sample buffer (Invitrogen) in NuPAGE gel tanks (Invitrogen). Gels were run at 200V until the gel front reached the bottom of the gel.

2.4.3. Immunoblotting or western blotting

Proteins were separated as above (2.4.2) in NuPAGE gels. To identify separated proteins/ peptides, the proteins were transferred from the gels to Hybond nitrocellulose membranes (Amersham bioscieces) using a semi-dry transfer unit (Hoeffer) and NuPAGE Transfer Buffer (Invitrogen). Non-specific binding of antibodies was prevented by blocking membranes with either 5 % non-fat milk powder (wt/vol) or 5 % BSA (wt/vol) dissolved in either PBS (most antibodies) or in Tris Buffered Saline (TBS) (Phosphoantibodies, and most Cell Signal Technology antibodies), with 0.1 % Tween. Blocking was performed for either 1 hour at RT or overnight at 4 °C in a 50 mL falcon tube with gentle rotation. Blocked membranes were then washed at least three times with PBS/ 0.1 % Tween (majority of antibodies) or TBS/ 0.1 % Tween (phosphoantibodies and Cell Signal Technology

antibodies) prior to incubation with primary antibodies. Primary antibodies were incubated in either PBS/0.1 % Tween/ 5 % non-fat milk powder or TBS/0.1 % Tween/ 5 % BSA for 1 hour at RT, or overnight at 4 °C. Unless the primary antibody was directly conjugated, the membrane was then extensively washed 3-6 times with PBS or TBS/Tween, and incubated with an appropriate horseradish peroxidase (HRP)-conjugated secondary antibody. The membrane was finally washed a further three times, and then visualised with enhanced chemilluminescence (ECL) reagents (Amersham) and film (Amersham), according to the manufacturer's instructions.

2.4.4. Native protein assessment

NuPAGE gels were stained for protein or peptide using a silver staining kit (Silverquest, Invitrogen or Silver stain for mass spectrometry, Pierce). In all instances kits were used according to the manufacturer's standard protocols. Gels were visualised using either visible light (silver staining) or Imagequant (GE Healthcare).

2.4.5. Phosphoprotein purification

Cells were harvested, washed repeatedly in HBS supplemented with 0.1 % phosphatase inhibitor cocktail 1 or 3 (Sigma) at 4 °C, and lysed as described above in 2.4.1 and as follows. To enable binding of phosphoproteins to the column resin the concentration of the lysates were normalised to 0.1 mg mL^{-1}, using phosphoprotein lysis buffer (Qiagen) with CHAPS 25 µl mL^{-1}. Phosphoproteins were purified from lysates using a Phosphoprotein Purification Kit (Qiagen). The kit was used according to the manufacturer's protocols, except for the following modifications: 1 protease inhibitor tablet was used per 5 mL not per 7 mL; if

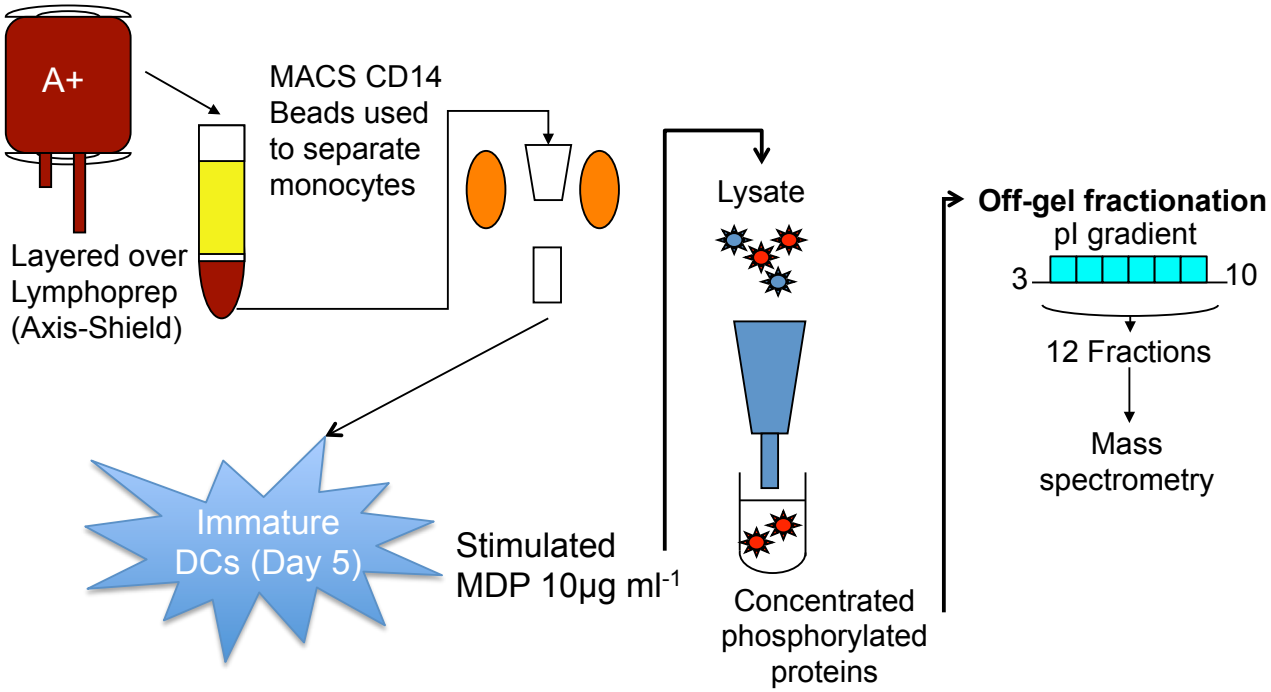


Figure 8: Cartoon of Phosphoprotein protocol: Monocyte derived DCs harvested and stimulated in R10 with MDP 10 µg ml^{-1} or RPMI, lysed using phosphoprotein lysis buffer (Qiagen) and phosphorylated proteins extracted and concentrated. Proteins separated using Off-gel fractionation before analysis by mass spectrometry.

protease inhibitor tablets were unavailable Complete Mini EDTA-free protease inhibitor tablets (Roche) were used on the recommendation of Qiagen; lysis was extended from 30 minutes to 40 minutes and the lysis buffer was supplemented with Phosphatase inhibitor cocktail 1 or 3 (Sigma); the centrifugation of the lysate occurred in 7 x 1.5 mL eppindorfs and supernatants combined before protein concentration was determined by Bradford Assay (BioRad); finally, 2 mL of phosphoprotein eluate was collected, rather than 500 µL suggested in the protocol. To speed sample preparation and reduce sample loss, the eluate was concentrated using higher volume iCon ultrafiltration concentrators (Pierce) rather than 500 µl colunns provided in the kit. Cell lysates, both concentrated and diluted, column flow-through, and phosphoprotein eluates were retained for immnoblotting and native protein staining as described above (2.4.3 and 2.4.4). Electrophoresis of

aliquots was undertaken, while the remainder of the eluate sample was stored at -80 °C until sufficient samples were accumulated for LC MS/MS analysis.

2.4.6. Protein desalting using methanol chloroform precipitation and other methods

Desalting, removal of detergents or concentrating proteins was done by methanol-chloroform precipitation as per Kessler laboratory protocol: 600 μL of methanol and 150 μL of chloroform were added to 200 μL of protein solution, and vortexed. 450 μL of ultrapure water was then added, and the mixture vortexed, and centrifuged at 15.7 g (13000 rpm) in a microfuge for 2 minutes at RT. The upper aqueous solution was then removed without disrupting the precipitate at the interface. 450 μL of methanol was then added, the mixture vortexed, and centrifuged at 15.7 g (13000 rpm) in a microfuge for 2-30 minutes, at RT. The supernatant was then removed from the precipitated proteins.

In phosphoproteomic experiments, sample loss at the resuspension stage of precipitated protein pellets was prevented and handling of large numbers of samples improved by using small and large volume Zeba desalting columns (Thermo Scientific/Pierce), which were used according to the manufacturer's standard protocols, as an alternative to methanol-chloroform precipitation.

2.4.7. Tandem Mass Tagging (TMT) Labelling

Protein samples from phospho-enrichment were concentrated to 40 μL, with a protein level of >2 mg mL^{-1} and a total protein amount of 100 μg. 45 μL of 200 mM TEAB was added and made up to 100 μL with ultrapure water. 5 μL of 200 mM TCEP

was added and mixed before incubation for 1 hour at 55 °C. 5 µL of 375 mM iodoacetamide was added and incubated out of light for 30 minutes. The samples were desalted using methanol/chloroform protein precipitation described (2.4.6). The protein precipitate was resuspended in 100 µL of 200 mM TEAB and 2.5 µg of trypsin per 100 µg of protein was added, and allowed to digest at 37 °C overnight. 41 µL of TMT label reagent was added per 100 µg of protein and incubated for 1 hour at RT. 8 µL of 5 % hydroxylamine was added for 15 minutes at RT to quench. Samples were combined in a 1:1 ratio, and a small aliquot was run on mass spectrometer to confirm labelling efficiency. Once labelling was confirmed as >99 %, samples were desalted using Sepak C18 columns (see 2.4.8). Samples were subject to OFFGEL fractionation as described earlier and each fraction was desalted again on Sepak C18 columns before storing at -20 °C until a mass spectrometry analysis was performed.

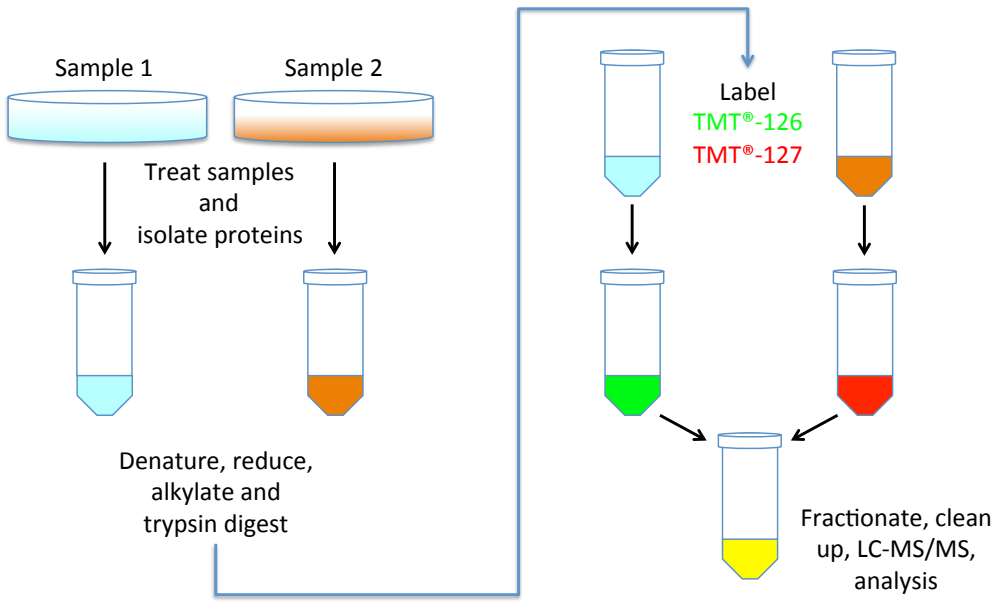


Figure 9: Tandem Mass Tagging methodology (adapted from Pierce's TMT reagents page, www.piercenet.com). Samples were obtained, denatured, reduced, alkylated and trypsinised before labelling with differentially weighted label. Samples were combined, fractionated and then analysed using LC-MS/MS.

2.4.8. Sep-Pak purification

Sep-Pak plus C18 cartridges (Waters WAT020515) were used to prepare trypsin-digested peptide samples for analysis by mass spectrometry. To enable the unfolding of C18 peptides the column was first primed by flushing with 5 mL of Buffer B (80% acetonitrile, 20% ultrapure water, 0.1% Formic acid), and washed with 2x 5 mL aliquots of Buffer A (98% ultrapure water, 2% acetonitrile, 0.1% Formic acid) using a vacuum manifold. The peptide digest sample was then passed through the column in 10 mL of Buffer A, and the column washed with a further 2 x 5 mL of Buffer A. The sample was then eluted from the column with 2 x 0.6 mL of Buffer B, and dried down completely in a vacuum centrifuge. The dried sample was then resuspended in 20 μL of Buffer A for OFFGEL fractionation or Buffer B for mass spectrometry analysis.

2.4.9. OFFGEL isoelectric protein and peptide separation

Protein samples were desalted, either by methanol chloroform precipitation or using resin-based Zeba desalting columns as described above (2.4.6). After TMT labelling, peptides were desalted using Sepak C-18 columns (see 2.4.8). Desalted protein or peptide solutions were diluted in relevant 1.25X stock solutions (see 2.5.1) then subjected to liquid iso-electric focusing, over a pH 3-10 range in a low-resolution 12-well system, using an Agilent 3100 OFFGEL fractionator (Agilent). The fractionation was continued until complete (typically 24-36 hours) at RT, after which the liquid fractions were harvested, and each fraction desalted using either methods described above (see 2.4.6). Desalted fractions were then taken either for electrophoresis and blotting/native protein staining (see 2.4.3 and 2.4.4) or for mass spectrometry analysis (see 2.4.10).

2.4.10. Mass spectrometry

Purified peptide samples generated as described above (2.4.7) were separated for 60 minutes with a nano-liquid chromatography system (Ultimate Plus; LC packings) on a reverse phase C18 column (10 cm length, 75 μm internal diameter, Dionex; LC packings) on a gradient of 0-55 % Buffer B, coupled to a high capacity ion-trap mass spectrometer (MS/MS HCT plus, Brucker Daltonics) [436]. MS data was analysed using the MASCOT programme, which was designed through a collaboration between Dr Benedikt Kessler (Core Proteomics Facility, University of Oxford), the Computational Biology Research Group (University of Oxford), and the SwissProt proteomics database.

2.4.11. Enzyme-linked Immunosorbent Assays (ELISAs) and Cytometric bead assays

After cells were cultured with appropriate stimulation conditions, supernatants were harvested and cleared of cellular debris by centrifugation, and frozen in aliquots at -80 °C until required for analysis. Human IL-1β, IL-8, IL-10, IL-12p40, IL-17, and IL-23 Enzyme-linked Immunosorbent Assays (ELISA) Duoset kits (R&D Systems), IL-18 (MBL International Corporation) and HMGB1 ELISA (Shino-Test Corporation) were obtained. Maxisorp flat-bottomed 96-well plates (Nunc) were coated with capture antibody, and the ELISA performed according to the manufacturer's instructions. Each sample was assayed in duplicate, and where necessary at a range of dilutions. Standard curves using 7- to 9-point serial dilutions were prepared freshly for each plate, using the internal standards provided with the assay kits. Developed ELISA plates were read using a Microplate 680 reader (BioRad) or FLUOStar Optima (BMG Labtech) with dual wavelength correction.

Protein	Species	Company	Clone	Product ID	Concentration used	
					Immunoblotting	Confocal
Alix	Mouse	Santa Cruz Biotechnology	1A12	sc-53540	1:200	
APG7	Rabbit	Abcam	EP1759Y	ab52472	1:100000	
β-Actin	Mouse	Sigma-Aldrich	AC-15	A1978	1:2500	
β-Arrestin 1/2	Rabbit	Cell Signaling Technology	D24H9	4674	1:1000	
Caspase 1	Rabbit	Cell Signaling Technology	D7F10	3866	1:1000	
CD63	Mouse	Abcam	CLB-180	ab23792		
CD74	Mouse	Abcam	LN2	ab9514		
CIASI/NALP3	Mouse	Abcam	nalpy3-4	ab17267		
Cofilin	Rabbit	Cell Signaling Technology	D3F9	5175	1:1000	
Cryopyrin	Rabbit	Santa Cruz Biotechnology	H-66	sc-66846		
DAPK1	Rabbit	Assay Biotech		B0898		1:100
DAPK1	Rabbit	Cell Signaling Technology		3008	1:1000	
DC-SIGN	Rabbit	Santa Cruz Biotechnology	H-200	sc-20081	1:200	
EEA1	Mouse	BD Transduction Laboratories	14/EEA1	610457		
EEA1	Rabbit	Cell Signaling Technology	C45B10	3288	1:1000	
Ezrin	Rabbit	Cell Signaling Technology		3145	1:1000	
GDI1	Mouse	Sigma-Aldrich	1H3	WH0002664M8	1:333	
GNB2L1	Rabbit	Lifespan Biosciences		LS-C99963	1:200	
HCLS1	Mouse	Abnova	2A8	H00003059-M05	1:200	
HLA-C	Mouse	Santa Cruz Biotechnology	D-9	sc-166057		
HLA-DM	Mouse	Abcam	TAL 18.1	ab20170		
HLA-DM	Mouse	BD Pharmingen	MaP.DM1	555982		
HMGB1	Rabbit	Cell Signaling Technology		3935		
HNP	Goat	Santa Cruz Biotechnology		sc-22916		
HS1	Rabbit	Cell Signaling Technology	D83A8	3890	1:1000	
HSPB1/HSP27	Mouse	Cell Signaling Technology	G31	2402	1:1000	
HSP70	Rabbit	Cell Signaling Technology	D69	4876	1:1000	
IGFIRB	Rabbit	Cell Signaling Technology	111A9	3018	1:1000	
IKKα	Rabbit	Cell Signaling Technology		2682	1:1000	
IL-1β	Rabbit	Cell Signaling Technology		2022	1:1000	
IL-1β	Mouse	R&D Systems	8516	MAB201	1:250	
IL-1β (Cleaved Asp116)	Rabbit	Cell Signaling Technology		2021	1:1000	
LAMP1	Mouse	Santa Cruz Biotechnology	H4A3	sc-20011		1:100
LC3B	Rabbit	Cell Signaling Technology	D11 XP	3868		1:100
LCP1	Rabbit	Cell Signaling Technology		5350	1:1000	
LRRFIP1	Mouse	Sigma-Aldrich	2D3	WH0009208M2	1:333	
LRRFIP2	Mouse	Abnova	B01P	H00009209-B01P	1:1000	
Lysine 48-Linkage Specific Polyubiquitin	Rabbit	Cell Signaling Technology		4289	1:1000	
MEK1/2	Mouse	Cell Signaling Technology	L38C12	4694	1:1000	
MRP8	Rabbit	Abcam	EPR3554	ab92331	1:2000	
NALP1	Mouse	Santa Cruz Biotechnology	6D598	sc-71641		
NF-κB p65	Rabbit	Cell Signaling Technology	C22B4	4764	1:1000	
NOD2	Mouse	Abcam	2D9	ab31488		
NOD2	Goat	Santa Cruz Biotechnology	P-18	sc-23587		
NOD2	Mouse	Santa Cruz Biotechnology	2D9	sc-56168		
NOD2	Rabbit	Santa Cruz Biotechnology	H-300	sc-30199		
p38 MAPK	Rabbit	Cell Signaling Technology		9212	1:1000	
Phospho-β-Arrestin 1 (Ser412)	Mouse	Cell Signaling Technology	6-24	2416	1:1000	
Phospho-Cofilin (Ser3)	Rabbit	Cell Signaling Technology	77G2	3313	1:1000	
Phospho-HS1 (Tyr397)	Rabbit	Cell Signaling Technology		4507	1:1000	
Phospho-IKKα (Ser176)/IKKβ (Ser177)	Rabbit	Cell Signaling Technology	C84E11	2078	1:1000	
Phospho-LCP1 (Tyr28)	Rabbit	Cell Signaling Technology		5277	1:1000	
Phospho-MLC2	Rabbit	Cell Signaling Technology	519	3671	1:1000	
Phospho-NF-κB p65 (Ser276)	Rabbit	Cell Signaling Technology		3037	1:1000	
Phospho-p38 MAPK (thr180/Tyr182)	Rabbit	Cell Signaling Technology	3D7	9215	1:1000	
Phospho-p44/42 MAPK (Thr202/Tyr204)	Rabbit	Cell Signaling Technology		9101	1:1000	
Phospho-VASP (Ser157)	Rabbit	Cell Signaling Technology		3111	1:1000	
Phospho-VASP (Ser239)	Rabbit	Cell Signaling Technology		3114	1:1000	
Phospho-Vimentin (Ser56)	Rabbit	Cell Signaling Technology		3877	1:1000	
Phospho-YB1 (Ser102)	Rabbit	Cell Signaling Technology	C34A2	2900	1:1000	
Plastin L	Mouse	Abcam	LPL4A.1	ab80729		1:200
Radixin	Rabbit	Cell Signaling Technology	C4G7	2636	1:1000	
RIP2	Rabbit	Cell Signaling Technology		4982	1:1000	
S100-A9	Mouse	AbD Serotec	1C10	MCA3438Z	1:200	
SAMHD1	Mouse	Sigma-Aldrich		SAB1400478	1:125	
SGTA	Rabbit	Cell Signaling Technology		3349	1:1000	
SH3BP1	Goat	Lifespan Biosciences		LS-C55462/20020	1:250	
SHP-1	Rabbit	Cell Signaling Technology	C14H6	3759	1:1000	
SQSTM1/p62	Rabbit	Cell Signaling Technology	D5E2	8025	1:1000	
Talin1	Mouse	Abcam		ab57758	1:250	
TEBP	Mouse	Abnova	3H1-2AB	H00010728-M01		
TGN46	Sheep	AbD Serotec		AHP500	1:1000	
TNPO3	Rabbit	Abcam		ab65016		
TREX-1	Mouse	Sigma-Aldrich	2F10	WH0011277M1	1:1000	
Ubiquitin	Mouse	Cell Signaling Technology	P4D1	3936	1:1000	1:25
Ubiquitinylated proteins	Mouse	Millipore	FK1	04-262	1:1000	
Ubiquitinylated proteins	Mouse	Millipore	FK2	04-263	1:1000	
VASP	Rabbit	Cell Signaling Technology	9A2	3132	1:1000	
Vimentin	Rabbit	Cell Signaling Technology	R28	3932	1:1000	

Table 7: Primary antibodies used

A 17-plex human cytometric (Luminex) bead immuno-assay was performed using a 17-plex human cytokine kit (Bio-Rad), according to the manufacturer's instructions. Data were extracted using a Bio-Plex 200 reader.

					Concentration used	
Fluorochrome/HRP	**Host species**	**Target Species**	**Company**	**Product ID**	**Immunoblotting**	**Confocal**
HRP	Goat	Mouse	Cell Signaling Technology	7076	1:2500	
HRP	Goat	Rabbit	Cell Signaling Technology	7074	1:5000	
HRP	Goat	Rabbit	Sigma-Aldrich	A9169	1:2500	
HRP	Rabbit	Mouse	Sigma-Aldrich	A9044	1:2500	
HRP	Rabbit	Rat	Sigma-Aldrich	A5795	1:2500	
HRP	Donkey	Sheep	Sigma-Aldrich	A3415	1:2500	
AlexaFluor488	Goat	Mouse	Invitrogen	A11001		1:100
AlexaFluor488	Goat	Rabbit	Invitrogen	A11034		1:100
AlexaFluor568	Goat	Mouse	Invitrogen			1:100
AlexaFluor568	Goat	Rabbit	Invitrogen	A11036		1:100

Table 8: Secondary antibodies used

Protein	**Conjugate**	**Company**	**Clone**	**Product ID**
CCR5	PeCy5	BD Pharmingen	2D7/CCR5	561750
CCR7	APC	Ebiosciences	3D12	17-1979-42
CD11b	FITC	Ebiosciences	ICRF44	11-0118-41
CD11b activated		Biolegend	CBRM1/5	301409
CD11c	PeCy7	Ebiosciences	3.9	25-0116-42
CD11c	PerCP/Cy5.5	Biolegend	3.9	301624
CD18	APC	Biolegend	TS1/18	302124
CD29	PE	Biolegend	TS2/16	303004
CD51/aV	PE	Biolegend		327910
CD80	PE	Ebiosciences	2D10.4	12-0809-42
CD80	FITC	Ebiosciences	2D10	11-0809-73
CD86	FITC	BD Pharmingen		555657
CD86	PeCy5	Ebiosciences	IT2.2	15-0869-73
CD163	PE	BD Pharmingen	GHI/61	556018
CD206	APC	BD Pharmingen	19.2	550889
CLIP	FITC	BD Pharmingen		555981
HLA-DR	eFluor450	Ebiosciences	L243	48-9952-42
IgG1	FITC	Ebiosciences	P3	11-4714-82
IgG1	APC	Ebiosciences	P3.6.2.8.1	17-4714-82
IgG1	FITC	BD Pharmingen		349041

Table 9: Flow Cytometry antibodies used

2.5. **Materials, Solutions and Chemicals used**

All chemicals are from Sigma unless otherwise stated.

2.5.1. Nucleic Acid analysis

2.5.1.1. Tris Borate EDTA (TBE)

Stored as a 5X stock solution in 1000 mL of ultrapure water: 54 g Tris Base, 27.5 g Boric Acid, 10 mL 0.5 M EDTA (pH 8.0).

2.5.1.2. Agarose gel

0.5 g Agarose added to 50 mL 1X TBE and boiled in a microwave before adding 2.5 μL Ethidium bromide or 2.5 μL Gel Red (Biotium)

2.5.1.3. Gel Red (Biotium)

Used at 2.5 μL 50 mL^{-1}

2.5.2. Lysis Buffers and Solutions

2.5.2.1. NP40

1 % Nonidet P40/ Igepal, 450 mM NaCl, 50 mM Tris at pH 8.0, 5 mM EDTA

2.5.2.2. Triton X114

2 % Triton X-114 supplemented with Roche Complete Mini protease inhibitors (Roche), 1 mM NaF and 1 mM activated Sodium Orthovanadate

2.5.2.3. Sodium Fluoride (NaF)

200 mM concentration stored at RT, then used at 1 mM

2.5.2.4. Activated Sodium Orthovanadoate

Diluted to 200 mM water pH 10.0, then used at 1 mM

2.5.2.5. EDTA

0.5 M EDTA pH 8.0, stored at RT

2.5.3. Immunoblotting

2.5.3.1. TBS Tween

Tris Buffered Saline (10 mM Tris pH 7.4, 150 mM NaCl, 0.75 % Tween 20 in 1 L ultrapure water). PBS Tween is made by dissolving 1 PBS tablet (Sigma) in 100 mL ultrapure water and adding 0.75 % Tween 20.

2.5.3.2. Blocking Buffer

TBS Tween or PBS Tween supplemented with skimmed milk powder 5 % (wt/vol, Marvel) or 5 % BSA (wt/vol).

2.5.3.3. Precast SDS-PAGE Gels (Invitrogen)

4-12 % 1.5 mm 10 well or 10 % 1.0 mm 12 well

2.5.3.4. Other products used

MOPS Buffer, MES Buffer, Transfer Buffer, 4x Loading Buffer (all from Invitrogen) and ECL Developing Reagents and Full Range Rainbow Marker (both from Amersham).

2.5.4. Tissue Culture

2.5.4.1. R10

RPMI-1640 supplemented with Fetal Calf Serum (FCS) 10 % (vol/vol), glutamine 1 % (vol/vol), Penicillin/ Streptomycin 1 % (vol/vol).

2.5.4.2. Macrophage R1

RPMI-1640 supplemented with 1 % autologous serum (heat inactivated at 54 °C for 30 minutes then centrifuged 3273 g (3750 rpm) for 30 minutes and sterile filtered.

2.5.4.3. MACS Buffer

Sterile Dulbecco's PBS supplemented with sterile filtered 5 % BSA (wt/vol) and 2

mM EDTA.

2.5.4.4. Leucocyte separation solution

Sodium Diatrizoate/Polysaccharide solution (Lymphoprep, Axis-Shield)

2.5.5. Microbiological media

2.5.5.1. Leuers Broth

10 g tryptone, 5 g yeast extract, 10 g NaCl at pH 7.0, make up to 1 L with ultrapure water and autoclaved before use.

2.5.5.2. LB Agar

LB supplemented with 15 g agar

2.5.5.3. Gentamicin

Aliquoted and stored at -20 °C, used at 50 μg mL^{-1}

2.5.6. Confocal and Flow Cytometry

2.5.6.1. PBA

Dulbecco's PBS supplemented to 0.5 % or 1 % with BSA (wt/vol)

2.5.6.2. ToPro (Invitrogen)

Stored in aliquots in dark at -20 °C, used diluted 0.05 % (vol/vol) in PBA

2.5.6.3. Pepstatin

20 mg mL^{-1} dissolved in 100% ethanol in a water bath at 60 °C for 45 minutes, used at working dilution of 10 μg mL^{-1}

2.5.6.4. E64d

20 mg mL^{-1} in DMSO, used at working dilution of 10 μg mL^{-1}

2.5.6.5. Lysotracker-Red (Invitrogen)

Stored at -20 °C, used at 0.2 % (vol/vol) and incubated with cells for 2 hours prior to

fixation and staining.

2.5.6.6. PFA

8 % paraformaldehyde was aliquoted and stored at -20 °C until required. It was then defrosted at 37 °C and vortexed to dissolve before diluting to working concentration of 4 % with 2X PBS.

2.5.6.7. Triton X-100

Used at 0.1 % (vol/vol) in PBS

2.5.6.8. Vectashield (Vector Laboratories)

2.5.7. OFFGEL Fractionation

Kit was purchased from Agilent and used according to manufacturer's instructions.

2.5.7.1. Protein OFFGEL Stock Solution (1.25X) (Agilent)

Made according to manufacturer's guidelines: contains Thiourea, DTT, Glycerol 6 mL, OFFGEL buffer 600 μL, ultrapure water to bring to 50 mL and warm at 37 °C to aid dissolving.

2.5.7.2. Peptide OFFGEL Stock Solution (1.25X) (Agilent)

Made according to manufacturer's guidelines: contains Glycerol 6 mL, OFFGEL buffer 600 μL, ultrapure water to bring to 50 mL.

2.5.8. Mass spectrometry

2.5.8.1. Buffer A

Acetonitrile 1 %, Formic acid 0.2 %, HPLC grade water 98.8 %

2.5.8.2. Buffer B

Acetonitrile 80 %, Formic acid 0.2 %, HPLC grade water 19.8 %

2.5.9. ELISA and cytometric bead assays (Luminex, BioRad)

IL-1β, IL-10, IL-12p40, IL-17 and IL-23 DuoSet ELISA (R&D Systems) were used according to manufacturer's instructions. IL-18 (MBL International Corporation) and HMGB1 (Shino-Test Corporation) was also used according to manufacturer's instructions. Luminex (BioRAD) was used according to manufacturer's instructions.

3. Dissecting the NOD2 and NOD2/TLR2 signalling cascade

3.1. Introduction

The molecular basis of NOD2 signalling remains poorly characterised, especially in cooperation with TLRs. Whilst NOD2 is known to activate and signal via RIPK2, MAPK and NF-κB, the mechanism by which it cross-talks with other PRRs, particularly TLR2 remains unclear. TLR2 recognises PAM, another component of peptidoglycan and it is unlikely either receptor could be activated in isolation in physiological circumstances. Wild-type NOD2 synergises with TLR2 to multiply differential regulation of a variety of mediators [309], but the mechanism by which this occurs is unclear. In addition the transcriptional control of NOD2 signalling remains poorly defined. I undertook a phospho-proteomics approach to define NOD2 signalling, alone and in cooperation with TLR2, to try and cast light on mechanisms involved in NOD2-mediated microbe recognition.

3.2. Results

3.2.1. Schema of approach

Previous work carried out in the laboratory included optimisation of a method to pull-down phosphorylated proteins to analyse the signalling cascades downstream of key immune regulators, such as NOD2. Traditional phospho-proteomic techniques involve affinity purification of phospho-proteins with either phospho-tyrosine, phospho-serine or phospho-threonine antibodies. An example of immunoprecipitation using this approach is shown in Figure 10A. Here DCs were stimulated with MDP, PAM or both ligands (MDP and PAM) and phosphorylated proteins enriched using anti-phospho-serine, -threonine and -tyrosine antibodies. However, this approach is notoriously non-specific, particularly for anti-phospho-serine and -threonine antibodies. To enable more specific enrichment of phosphorylated residues, a different methodological approach was required. I elected to use phospho-enrichment columns from Qiagen to enrich phosphoproteins from DC whole cellular lysate (WCL) left unstimulated or stimulated with MDP, PAM or MDP/PAM (Figure 10B). Known intermediates of NOD2/TLR2 signalling cascades, p38 MAPK and p44/42 MAPK, were immunoblotted in DCs stimulated with MDP for 30 minutes and the lysate, diluted lysate and concentrated phospho-column eluate. This approach demonstrated a clear increase in phosphorylation on stimulation (right panel Figure 10B). Loading controls were total p38 and p44/42 MAPK, total phosphotyrosine levels and β-actin. Figure 10B shows how this approach facilitates removal of ubiquitous housekeeping proteins, such as actin, and increases concentration of low-abundance phosphoproteins. The original

methodology was carried out in DCs held on ice for 30 minutes as the unstimulated control. However, I improved the comparison of stimulated and unstimulated samples by leaving unstimulated cells at 37 °C for 30 minutes, and signalling by NOD2 via p44/42 MAPK was further confirmed in DCs stimulated with MDP and compared to unstimulated cells, Figure 10C. Marked phosphorylation of p44/42 MAPK was demonstrated (lane 6 compared to lane 5) with loss of housekeeping proteins such as β-actin.

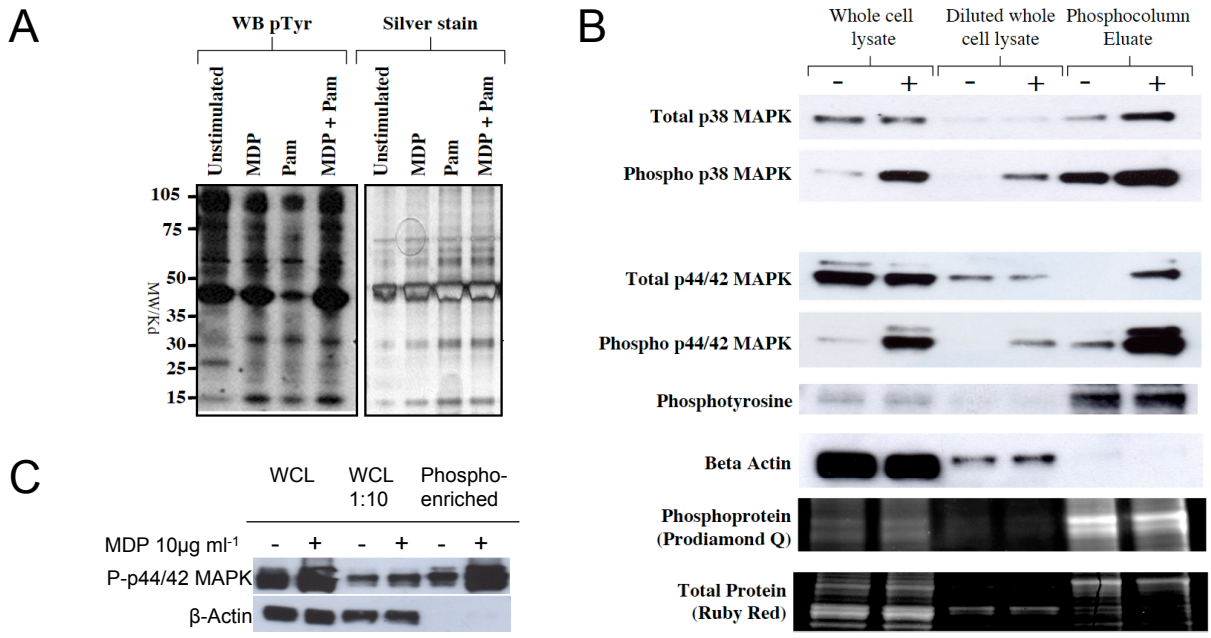


Figure 10: Demonstration of different methods of determining intermediates in the NOD2 signalling cascade. A) Left panel shows DCs left unstimulated or stimulated with MDP, PAM, MDP and PAM for 30 minutes, lysed and immunoblot for anti-phosphotyrosine. Right panel shows SDS-PAGE gel of lysates from left panel silver stained for total protein. B) Left panel shows DCs unstimulated or stimulated for 30 minutes with MDP, lysed and immunoblot for total and phosphorylated p38 MAPK or p44/42 MAPK, phosphotyrosine and βactin; or stained for phospho-proteins using Prodiamond Q or total protein using Ruby Red. Middle panel is lysate diluted to 0.1mg mL^{-1} and stained as above. Right panel is the concentrated eluate from the phospho-column stained as above. C) Confirmation of NOD2 signalling via p44/42 MAPK on MDP (10 µg mL^{-1}) stimulation of NOD2 for 30 minutes in DCs with unstimulated and stimulated in similar conditions.

3.2.2. Preparation of NOD2 stimulated samples for mass spectrometry

To undertake phosphoproteomic analysis by MS, Qiagen column purified phospho-eluates were obtained from DCs that had been stimulated with MDP or cells left unstimulated and prepared for MS. In depth description of preparation of samples for MS can be found in Chapter 2.4.10, but in essence, the eluate from a number of buffy coats were pooled, concentrated and desalted by ZeBa desalting columns. The samples were then subject to OFFGEL fractionation to separate the proteins according to their electrical charge or isoelectric point. The recovered 12 fractions were then desalted again and then denatured, reduced, alkylated and finally trypsin digested. The trypsin digested peptides were desalted on C18 columns, dried and resuspended in water before being loaded onto the mass spectrometer, liquid-chromatography mass spectrometry/mass spectrometry (LC-MS/MS) with both ion trap and quadruple-time of flight (Q-TOF) capabilities. A selection of MS data targets are listed in Appendix Table 1, and were placed in order of increasing MASCOT score. Putative targets from the MS data that might be either novel signalling intermediates or known to be involved in innate immunity, antigen presentation or autophagy were drawn into a list. The list of potential targets was filtered depending on known or similar functions, recent published activity or interesting targets.

3.2.3. Verification of some targets does not concur with mass spectrometry data

In order to confirm that proteins identified by the MS data were true mediators of NOD2 signalling, phospho-eluates were obtained from DCs left unstimulated or stimulated with MDP, and immunoblotted for putative targets, as seen in Figure 11. Table 10 gives details of MASCOT score, whether the protein was preferentially phosphorylated (P) or dephosphorylated (D) and the fraction that it was identified in, for example fraction 5 is denoted by "5". In addition, some proteins were identified in an ion trap MS and these are denoted by a "Yes" in the ion trap column.

β-arrestin1 (Table 10, row 1) showed no change in phosphorylation between unstimulated or stimulated in lanes 5-6 (Figure 11). MEK1/2 (Table 10, row 2) was barely visible in the diluted WCL lanes, lanes 3-4, and did not demonstrate any difference between unstimulated or stimulated in lanes 5-6 of Figure 11. Vasodilator-stimulated phosphoprotein (VASP) (Table 10, row 3) appeared to have more protein loaded in the diluted sample, lane 4 compared to lane 3, but no difference was seen on concentration of the eluate, lanes 5-6. S100A9 (Table 10, row 4) was not phosphorylated on stimulation of NOD2 by MDP as seen in lane 5-6. SH3BP1 (Table 10, row 5), Ezrin (Table 10, rows 6-7), Radixin (Table 10, row 8), and ATG7 (Table 10, row 9) showed no difference on stimulation in the phospho-eluate, lanes 5-6. Confirmation of stimulation was demonstrated through marked phosphorylation of p44/42 MAPK (thr202/tyr204), both in the WCL, lane 2, and in the concentrated eluate, lane 6 of Figure 11.

Protein	Protein symbol	Uniprot Accession number	MASCOT score	Phosphorylated (P) Dephosphorylated (D)	Fraction identified	Ion trap
β-arrestin 1	ARRB1	P49407	64	D	6	
Dual specificity mitogen-activated Protein Kinase kinase 1	MEK1	Q02750	52	P	6	
Vasodilator-stimulated phosphoprotein	VASP	P50552	103	D	10	
Protein S100-A9	S100-A9	P06702	256	D	5	Yes
SH3 domain-binding protein 1	SH3BP1	Q9Y3L3	68	P	6	
Ezrin	EZR	P15311	106	D	7	
			83	P	6	
Radixin	RDX	P35241	55	D	7	
Autophagy-related protein 7	ATG7	O05352	148	P	6	Yes
Rab GDP dissociation inhibitor alpha	GDI1	P31150	82	P	6	Yes
Leucine-rich repeat flightless interacting protein 1	LRRFIP1	Q32MZ4	57	D	1	
			108	D	2	
Protein S100-A8	S100-A8/ MRP8	P05109	66	P	9	
SAM domain and HD domain containing protein 1	SAMHD1	Q9Y3Z3	52	P	8	

Table 10: Selection of proteins identified by MS with their MASCOT score, fraction and whether preferentially phosphorylated or dephosphorylated.

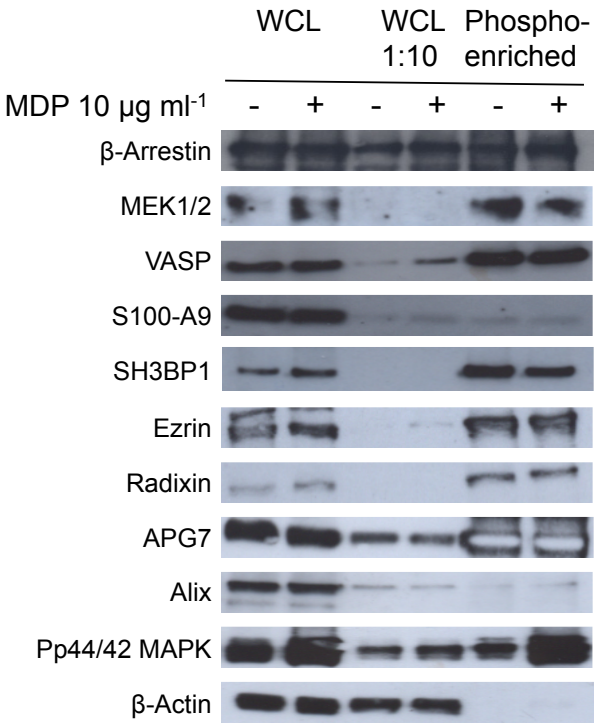


Figure 11: Immunoblot of proteins identified by MS but with no identifiable change in phosphorylation status between unstimulated or stimulated conditions. Confirmation of presence of putative targets from **Table 10** on stimulation of DCs by MDP at 10 µg mL^{-1} for 30 minutes in the phospho-eluate. Immunoblotting was done for HMGB1, β-Arrestin, MEK 1/2, VASP, S100-A9, SH3BP1, SHP-1, Ezrin, Radixin, APG7, Alix, P-p44/42 MAPK, and β-Actin as loading control. This demonstrated that these proteins were not differentially phosphorylated by MDP stimulation of NOD2. N=3.

3.2.4. Targets validated and in agreement with MS data

Differential phosphorylation of proteins in agreement with the MS data, with details of MASCOT score, preferential phosphorylation status and fraction can be seen in Table 11 and the relevant immunoblots in Figure 12. LCP1 (Table 11, row 1) was phosphorylated more on stimulation with MDP in the phospho-eluate (Figure 12, lane 4 compared to 3). HMGB1 (Table 11, row 2) was dephosphorylated on MDP stimulation (Figure 12, lane 3 compared to 4). GNB2L1, according to the MS data should be dephosphorylated (Table 11, row 3) and this was in agreement with what was immunoblotted on stimulation with MDP (Figure 12, lane 3 compared to 4). SHP1 (Table 11, row 4-5) was markedly phosphorylated on stimulation with MDP (Figure 12, lane 4). The immunoblot controls were provided by phospho-p44/42 MAPK and β-actin (Figure 12, rows 5-6).

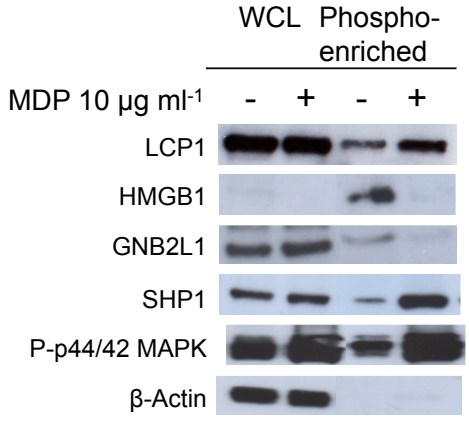


Figure 12: Immunoblot of proteins found to be differentially phosphorylated on NOD2 stimulation with its ligand MDP. Confirmation of proteins with differential phosphorylation status on stimulation of DCs with MDP (10 µg mL^{-1} for 30 minutes). Immunoblotting for the following proteins: LCP1 (or L-plastin), HMGB1, GNB2L1, SHP1; confirmation of signalling via NOD2 by immunoblot of phosphorylated p44/42 MAPK, and loading control by β-actin. N=3.

Protein	Protein symbol	Uniprot Accession number	MASCOT score	Phosphorylated (P) Dephosphorylated (D)	Fraction identified	Ion trap
L-plastin/Plastin-2	LCP1	P13796	139	P	4	
High Mobility Group B1	HMGB1	P09429	140	D	7	Yes
Guanine nulceotide-binding Beta-2 like	GNB2L1	P63244	103	D	10	
Protein Tyrosine Phosphatase Non-receptor Type 6 or Src-Homology Protein 1	PTPN6/SHP1	P29350	73	p	8	
			59	P	9	

Table 11: Details of proteins verified positively by immunoblot, with their MASCOT score, fraction identified in and whether phosphorylated or dephosphorylated.

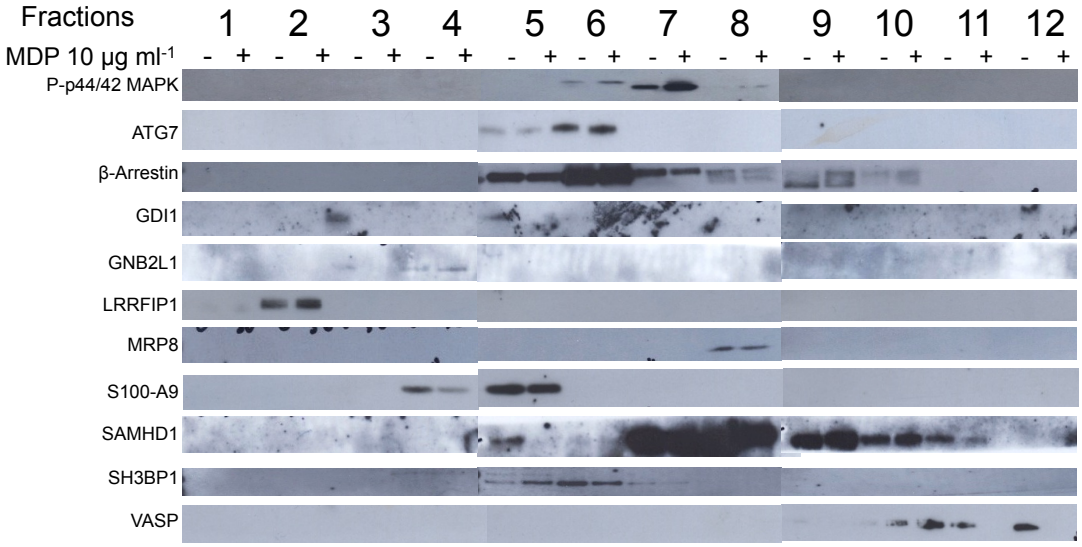


Figure 13: Immunoblot of OFFGEL fractionated phospho-enriched eluate. Samples were obtained from DC lysates unstimulated or stimulated with MDP and demonstrating changes in phosphorylation that affected isoelectric point (pI) of each protein. Proteins immunoblotted included: ATG7, β-Arrestin, GDI1, GNB2L1, LRRFIP1, MRP8, S100-A9, SAMHD1, SH3BP1, and VASP. Differential phosphorylation demonstrated in β-arrestin, GNB2L1, S100-A9, SAMHD1, and VASP. N=2.

3.2.5. OFFGEL fractionation has the potential to reveal post-translational modifications, such as phosphorylation

A number of proteins suggested to be differentially phosphorylated on NOD2 stimulation by MS were not validated by phosphoenrichment and subsequent immunoblot. In some cases phospho-specific antibodies were not available to proteins concerned, so to be sure no change in phosphorylation was occurring I used OFFGEL fractionation to separate eluates by their isoelectric point (or pI) prior to immunoblot. DC phospho-eluate obtained as before, was diluted with urea/glycerol solution supplemented with OFFGEL ampholytes and subject to OFFGEL fractionation (Figure 13). The 12 fractions from the unstimulated eluate and the 12 from the stimulated eluate were recovered, desalted and then immunoblotted comparing unstimulated and stimulated fractions.

Internal validation of the technique was provided by changes demonstrated by phospho-p44/42 MAPK (thr203/tyr204) (Figure 13). Using OFFGEL fractionation differences in abundance of proteins was observed for β-arrestin1, S100-A9, SAMHD1, SH3BP1, and VASP on stimulation with MDP consistent with post-translational modification, most likely phosphorylation. For proteins ATG7, GDI1, GNB2L1, LRRFIP1, and MRP8 (or S100-A8) no differences were observed meaning they were unlikely to be involved in the signalling cascade.

3.2.6. Investigating NOD2/TLR2 crosstalk by MS

Identifying signalling molecules in NOD2 stimulated cells provided insight into the function of NOD2. To investigate how NOD2 cross-talks and synergises with TLR2, phospho-eluates were obtained from DCs stimulated with MDP and PAM or left unstimulated in R10, and immunoblotted as before. The concentrated eluate from 6 of the 12 biological replicates most clearly demonstrating differential phosphorylation of p44/42 MAPK (see Figure 14) were combined and prepared for MS, but in this experiment I improved the technical approach.

To enable analysis of relative changes in protein phosphorylation between stimulated and unstimulated samples, a differentially weighted marker was attached to the trypsin-digested peptides, known as TMT. iTRAQ [347] and isotope-free TMT [348] are similar techniques, but the benefit of TMT over iTRAQ is that it is an isotope-free methodology, the differentially weighted reporter ions attach to free amino-terminus peptides or lysine residues and so are not restricted toward a particular class of peptide, and the reporter ions are isobaric, that is they do not interfere with peptide identification. The differentially weighted ions have a predetermined mass/charge (*m/z*), such as in the 2-plex TMT the ions are 126 or 127. I attached the 126 label to the dual stimulated pooled samples, and 127 to the unstimulated samples. On analysis therefore, fold change is expressed as 126/127 so a value greater than 1 is evidence of more protein in the stimulated sample (that is differentially phosphorylated) and a value less than 1 is evidence of less (that is differentially dephosphorylated).

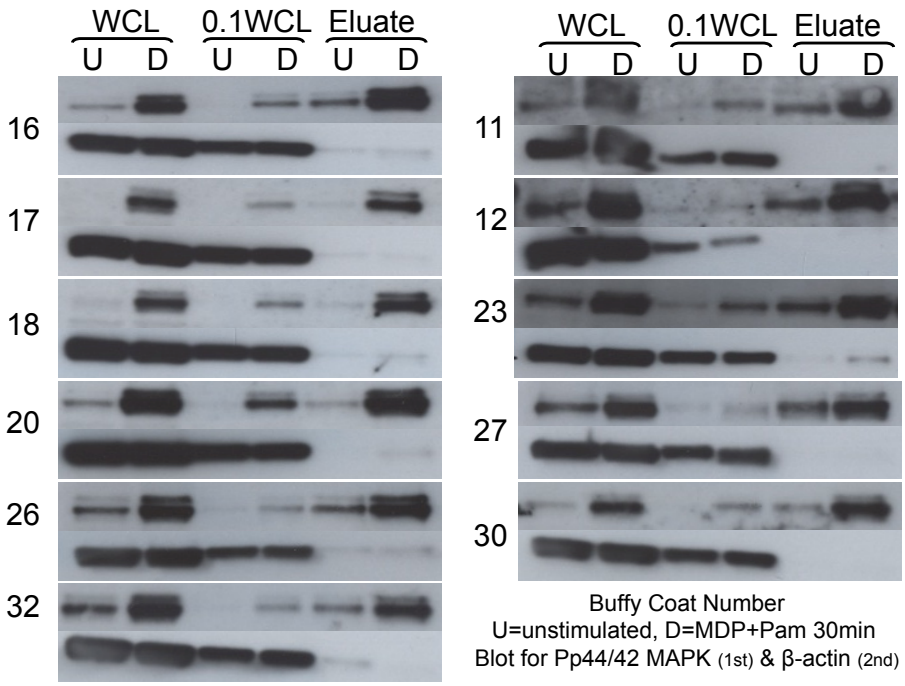


Figure 14: Selection of 6 biological replicates for MS analysis (Donor 16, 17, 18, 20, 26 and 32) and 5 rejected replicates (11, 12, 23, 27, and 30).

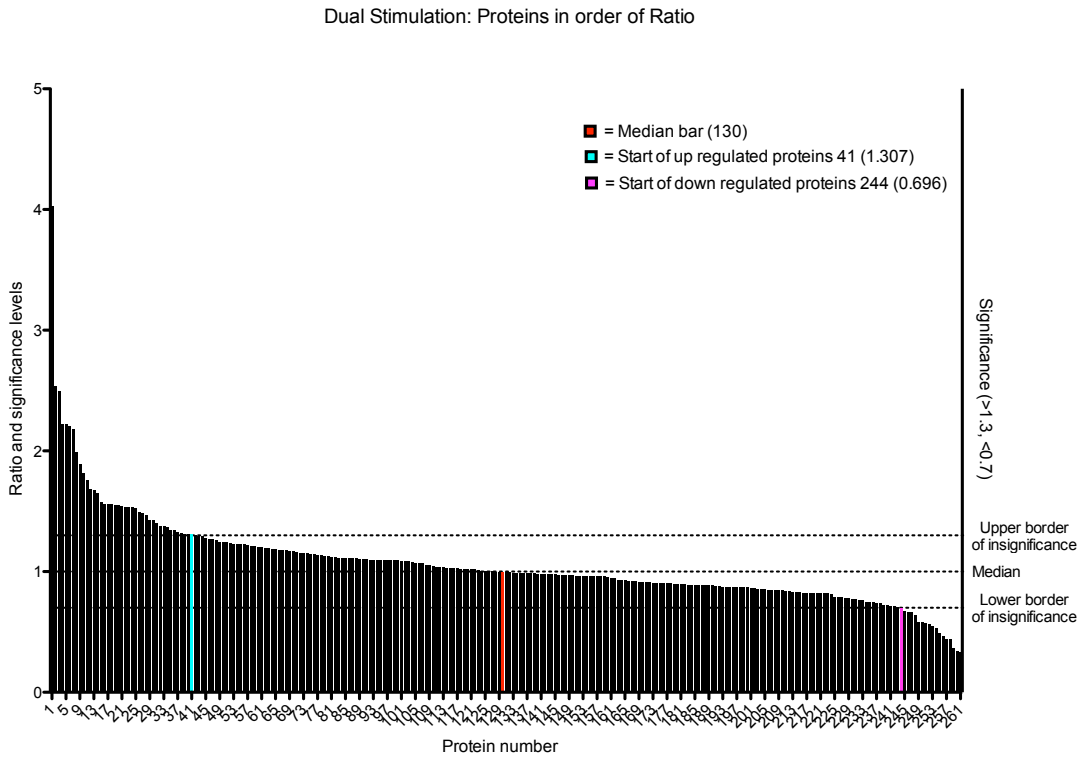


Figure 15: Graph showing linearization of the 126/127 ratios. Levels of significance were set at >1.35 (turquoise bar) or <0.7 (violet bar) and median ratio of 1 (red bar).

The resulting data gave proteins identified by a Uniprot number and MASCOT score. The sample was normalised about the median value, and proteins where only 1 peptide was used to identify it were excluded. The Matrix science software then calculated the fold change with the unstimulated sample (ion 127) being the denominator and the stimulated sample (ion 126) the numerator. In order to determine which targets should be further validated, the proteins identified were ordered according to fold change in order of magnitude. The curve change from being linear to exponential at either end determined the level of significant change in phosphorylation. Thus, with a median of 1, the significant phosphorylation was set at 1.307 and dephosphorylation was 0.696 (see Figure 15). This identified 53 proteins differentially phosphorylated and 49 proteins differentially dephosphorylated. 334 proteins identified showed no significant difference in phosphorylation. The greatest phosphorylated was 3.328, and the greatest dephosphorylated was 0.271 which equates to a 3.690 fold decrease in phosphorylation (Figure 15).

Comparing the proteins identified through MDP stimulation on MS with those identified now produced a list of 14 proteins that were differentially phosphorylated on both MDP and MDP+PAM stimulation (see Table 12). As seen in Table 12, eight proteins had their preferential phosphorylation state changed between single and dual stimulation. ATG7, PSMB10, EEF2, ANP328 and MEK1 were phosphorylated on MDP alone but were found to be dephosphorylated on NOD2/TLR2 triggering. Conversely, S100-A9 and HSPB1 were originally dephosphorylated but now were phosphorylated on NOD2/TLR2 stimulation.

Gene	Accession Number	Ratio: 127/126	IPA Fold change	Dual stimulation Mascot score	Single Fraction	MDP only Mascot score	Phosphorylation status different?
PSMA2	P25787	0.597	-1.675	97	D8	54	
LRRFIP1	Q32MZ4	0.650	-1.538	143	D1	108	
LRRFIP1	Q32MZ4	0.650	-1.538	143	D2	57	
EEF2	P13639	0.681	-1.468	115	D7	145	
EEF2	P13639	0.681	-1.468	115	D10	64	
EEF2	P13639	0.681	-1.468	115	D8	42	
SEPT2	Q15019	0.681	-1.468	144	D7	89	
ATG7	O95352	0.632	-1.582	73	P6	58	Opposite
ATG7	O95352	0.632	-1.582	73	P6	148	Opposite
PSMB10	P40306	0.646	-1.548	248	P6	35	Opposite
EEF2	P13639	0.681	-1.468	115	P7	95	Opposite
ANP32B or APRIL	Q92688	0.702	-1.425	90	P6	63	Opposite
MAP2K1 or MEK1	Q02750	0.737	-1.357	35	P6	52	Opposite
MAP2K1 or MEK1	Q02750	0.737	-1.357	35	P6	28	Opposite
S100-A9	P06702	1.368	1.368	116	D5	256	Opposite
NT5C2	P49902	1.516	1.516	134	D7	39	Opposite
HSPB1	P04792	1.520	1.520	96	D6	31	Opposite
HSPB1	P04792	1.520	1.520	96	D6	59	Opposite
NT5C2	P49902	1.516	1.516	134	P7	49	
HSPB1	P04792	1.520	1.520	96	P5	69	
HSPB1	P04792	1.520	1.520	96	P6	39	
HSPB1	P04792	1.520	1.520	96	P5	42	
VIM	P08670	1.527	1.527	48	P2	77	
RPS6	P62753	2.350	2.350	37	P5	41	
LCP1	P13796	2.360	2.360	345	P4	139	

Table 12: Proteins that are differentially phosphorylated on both MDP stimulation alone (10 µg mL^{-1}) and dual MDP (10 µg mL^{-1}) and PAM (1 µg mL^{-1}) stimulation for 30 minutes. The proteins listed are grouped according to differential phosphorylation on dual stimulation then according to dephosphorylated or phosphorylated by MDP alone. Those proteins that demonstrate a different phosphorylation state are marked 'Opposite' in the final column. Orange numbers in Single Fraction column denote ion trap results.

3.2.7. Verification of proteins identified as differentially phosphorylated on NOD2/TLR2 stimulation

In order to verify the results of the MS further, DCs stimulated with MDP and PAM or R10 alone as before were immunoblotted. This demonstrated that there was increased signalling capacity through p44/42 MAPK due to the increased strength of stimulation in dual compared to MDP alone. Despite this increase in signal capacity this was not translated into differential phosphorylation of the targets as seen in Figure 16. ATG7 (Fold change -1.582, MASCOT 73), which on MS data was above the threshold for differential dephosphorylation of 0.699 or -1.4, was unchanged on stimulation with MDP+PAM (Figure 16, row 1). β-arrestin1 did not appear in the dual stimulation MS data but was immunoblotted and no difference was found, including looking at the phosphorylation site serine 412 (ser412) (Figure 16, row 3-4). LRRFIP1 (-1.538, MASCOT 143) was differentially phosphorylated in both data sets, but on immunoblot was found to have an imperceptible decrease in phosphorylation on stimulation of NOD2 and TLR2 (Figure 16, row 4). According to the MS data Ezrin (-1.112, MASCOT not available) was no longer differentially phosphorylated on dual stimulation and this concurred with the immunoblot (Figure 16, row 5). S100-A9 (1.368, MASCOT 168), which had changed preference in the MS data from dephosphorylated on MDP stimulation to phosphorylated on dual, was barely present in the phospho-eluate and certainly to no level to distinguish whether there was a difference (Figure 16, row 6). SAMHD1 (1.095, MASCOT 209) was not differentially phosphorylated and immunoblot agreed (Figure 16, row 7). VASP (-1.35, MASCOT 78) was no longer differentially phosphorylated and on immunoblot there was a suggestion of phosphorylation on stimulation. To ensure

that this was correct the sample was probed for two phosphorylation sites on VASP: ser157 did not demonstrated any difference (Figure 16, row 8-9), nor did ser239, though it was not present in WCL or eluate (data not shown).

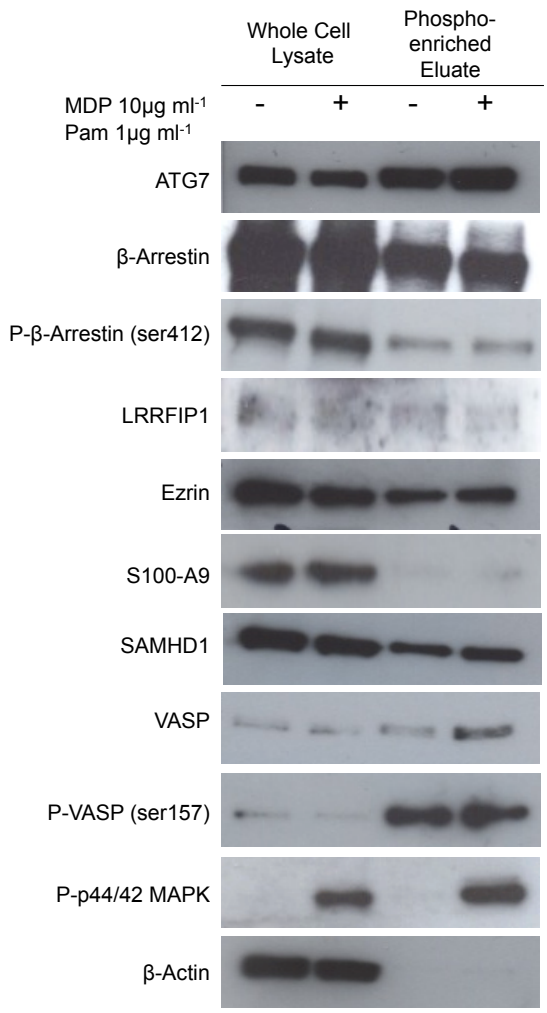


Figure 16: Immunoblot to verify potential proteins differentially phosphorylated on NOD2/TLR2 cross-talk. Proteins identified by MS from single stimulation used to verify if proteins are differentially phosphorylated on dual stimulation. 23 x 10^6 DCs were left unstimulated or stimulated with MDP (10 µg mL^{-1}) and PAM (1 µg mL^{-1}) stimulation for 30 minutes and phosphoproteins enriched. Positive control provided by phosphorylated p44/42 MAPK and loading verified by β-actin. N=2.

3.2.8. LCP1 and DAPK1 verified in NOD2/TLR2 crosstalk signalling cascade

Some proteins that appeared in both the single and dual data sets were differentially phosphorylated, and one protein from the dual set alone, DAPK1 was also differentially phosphorylated (Figure 17). The proteins verified are shown in Table 13.

Protein	Protein symbol	Uniprot Accession number	MASCOT score	Ratio 126/127	Fold Change
Death-Associated Protein Kinase 1	DAPK1	P53355	n/a	2.19	2.19
L-plastin/Plastin-2	LCP1	P13796	345	2.36	2.36
Dual specificity mitogen-activated Protein Kinase kinase	MEK1	Q02750	35	0.737	-1.36
Heat-Shock Protein 27/ Beta1	HSP27/ HSPB1	P04792	96	1.52	1.52

Table 13: Induction of phosphorylation of key intermediates in the NOD2/TLR2 signalling cascade. Detailed within are MASCOT score, ratio and thus fold change between unstimulated and dual stimulated conditions.

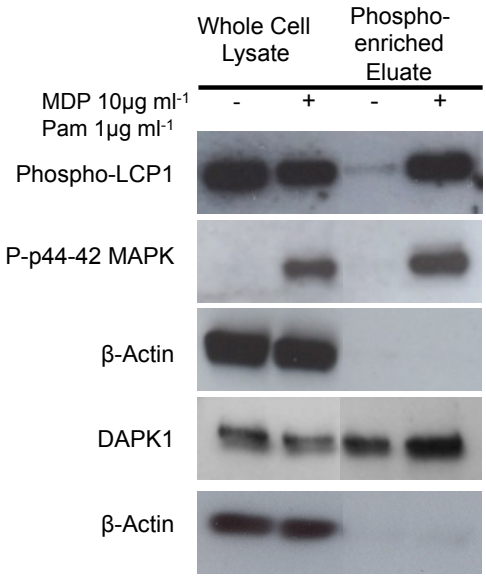


Figure 17: Immunoblot of verified proteins differentially phosphorylated on dual stimulation of DCs. Immunoblot of verified protein targets identified by MS from dual stimulated DCs by MDP (10 µg mL^{-1}) and PAM (1 µg mL^{-1}) stimulation for 30 minutes. Proteins verified are LCP1 (L-plastin) and phosphorylated p44/42 MAPK with a loading control provided by β-actin; and secondly demonstration of DAPK1 with a loading control provided by β-actin. N=3.

LCP1 (2.36, MASCOT 345) was differentially phosphorylated on dual stimulation (Figure 17, row 1), as well as seen previously with MDP alone (Figure 12, row 1). The immunoblot demonstrated highlights a difference in phospho-LCP1 (tyr28), but due to differences in the WCL, it is not the site of differential phosphorylation (Figure 17, row 1, and see Chapter 5). Phospho-p44/42 MAPK is provided as a positive control (Figure 17, row 2). DAPK1 (2.19, MASCOT not available) was preferentially phosphorylated on dual stimulation (Figure 17, row 4).

3.2.9. The determination of whether the verification targets are involved in the TLR signalling cascade and not NOD2 signalling cascade

Immunoblots were used to determine whether these positive results from the dual stimulation with MDP and PAM were from the NOD2 signalling cascade, the TLR2 signalling cascade, or new to the dual stimulation signalling cascade. Furthermore, stimulation with other TLR ligands was investigated to see if the response was restricted to NOD2/TLR2 or included other PRRs. DCs were separated into six aliquots and stimulated with MDP, PAM, MDP and PAM, LPS (TLR4 ligand) or FLA (TLR5 ligand). In all cases it is shown that there was preferential phosphorylation on TLR signalling particularly to TLR2 and TLR5 (Figure 18A, lanes 9-12).

MEK1 (-1.357, MASCOT 35) was previously seen to be equivocally dephosphorylated on MDP stimulation alone (Figure 11, row 2) and yet was clearly phosphorylated on dual stimulation on immunoblot (Figure 18A, row 4, lane 10). This was contrary to the MS data, where it was dephosphorylated (-1.357), so demonstrating a change in its phosphorylation preference between MS and immunoblot. Interestingly MEK1 did not show phosphorylation on TLR4 stimulation (Figure 18A, row 4, lane 12).

HSPB1 (HSP27) (1.52, MASCOT 96), which was phosphorylated on MDP alone was demonstrated to be phosphorylated on dual stimulation (Figure 18A, row 5, lane 10) and HSP27 was more involved in the TLR2 signalling cascade than any other (Figure 18A, row 5, lane 9-10).

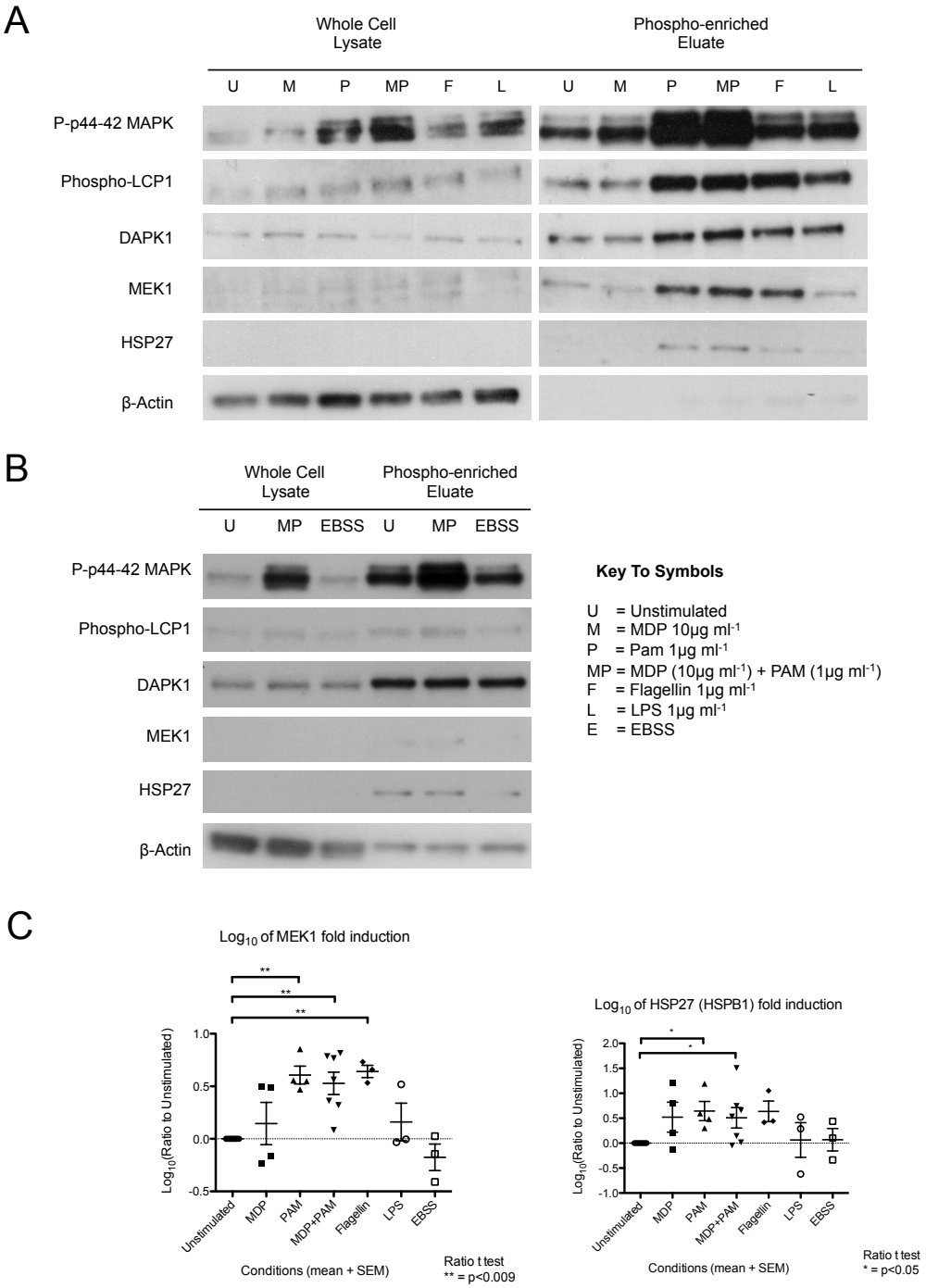


Figure 18: A panel of PRR ligands differentially phosphorylate proteins in the NOD2/TLR2 signalling cascade but not on starvation. A) 3.5 x 10^6 DCs were left unstimulated or stimulated with MDP (10 μg mL^{-1}), PAM (1 μg mL^{-1}), dual (MDP 10 μg mL^{-1} + PAM 1 μg mL^{-1}), Flagellin (1 μg mL^{-1}), LPS (1 μg mL^{-1}) for 30 minutes then immunoblot of concentrated phospho-eluate for phospho-LCP1, DAPK1, MEK1, HSP27, phospho-p44/42 MAPK and β-actin in WCL (left panel) and phospho-enriched eluate (right panel). B) 3.5 x 10^6 DCs were left unstimulated or stimulated with MDP and PAM together or starved in EBSS for 30 minutes. Immunoblot of WCL and eluate as for A. C) Quantification of immunoblot intensity using Imagequant (GE Healthcare) system demonstrating Log_{10} [fold induction] of MEK1 and HSP27 (HSPB1) phosphorylation over unstimulated demonstrating phosphorylation on PRR stimulation but not on EBSS stimulation. N=4.

All the proteins were correlated against p44 MAPK and the only one that was significant was MEK1 with a Spearman rank 0.8214, p=0.0341 (Figure 19).

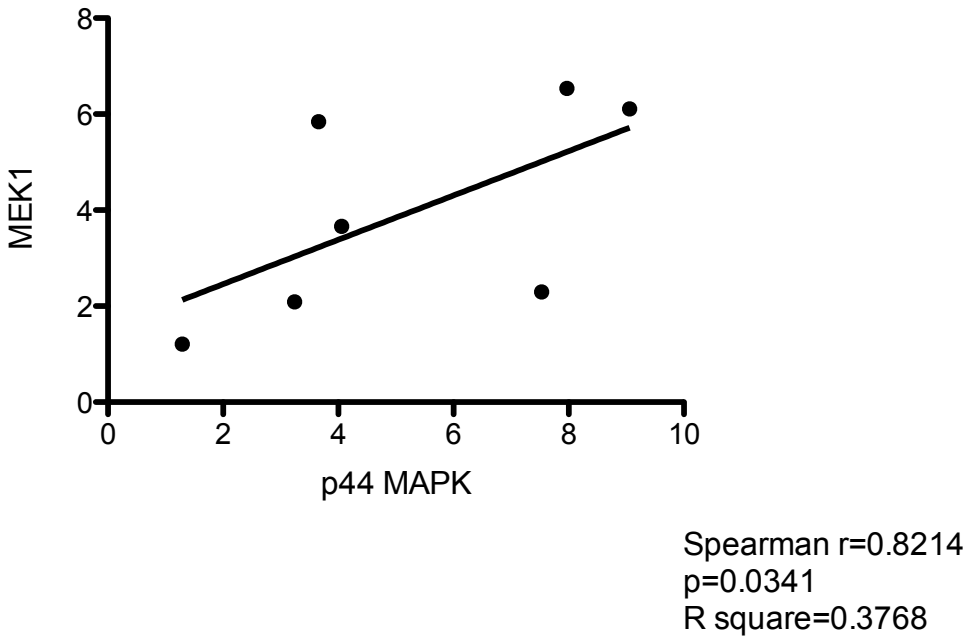


Figure 19: Correlation of phosphorylation of p44 MAPK and MEK1 expressed as a ratio of phosphorylation in dual stimulated cells compared to unstimulated.

3.2.10. Starvation-induced autophagy does not involve differential phosphorylation of LCP1, MEK1 or HSP27

To further determine whether these intermediates from the NOD2 and TLR2 signalling cascades were involved in the initiation signals for autophagy, EBSS, a known potent inducer of starvation induced autophagy was compared to dual MDP and PAM stimulated and unstimulated DCs. This showed a lack of signalling through any intermediates and less signalling when stimulated with EBSS (Figure 18B). HSP27 may be involved, but requires more donors to confirm this.

3.2.11. Quantification of signalling intermediates from NOD2/TLR2 signalling cascades

Quantification of the immunoblots performed previously was made on Imagequant for the biological replicates (Figure 18C) and mean, standard deviation (SD) and standard error of the mean (SEM) of the Log_{10} [ratio or fold change] compared to unstimulated samples were obtained. The Log_{10} [ratio] was used to calculate a ratio t-test to discover if the differences in ratios were significant.

MEK1 phosphorylation was compared to unstimulated and it was significantly phosphorylated when stimulated with PAM (mean 0.6069, p=0.0056), MDP+PAM (0.5280, p=0.0026) and FLA (0.6411, p=0.0082), whereas not with MDP, LPS and EBSS (Table 14). Similarly for HSP27, it was significantly phosphorylated on PAM stimulation (0.6428, p=0.0444) and the others were not (Table 15).

	Mean	SD	SEM	p value
MDP	0.1453	0.4021	0.1483	0.5220
PAM	0.6069	0.1698	0.0489	**0.0056**
MDP+PAM	0.528	0.2818	0.1065	**0.0026**
FLA	0.6411	0.1009	0.5825	**0.0082**
LPS	0.1609	0.3100	0.1790	0.4636
EBSS	-0.1754	0.219	0.1264	0.2996

Table 14: Mean Log_{10} [ratio] compared to unstimulated with SD, SEM and ratio t-test for MEK1 Highlighted in bold are significant values.

	Mean	SD	SEM	p value
MDP	0.5202	0.6002	0.3001	0.1815
PAM	0.6428	0.3851	0.1926	**0.0444**
MDP+PAM	0.5084	0.5414	0.2046	**0.0475**
FLA	0.6370	0.3582	0.2068	0.0912
LPS	0.0639	0.6037	0.3486	0.8714
EBSS	0.0681	0.3887	0.2244	0.7902

Table 15: Mean Log_{10} [ratio] compared to unstimulated with SD, SEM and ratio t-test for HSP27. Highlighted in bold are significant values.

3.3. Discussion

Traditional proteomic techniques often involve 2-Dimentional (2D) gels, that is separating proteins according to their isoelectric point or pI, followed by turning the blot through 90 ° and undertaking SDS-PAGE gel separation. The resulting scatter dot-blot makes protein matching between two experiments challenging. In this method of extraction of phospho-serine, -threonine, and -tyrosine residues by a column, the sample complexity still remained. This was reduced by OFFGEL fractionation, which similarly to 2D-gels, separated proteins according to their charge. The samples from sequential fractions were then separated by SDS-PAGE prior to immunoblot. Differences observed in the abundance of a protein between different fractions were indicative of a post-translational modification (most likely phosphorylation) occurring. The trypsin-digested fraction samples were then analysed using LS-MS/MS analysis providing the basis of experiments for this part of the research.

The data presented here demonstrates that on stimulation of NOD2 by its ligand MDP, downstream phosphorylation of p44/42 MAPK occurs. In addition novel signalling targets, such as LCP1, SHP1 and HMGB1 are phosphorylated or dephosphorylated at the early time point of 30 minutes post commencement of stimulation (Figure 12). These intermediates have previously been determined as negative regulators of signalling [382] [383], cytoskeletal conformational changes [368], gene translation [437] and modulation of apoptosis [371]. Furthermore, when NOD2 signals in conjunction with TLR2, the phosphorylation of p44/42 MAPK is increased. Targets identified on NOD2 signalling also have greater phosphorylation on dual

stimulation, such as LCP1. Other mediators identified, for example DAPK1, MEK1 and HSP27, are involved in functions such as apoptosis control, autophagy induction, signalling propagators and protein chaperones. These proteins, differentially phosphorylated by NOD2 and NOD2/TLR2 signalling cascades, are further investigated in the subsequent chapters.

NOD2 signalling, being cytosolic, initially occurs via RIP2, and may have additional support from CARD9 [438]. Poly-ubiquitination of RIP2 causes activation of the signalling cascade via phosphorylation of TAK1 with IκB degradation and activation of p85 and Rel (p50) parts of NF-κB. Eliciting different members of the signalling process enables a greater understanding of other scaffolding support proteins, signalling intermediates or negative regulators.

Of the signalling intermediates outlined in the introduction above only two appeared in the dual stimulation analysis (TAK1 (fold change 0.809) and CARD9 (1.098)), and both had insignificant phosphorylation changes (see Appendix Table 4). This is not surprising, as firstly, MS does not pick up all proteins present. Secondly, at 30 minutes, their differential phosphorylation may be over, or not yet involved in the dual stimulation of NOD2 and TLR2.

HSP27 is involved in actin organisation and a chaperone in stress-induced circumstances [422] [423]. The phosphorylation of HSP27 may occur at 4 different sites, ser15, ser78, ser82 and ser86. Not only is it part of the p38-MAPKAP K-HSP27 axis [418], it is important for autophagy. Further work on HSP27 in this setting would be to determine the phosphorylation site to guide future work on HSP27.

In contrast to p44/42 MAPK, which was not identified in the MS data but was verified by immunoblotting, MEK1 was identified in the NOD2/TLR2 signalling pathway. MEK1 is a well known intermediate of the TLR signalling cascade [430], acting downstream of MAP4K then MAP3K, and from there binds β-arrestin and activates ERK2 [433]. The data suggests that MEK1 was involved in TLR signalling, but for the first time was also associated with NOD2 signalling.

As MEK1 has been confirmed as a NOD2/TLR2 signalling mediator, the identification of β-arrestin1 in the MS data was important, due to the role of β-arrestin1 as a negative regulator of TIR signalling. β-arrestin1 restricts TRAF6 ubiquitination by direct association with TRAF6, and caused activation of IκBα on TLR4, RANKL and IL-1β stimulation [439]. The interference of TRAF6 by β-arrestin1 is not observed with TRAFs1-5. β-arrestins have been observed to negatively influence G-protein coupled receptor complexes (GPCR) [440] [441] [442] [443] and, similarly, NOD2 and TLR2 stimulation have previously been shown to alter the expression of GPCRs [444] [445]. Furthermore, interaction of β-arrestin with GPCR at the cellular membrane results in dephosphorylation of β-arrestin. Phosphorylation of β-arrestin at ser412 by ERK and, when enabled by MEK1, may prevent endocytosis from occurring [433]. This would have been the first time to link the NOD2 signalling pathway with β-arrestin1.

S100-A8 and S100-A9 are secreted in stools of patients with IBD [446] and they are useful to both differentiate IBD from other GI disorders and for monitoring disease activity. They are small DAMPs that form complexes [447] and on release, dependent

on PKC [448], signal via RAGE [397] and TLR4 [449]. Their involvement in the NOD2 signalling pathway would have been unusual, as their usual action is extracellular on surface receptors, though as PMA causes their release [448], it could be possible to stimulate their release via NOD2.

SAMHD1 was first reported as part of Aicardi-Goutieres Syndrome and a negative regulator of IFN responses to viruses [450], particularly as a restriction enzyme for human immunodeficiency virus 1 (HIV1) [451]. It is possible SAMHD1 is recruited in PRR sensing to destroy incoming microbial nucleic acid.

SH3BP1 is a Rac1 protein that may prevent membrane ruffling in fibroblasts [452] and so speculatively may be involved in autophagy in innate immune cells. It is also involved at the front end of cellular movement by inactivating Rac [453] so may be involved in DC migration or formation of dendrites.

Further analysis of the other proteins shown to be part of the NOD2 and TLR2 signalling cascades are going to be discussed in later chapters.

The figure demonstrating the interacting proteins originally presented here cannot be made freely available via ORA because of copyright. The image was sourced at IPA (**Ingenuity® Systems, www.ingenuity.com).**

Figure 20: An overview of the interaction of proteins involved in NOD2/TLR2 signalling. Orange lines denote new connections between proteins. Pathway designer created using IPA (Ingenuity® Systems, www.ingenuity.com).

3.4. Conclusion

Understanding the signalling cascades for both NOD2 and TLR2, and in particular the cross-talk that occurs between these two PRRs that recognise different breakdown products of peptidoglycan, is vital to understand the initial modulation of APCs such as DCs microbial recognition. The resulting data shown here demonstrated the involvement of novel NOD2 signalling proteins, including HSP27 and MEK1 and four others which will be discussed in later chapters: DAPK1, LCP1, SHP1, HMGB1. These six proteins have been demonstrated to be involved in either NOD2 triggering or in dual PRR triggering for NOD2 with TLR2 and TLR5, in particular.

MEK1 interacts with β-arrestin and is one of the main kinases in TLR signalling cascades. HSP27/HSPB1 is a chaperone protein and may be involved in autophagy.

Further work would be to further validate targets identified by MS. From there, analysis of the phospho-peptides using phospho-peptide enrichment would enable clear assessment of which peptides are phosphorylated in which stimulation scenarios and how the proteins therefore may be involved in the signalling cascades.

A summary figure produced using Ingenuity indicates the interaction of different proteins within the NOD2 signalling cascade (Figure 20). The proteins included are those known to interact based on previous literature (black line and dashed line) and the novel interactions from this work are highlighted in orange.

4. LCP1, SHP1 and HMGB1: novel downstream mediators of NOD2/TLR2 signalling

4.1. Overall Introduction

The proteins LCP1, SHP1 and HMGB1 were previously identified by phosphoproteomic analysis as acting downstream of NOD2/TLR2 stimulation in human DCs. All three of these proteins might function in antibacterial defence mediated by NOD2/TLR2 and in this chapter I investigate possible functional roles for these proteins in NOD2 signalling.

L-plastin or LCP1 is an actin bundling protein expressed in mammalian haematopoeitic cells and has been implicated in bacterial phagocytosis and cytokine release. SHP1 is a tyrosine phosphatase, and is a negative regulator of intracellular signalling that is necessary for the propagation of the phosphorylation signal from NOD2 through to p44/42 MAPK and control of cytokine release. Lastly, HMGB1 is a nuclear transcription factor.

4.2. L-plastin or Lymphocyte Cytosolic Protein 1 (LCP1)

4.2.1. Introduction

LCP1 was significantly phosphorylated both on MDP stimulation and MDP/PAM dual stimulation in human DCs. Plastins, such as LCP1, have had roles in bacterial handling [374] [454], protecting against TNF induced apoptosis [371], and migration of leucocytes [372] [373] [374]. This chapter seeks to demonstrate its function within DCs on triggering of PRRs by their ligand, and suggest a putative role for LCP1.

4.2.2. LCP1 Results

4.2.2.1. LCP1 is part of the PRR signalling cascades

The MS data suggested that LCP1 was phosphorylated in both MDP stimulated DCs (MASCOT score (MASCOT) 139, phosphorylated in fraction 4 of ion trap) and in MDP+PAM dual stimulated DCs (MASCOT 345, 126/127 ratio 2.36). In order to verify these results, an immunoblot for LCP1 was undertaken on samples derived from the WCL and phospho-eluate from MDP stimulated DCs. Examination of phospho-enriched material from either MDP stimulated (Figure 21A) or from MDP/PAM stimulated (Figure 21B) DCs using anti-phospho-LCP1 (tyr28) showed increased phosphorylation of LCP1 in NOD2 or NOD2/TLR2 activated DCs.

In order to probe whether phosphorylation of LCP1 was particular to NOD2 and TLR2 or occurred with other PRRs as well, DCs were stimulated for 30 minutes with a panel of PRR ligands as demonstrated by the immunoblot with phosphorylation of p44/42 MAPK as a control (Figure 21C). A number of immunoblots were analysed using Imagequant (Figure 21D and Table 16) and demonstrated significant phosphorylation, expressed as Log_{10} [ratio to unstimulated], in MDP and PAM dually stimulated DCs (mean 0.3811, p=0.0088) and on stimulation with FLA (0.5241, p=0.0337). To investigate if phosphorylation of LCP1 occurred on induction of autophagy, as was seen on PRR triggering, I treated DCs with EBSS for 30 minutes. No significant dephosphorylation of LCP1 (-0.2138, p=0.1236) was observed following treatment of DCs with this classical inducer of starvation-mediated

autophagy, suggesting that if LCP1 played a role in PRR-mediated autophagy it would be following a different route to that of starvation-mediated autophagic flux.

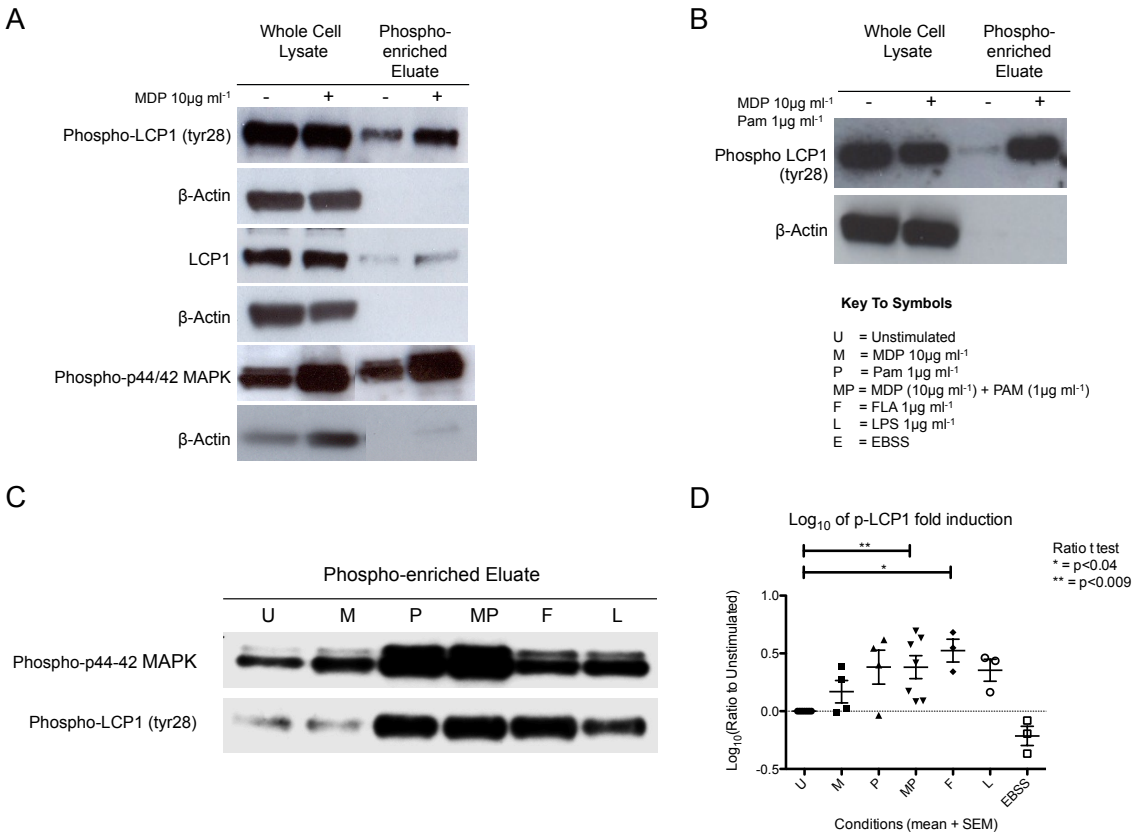


Figure 21: Assessment of LCP1 phosphorylation by a panel of PRR ligands. 3.5-15 x10^6 DCs were stimulated with MDP (10 µg mL^{-1}) and PAM (1 µg mL^{-1}). Comparison was made to total LCP1 and β-actin. A) Immunoblot of WCL or phospho-eluate from unstimulated or MDP stimulated DCs using antibodies to LCP1, phospho-LCP1, phospho-p44/42 MAPK and β-actin. B) Dual (MDP+PAM) stimulated DCs and immunoblot for phospho-LCP1 and β-actin. C) Immunoblot of phospho-enriched eluate from DCs stimulated with a panel or PRR ligands (U=unstimulated, M=MDP 10 µg mL^{-1}, P=PAM 1 µg mL^{-1}, FLA=Flagellin 1 µg mL^{-1}, LPS=Lipopolysaccharide 1 µg mL^{-1}, EBSS=starvation media). D) As for C) with Imagequant quantification of phosphorylation of LCP1 as a ratio to unstimulated. N=4-6.

	Mean	SD	SEM	± 95 % CI	p value
MDP	0.1689	0.1941	0.09703	0.3088	0.1801
PAM	0.3814	0.2928	0.1464	0.4659	0.0800
MDP+PAM	0.3811	0.264	0.09977	0.2441	**0.0088**
FLA	0.5241	0.1711	0.09878	0.425	**0.0337**
LPS	0.3543	0.165	0.09528	0.4099	0.0653
EBSS	-0.2138	0.1438	0.08305	0.3574	0.1236

Table 16: Mean of Log_{10} [ratio], SD, SEM, 95 % confidence interval (CI) and ratio t-test p value for LCP1 phosphorylation at tyr28 after PRR triggering. Significant p values in bold.

I sought to determine which residues of LCP1 were differentially phosphorylated on NOD2 triggering. Using an anti-phospho antibody that recognises tyr28 of LCP1, I could demonstrate that at least this residue was involved in the phospho-enriched eluate. I used kinase prediction programmes, such as <phosphonet.ca> and <www.cbs.dtu.dk/services/NetPhosK/> [455] to suggest which kinases might be involved in phosphorylating LCP1 at tyr28 downstream of NOD2; epidermal growth factor receptor (EGFR) and insulin receptor (INSR) were both predicted. Interestingly, while I could not detect EGFR expression in DCs by immunoblot or flow cytometry, an inhibitor of EGFR (EGFRi) inhibited phosphorylation of LCP1 at tyr28 in a dose response (data not shown). An explanation for this result may lie in the fact that EGFRi are non-specific and inhibit other kinases, including RIPK2. A better experiment would have been to use siRNAs and knockdown key kinases predicted to phosphorylate LCP1 downstream of NOD2.

4.2.2.2. Silencing LCP1 to enable investigation of function

In order to conduct experiments to investigate the function of LCP1, I used siRNAs to knockdown expression in primary human monocyte-derived DCs, and effective knockdown was demonstrated both at protein level (Figure 22A siRNA 8), message level relative to GAPDH (Figure 22B left) and mRNA normalised to a non-sense (NS) control siRNA (Figure 22C left). Furthermore, LCP1 was silenced in DCs by an equivalent amount using an LCP1 siRNA that had an AlexaFluor555 tag. The tagged siRNA had been obtained to aid determining which cells had been transfected, though later proved to be superfluous (Figure 22B right, Figure 22C right). Combining the data demonstrated a reduction of mRNA level by 90.0 % (mean Log_{10} [ratio]=-1.131, SEM=0.1942, p=0.0101) over 4 donors (Figure 22D).

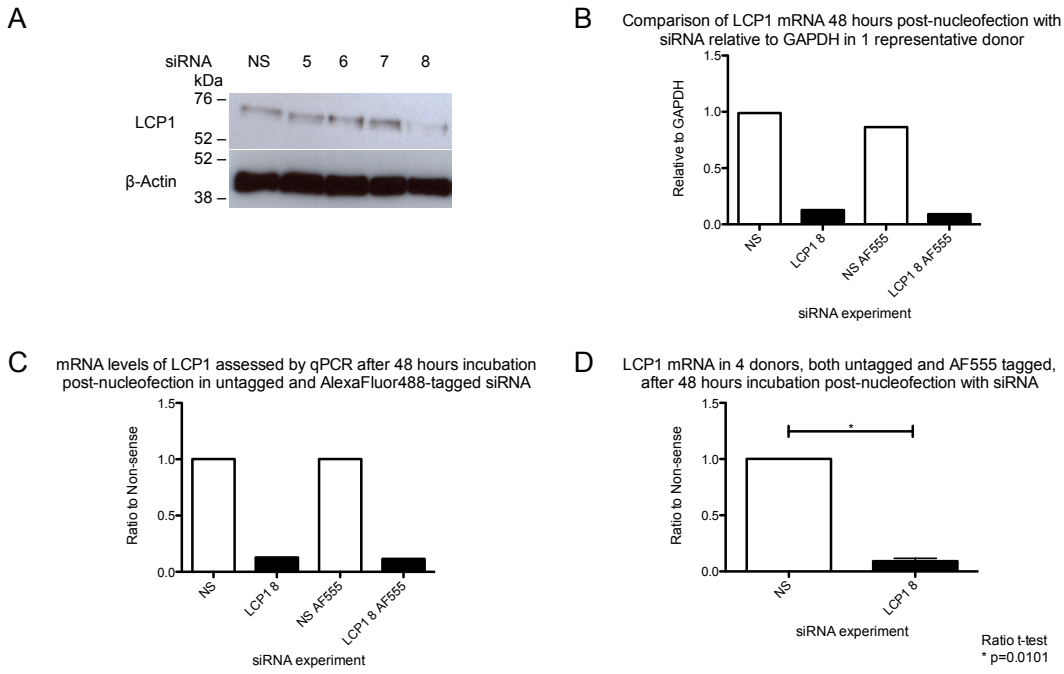


Figure 22: LCP1 is effectively silenced at mRNA and protein level by siRNA targeting LCP1. A) DCs transfected with NS or different LCP1 siRNA and immunoblot for LCP1 or β-actin. B) Comparison of quantity of mRNA of LCP1 in both untagged siRNA and AlexaFluor-555 (AF555) tagged siRNA number 8, relative to GAPDH. C) Comparison of LCP1 and AF555 tagged siRNA as a ratio to NS, demonstrating comparable knockdown of LCP1. D) Demonstration of mRNA levels in 4 donors to LCP1 siRNA (both untagged and AF555 tagged) with a 90.9 % reduction in mRNA level relative to NS.

4.2.2.3. LCP1 knockdown reduces phagocytosis but does not alter downstream bacterial killing in DCs

T-plastin is an LCP1/L-plastin homologue found in solid tissues such as kidney cells. T-plastin was found to be recruited to *S. typhimurium*-induced membrane ruffles in a CDC42-dependent manner where a complex formed between bacterial protein SipA and cellular proteins T-plastin and F-actin, which mediated bacterial invasion. Furthermore, a dominant negative form of T-plastin was shown to reduce invasion of *Salmonella* in HEK293 cells as early as 20 minutes, but this was overcome by 60 minutes incubation time [454]. Neutrophils from an LCP1$^{-/-}$ mouse fail to kill phagocytosed bacteria as they cannot mount an adequate respiratory burst on integrin signalling, but migrate and phagocytose bacteria normally [374].

I hypothesised that LCP1 might function in a similar way in DCs, such that removal of LCP1 would affect bacterial entry into the cell. I therefore investigated whether silencing LCP1 in DCs altered phagocytosis of GFP-*Salmonellae* (*S. typhimurium)*. DCs were transfected with NS or LCP1 siRNA for 48 hours before exposure of the cells to bacteria. I performed a time course and found a significant increase in the number of bacteria phagocytosed at 60 minutes (Figure 23B and Table 17) (0.08108 vs. 0.3600, p=0.0153) and there was a marked difference in the maximum number of bacteria in a single cell (1 vs. 7) in a similar number of cells counted (74 vs. 75).

In order to assess the effect of LCP1 on bacterial longevity within DCs, I then performed a bacterial persistence assay. There was no difference in the ratio of bacteria in LCP1 knockdown DCs compared to NS control transfected DCs from 9

biological replicates (Figure 23C). The mean ratio of the number of CFUs in the LCP1 knockdown group compared to the NS silenced groups was 1.173 and, in calculating a ratio t-test, the mean Log_{10} [ratio]=0.00939 p=0.914, was statistically insignificant (Figure 23D and Table 17).

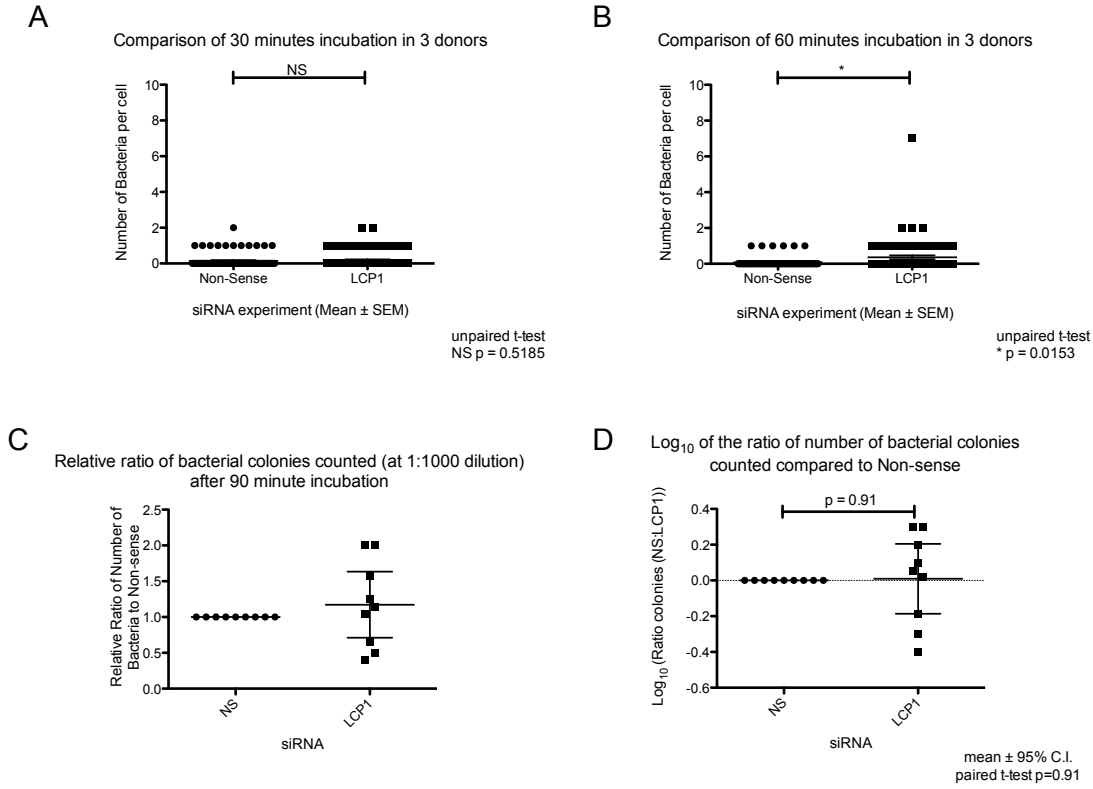


Figure 23: Assessment of the role of LCP1 in phagocytosis and bacterial persistence. A-B) 3 x 10^6 DCs were Amaxa nucleofected with NS or LCP1 siRNA, incubated for 48 hours then infected with GFP-*Salmonella* for A) 30, B) 60 minutes in 3 donors and then stained with anti-LCP1 (Abcam). 3 blinded representative photos were analysed and number of cells counted with or without bacteria and number of bacteria per cell. C-D) 3 x 10^6 DCs from 9 donors were nucleofected (Amaxa) with NS or LCP1 siRNA and incubated for 48 hours. Cells were incubated with GFP-*Salmonella* for 90 minutes and then incubated with gentamicin (100 μg mL^{-1}) for 2 hours. DCs were lysed plated onto agar plates to count colonies. C) Ratio of colonies counted compared to NS. D) Log_{10} of the ratio of number of colonies detected compared to NS, enabling a paired t-test to be done, demonstrating no significant difference between siRNAs.

	Non-sense		LCP1		
Time (min)	**Mean**	**± 95 % CI**	**Mean**	**± 95 % CI**	**p value**
30	0.148	0.082	0.186	0.081	0.519
60	0.081	0.064	0.360	0.216	**0.015**
90	0.123	0.102	0.150	0.087	0.695
180	0.603	0.302	0.723	0.335	0.597
Persistence	-	-	0.009	0.195	0.914

Table 17: Comparison of mean, SD, SEM and unpaired t-test for NS and LCP1 silenced cells infected with bacteria at different time points. Also included is the bacterial persistence assay.

4.2.2.4. LCP1 increases MCP1 release from DCs on MDP stimulation

The LCP1$^{-/-}$ mouse shows defects in cytokine production from T cells [378]. I hypothesised that LCP1 might be involved in cytokine production in innate immune cells such as DCs. In order to assess the role of LCP1 in NOD2 and TLR2 stimulation, DCs transfected with NS or LCP1 siRNAs were stimulated for 24 hours with MDP, PAM or MDP/PAM or left unstimulated. Cell supernatants were assessed for cytokine release using a 17-plex (Luminex) cytometric bead assay. LCP1 did not appear to be required for the release of cytokines such as TNFα, IFNγ, IL-10, or IL-1β. However, there was an increase in release of Monocyte chemotactic protein 1 (MCP1) on MDP triggering following LCP1 knockdown (mean Log_{10} [ratio]=0.03198, SEM=0.006672, ratio t-test p=0.0409) (Figure 24A-B), but not in PAM or MDP/PAM stimulated cells. The actual difference is very small as a ratio, but due to the very tight clustering of secretion as a result of NOD2 triggering by MDP it is statistically significant. The functional relevance of this will be discussed later.

Loss of LCP1 was also found to reduce IL-12p40 secretion in dual stimulated cells. Whilst it did not reach significance it certainly was trending towards significance with a ratio t-test p value at 0.0527, mean -0.1550, SEM 0.03707 (Figure 24C-D).

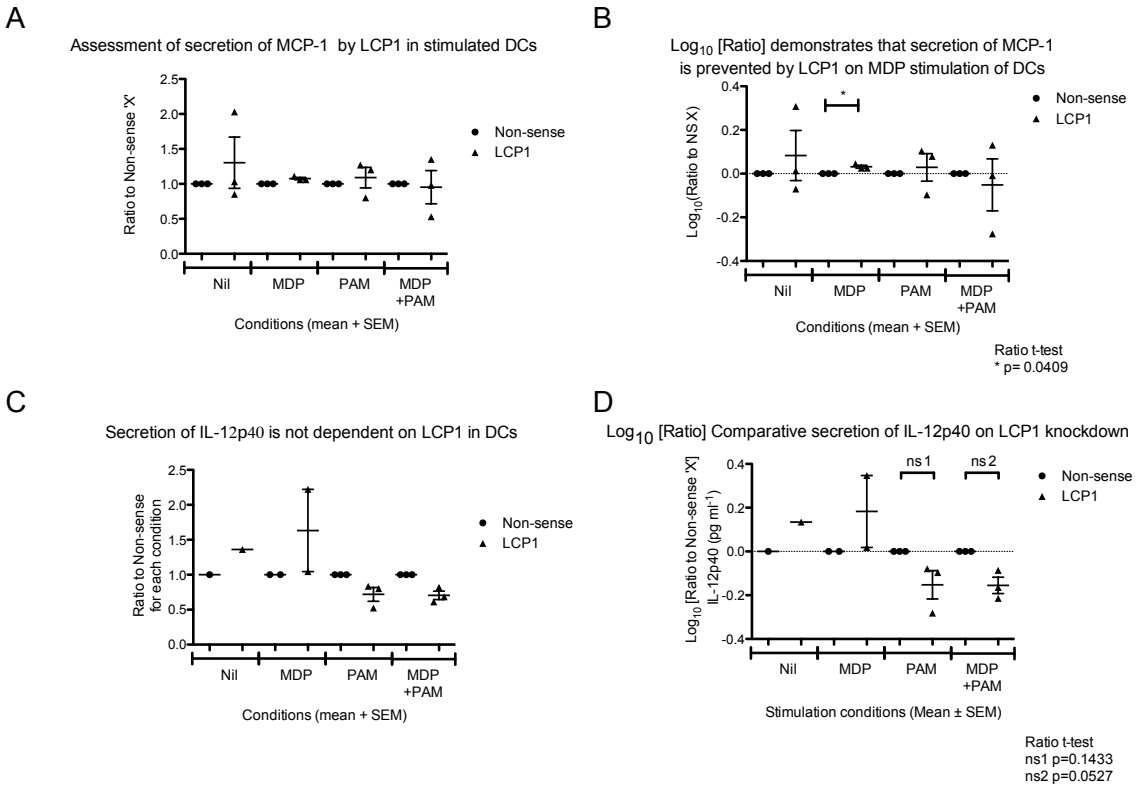


Figure 24: Assessment of the role of LCP1 on cytokine secretion. 6 x10^6 DCs silenced for NS or LCP1 and left unstimulated or stimulated by MDP (10 µg mL^{-1}), PAM (1 µg mL^{-1}) or dual. Supernatants analysed for MCP1 and IL-12p40 secretion. N=3 for each condition.

4.2.2.5. LCP1 does not affect DC survival or maturation

Phosphorylation of LCP1 has been shown to confer resistance to TNFα-induced apoptosis in breast cancer cells [371]. I investigated whether silencing LCP1 had any impact on cell survival or maturation, both in unstimulated and stimulated conditions. NS or LCP1 siRNA were used to silence LCP1 and after 24 hours incubation the cells were stimulated with MDP, PAM or MDP/PAM for a further 24 hours. Using flow cytometry I measured cell survival by using a fixable Live/Dead AlexaFluor660 marker and there was no difference in LCP1 silenced cells (Figure 25A). Furthermore, I examined the ability of the silenced cells to up-regulate co-stimulatory activation markers CD80 (Figure 25B) and CD86 (Figure 25C) and LCP1 silencing did not significantly change the maturation markers.

As LCP1 is an actin bundling protein, the role of LCP1 in shuttling of proteins to the cell surface by the cytoskeleton or in the effective loading of peptide onto MHC II receptors was investigated. I investigated this indirectly initially by determining levels of HLA-DR pre and post LCP1 knockdown and MDP/PAM stimulation. Antibody to Class II-associated invariant chain peptide (CLIP) recognises surface immature MHC II loaded with the invariant chain, and if LCP1 was involved in the efficient loading of peptide the amount of surface CLIP should reduce. In LCP1 silenced cells equivalent surface expression of both CLIP and HLA-DR was observed, and whilst there was a trend towards a reduction in CLIP in PAM stimulated cells it was not significant (Figure 25D-F).

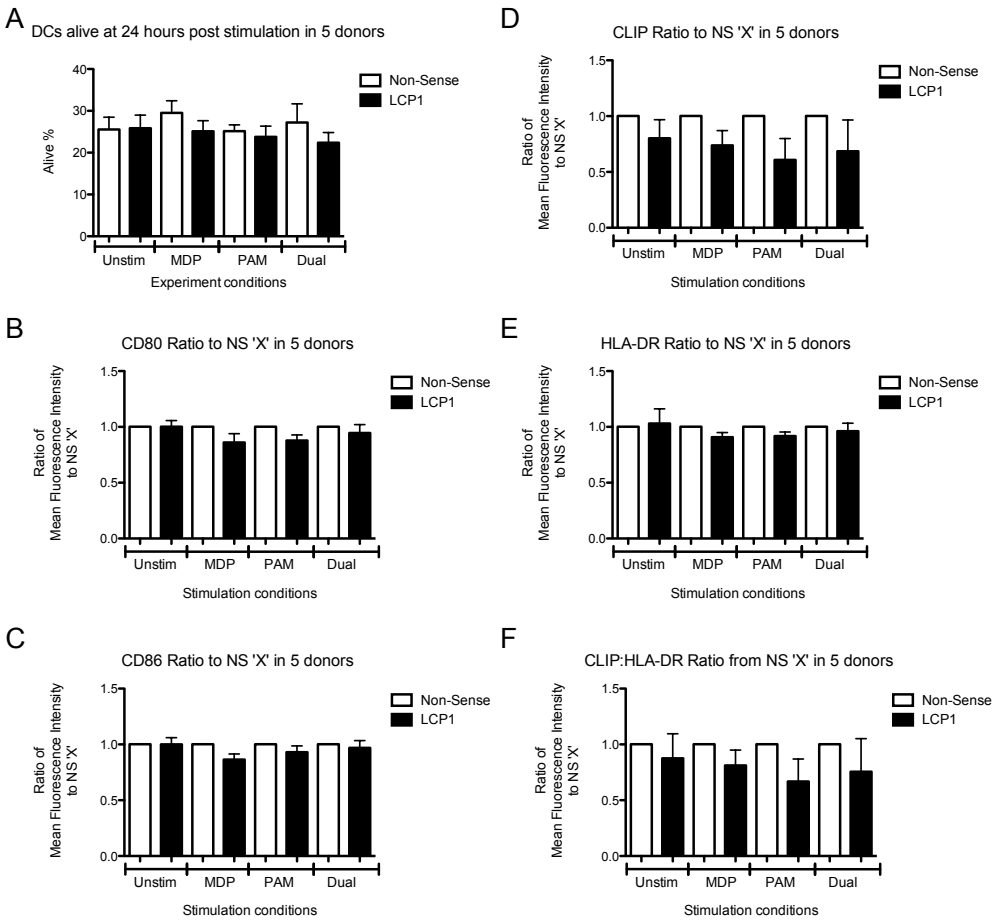


Figure 25: Assessment of the role of LCP1 in cell survival, maturation and MHCII loading/HLA-DR expression in DCs. 6 x 10^6 DCs were Amaxa nucleofected with NS or LCP1 siRNA and incubated for 24 hours before being harvested and replated in 6 well plate at 1.5 x 10^6 (of pre-nucleofected) cells per well, and stimulated for 24 hours with MDP (10 μg mL^{-1}), PAM (1 μg mL^{-1}), or dual (MDP 10 μg mL^{-1} and PAM 1 μg mL^{-1}). A) Cells stained with live/dead stain, analysed by flow cytometry and percentage alive calculated. Mean fluorescence intensity (MFI) for CD80 (B) and CD86 (C) on surface of DCs expressed as a ratio to the unstimulated of each condition, demonstrating no effect on maturation. MFI for CLIP (D) and HLA-DR (E) on surface of DCs expressed as a ratio to the unstimulated of each condition, demonstrating no effect on loading of peptide onto MHCII. F) Ratio of CLIP to HLA-DR demonstrating no effect seen between both.

4.2.3. LCP1 Discussion

4.2.3.1. LCP1 phosphorylation and effective silence by siRNA

LCP1 has been demonstrated to be phosphorylated when human DCs are stimulated with a panel of PRR ligands (Figure 21). Within the literature, LCP1 appears to be phosphorylated at Ser5 or Ser7 [456] [457]. To investigate this further would require immunoprecipitation of LCP1 stimulated by different PRR ligands, followed by MS analysis of enriched phospho-peptide or immunoblotting with a phospho-ser5/7 specific antibody. One was requested from one of these groups [457] but at the time of writing it had not arrived.

Understanding LCP1's function can readily be assessed by examining the effect removal of LCP1 has on cellular function when it is silenced by siRNA knockdown. An siRNA targeting sequence 5'-CAGAGTAAACAAACCGCCATA-3' (siRNA number 8) effectively silenced LCP1, and achieved 90.9 % knockdown at message level and clear loss of protein on the immunoblot (Figure 22).

4.2.3.2. LCP1 is important for phagocytosis but not bacterial persistence

The initial work on phagocytosis was attempted through beads to avoid the need for bacterial handling. Carboxylated beads may lack the virulence of live bacteria, but they can be modified to stimulate different PRRs by using different PRR ligands and change the phagocytic compartment the beads are processed in. Confocal and flow cytometry methods to utilise bead based assays were attempted, but bleeding of fluorescence into other channels prevented their use as a good assay (data not

shown). However, the bacteria were clearly evident on confocal microscopy and so proved a useful technique for assessing phagocytosis.

The data presented here is in agreement with the T-plastin data in that phagocytosis was altered on LCP1 silencing at 60 minutes, which was delayed compared to 20 minutes seen with T-plastin [454]. At later time points the differences between NS and LCP1 silencing disappear, which is in agreement with the T-plastin and neutrophil data [374]. However, unlike the inability of neutrophils to kill phagocytosed bacteria on LCP1 silencing [374] there was no difference seen in the bacterial persistence assay in DCs (Figure 23E+F). This may be explained by a difference in cell type, that of DCs compared to neutrophils, and that DCs kill bacteria in a manner that enables effective antigen presentation [458], rather than the destructive killing of phagocytosed bacteria by neutrophils [459]. LCP1 is involved in bacterial killing in neutrophils by activating the respiratory burst on integrin activation [374]. However, in DCs there is a less potent respiratory burst than in neutrophils [460] that can be increased by TLR stimulation [461], but may not be necessary for antigen presentation [462]. Therefore, the differences observed between neutrophils and DCs may be because, firstly, the respiratory burst in DCs utilises an LCP1-independent pathway. Secondly, this may confirm that in neutrophils LCP1 is an integral part of the integrin signalling pathway [463] [464], which is required for a functional respiratory burst in neutrophils [465] [466] [467].

In bacterial persistence assays, the infection and incubation time of the bacteria varies according to bacterial strain, cell type and author [468] [469] [470] but typically involves a total incubation time of 3 hours. In CD patients we had previously shown

1 hour infection followed by 2 hour incubation with gentamicin to be significant [190]. DCs were infected, to assess for bacterial persistence, for 90 minutes before extracellular bacteria were killed using gentamicin for 2 hours. There was no difference seen in the number of CFU between NS or LCP1 knockdown. Further work would compare the effect seen at 60 minutes, given the difference in phagocytosis. However, using a kill curve to assess bacterial killing by gentamicin, 10 minutes might have been sufficient (see Appendix 1 Figure 1) and would corroborate the 60 minute difference seen confocally, but risks being not a long enough incubation time to assess persistence effectively. Longer incubation times such as 4 hours would also be beneficial and comparison with AIEC may also provide further assessment.

4.2.3.3. LCP1 and cytokine production

MCP1 is a chemokine that is part of the family with a C-C motif. MCP1 is also known as CCL2 and it is secreted by monocytes, macrophages and DCs [471]. CCL2 is more expressed in $CD14^+$ tissue resident DCs rather than peripherally derived monocyte-derived DCs or $CD11c^-$ lymphoid DCs [472]. Co-stimulation of LPS with R848 or polyI:C reduced the production of CCL2, and this then had an effect on the production of IL-12 and the drive into T_H1 subset [473]. Interestingly, TB infection in Mexicans was found to be greater in SNPs for CCL2, with high levels of CCL2, seen in the at-risk alleles of AG or GG, to be inversely related to IL-12p40 levels [474]. The reduction in IL-12p40 was particularly seen in dual stimulated cells (Figure 24). Recently MCP1/CCL2 has been demonstrated to drive accumulation of inflammatory monocytes in the mucosa and cause colitis [475]. There is no data on LCP1 and IL-12p40.

4.2.3.4. LCP1 did not alter integrin expression

It is well recognised that integrins are integral to cellular function, both in terms of adhesion [476] [477] and signalling function [374]. Integrins function in a bidirectional fashion: they are activated internally, a mechanism of inside-out control, but also once activated inform internal cellular functions, an outside-in signalling pathway. Components of the signalling cascade that control integrin function have included Rho-GTPases, L-plastin [376] and Syk [374]. As noted above, LCP1$^{-/-}$ neutrophils phagocytose bacteria effectively but fail to kill them due to a lack of respiratory burst on integrin signalling [374]. As a result, integrin expression on DCs was investigated on LCP1 silencing, and there was a suggestion of decreased expression of β2-integrin on LCP1 silencing in dual stimulated cells, there was no significant difference seen in β1, β2, CD11b activated, and αV due to too few replicates (data not shown).

4.2.4. LCP1 Conclusion

LCP1 is highly differentially phosphorylated on PRR triggering generally, including via NOD2.

In the data presented here, I have shown that LCP1 has a role in phagocytosis but has no impact on killing of *Salmonella* in DCs. In the future, it would be useful to determine the relevance of this effect on phagocytosis for a broader range of bacteria, such as AIEC and other commensals, and to assess whether this defect has implications for bacterial inactivation or antigen presentation by DCs. I have also demonstrated that LCP1 is involved in release of MCP1/CCL2 and IL-12p40. MCP1/CCL2 has recently been implicated in recruitment of inflammatory monocytes required to clear enteric bacteria, such as *Citrobacter rodentium* in mice that models human infection with pathogenic *E. coli* [475]. Furthermore, the role of LCP1 on NOD2 triggering could be investigated by measuring the release of CCL2 and IL-12p40 in DCs from cells of FS1007insC CD patients.

4.3. Src homology domain 2 containing protein tyrosine phosphatase 1 (SHP1) or Protein Tyrosine Phosphatase Non-receptor 6 (PTPN6)

4.3.1. Introduction

SHP1 is a tyrosine phosphatase that is important in dephosphorylation of phosphorylated residues in immune cells. SHP1 is expressed in haematopoietic cells [478], smooth muscle [380] and epithelial cells [381]. Activation of SHP1 by phosphorylation has been described on stimulation of the INSR [384], CCR5 [385], TLR4 [386] and of CD4 [387]. Phosphorylation of SHP1 is dependent on c-Src [388].

Knowledge of the function of SHP1 was delineated in the 'motheaten' knockout mouse, where $SHP1^{-/-}$ knockout mice display cutaneous abscesses, proteinuria, elevated anti-dsDNA antibody levels and deranged cytokines, such as increased expression of IFNγ, TNFα and IL-6, but reduced IL-2, and equivocal IL-10 and GM-CSF [479]. Other downstream effects of SHP1 include negative regulation of ITIMs within leucocytes and epithelial cells [382] [383], resulting in reduced inflammation due to cytokine [386] [389] [390] [391] [392] and chemokine release [480]. Loss of SHP1 in T cells prolongs tyrosine phosphorylation of the T cell receptor and results in T cell hyper-proliferation and an autoimmune phenotype [387].

4.3.2. SHP1 Results

4.3.2.1. SHP1 is phosphorylated on MDP stimulation

SHP1 was a putative target on the MS data on MDP stimulation of DCs (MASCOT 73 in fraction 8 and 59 in fraction 9), but on dual stimulation with MDP/PAM it was not significantly phosphorylated (MASCOT 139, 126/127 -1.095). To clarify if it was differentially phosphorylated on MDP stimulation I activated DCs with MDP, lysed the cells and phosphoprotein-enriched the sample prior to immunoblotting with anti-SHP1. This revealed marked phosphorylation on MDP stimulation (Figure 26A, lane 6).

4.3.2.2. Silencing of SHP1 by siRNA

In order to then understand the function of SHP1 in the context of DC stimulation by MDP, SHP-1 was silenced by siRNA effectively at protein level at 24 hours (Figure 26B, lane 5), and at the mRNA level (relative to GAPDH Figure 26C), with 55.63 % knockdown achieved at 24 hours (Figure 26D, SEM=0.1804, 1way ANOVA not statistically significant).

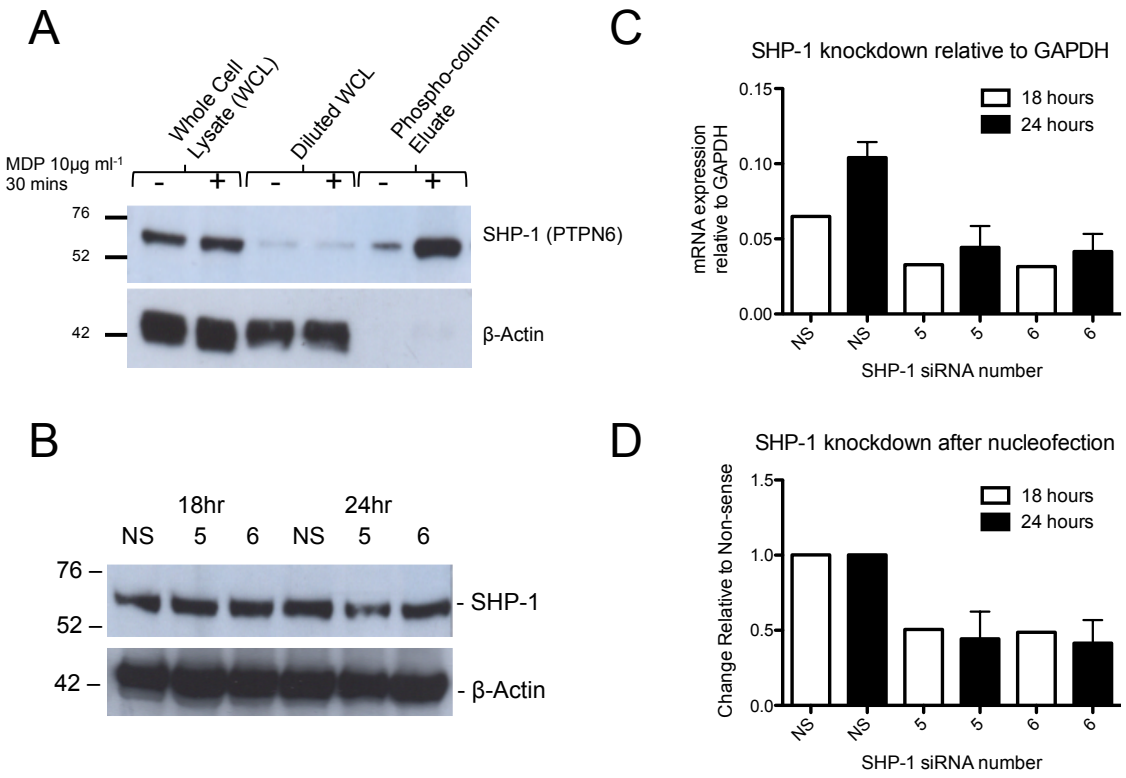


Figure 26: Investigation of SHP1 phosphorylation by MDP and knockdown of SHP1 using siRNA. A) 30 x 10^6 DCs were left unstimulated or stimulated with MDP (10 µg mL^{-1}) for 30 minutes, phosphoproteins extracted as described earlier, concentrated and immunoblot for SHP-1. B) 3 x 10^6 DCs were nucleofected (Amaxa) with NS or SHP-1 siRNA (Qiagen) and incubated for 18 or 24 hours and immunoblotted for SHP-1 demonstrating knockdown at the protein level in siRNA 5. β-Actin provided as loading control. C-D) Graphs demonstrating mRNA level of SHP-1 after nucleofection of 3 x 10^6 DCs with NS and SHP-1, shown as relative to GAPDH (C) and to NS (D). N=3.

4.3.2.3. Loss of SHP1 alters signalling via p44/42 MAPK

In LPS stimulated BMDCs silencing of SHP1, by stibogluconate or siRNA, resulted in reduced p38 signalling but increased phosphorylation of p44/42 MAPK and phosphorylation of JNK [389]. Using RAW 264.7 murine macrophage cell line, overexpressing C453S mutant SHP1, whose protein exhibited loss of phosphatase activity, ERK1/2 was phosphorylated pre-stimulation and dephosphorylated post-stimulation. Furthermore IRAK1 was more phosphorylated by SHP1 and resulted in greater STAT1 phosphorylation when compared to wildtype SHP1 [390].

Being a phosphatase and a negative regulator of cellular signalling, it was hypothesised that loss of SHP1 would impact intracellular signalling on MDP stimulation. DCs were silenced by nucleofection of NS or SHP1 siRNA for 24 hours and then stimulated with MDP and phosphorylation of different intracellular signalling proteins such as p38 MAPK, p44/42 MAPK, NF-κB, and IKKα were compared (Figure 27). Phosphorylation of p38 occurred at 60 minutes and was reduced following SHP1 knockdown (compare in row 2 lane 4 with lane 8 in Figure 27); of p44/42 it occurred at 30-60 minutes (row 4 lanes 3-4, Figure 27) and again reduced following SHP1 knockdown (row 4 lanes 7-8, Figure 27), and there was less phosphorylation of NF-κB at 30-60 minutes (in row 6 compare lanes 3-4 with 7-8, Figure 27). Phosphorylation of IKKα appeared to be greater and more sustained following SHP1 knockdown (row 8 lane 8, Figure 27) whereas by 60 minutes in nonsense it was dephosphorylated (row 8 lane 4, Figure 27). In order to confirm this using another technique, the phosphorylation of intracellular signals such as p44/42 and NF-κB was further confirmed using Phosflow technique (Figure 28).

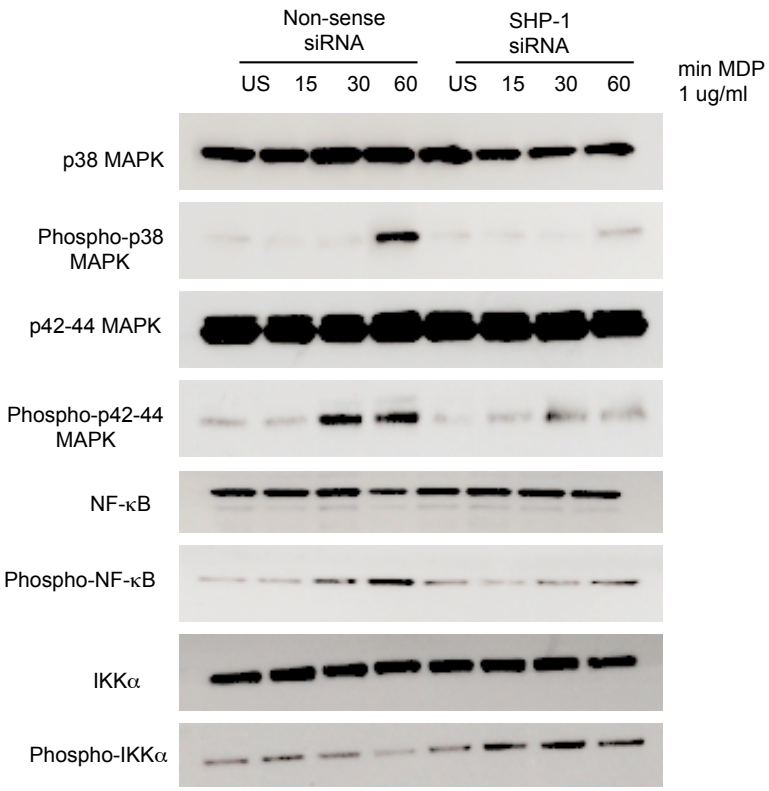


Figure 27: Effect of SHP1 knockdown on MDP-mediated MAPK and NF-κB activation. 3 x10^6 DCs nucleofected with NS siRNA or SHP1 siRNA number 5 (Qiagen) and incubated for 24 hours, then stimulated for the times shown with MDP 1 μg mL^{-1} or RPMI. N=3.

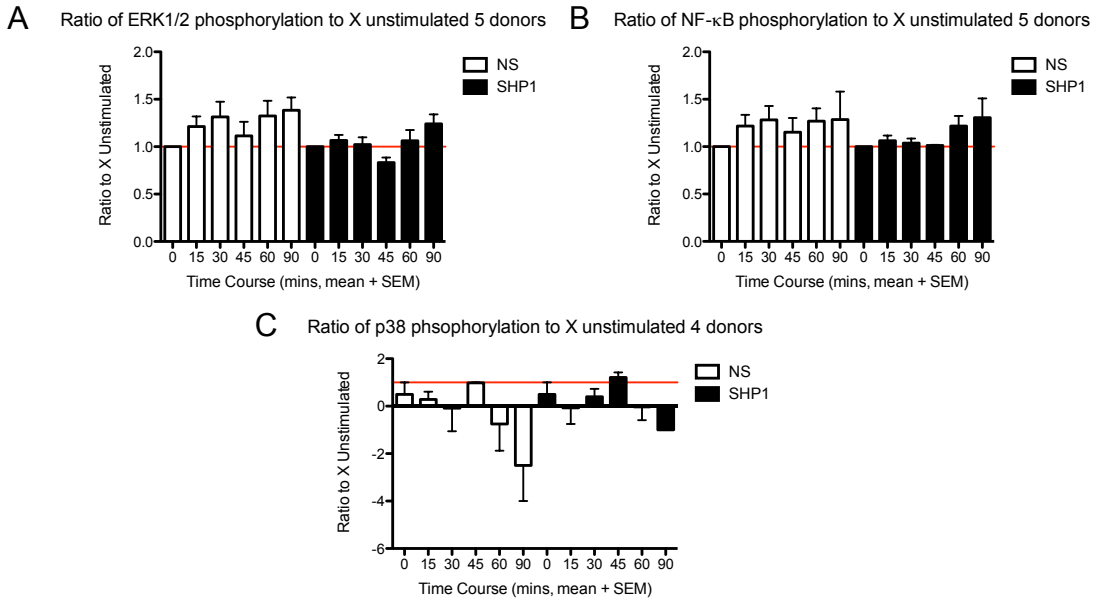


Figure 28: Comparison of phosphorylation of known intermediates ERK1/2, NF-κB or p38 MAPK using Phosflow technique demonstrating loss of signalling in SHP1 knockdown cells.

4.3.2.4. Loss of SHP1 increases secretion of MIP1β or CCL4

SHP1 has been previously shown to downregulate receptor function, such as CD300F [391] or TLR2 p85 subunit [392] to reduce IL-8 release. Secretion of IL-1β in neutrophils [393], IL-1β and IL-12p70 in bone marrow derived macrophages (BMDMs) [389], and IL-12p40 from BMDMs [386] are all dependent on SHP1. SHP1 has also been implicated in TNFα release, although its effect is different in different cell types; some have found that there is SHP1-dependent TNFα release in alternatively-activated macrophages [389] and in splenocytes and macrophages [390], yet others have found SHP1-independent TNFα release in BMDMs [386].

Being a negative regulator of cellular signals, it was hypothesised that potential loss of p44/42 MAPK and NF-κB activation by removal of SHP1 would affect cytokine production. I assessed this by using a Luminex assay. Here DCs were transfected with NS or SHP1 siRNAs and after 24 hours incubation were left unstimulated or stimulated with MDP, PAM or MDP/PAM for a further 24 hours. There was no appreciable difference in cytokine production from the supernatant in any scenario except MIP1β, where there was a statistically significant increase in MIP1β release on MDP stimulation (mean Log_{10} [ratios]=0.08022, SEM=0.008459, ratio t-test p=0.0109) and this was not seen on TLR2 or NOD2/TLR2 stimulation (Figure 29A). Assessment of IL-12p40 was investigated using an ELISA and it was observed that there was increased release of IL-12p40 on NOD2 stimulation (mean Log_{10} [ratios]=0.4859, SEM=0.1238, ratio t-test p=0.0294) but not on TLR2 or NOD2/TLR2 stimulation (Figure 29B). Cytokines, such as TNFα and IL-10 (Figure 29C), or IL-1β and IL-8 (data not shown) were not affected.

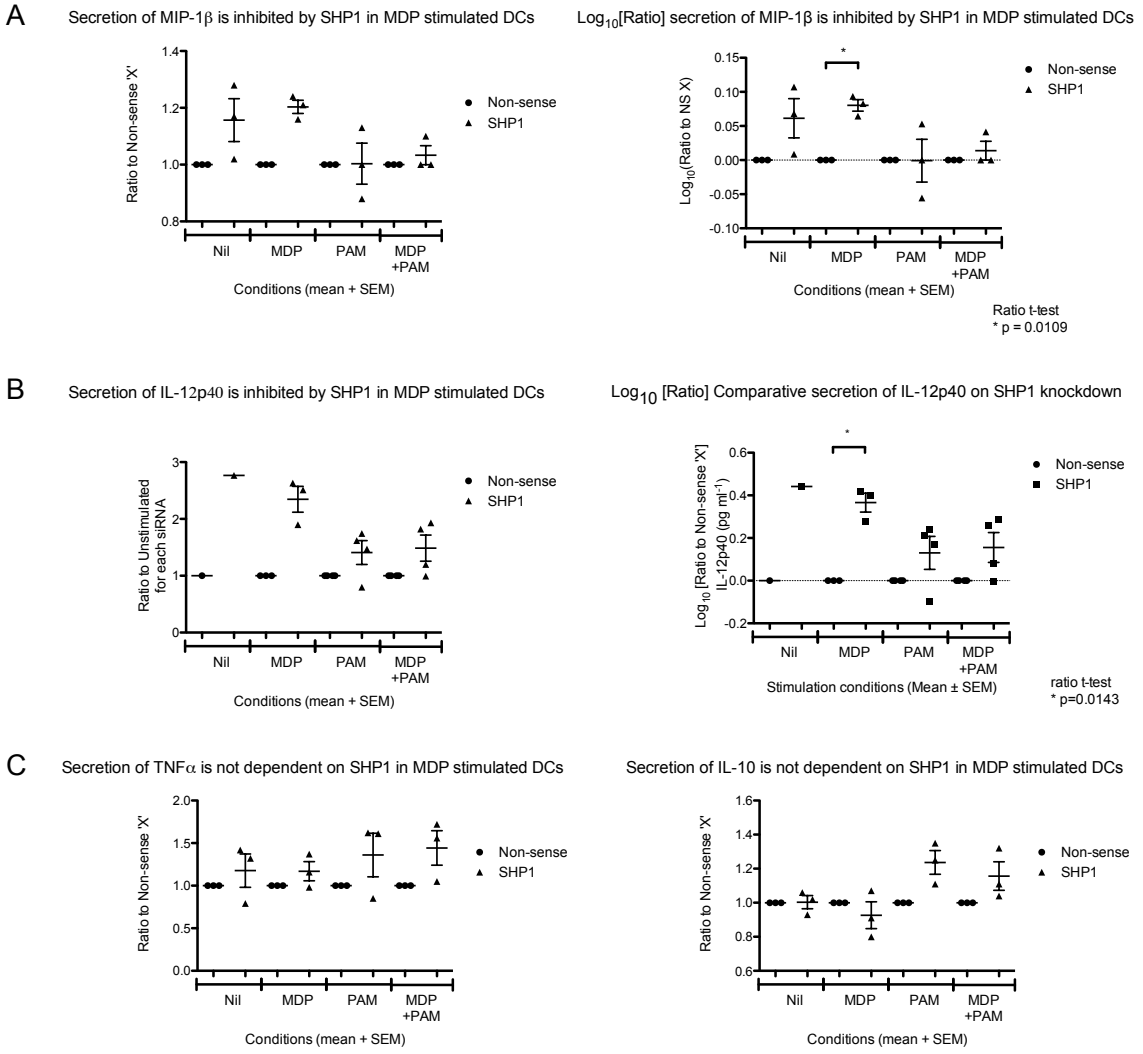


Figure 29: Effect of SHP1 on MIP1β (CCL4) and IL-12p40 but not TNFα or IL-10 secretion in MDP stimulated cells. DCs silenced for NS or SHP1 were incubated for 24 hours then stimulated for a further 24 hours with MDP (10 μg mL^{-1}), PAM (1 μg mL^{-1}), or dual (MDP 10 μg mL^{-1} and PAM 1 μg mL^{-1}). Supernatants were collected for analysis by cytometric bead assay (A+C) or ELISA (B). N=3-4.

4.3.2.5. Loss of SHP1 does not impact DC survival or maturation

Finally to assess if SHP1 affects DC maturation or survival, DCs were transfected with NS and SHP1 siRNAs, as before, prior to stimulation with different PRR ligands. No difference in survival was observed following SHP1 knockdown (Figure 30A). Furthermore, whilst stimulation occurred normally there was no difference between NS or SHP1 for markers of activation, CD80 (Figure 30B) and CD86 (Figure 30C), or MHC II expression (Figure 30E), or of immature CLIP loaded HLA-DR on the surface of DCs (Figure 30D).

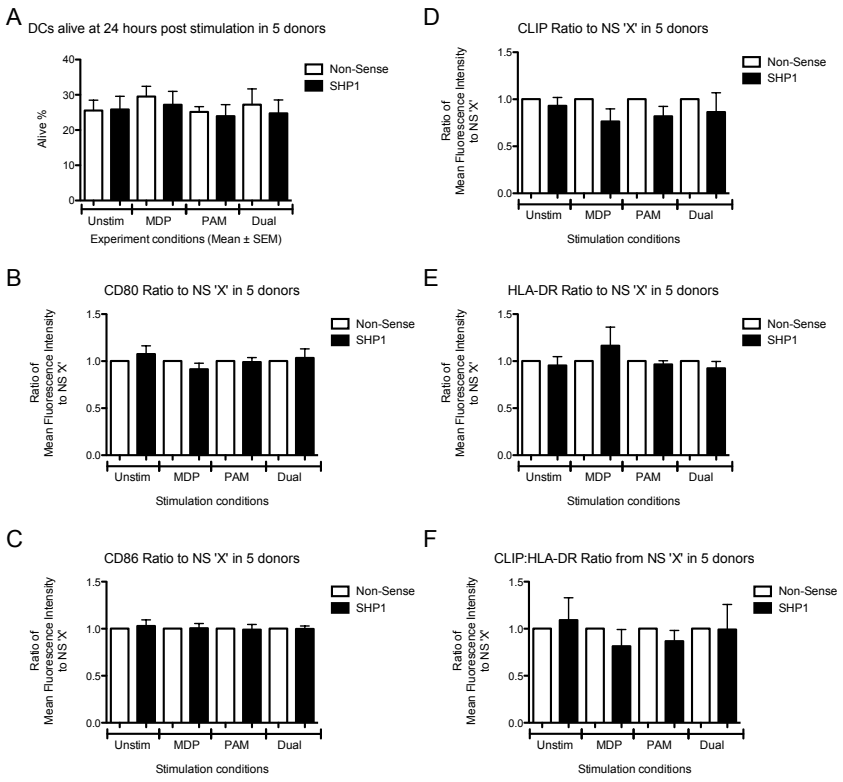


Figure 30: Assessment of SHP1 function in survival, maturation or MHCII loading/HLA-DR expression in DCs. 6 x 10^6 DCs were Amaxa nucleofected with NS or LCP1 siRNA and incubated for 24 hours before being harvested and replated in 6 well plate at 1.5 x 10^6 (of pre-nucleofected) cells per well, and stimulated for 24 hours with MDP (10 μg mL^{-1}), PAM (1 μg mL^{-1}), or dual (MDP 10 μg mL^{-1} and PAM 1 μg mL^{-1}). A) Cells stained with live/dead stain, analysed by flow cytometry and percentage alive calculated. MFI for CD80 (B) and CD86 (C) on surface of DCs expressed as a ratio to the unstimulated of each condition, demonstrating no effect on maturation. MFI for CLIP (D) and HLA-DR (E) on surface of DCs expressed as a ratio to the unstimulated of each condition, demonstrating no effect on loading of peptide onto MHCII. F) Ratio of CLIP to HLA-DR demonstrating no effect seen between both.

4.3.3. SHP1 Discussion

4.3.3.1. SHP1 and its role in NOD2 signalling

Stimulation of NOD2 by MDP resulted in marked phosphorylation of SHP1. Stimulation of different receptors results in SHP1 phosphorylation and was first described by stimulation of the insulin receptor [384], and subsequently others such as CCR5 [385], TLR4 [386], and by CD4 stimulation [387]. SHP1 has since been involved in a number of different signalling cascades, where it dephosphorylates ITIM residues.

4.3.3.2. SHP1 and cytokine production

One of the main downstream effects of SHP1 is control of cytokine release. Stimulation of $SHP1^{mev/mev}$ BMDMs have been shown to produce increased secretion of IL-12p70 and IL-1β [389] but others have demonstrated reduced levels of IL-12p40 on stimulation with LPS and PAM due to hyperphosphorylated PI(3)K [386]. In contrast, TNFα was unaffected in its production from $SHP1^{mev/mev}$ cells with LPS stimulation [386], which contradicted the experience of another group where stimulation of $SHP1^{mev/mev}$ cells and of cells with SHP1 silenced by siRNA and stimulated with LPS resulted in TNFα and IL-1β overproduction and a reduction in IFNβ at both mRNA and protein levels [390]. TNFα release has further been shown to increase on IL-4 stimulation of macrophages co-exposed to stibogluconate [389]. Co-stimulation of the ITIM CD300F, with anti-CD300F antibodies, and TLR4, with LPS, resulted in loss of TRIF and MyD88 dependent IL-8 production, and this effect was dependent on functional SHP1 [391]. Co-stimulation of the ITIM CEACAM1 and TLR2 resulted in SHP1-dependent dephosphorylation of TLR2 p85 subunit and a reduction of IL-8 when compared with TLR2 stimulation alone [392].

In keeping with these contradictory results, whilst SHP1 knockdown by siRNA in primary human DCs resulted in no increased release of TNFα, it did result in increased release of MIP1β/CCL4 and IL-12p40 on NOD2 stimulation (Figure 29). If loss of these effectors occurred in NOD2 FS1007insC expressing cells, this would result in defective immunity against microbes, whose abnormal persistence would become a trigger for inflammation.

4.3.3.3. Cell migration and control by SHP1

In a recent study, cell migration was studied in vivo by injecting NS or SHP1 silenced BMDCs into the footpad of mice then 24 hours later the lymph nodes were removed and analysed for CSFE labelled cells, and a 4-fold increase in cells migrated with SHP1 silencing than without was found [389]. Higher levels of activated PI(3)K products were associated with increased stickiness of macrophages, which was reversed using wortmannin, resulting in a reduction in macrophage migratory ability [394]. In the future I would want to investigate this aspect further by measuring the activated PI(3)K products and optimise a migration assay that I had started to develop for LCP1 silenced cells. The changes in DC migration in the context of CCL21 stimulated cells for the chemokine receptor CCR7 in NS or SHP1 siRNA cells would further demonstrate the role of SHP1 in DC function on NOD2 stimulation.

4.3.3.4. SHP1 determines phagocytic potential

SHP1 has also been implicated in phagocytosis. Removing SHP1 has been shown to increase the phagocytosis of an encapsulated *Streptococcus suis* compared to a non-silenced cell line, with associated phosphorylation of Akt and PKC [356]. The authors

postulate that SHP1 may be one of the negative regulators of phagocytosis that enables *Streptococcus suis* to evade phagocytosis. Furthermore, stimulation of the ITIM CD300F prevents the blockade of phagocytosis caused by the activation of B-cell activation factor of the tumour necrosis factor family (BAFF) in an SHP-1 and PI(3)K dependent manner [481].

Phagocytosis in DCs is a vital function, and this could have been investigated more fully using an optimised phagocytosis assay or by using GFP-*S. typhimurium*. Indeed if phagocytosis was shown to be defective following SHP1 reduction, the killing of the bacteria that do make it into the cells could then be assessed using a bacterial persistence assay.

4.3.4. SHP1 Conclusion

SHP1 is a phosphatase that is vital for the signalling pathways of a number of different inhibitory and stimulatory receptors, resulting in the production of different cytokines, such as IL-8, TNFα and IFNγ. However, in DCs its phosphorylation at 30 minutes on stimulation of NOD2 with MDP is a novel finding. I also found a requirement for SHP1 in production of IL-12p40 and MIP1β/CCL4 following NOD2 stimulation by MDP. If FS1007insC expressing cells show defective SHP1 activation, this might lead to dysregulated IL-12p40 and CCL4 release in tissues.

4.4. High Mobility Group Protein B1 (HMGB1)

4.4.1. Introduction

HMGB1, a DAMP, has two main functions: as a DNA-transcription regulator and as a cytokine that binds the RAGE receptor. Its phosphorylation status determines its localisation within the cell, with phosphorylated HMGB1 exiting the nucleus and entering the cytoplasm [482] and in its dephosphorylated state residing within the nucleus. HMGB1 is phosphorylated by PKC [400] on a serine residue necessary for secretion. HMGB1 has been shown to translocate out of the nucleus into the cytoplasm in response to starvation and ROS, where it induces autophagy by associating with Beclin1 and causing the dissociation of Beclin1 from BCL2 [402].

4.4.2. HMGB1 Results

4.4.2.1. HMGB1 is dephosphorylated on MDP stimulation of DCs

HMGB1 was identified in the MS data for MDP stimulation alone (MASCOT 140 phosphorylated in unstimulated fraction 7) but was subsequently found on dual stimulation data to be not significantly phosphorylated (MASCOT 49, 126/127 - 1.009).

In order to verify if HMGB1 was dephosphorylated on stimulation of DCs by MDP an immunoblot of HMGB1 was done on the phospho-eluate demonstrating low levels of HMGB1 in WCL (row 1, lanes 1-2, Figure 31A). HMGB1 was dephosphorylated in the phospho-eluate (in row 1, compare lane 5 with lane 6, Figure 31A).

4.4.2.2. Transcription of HMGB1 is unaffected by PRR stimulation

As HMGB1 is a nuclear transcription protein, to assess if there was any transcriptional upregulation of HMGB1 on PRR stimulation, mRNA levels of HMGB1 were assessed over different stimulation of PRRs, and found to be no different to NS compared to NOD2 knockdown (Figure 31B).

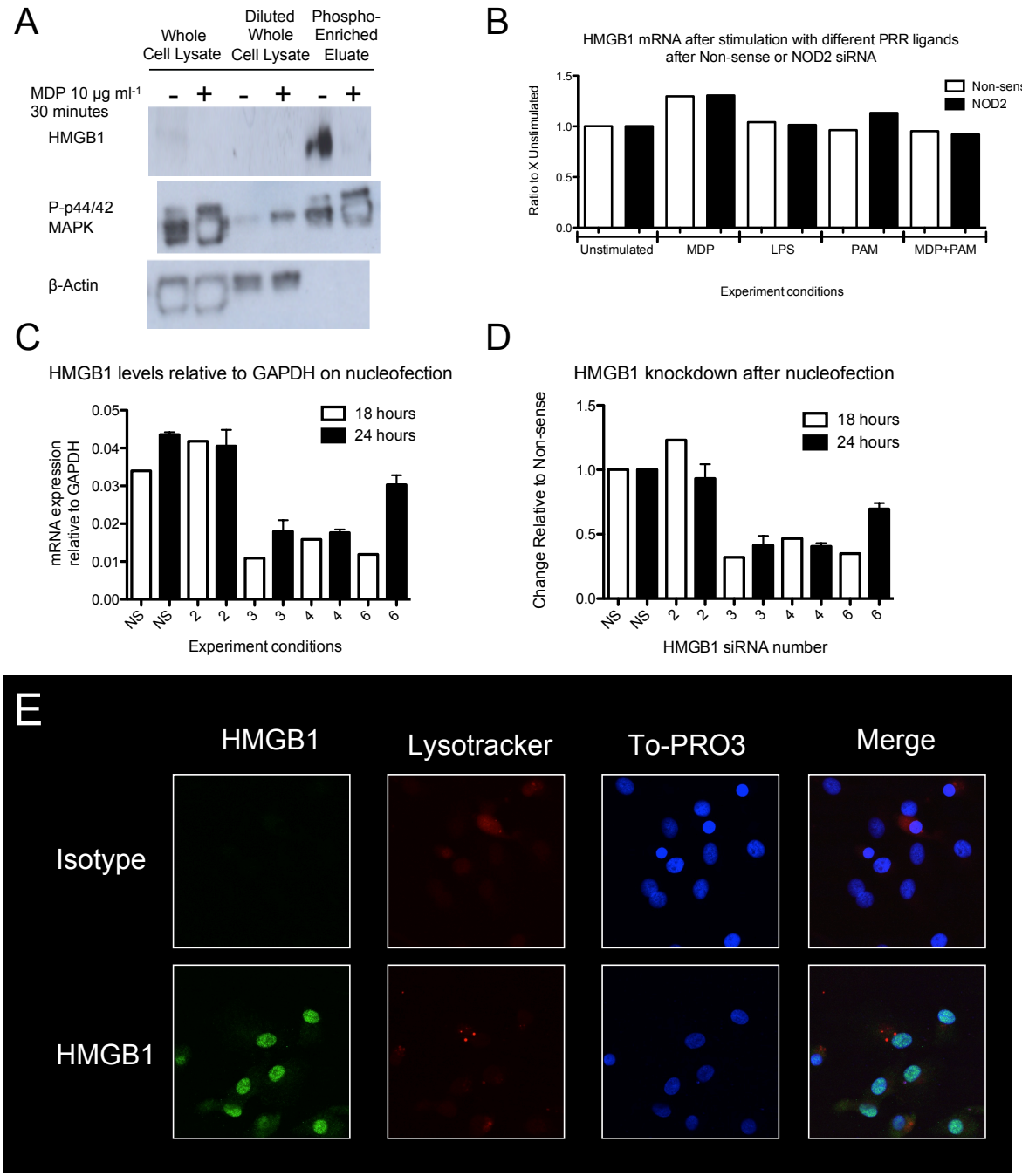


Figure 31: HMGB1 phosphorylation status is dependent on NOD2 stimulation by its ligand MDP, but its mRNA transcription level is not. A) Demonstration of dephosphorylation of HMGB1 in the phospho-enriched eluate by NOD2 stimulation with MDP 10 µg mL^{-1} for 30 minutes. B) Comparison of HMGB1 mRNA on 24 hours stimulation of DCs by different PRR ligands with NOD2 or non-sense siRNA demonstrating that HMGB1 transcription is not under PRR control. C) and D) qPCR of mRNA levels of HMGB1 relative to GAPDH (C) and relative to non-sense (D). E) Confocal study to demonstrate nuclear localisation of HMGB1 at rest compared to isotype. Lysotracker demonstrates cytosol localisation, and To-PRO3 as a nuclear stain.

4.4.2.3. HMGB1 can be silenced in DCs

HMGB1 is readily knocked down to 50 % baseline levels by siRNA on qPCR (Figure 31C+D). Protein level was not quantified except by confocal visualisation.

4.4.2.4. HMGB1 is localised to the nucleus

HMGB1 usually resides in the nucleus as shown on this confocal image (Figure 31E) comparing HMGB1 and an isotype control. Lysotracker was used as a marker of cytoplasmic organelles.

4.4.2.5. HMGB1 and CCR7 surface expression

Extracellular HMGB1 reduction by anti-HMGB1 antibodies was shown to reduce CCR7 expression [401] and as a result reduce DC migration in response to CCL19. In order to test whether HMGB1 release increases CCR7 expression on DCs, human DCs were silenced for NS or HMGB1 by siRNA and incubated for 24 hours before stimulation with MDP. In a single donor, there was no appreciable induction of CCR7 on the surface of DCs, or any surface marker. However, in the light of experiments done more recently on LCP1, where incubation for 48 hours of stimulation found up-regulation of CCR7, perhaps the cells should be incubated for 48 hours to see if there was a difference in surface expression of CCR7. As an interim mRNA levels could have been interrogated to see if they were induced or not.

4.4.3. HMGB1 Discussion

HMGB1 is dephosphorylated on NOD2 stimulation with MDP. Phosphorylation of insect homologues of HMGB1 prevents nuclear translocation [483], which was then confirmed in human cells [482]. Phosphorylation of HMGB1 occurs after TNFα [482] and LPS stimulation [400].

Release of HMGB1 into the cytoplasm is dependent on calcium concentrations and phosphorylation of HMGB1 on its serine residue, which on LPS stimulation is mediated by PKC [400]. PI(3)K inhibitors were found to reduce secretion of HMGB1 as did JNK inhibitors, but not ERK, NF-κB or p38 inhibitors. In SHP1 silenced cells, PI(3)K is overactive [386]. I would investigate this further by silencing SHP1 and measuring release of HMGB1 on PRR stimulation. As extracellular anti-HMGB1 reduced CCR7 expression and CCL19-mediated DC migration [401], this could be investigated by repeating the experiment above (4.4.2.5) for 48 hours stimulation not 24 hours and then study the effect of SHP1 knockdown on HMGB1-dependent CCR7 expression.

In response to starvation and ROS, HMGB1 has been shown to translocate out of the nucleus into the cytoplasm where it induces autophagy by associating with Beclin1 and causing the dissociation of Beclin1 from BCL2 [402]. In the presence or absence of HMGB1, autophagosome formation could be investigated on MDP stimulation, and whether HMGB1 co-localises with LC3 or Beclin1 in DCs stimulated with PRRs.

4.4.4. HMGB1 Conclusion

HMGB1 is dephosphorylated on initial stimulation by NOD2. This should facilitate HMGB1 recruitment to the nucleus to enable DNA transcription on NOD2 signalling. It would be interesting to investigate the transcriptional targets of HMGB1 using chromatin immunoprecipitation DNA sequencing (ChIP-seq). The role of HMGB1 in autophagy induction, CCR7 expression and cell migration would also make interesting areas of future research. Furthermore, cellular maturation and cytokine release may also be under the influence of HMGB1 phosphorylation by NOD2.

4.5. Overall Discussion and Conclusion

In this chapter I have examined the function of three proteins I found to be differentially phosphorylated on NOD2 or NOD2/TLR2 co-triggering: LCP1, SHP1 and HMGB1. I have suggested that both from the experimental evidence demonstrated here, and in conjunction with evidence from the literature, LCP1, SHP1 and HMGB1 may all be involved in cellular processes such as production of pro-inflammatory cytokines, DC activation and maturation and finally migration of DCs. Future work in this area would include assessing the role of the excess pro-inflammatory cytokine release of MCP1/CCL2 occurring on NOD2 stimulation following LCP1 knockdown; and of increased IL-12p40 and MIP1β/CCL4 release following SHP1 silencing. Finally I would investigate how HMGB1 is involved in NOD2-mediated autophagy.

5. Assessing the function of DAPK1 in the NOD2/TLR2 signalling cascade

5.1. Introduction

DAPK1 was found to be a putative downstream mediator of NOD2/TLR2 signalling by phosphoproteomic analysis. DAPK1 has been demonstrated to increase apoptosis [403] [405] [484] [485] [486] [487], increase stress fibres [488] [489], reduce migration [490], increase autophagy [329] [491] [492] and alter T cell activation [493]. In this context I examined DAPK1 function downstream of PRR triggering biologically and investigated whether DAPK1 played a role in MHC II loading, pro-inflammatory cytokine production, DC maturation and survival.

5.2. DAPK1 Results

5.2.1. Verification of DAPK1 in NOD2/TLR2 signalling cascade

Phosphorylation of DAPK1 has been reported at a number of different sites with different functional outcomes. The phosphorylation of DAPK1 has not been investigated after PRR triggering before, only after generic leucocyte stimulation by phorbol 12-myristate 13-acetate (PMA) where it caused receptor Ser/Thr kinase (RSK)-mediated phosphorylation at ser289 [407] and ERK-mediated phosphorylation at ser735 [494]. RSK is a downstream mediator of ERK. Activation of the kinase domain of DAPK1 requires the dephosphorylation of the autophosphorylation site, ser308, by PP2A [406] and of ser289 to enable the binding of calmodulin [407], which together causes a conformational change so opening the binding domain for kinase activity [408] [409] [410]. Another phosphorylation site previously determined in DAPK1 is at tyr491/tyr492 in the cytoskeleton-binding domain that occurred via EGFR-mediated activation of Src. Conversely, this site is dephosphorylated by leucocyte common antigen-related protein (LAR) [495]. Phosphorylation at each of these different sites then has an impact on the function of DAPK1: ser 289 and ser734 results in loss of apoptosis, tyr491/492 results in increased adhesion, increased migration and less apoptosis, and phosphorylation at ser308 prevents kinase function.

DCs stimulated by NOD2/TLR2 ligands, MDP/PAM, demonstrated phosphorylation of DAPK1 by MS analysis (fold ratio 2.19, Chapter 3 Table 13). I examined whether this could be observed biologically by stimulating DCs with NOD2/TLR2 ligands,

enriching phosphorylated proteins and immunoblotting with anti-DAPK1. There was marked phosphorylation of DAPK1 on stimulation of DCs with MDP and PAM (lane 6, Figure 32A).

To establish whether other PRRs might exert the same effect, or whether this was an observation exclusive to NOD2/TLR2, DAPK1 phosphorylation was investigated pre- and post-PRR triggering by a panel of PRR ligands (Figure 32B). DAPK1 was phosphorylated with TLR2, dual, TLR4 and TLR5 (Figure 32B, lanes 3-6). 2 biological replicates had significant phosphorylation (see Figure 32D) with one donor having a fold change range of 19.74-30.05 and the other of 0.95-2.38. In the biological replicate demonstrated by immunoblot (Figure 32B), this was associated with an increased phosphorylation of DAPK1 at ser308 and with greater levels of phosphorylation of p44/42 MAPK (thr202/tyr204).

One of the key functions ascribed to DAPK1 in the literature is a role in autophagy [329] [333]. To ask whether DAPK1 was phosphorylated on autophagy induction and obtain indirect evidence that PRR phosphorylation of DAPK1 might be relevant to xenophagy, DCs were starved in EBSS, a classical autophagy inducer, for 30 minutes. The level of DAPK1 phosphorylation on PRR triggering with MDP and PAM dual stimulation was measured (Chapter 3 Figure 17) and compared with that observed on EBSS stimulation, which demonstrated no difference or a mild reduction in phosphorylation (Figure 32E+F).

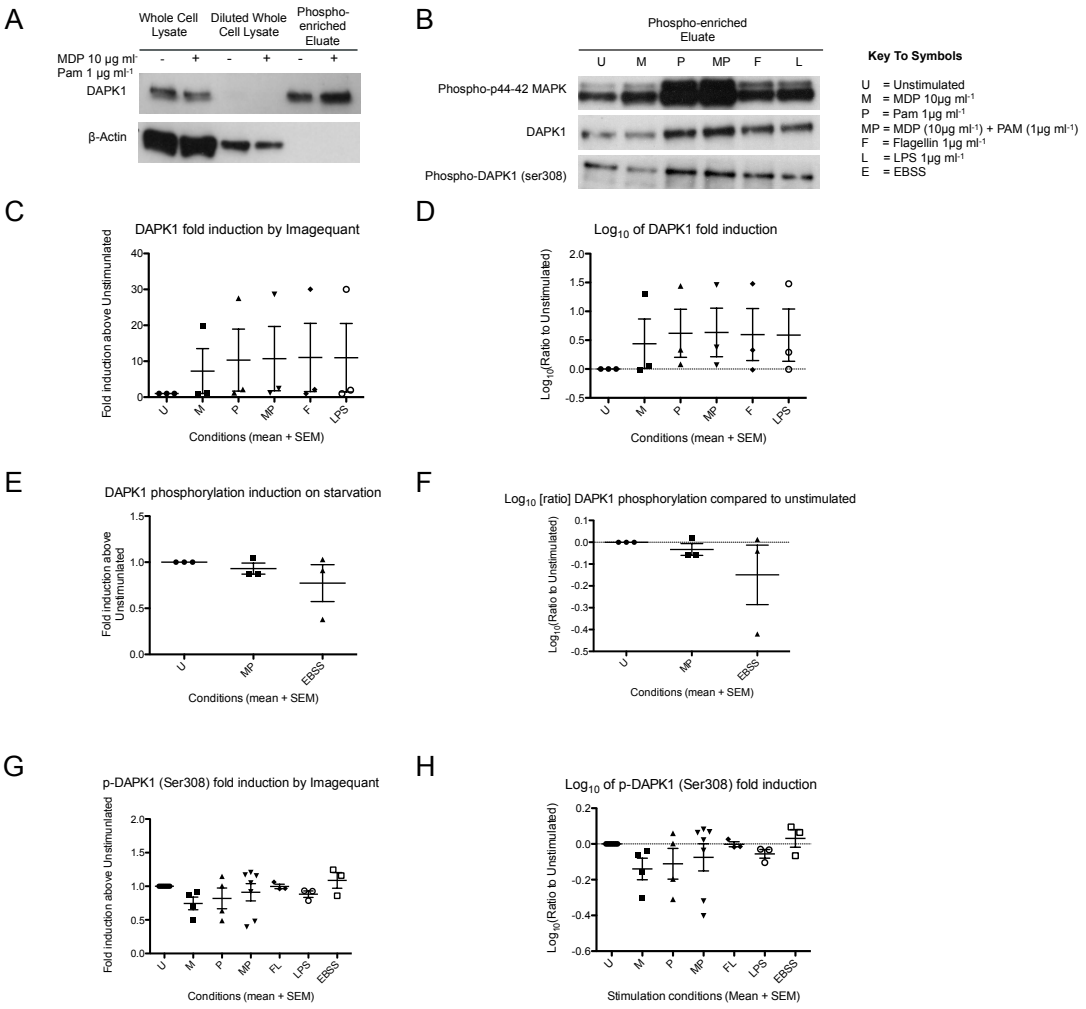


Figure 32: Verification of DAPK1 phosphorylation by immunoblot in phospho-eluate in dual stimulated DCs. A) Immunoblot demonstrating DAPK1 was phosphorylated by stimulation of DCs with MDP (10 µg mL^{-1}) and PAM (1 µg mL^{-1}). Comparison was made to β-actin. B) Comparison of DAPK1 phosphorylation on PRR stimulation measured by whole DAPK1 in the phospho-eluate and phosphorylated DAPK1 at serine308 in 1 representative donor; phosphorylation of p44/42 MAPK was provided as positive control. C) and D) Imagequant quantification from the western blots E) and F) Imagequant quantification of 3 replicate experiments of dual stimulation and starvation in EBSS. G) and H) Imagequant quantification of PRR ligands and EBSS stimulation on phosphorylation of phospho-DAPK1 ser308. N=3-6.

In the inactive state, DAPK1 is autophosphorylated at ser308 preventing the kinase site from being opened. Therefore, phosphorylation of DAPK1 ser308 was examined using anti-ser308 specific antibody. There were variable levels of phosphorylation of DAPK1 ser308 (Figure 32B+G-H). In some cases of MDP, PAM and MDP/PAM stimulation, there was approximately a 50 % reduction in phosphorylation of DAPK1 ser308, and in others a 20 % increase. In conjunction with the total

phosphorylated DAPK1 data (Figure 32B) this would suggest that phosphorylation of DAPK1 occurred and resulted in excess phosphorylation of DAPK1 despite dephosphorylation of ser308 and activation of its kinase site. None of the changes in phosphorylation of DAPK1 ser308 reached statistical significance.

Phosphorylation of DAPK1 ser308 was further examined using the Phosflow technique (Figure 33). Having chosen the gating strategy (Figure 33A-B) cells were intracellularly stained for phospho-DAPK1 (ser308). In 2 biological replicates there was no statistical difference in staining (Figure 33C+D).

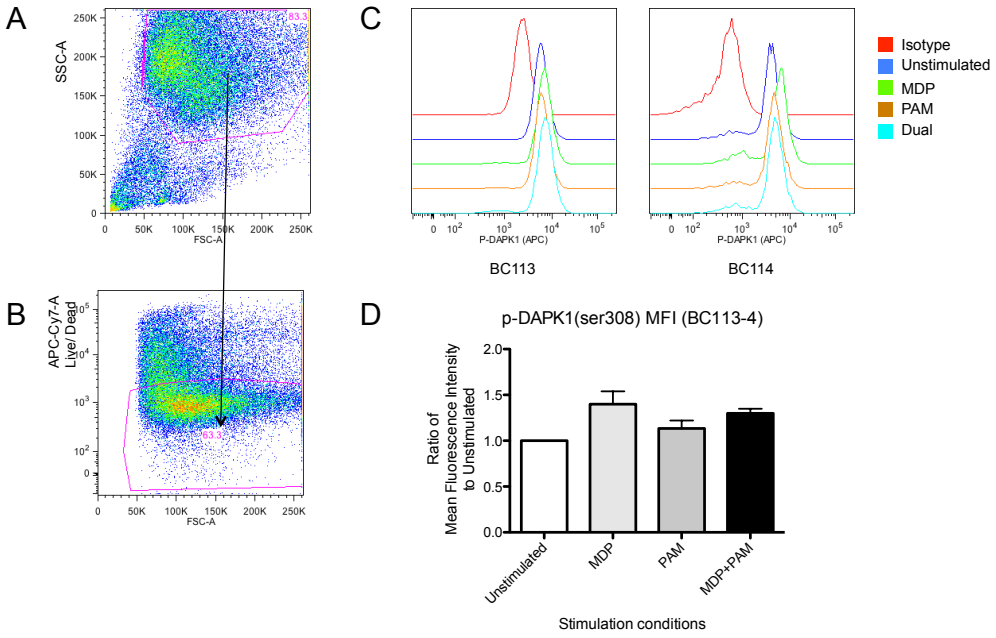


Figure 33: Phosphorylated DAPK1 at serine 308 (p-DAPK1 (ser308)) demonstrating Phosflow technique. 0.5 x 106 DCs were prestained in live-dead stain and HLA-DR for 30 minutes on ice, washed in PBS and plated in R10 in 96 well plate and stimulated for 30 minutes with R10, MDP (10 μg mL^{-1}), PAM (1 μg mL^{-1}), or dual (MDP 10 μg mL^{-1} and PAM 1 μg mL^{-1}). The cells were stained for phospho-DAPK1 (ser308) (Sigma) and a secondary or isotype control and then analysed by flow cytometry and by FlowJo. N=2.

5.2.2. Silencing DAPK1 effectively

In order to examine the function of DAPK1 further I used siRNAs targeting DAPK1 to reduce its expression in DCs. Cells were transfected with siRNA and both qPCR and immunoblot performed. This demonstrated reduction in mRNA level at both 24 hours incubation (0.3397, SEM 0.02895) and 48 hours (0.43, SEM 0.04039) demonstrating 57-66% knockdown (Figure 34A). This was further confirmed by immunoblot at protein level in 2 donors compared to NS siRNA (Figure 34B).

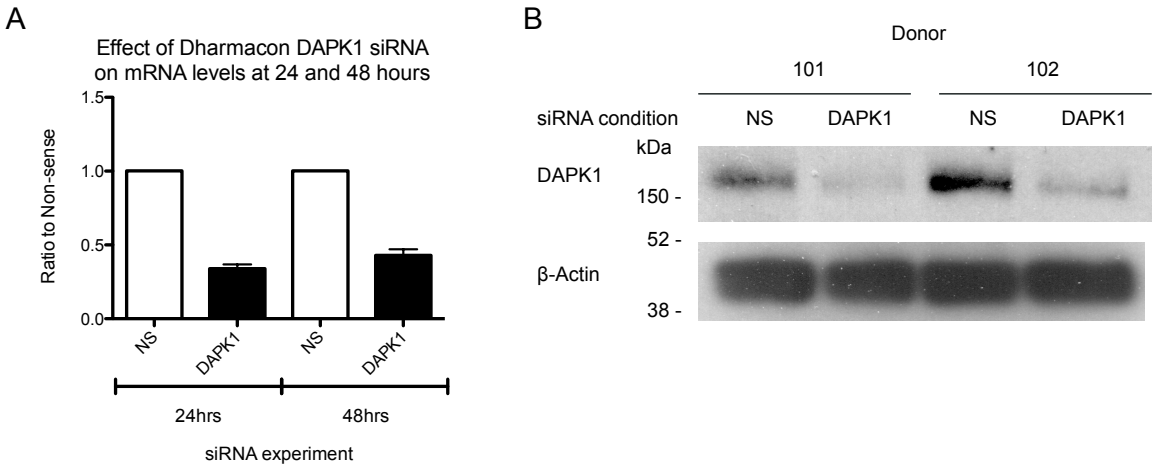


Figure 34: Demonstration of DAPK1 reduction by siRNA measured by quantitative PCR (qPCR) and immunoblot. A) Demonstration of mRNA levels in 2 donors to DAPK1 siRNA with a 66.1 % reduction in mRNA level relative to NS. B) Protein levels at 48 hours incubation demonstrating knockdown.

5.2.3. DAPK1 associates with MHC II-loading compartment and this is not under the control of NOD2

DAPK1 has previously been shown to interact with MHC II loading in MHC II-expressing cells [496]. I sought to investigate whether DAPK1 might be involved in the MHC II antigen presentation pathway.

DCs were stimulated over time to determine if DAPK1 co-localised with HLA-DM, a marker for MHC II-loading compartment. There appeared to be co-localisation (data not shown) so the study was repeated using NOD2 silenced cells to determine if it was under the control of NOD2 (Figure 35). There appeared to be more co-localisation of DAPK1 and HLA-DM in PAM and MDP/PAM stimulated cells (Figure 35B) than in unstimulated or MDP stimulated cells (Figure 35A), and this was independent of NOD2 expression.

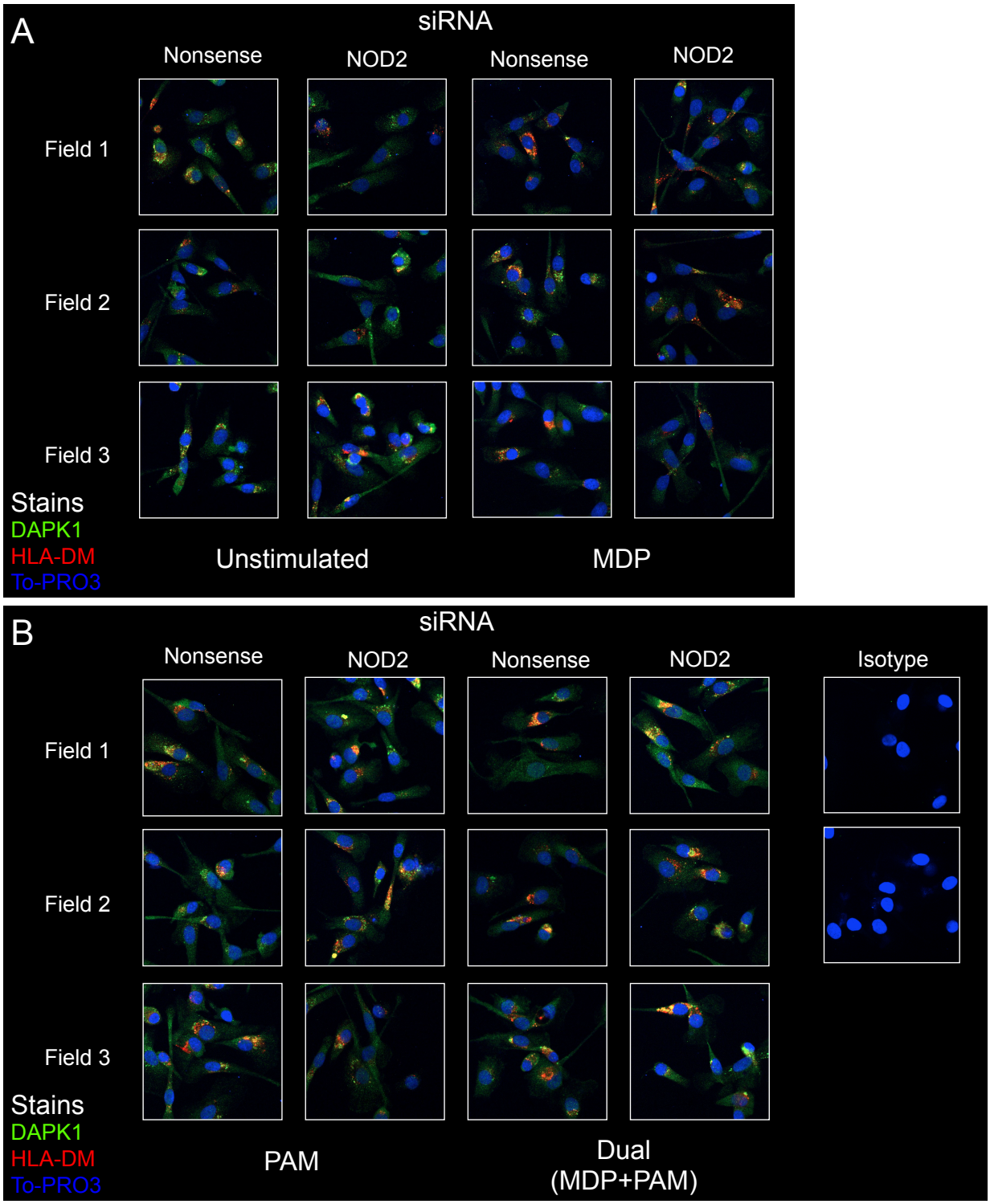


Figure 35: Assessment of DAPK1 localisation with HLA-DM in the MHC Class II loading compartment. 3 x 10^6 DCs were nucleofected (Amaxa) with NS or NOD2 siRNA for 48 hours then replated at 2 x 10^5 per well in confocal slides (BD) coated with poly-L-lysine (Sigma) and stimulated for 2 hours. A) Unstimulated and MDP (10 μg mL^{-1}) stimulated cells and B) PAM (1 μg mL^{-1}) and dual (MDP (10 μg mL^{-1}) and PAM (1 μg mL^{-1})) and isotype for NS (upper image) and NOD2 (lower image).

5.2.4. Levels of CLIP-loaded immature HLA-DR and mature HLA-DR are not affected by DAPK1 protein silencing

DAPK1 has previously been shown to alter surface expression of MHC II in MHC II-expressing cells [496], and having demonstrated that DAPK1 might play a role in the MHC II antigen presentation pathway, the function of DAPK1 and the effect of its absence was further assessed in terms of surface expression of CLIP loaded HLA-DR and mature HLA-DR.

The optimised gating strategy (Figure 36A) and staining of CLIP (Figure 36B, left panel) and HLA-DR (Figure 36B, right panel) was determined. There was increased fluorescence with increasing concentration of antibody on stimulation with MDP+PAM on the CLIP stained cells. On dual staining of cells there appeared to be competitive staining occurring whereby CLIP was displaced by HLA-DR (Figure 36E, left panel), which is presented as per MFI (Figure 36F). As a result the experimental concentrations of 1:10 for CLIP and 1:50 for HLA-DR were used.

In order to assess if DAPK1 altered CLIP and HLA-DR expression, DCs from 4 biological replicates were stimulated for 24 hours and surface expression analysed (Figure 37). There was no difference in expression of CLIP or HLA-DR on stimulation of DCs with different PRR ligands (Figure 37A-D with MFI as a ratio to 'X' unstimulated Figure 37E-F). This was not due to lack of cellular activation as, in dual stimulated cells, the mean fold increase for co-stimulatory markers CD80 in non-sense was 2.81 (SEM 0.1286) versus 2.948 (SEM 0.2843) in DAPK1 silenced

cells, and for CD86 was 1.943 (SEM 0.2331) in non-sense and 1.788 (SEM 0.1922) in DAPK1 silenced cells. Neither result was significantly different.

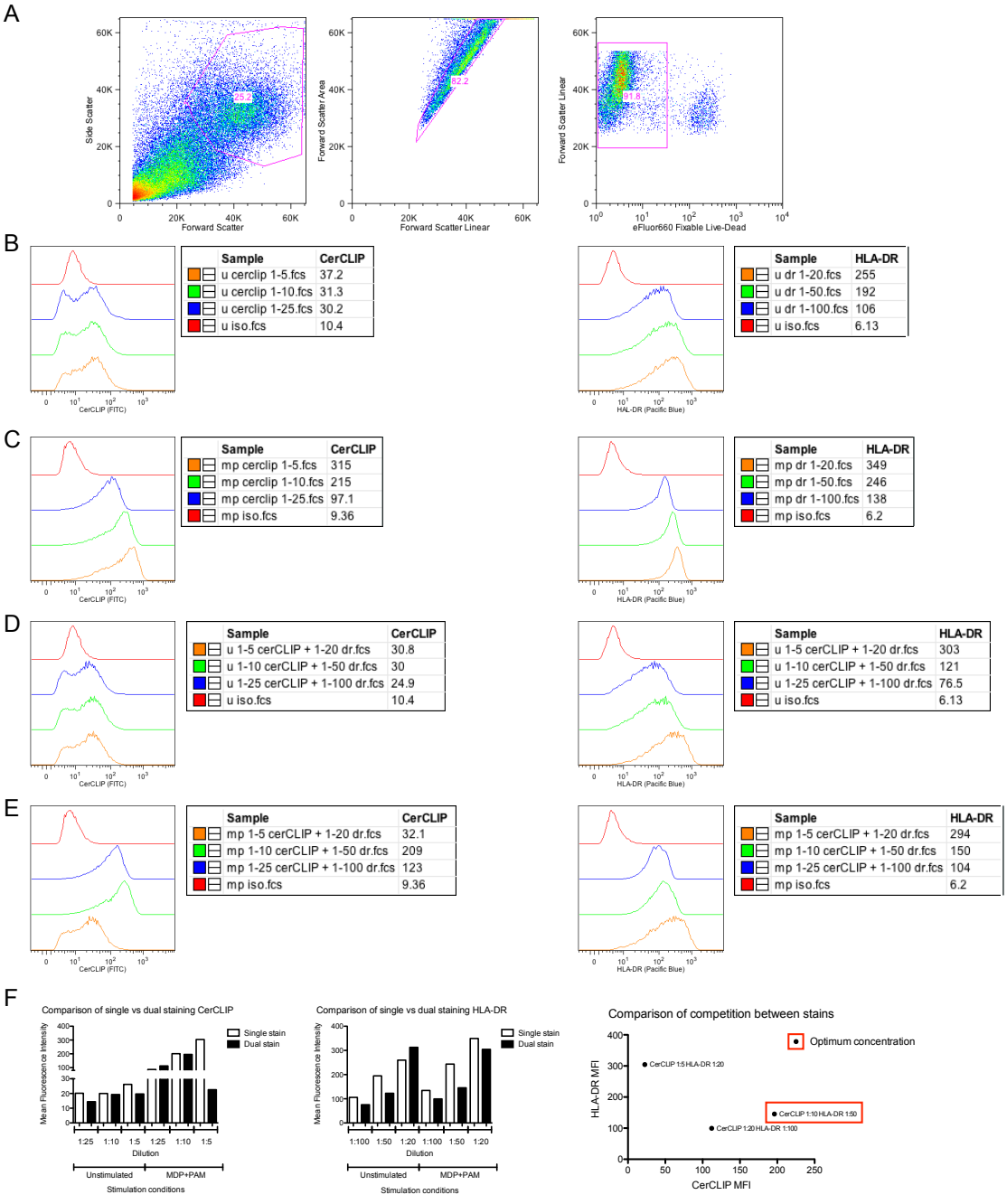


Figure 36: Optimisation of CerCLIP and HLA-DR staining for flow cytometry. 0.5 x 10^6 DC were harvested on day 5, and left unstimulated for 24 hours or dual stimulated (MDP 10 µg mL^{-1} and PAM 1 µg mL^{-1}) for 24 hours, and then stained with eFluor660 Fixable Live-Dead (L/D) stain and CerCLIP (fluorochrome FITC, left panels) or HLA-DR (fluorochrome Pacific blue, right panels). Cellular staining was measured by flow cytometry and analysed on FlowJo. A) Gating strategy: forward scatter (FS):side scatter (SS), FS linear:FS area, and L/D:FS linear. MFI in B+D) Unstimulated cells, C+E) dual stimulated cells, B+C) increasing single stained antibody concentration, D+E) as for B+C) but dual stained cells. F) MFI for CLIP (left panel) and HLA-DR (middle panel) and correlation of dual staining for optimal concentration (right panel).

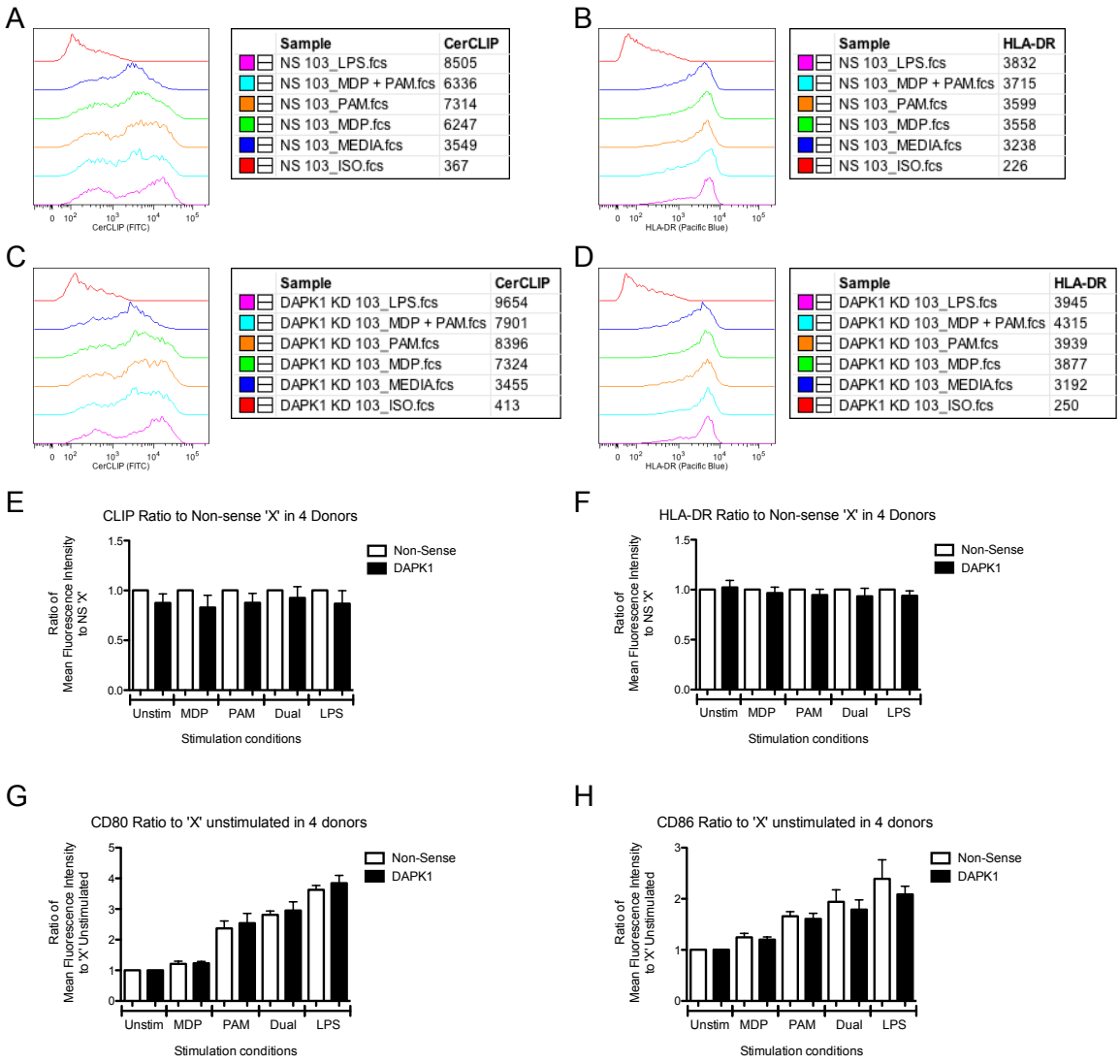


Figure 37: Assessment of the effect of DAPK1 on MHC Class II cell surface expression. 6 x 10^6 DCs were Amaxa nucleofected with nonsense (NS) or DAPK1 siRNA (Dharmacon) and incubated for 24 hours before being harvested and replated in a 96 well plate at 1 x 10^6 (of pre-nucleofected) cells per well, and stimulated for 24 hours with MDP (10 µg mL^{-1}), PAM (1 µg mL^{-1}), dual (MDP 10 µg mL^{-1} and PAM 1 µg mL^{-1}), or LPS (1 µg mL^{-1}). Representative offset histogram plots of fluorescence and tables of mean fluorescence intensity (MFI) for CLIP (A, C) and HLA-DR (B, D), and ratio to NS 'X' plotted as a mean of 4 biological replicates for CLIP (E) and HLA-DR (F). To demonstrate activation of the DCs in all conditions, MFI ratios to 'X' unstimulated for co-stimulatory markers CD80 (G) and CD86 (H) are also shown.

5.2.5. Loss of DAPK1 does not impact on cell survival or activation in DCs

DAPK1 plays a role in cell death and has been demonstrated to be both pro- and anti-apoptotic depending on the experimental systems used. It is pro-apoptotic when overexpressed in cells lacking p55 [491], and in response to a number of different ligands: TNFα [484], Fas [484], IFNγ [403], ceramide [485] [486], oncogenes c-Myc and E2F [487] and finally TGFβ, where DAPK1 activates the intrinsic apoptotic pathway [405]. Yet, DAPK1 is anti-apoptotic in TNFα-stimulated HEK293 cells [484], TGFβ-stimulated Hep3B cells [405] and in TNFα-induced DIP1-mediated reduction of murine DAPK1 resulting in increased apoptosis [497] [498].

To discover, therefore, if DAPK1 was involved in cell death in DCs during PRR triggering, flow cytometry was used to assess survival of DCs on PRR stimulation in the presence or absence of DAPK1 knockdown. Survival was unaffected after 24 hours incubation post-electrical nucleofection, nor after 24 hours stimulation with typical PRRs, such as MDP, PAM or LPS, on survival (Figure 38A). Confirmation of cellular activation by MDP/PAM or LPS was elicited by measuring up regulation of co-stimulatory surface proteins (CD80 and CD86), and the cells were activated appropriately in both NS and DAPK1 silenced cells as seen for CD80 (Figure 38B+D respectively) and CD86 (Figure 38C+E respectively). CD80 (Figure 38F) and CD86 (Figure 38G) levels were represented as a ratio to NS or DAPK1 unstimulated and graphically demonstrated for 4 biological replicates. Ratios comparing the difference between each stimulation condition were analysed for CD80 (Figure 38H) and CD86 (Figure 38I) and there was no statistical difference.

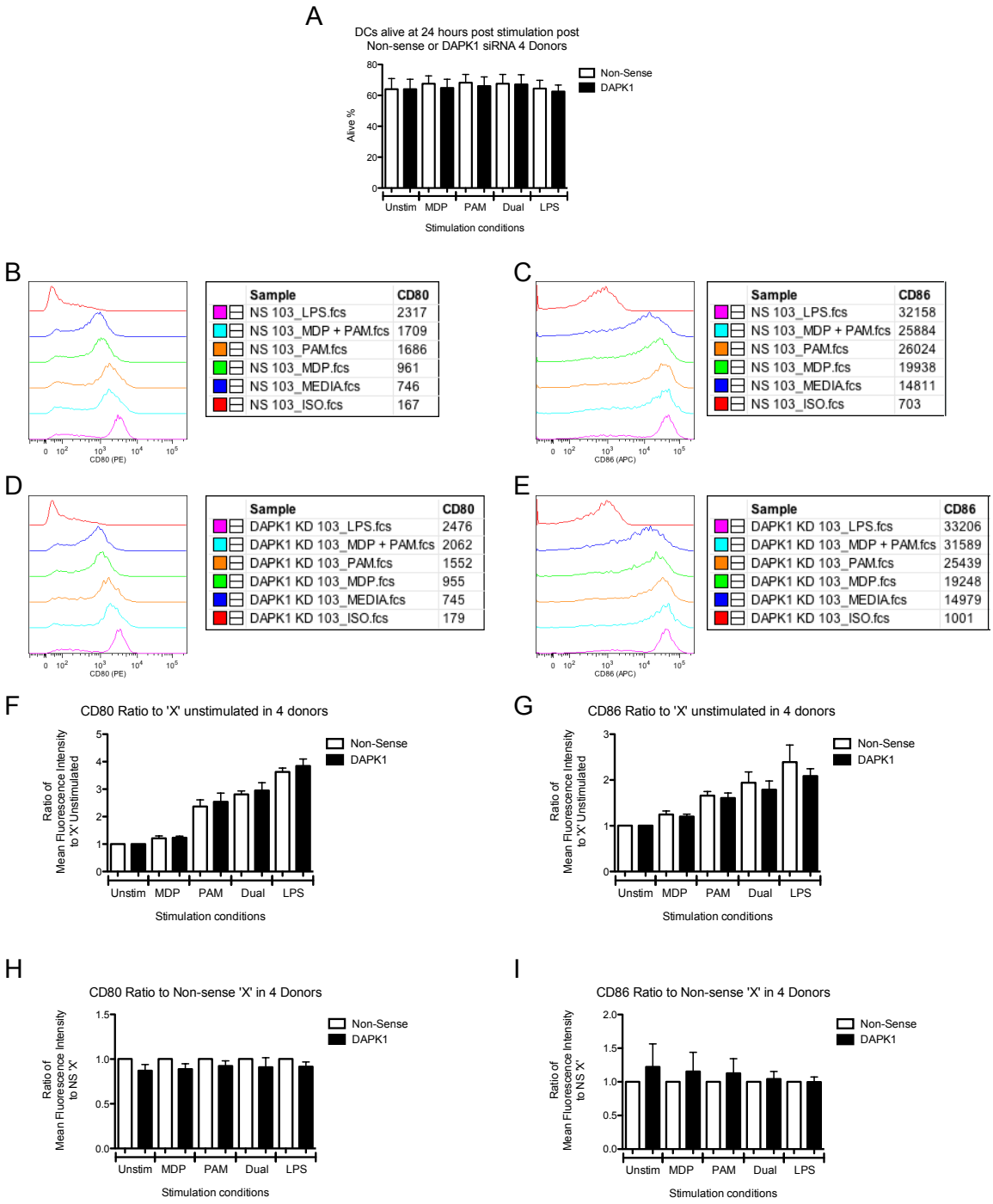


Figure 38: Effect of DAPK1 on cell death and DC maturation. 6 x 10^6 DCs were Amaxa nucleofected with NS or DAPK1 siRNA (Dharmacon) and incubated for 24 hours before being harvested and replated in 96 well plate at 1 x 10^6 (of pre-nucleofected) cells per well, and stimulated for 24 hours with MDP (10 µg mL^{-1}), PAM (1 µg mL^{-1}), dual (MDP 10 µg mL^{-1} and PAM 1 µg mL^{-1}), or LPS (1 µg mL^{-1}). A) Cells stained with live/dead stain, analysed by flow cytometry and percentage alive calculated. Representative offset histogram plots of fluorescence and tables of mean fluorescence intensity (MFI) for CD80 (B, D) and CD86 (C, E) showing activation of both siRNA groups by PRR ligands. MFI ratios to 'X' unstimulated for CD80 (F) and CD86 (G) and NS 'X' for CD80 (H) and CD86 (I) plotted as a mean of 4 biological replicates to demonstrate no effect of siRNA on DC maturation.

5.2.6. DAPK1 silencing does not interfere with cytokine production

IL-1β secretion has been previously shown to be dependent on DAPK1 [499] and phosphorylation of DAPK1 was therefore hypothesised to have a role in cytokine production generally. I examined the ability of DAPK1 to affect IL-1β secretion in DCs stimulated with different PRR ligands. ELISA quantification of IL-1β showed no difference between NS or DAPK1 silencing as a ratio to unstimulated for either NS or DAPK1 (Figure 39A). Furthermore, Log_{10} [ratio] for these ratios and a ratio t-test was non-significant (Figure 39B).

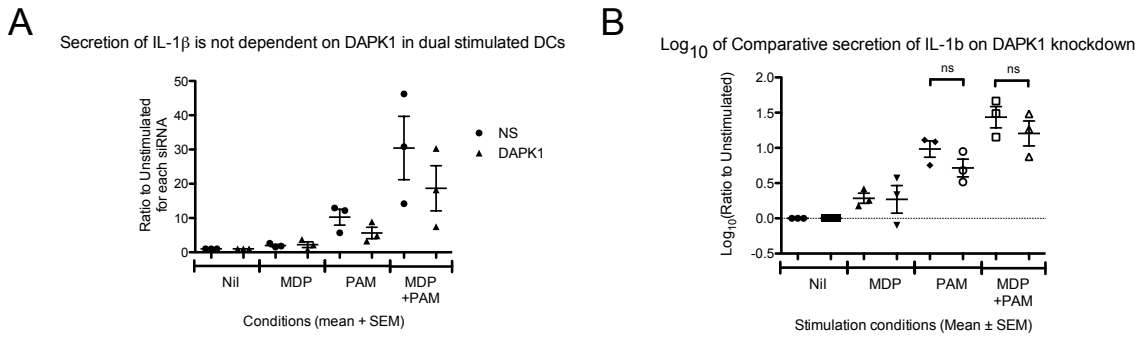


Figure 39: Assessment of DAPK1 in IL-1β secretion. ELISA performed on the supernatants from 6 x 10^6 DCs silenced with NS or DAPK1 siRNA (Qiagen) and incubated for 24 hours before being harvested and replated in 96 well plate at 1 x 10^6 (of pre-nucleofected) cells per well, and stimulated for 24 hours with MDP (10 μg mL^{-1}), PAM (1 μg mL^{-1}), dual (MDP 10 μg mL^{-1} and PAM 1 μg mL^{-1}).

DAPK1 has been demonstrated to stabilise the inflammasome [499]. In inflammasome biology activation is a two-step process: the first signal causes the transcription of pro-IL-1β and the second signal activates the inflammasome cleaving pro-Caspase-1 into Caspase-1, which then in turn cleaves pro-IL-1β into mature IL-1β [500]. Whilst TLR4-induced pro-IL-1β is not dependent on DAPK1, TLR2-induced transcription [499] and the second activating signal are dependent on DAPK1 [499]. Stimulation of PRRs is often insufficient for both the priming and activating signal [501]. In this

experiment, IL-1β was measured by ELISA (Figure 39), and whilst there was no difference demonstrated, IL-1β was detected. Future work would be to stimulate DAPK1 silenced DCs, measure pro-IL-1β and then activate the second signal through ATP stimulation and measure the release of IL-1β.

5.2.7. DAPK1 and the immunological synapse

Antigen presentation is required for activation of the adaptive immune system. To investigate this further autologous CSFE-stained $CD4^+$ T cells from peripheral blood mononuclear cells (PBMCs) were incubated with DCs pulsed with Tetanus toxoid C fragment coated latex beads. After 1 week incubation CSFE staining was assessed but unfortunately the experiment did not work due to pre-activation of the CD4+ T cells whilst awaiting monocyte incubation. Investigating CSFE levels at 1 week is a normal time point, but we had previously demonstrated a difference at days 3-4 of culture with 18 hours of radiolabelled nucleic acid incorporation [190]. In future, an earlier time point would be used and optimisation of incubation conditions to prevent T cell activation and use Tetanus toxoid expressing bacteria instead of beads.

5.2.8. DAPK1 and autophagy induction

DAPK1 has been implicated in autophagy [329] [491] [492]. The hypothesis, therefore, was that PRR triggering phosphorylated DAPK1 so deactivating it. This prevented DAPK1-mediated phosphorylation of PIN1 or TSC2 so maintains mTOR's control of autophagy [329] [502]. Conversely, EBSS starvation media should cause

dephosphorylation of DAPK1 if it were able to differentiate between situations of starvation compared to xenophagy. Initially comparison of the formation of autophagosomes as defined by punctate staining of LC3 on confocal images and their co-localisation to lysosomes (a marker of acidic compartments, most notably lysosomes) was done. Despite the knockdown of DAPK1, EBSS proved a very convincing positive control and PRR triggering did not demonstrate difference in DAPK1 silenced DCs. To study this further would require investigation of other markers of autophagy activation, such as the flux of LC3-I and LC3-II or p62 (SQSTM1).

5.3. Discussion

Here DAPK1 has been validated as being phosphorylated downstream of NOD2/TLR2 stimulation. The increased phosphorylation demonstrated appears to be more on TLR triggering than NOD2 (Figure 32). On PRR triggering, DAPK1 co-localises with HLA-DM but there is no clear effect of DAPK1 on mature HLA-DR surface expression. The silencing of DAPK1 did not prevent DC maturation from occurring, and whilst DAPK1 has previously been demonstrated to regulate apoptosis, silencing DAPK1 did not alter cell survival.

5.3.1. DAPK1 forms part of the NOD2/TLR2 signalling cascade

DAPK1 was validated in the NOD2/TLR2 signalling cascade (Figure 32A), and increased phosphorylation of DAPK1 ser308 was demonstrated on immunoblot (Figure 32B, E-F) and Phosflow (Figure 33). Phosphorylation of DAPK1 has been reported at a number of different sites with different mediators of phosphorylation/dephosphorylation: ser289 (RSK/unknown [407]), ser308 (autophosphorylation/PP2A [406]), tyr491/tyr492 (Src/LAR [495]) and ser735 (ERK/unknown [494]). The phosphorylation of DAPK1 had not been investigated after PRR triggering before, only after phorbol 12-myristate 13-acetate (PMA) [407] [494]. What role phosphorylation of DAPK1 in DCs is having will be discussed later.

5.3.2. DAPK1 is not degraded on initial PRR stimulation

Once dephosphorylated at ser308 and active, DAPK1's homeostasis is maintained due to rapid degradation by the proteasome. DAPK1 ubiquitination by DIP1/Mindbomb1 has previously been observed within 30 minutes [498] but degradation of DAPK1 has been observed only as early as 6 hours by carboxyl terminus of HSP70-interacting protein (CHIP) [503] and ubiquitination by Cullin3, keitch-like homologue protein 20 (KLH20) and regulator of cullins 1 (ROC1) at 16 hours could be reversed by IFNγ [504]. DAPK1 total levels were unaffected by PRR triggering, as demonstrated on WCL, but this could be further investigated by stimulating for longer time periods and also by immunoblotting for ubiquitination of DAPK1.

5.3.3. DAPK1 and MHC II loading

DCs are highly efficient at presenting processed antigen to the adaptive immune system to activate it or induce tolerance, and the antigenic peptides are loaded on MHC II molecules. MHC II loading and effective transport to the surface is a complex pathway requiring a number of different steps. Previously, a siRNA library to interrogate the role of different proteins on MHC II expression in an MHC II-expressing melanoma cell line was done by measuring surface expression of HLA-DR, a marker of total mature MHC II on the surface of the cell, compared to expression of CLIP, a marker of immature invariant chain load MHC II on the cell surface [496]. DAPK1 was reported to affect mature MHC II. Over a number of different donors I repeated the experiment looking at surface expression of CLIP and HLA-DR (Figure 36) and found that I could not replicate the findings of the melanoma cell line. Instead, whilst CLIP and HLA-DR increased on stimulation (Figure 36A-D), removal of DAPK1 by siRNA did not exaggerate this increase, nor was it starting from a reduced level of expression (Figure 36E-F). Whilst the limitations of my study was only 4 donors compared to a high throughput model system, the limitations of theirs was a study in a non-haematopoeitic atypical MHC II-expressing cell line compared to primary human DCs, and may explain why the same results were not observed.

Kinase prediction websites, such as <www.phosphonet.ca>, predicted that DAPK1 would be potentially able to phosphorylate HLA-DM, which is made of two subunits HLA-DMA and HLA-DMB. Accordingly, it would be able to phosphorylate HLA-DMB, but not HLA-DMA, at ser116, ser246, and ser247. Using confocal images to

investigate if HLA-DM and DAPK1 were associated, primary human DCs stimulated, with MDP and PAM or left unstimulated over time (0-24 hours), were stained with HLA-DM and DAPK1 for co-localisation (data not shown). In an experiment to determine if DAPK1 function may be dependent on NOD2, silencing NOD2 had no impact on co-localisation between NS or NOD2 but there was co-localisation of DAPK1 and HLA-DM at 2 hours (shown in Figure 35). Further work on this area would include more biological replicates, and immunoprecipitation of DAPK1 and blot for HLA-DM. DAPK1 interacts with ERK1/2 [494] and ERK1/2 is also a putative kinase for HLA-DMA and HLA-DMB (<www.phosphonet.ca>).

5.3.4. Silencing DAPK1 to assess function

Physiological investigation of a protein's function can be accentuated by studying effects with it present or absent, and here a suitable siRNA was used (Figure 33). Whilst the site of phosphorylation on stimulation of DCs with MDP and PAM remains unknown, the phosphorylation of ser308 (Figure 32B, E-F) is highly suggestive of decreased kinase function. Autophosphorylation of DAPK1 ser308 renders the kinase domain inactive, but dephosphorylation is required to activate it [408]. DAPK1 removal by siRNA may, therefore, produce no appreciable difference between non-sense silencing and DAPK1 silencing, as it is the phosphorylation status of DAPK1 ser308 that determines the functionality of DAPK1. This might explain why silencing of DAPK1 did not result in a clear phenotype in cytokine production, MHC II expression or autophagy induction. The balance of charge from phosphorylation at one site and dephosphorylation at another, such as ser308, would not be differentiated by the methodology used here. Instead, OFFGEL

fractionation would demonstrate a difference, and in future would need to be used to assess DAPK1 phosphorylation on PRR triggering. Secondly, MS analysis of enriched phospho-peptides from DAPK1 immunoprecipitated after PRR triggering would provide further information of phosphorylation sites.

Initial immunoblots clearly and reproducibly demonstrated the phosphorylation of DAPK1 on PRR stimulation, but later repeated blots to verify this finding became equivocal suggesting a lack of definitive evidence of differential phosphorylation (see Figure 32E+F). This is most probably due to the inherent variability within the donors exacerbated by the handling of the donated sample (from donation at Blood Donor site to obtaining it) despite exact handling within the laboratory. The non-differentially phosphorylated donors were not due to pre-stimulated DCs as morphologically the cells looked immature, naïve and unactivated prior to stimulation. Moreover, p44/42 MAPK phosphorylation appeared differentially phosphorylated across stimulation conditions so corroborating lack of cellular stimulation in the unstimulated cells (data not shown).

5.4. Conclusion

DAPK1 is a pivotal protein in a number of key cellular functions involving apoptosis, autophagy, and inflammasome stability. Its function as a kinase phosphorylating key proteins, most notably MLC, PIN1, and TSC2, make it interesting to study in the context of NOD2/TLR2 signalling.

In these experiments on DAPK1, silencing of DAPK1 by siRNA may exert no demonstrable difference in function of DAPK1 and may be no different to phosphorylation of DAPK1 at ser308, which inactivates the kinase function. A reduction in DAPK1 level does not affect cell survival, maturity or cytokine release. However, in non-silenced DCs DAPK1 co-localises with HLA-DM, a marker of recruitment to the MHC II loading compartment, but does not affect the loading of MHC II as assessed by CLIP levels.

Further work on DAPK1 to ascertain the function of DAPK1 in NOD2/TLR2 signalling would be to optimise the immunoprecipitation of DAPK1 on PRR triggering, and perform an in vitro kinase assay of DAPK1. This could be further investigated by using overexpression of naïve, inactive and constitutively active mutants of DAPK1 in DCs by using lentivectors to obtain good levels of expression whilst avoiding excessive cell death. These mutants would then be used to investigate further autophagy induction, cytokine release, and the role of DAPK1 in antigen presentation.

6. Discussion and Conclusion

6.1. Investigating the NOD2 signalling cascade

The work presented in this thesis has investigated the function of NOD2 in human APCs. The role of this work was to further elucidate the underlying signalling cascade induced on NOD2 stimulation with its ligand, MDP. This involved using large-scale proteomic techniques to delineate the proteins present in the signalling cascade and to attempt to investigate their immune function normally and to shed light on how innate recognition breaks down in CD.

The NOD2 signalling cascade is a dynamic and complex network of intersecting pathways, and becomes more so on co-triggering TLR2, with which NOD2 synergises. Microorganism PAMPs are not available in isolation during digestion and processing of intracellular pathogens or phagocytosed material. Whilst a reductionist approach looking at one pathway in isolation enables the cleanest environment for discovery of novel signalling proteins and pathways, this is not a true physiological or immunological setting.

In order to investigate the signalling cascades that result from NOD2 triggering, phospho-proteomics and MS were used to investigate NOD2 signalling alone, and then expanded to investigate the role of NOD2/TLR2 cross-talk. The proteins identified were confirmed by immunoblot and their functions investigated by siRNA paying particular attention to maturation, cytokine production, antigen presentation, migration and autophagy.

A number of novel proteins were identified on NOD2 triggering: LCP1, SHP1 and HMGB1. On dual stimulation of NOD2 and TLR2, LCP1 was again phosphorylated, and there were novel findings of DAPK1, MEK1, and HSP27. The subsequent experimentation investigated the function within the NOD2 signalling cascade of LCP1, a cytoskeletal protein; SHP1, a negative regulator of ITIM signalling; HMGB1, a DAMP and DAPK1, a cytoskeletal binding serine/threonine kinase usually involved in apoptosis.

Future investigation of the NOD2 signalling cascade with or without other PRRs such as TLR2 should be expanded to include TLR5, another protein that NOD2 synergises with. These should be studied in isolation and in conjunction to ascertain which signalling cascades are pertinent to NOD2 alone, TLR2 or TLR5 alone and in combination with NOD2/TLR2 or NOD2/TLR5. These phospho-proteomic studies were carried out on monocyte-derived dendritic cells all of whom were wild-type NOD2, and any donors found to have alleles with NOD2 variants were excluded from any analysis. In order to determine the effect of NOD2 variants in naïve cells, pooled concentrated phospho-eluates from different stimulation conditions would enable study of the effect of NOD2 variants and the subsequent signalling cascade without 'noise' from gene silencing techniques.

6.2. The role of LCP1 in the NOD2 signalling cascade

LCP1, or L-plastin, is an actin-bundling protein necessary for cytoskeletal functions [367] [368]. The majority of work on LCP1 has been in neutrophils, demonstrating that LCP1$^{-/-}$ affects ROS production as part of the respiratory burst, but not migration or

phagocytosis [374]. Yet in DCs, this study has demonstrated that LCP1 is involved in either being the gatekeeper of bacterial phagocytosis or bacterial killing once phagocytosed, as more bacteria were present in cells at 60 minutes post infection after LCP1 knockdown (Chapter 5 Figure 23).

Integrin function is vital for survival of cells and for informing cells of their immediate environment [375]. Whilst no difference in integrin levels or migration was demonstrated in initial experiments looking at these potential functions of LCP1, there remains the possibility that LCP1 may be part of the mechanism by which DCs are prepared for antigen presentation, migration to the lymph node or cytokine production. I observed a novel use for LCP1 in the induction of MCP1 (CCL2) on MDP triggering. MCP1 is interesting as it has previously been shown to drive accumulation of inflammatory monocytes in the mucosa via NOD2 [475].

6.3. The role of SHP1 in the NOD2 signalling cascade

SHP1 is a protein tyrosine phosphatase that is mainly involved in the regulation of ITIMs [382] [383]. The motheaten mouse has provided a very valuable resource in understanding the role of SHP1 [479], but the role of SHP1 within DCs has not been widely studied, particularly after stimulation of PRRs, such as NOD2.

I found SHP1 phosphorylated on NOD2 triggering and SHP1 knockdown resulted in reduced p38, p44/42 and NF-κB signalling but sustained IKKα phosphorylation. This is suggestive of activation of the alternative pathway of NF-κB signalling that results in tertiary lymphoid organs forming in areas of inflammation, such as the gut

[505]. SHP1 knockdown resulted in increased MIP1β or CCL4 expression and IL-12p40 expression on MDP triggering (Chapter 5 Figure 29). This warrants further investigation for a functional effect on the recruitment of $CCR5^+$ $CD4^+$ T cells and comparison with the effect occurring in FS1007insC NOD2 expressing cells.

6.4. The role of DAPK1 in the NOD2 signalling cascade

DAPK1, a serine/threonine kinase, has been found to be involved in a number of different cellular functions, particularly with induction of apoptosis mediating cell death. Phosphorylation of DAPK1 at ser289 [407], tyr491/492 [495] and ser734 [494] prevents apoptosis but activation of apoptosis requires dephosphorylation of DAPK1 at ser308 and the presence of the death domain [484 487]. In this present study the phosphorylation site remains unknown and despite an increased phosphorylation of DAPK1 on PRR triggering there was no difference seen in levels of cell death over 48 hours (Chapter 5 Figure 38A).

DAPK1 has previously been shown to alter the surface expression of mature HLA-DR or CLIP-loaded immature HLA-DR [496]. In primary human DCs there was no difference demonstrated between the surface expression of mature HLA-DR or CLIP-loaded immature HLA-DR. There is, however, a putative kinase site on HLA-DM, a marker for the MHC II loading compartment. Confocal experiments revealed that DAPK1 co-localises with HLA-DM.

DAPK1 has been shown to stabilise the inflammasome and be necessary for TLR2 or TLR4 induced pro-IL-1β mRNA levels [499]. In this study, the ability of DCs silenced

with DAPK1 did not seem to affect the production of IL-1β after PRR stimulation (Chapter 5 Figure 39) and may require further work on the activation of the inflammasome to demonstrate any difference.

Further optimisation of immunoprecipitation and kinase experiments on DAPK1 would enable experiments studying autophagy induction, HLA-DM co-localisation, antigen presentation and cytokine production.

6.5. Other proteins identified

This thesis identified a number of different proteins that warrant further study. HMGB1, a DAMP, whose release from dying cells acts as a cytokine, yet intracellularly is involved in DNA transcription. HMGB1 plays a role in autophagy induction by facilitating dissociation of Beclin from BCL2 [402]. Further study on HMGB1 would be to assess if there is a role for HMGB1 in autophagy induction on stimulation of NOD2.

HSP27 is a chaperone protein whose transcription is increased by HMGB1. It is involved in autophagy induction caused by the UPR [429] and so further work on the role of HSP27 in PRR stimulation would be to assess if it was necessary for autophagy.

MEK1 is a key signalling intermediate, whose role in β-arrestin-mediated endocytosis [433] would make investigation of MEK1 in phagocytosis an interesting

new pathway. In addition, β-arrestin was identified in the original screen for MDP stimulation and that too would warrant further investigation.

6.6. Conclusion

A number of new mediators of NOD2 and TLR2 signalling have been highlighted using phospho-proteomics, including LCP1, SHP1, HMGB1, DAPK1, MEK1 and HSP27. The function of these proteins within DC maturation, antigen presentation and bacterial handling has been investigated. Future work will involve further characterisation of these proteins within host innate defence and how their functional role is affected in the presence of NOD2 polymorphisms associated with Crohn's Disease.

7. Bibliography

1. Kirsner, J.B. The Historical Basis of the Idiopathic Inflammatory Bowel Diseases. *Inflammatory bowel diseases* **1**, 2-26 (1995).
2. Dalziel, T. Chronic interstitial enteritis. *Br Med J* **2**, 1068-1070 (1913).
3. Crohn, B. & Berg, A. Right-side (regional) colitis. *JAMA* **110**, 32-38 (1932).
4. Molodecky, N.a., *et al.* Increasing Incidence and Prevalence of the Inflammatory Bowel Diseases with Time, Based on Systematic Review. *Gastroenterology* **142**, 46-54.e42 (2012).
5. Thompson, N.P., Fleming, D.M., Charlton, J., Pounder, R.E. & Wakefield, A.J. Patients consulting with Crohn's disease in primary care in England and Wales. *Eur J Gastroenterol Hepatol* **10**, 1007-1012 (1998).
6. Wilson, J., *et al.* High incidence of inflammatory bowel disease in Australia: a prospective population-based Australian incidence study. *Inflammatory bowel diseases* **16**, 1550-1556 (2010).
7. Bernstein, C.N., *et al.* The epidemiology of inflammatory bowel disease in Canada: a population-based study. *The American journal of gastroenterology* **101**, 1559-1568 (2006).
8. Cottone, M., *et al.* Incidence of Crohn's disease and CARD15 mutation in a small township in Sicily. *European journal of epidemiology* **21**, 887-892 (2006).
9. Ehlin, A.G.C., Montgomery, S.M., Ekbom, A., Pounder, R.E. & Wakefield, A.J. Prevalence of gastrointestinal diseases in two British national birth cohorts. *Gut* **52**, 1117-1121 (2003).
10. Thia, K.T., Loftus, E.V., Sandborn, W.J. & Yang, S.-K. An update on the epidemiology of inflammatory bowel disease in Asia. *The American journal of gastroenterology* **103**, 3167-3182 (2008).
11. Ahuja, V. & Tandon, R.K. Inflammatory bowel disease in the Asia-Pacific area: a comparison with developed countries and regional differences. *Journal of digestive diseases* **11**, 134-147 (2010).
12. Cosnes, J., Gower-Rousseau, C., Seksik, P. & Cortot, A. Epidemiology and natural history of inflammatory bowel diseases. *Gastroenterology* **140**, 1785-1794.e1784 (2011).
13. Lloyd, D.A.J., *et al.* Crohn's disease and ulcerative colitis: divergent trends in hospital admission rates, 1989/90 to 1999/2000. *Health Statistics Quarterly* **16**, 19-25 (2002).
14. Dretzke, J., *et al.* A systematic review and economic evaluation of the use of tumour necrosis factor-alpha (TNF-α) inhibitors, adalimumab and infliximab, for Crohn's disease. *Health technology assessment (Winchester, England)* **15**, 1-244 (2011).
15. Sands, B.E. Therapy of inflammatory bowel disease. *Gastroenterology* **118**, S68-82 (2000).
16. Akobeng, A. & Gardener, E. Oral 5-aminosalicylic acid for maintenance of medically-induced remission in Crohn's disease (Review). *Cochrane Database of Systematic Reviews* (2005).
17. Ford, A.C., *et al.* Efficacy of 5-aminosalicylates in Crohn's disease: systematic review and meta-analysis. *The American journal of gastroenterology* **106**, 617-629 (2011).
18. Colombel, J.-F., *et al.* Comparison of two adalimumab treatment schedule strategies for moderate-to-severe Crohn's disease: results from the CHARM trial. *The American journal of gastroenterology* **104**, 1170-1179 (2009).
19. Colombel, J.F., *et al.* Infliximab, Azathioprine, or Combination Therapy for Crohn's Disease. *New England Journal of Medicine* **362**, 1383-1395 (2010).
20. Bernell, O., Lapidus, A. & Hellers, G. Risk Factors for Surgery and Postoperative Recurrence in Crohn's Disease. *Annals of Surgery* **231**, 38-45 (2000).

21. Binder, V., Hendriksen, C. & Kreiner, S. Prognosis in Crohn's disease - based on results from a regional patient group from the county of Copenhagen. *Gut* **26**, 146-150 (1985).
22. Michelassi, F., Balestracci, T., Chappell, R. & Block, G. Primary and Recurrent Crohn's Disease, experience with 1379 patients. *Annals of Surgery* **214**, 230-240 (1991).
23. Goldberg, P., Wright, J., Gerber, M. & Claassen, R. Incidence of Surgical Resection for Crohn's Disease. *Diseases of the colon and rectum* **36**, 736-739 (1993).
24. Simillis, C.*, et al.* A meta-analysis comparing incidence of recurrence and indication for reoperation after surgery for perforating versus nonperforating Crohn's disease. *The American journal of gastroenterology* **103**, 196-205 (2008).
25. Abraham, C. & Cho, J. Inflammatory bowel disease. *New England Journal of Medicine* **361**, 2066-2078 (2009).
26. Monsén, U., Broström, O., Nordenvall, B., Sörstad, J. & Hellers, G. Prevalence of inflammatory bowel disease among relatives of patients with ulcerative colitis. *Scandinavian journal of gastroenterology* **22**, 214-218 (1987).
27. Farmer, R., Michener, W. & Mortimer, E. Studies of family history among patients with inflammatory bowel disease. *Clinical Gastroenterology* **9**, 271-277 (1980).
28. Korelitz, B. From Crohn to Crohn's Disease: 1979 - an epidemiological study in New York City. *Mount Sinai Journal of Medicine* **46**, 533-540 (1979).
29. ZLotogora, J., Zimmerman, J. & Rachmilewitz, D. Prevalence of Inflammatory Bowel Disease in Family Members of Jewish Crohn's Disease Patients in Israel. *Digestive Diseases and Sciences* **36**, 471-475 (1991).
30. Yang, H.*, et al.* Familial empirical risks for inflammatory bowel disease: differences between Jews and non-Jews. *Gut* **34**, 517-524 (1993).
31. Probert, C.S.J.*, et al.* Prevalence and family risk of ulcerative colitis and Crohn's disease: an epidemiological study among Europeans and South Asians in Leicestershire. *Gut* **34**, 1547-1551 (1993).
32. Tsironi, E.*, et al.* Incidence of inflammatory bowel disease is rising and abdominal tuberculosis is falling in Bangladeshis in East London, United Kingdom. *The American journal of gastroenterology* **99**, 1749-1755 (2004).
33. Halfvarson, J., Bodin, L., Tysk, C., Lindberg, E. & Järnerot, G. Inflammatory bowel disease in a Swedish twin cohort: a long-term follow-up of concordance and clinical characteristics. *Gastroenterology* **124**, 1767-1773 (2003).
34. Spehlmann, M.E.*, et al.* Epidemiology of inflammatory bowel disease in a German twin cohort: results of a nationwide study. *Inflamm Bowel Dis* **14**, 968-976 (2008).
35. Lander, E. & Kruglyak, L. Genetic dissection of complex traits: guidelines for interpreting and reporting linkage results. *Nat Genet* **11**, 241-247 (1995).
36. van Heel, D.a.*, et al.* Inflammatory bowel disease susceptibility loci defined by genome scan meta-analysis of 1952 affected relative pairs. *Human molecular genetics* **13**, 763-770 (2004).
37. Achkar, J.-P.*, et al.* Phenotype-stratified genetic linkage study demonstrates that IBD2 is an extensive ulcerative colitis locus. *The American journal of gastroenterology* **101**, 572-580 (2006).
38. Ogura, Y.*, et al.* A frameshift mutation in NOD2 associated with susceptibility to Crohn's disease. *Nature* **411**, 603-606 (2001).
39. Hampe, J.*, et al.* Association between insertion mutation in NOD2 gene and Crohn's disease in German and British populations. *The Lancet* **357**, 1925-1928 (2001).
40. Hugot, J.P.*, et al.* Association of NOD2 leucine-rich repeat variants with susceptibility to Crohn's disease. *Nature* **411**, 599-603 (2001).
41. Hugot, J.-P.*, et al.* Mapping of a susceptibility gene locus for Crohn's disease on chromosome 16. *Nature* **379**, 821-823 (1996).
42. Cho, J.*, et al.* Identification of novel susceptibility loci for inflammatory bowel disease on chromosomes 1p, 3q, and 4q: Evidence for epistasis between 1p and

IBD1. *Proceedings of the National Academy of Sciences of the United States of America* **95**, 7502-7507 (1998).
43. Consortium, T.I.H. A haplotype map of the human genome. *Nature* **437**, 1299-1320 (2005).
44. Yamazaki, K.*, et al.* Single nucleotide polymorphisms in TNFSF15 confer susceptibility to Crohn's disease. *Human molecular genetics* **14**, 3499-3506 (2005).
45. Tremelling, M.*, et al.* Contribution of TNFSF15 gene variants to Crohn's disease susceptibility confirmed in UK population. *Inflammatory bowel diseases* **14**, 733-737 (2008).
46. Franke, A.*, et al.* Genome-wide meta-analysis increases to 71 the number of confirmed Crohn's disease susceptibility loci. *Nat Genet* **42**, 1118-1125 (2010).
47. Duerr, R.H.*, et al.* A genome-wide association study identifies IL23R as an inflammatory bowel disease gene. *Science (New York, N.Y.)* **314**, 1461-1463 (2006).
48. Jonasdottir, A.*, et al.* A whole genome association study in Icelandic multiple sclerosis patients with 4804 markers. *Journal of Neuroimmunology* **143**, 88-92 (2003).
49. Goertsches, R.*, et al.* A genomic screen of Spanish multiple sclerosis patients reveals multiple loci associated with the disease. *Journal of Neuroimmunology* **143**, 124-128 (2003).
50. Consortium, T.W.T.C.C. Genome-wide association study of 14,000 cases of seven common diseases and 3,000 shared controls. *Nature* **447**, 661-678 (2007).
51. Smyth, D.J.*, et al.* A genome-wide association study of nonsynonymous SNPs identifies a type 1 diabetes locus in the interferon-induced helicase (IFIH1) region. *Nat Genet* **38**, 617-619 (2006).
52. Tamiya, G.*, et al.* Whole genome association study of rheumatoid arthritis using 27 039 microsatellites. *Human molecular genetics* **14**, 2305-2321 (2005).
53. van Heel, D.a.*, et al.* A genome-wide association study for celiac disease identifies risk variants in the region harboring IL2 and IL21. *Nat Genet* **39**, 827-829 (2007).
54. Zhernakova, A.*, et al.* Novel association in chromosome 4q27 region with rheumatoid arthritis and confirmation of type 1 diabetes point to a general risk locus for autoimmune diseases. *American journal of human genetics* **81**, 1284-1288 (2007).
55. Hampe, J.*, et al.* A genome-wide association scan of nonsynonymous SNPs identifies a susceptibility variant for Crohn disease in ATG16L1. *Nat Genet* **39**, 207-211 (2007).
56. Rioux, J.D.*, et al.* Genome-wide association study identifies new susceptibility loci for Crohn disease and implicates autophagy in disease pathogenesis. *Nat Genet* **39**, 596-604 (2007).
57. Parkes, M.*, et al.* Sequence variants in the autophagy gene IRGM and multiple other replicating loci contribute to Crohn's disease susceptibility. *Nat Genet* **39**, 830-832 (2007).
58. Libioulle, C.*, et al.* Novel Crohn disease locus identified by genome-wide association maps to a gene desert on 5p13.1 and modulates expression of PTGER4. *PLoS genetics* **3**, e58 (2007).
59. Bagnoli, S.*, et al.* Susceptibility to refractory ulcerative colitis is associated with polymorphism in the hMLH1 mismatch repair gene. *Inflammatory bowel diseases* **10**, 705-708 (2004).
60. Lee-Kirsch, M.A.*, et al.* Mutations in the gene encoding the 3'-5' DNA exonuclease TREX1 are associated with systemic lupus erythematosus. *Nat Genet* **39**, 1065-1067 (2007).
61. Szalai, C.*, et al.* Chemokine receptor CCR2 and CCR5 polymorphisms in children with insulin-dependent diabetes mellitus. *Pediatric research* **46**, 82-84 (1999).

62. Truelove, S., Ellis, H. & Webster, C. Place of a double-barrelled ileostomy in ulcerative colitis and crohn's disease of the colon: a preliminary report. *British Medical Journal* **5428**, 150-153 (1968).
63. Oberhelman, H.A., Kohatsu, S., Taylor, K.B., Kivel, R.M. & Alto, P. Diverting Ileostomy in the Surgical of Crohn ' s Disease of the Colon * Management. *Atlantic* **115**(1968).
64. Moss, A.A., Carbone, J.V. & Kressel, H.Y. Radiologic and Clinical Assessment in Crohn's of Broad-Spectrum Disease Antibiotic Therapy. *American Journal of Roentgenology* **131**, 787-790 (1978).
65. Vallance, B.A., Deng, W., Knodler, L.A. & Finlay, B.B. Mice Lacking T and B Lymphocytes Develop Transient Colitis and Crypt Hyperplasia yet Suffer Impaired Bacterial Clearance during Citrobacter rodentium Infection. *Infection and Immunity* **70**, 2070-2081 (2002).
66. Sacco, R.E.*, et al.* Reduction in inflammation following blockade of CD18 or CD29 adhesive pathways during the acute phase of a spirochetal-induced colitis in mice. *Microbial pathogenesis* **29**, 289-299 (2000).
67. Kullberg, M.C.*, et al.* Helicobacter hepaticus Triggers Colitis in (IL-10)-Deficient Mice through an IL-12- and Gamma Interferon-Dependent Mechanism. *Infection and immunity* **66**, 5157-5166 (1998).
68. Sacco, R.E., Haynes, J.S., Harp, J.A., Waters, W.R. & Wannemuehler, M.J. Short communication: Cryptosporidium parvum initiates inflammatory bowel disease in germfree T cell receptor-a-deficient mice. *American Journal of Pathology* **153**, 1717-1722 (1998).
69. Prindiville, T., Cantrell, M. & Wilson, K.H. Ribosomal DNA Sequence Analysis of Mucosa-Associated Bacteria in Crohn's Disease. *Inflammatory Bowel Diseases* **10**, 824-833 (2004).
70. Frank, D.N.*, et al.* Molecular-phylogenetic characterization of microbial community imbalances in human inflammatory bowel diseases. *Proceedings of the National Academy of Sciences of the United States of America* **104**, 13780-13785 (2007).
71. Sartor, R.B. Microbial influences in inflammatory bowel diseases. *Gastroenterology* **134**, 577-594 (2008).
72. Bäckhed, F., Ley, R.E., Sonnenburg, J.L., Peterson, D.a. & Gordon, J.I. Host-bacterial mutualism in the human intestine. *Science (New York, N.Y.)* **307**, 1915-1920 (2005).
73. Turnbaugh, P.J.*, et al.* An obesity-associated gut microbiome with increased capacity for energy harvest. *Nature* **444**, 1027-1031 (2006).
74. Mazmanian, S.K., Liu, C.H., Tzianabos, A.O. & Kasper, D.L. An immunomodulatory molecule of symbiotic bacteria directs maturation of the host immune system. *Cell* **122**, 107-118 (2005).
75. Collier-Hyams, L.S., Sloane, V., Batten, B.C. & Neish, A.S. Cutting Edge: Bacterial Modulation of Epithelial Signaling via Changes in Neddylation of Cullin-1 1. *Journal of Immunology* **175**, 4194-4198 (2005).
76. Tien, M.-T.*, et al.* Anti-inflammatory effect of Lactobacillus casei on Shigella-infected human intestinal epithelial cells. *Journal of immunology (Baltimore, Md. : 1950)* **176**, 1228-1237 (2006).
77. Segawa, S.*, et al.* Probiotic-Derived Polyphosphate Enhances the Epithelial Barrier Function and Maintains Intestinal Homeostasis through Integrin–p38 MAPK Pathway. *PLoS ONE* **6**, e23278 (2011).
78. MacPherson, A.J. A Primitive T Cell-Independent Mechanism of Intestinal Mucosal IgA Responses to Commensal Bacteria. *Science* **288**, 2222-2226 (2000).
79. MacPherson, A.J. & Uhr, T. Induction of protective IgA by intestinal dendritic cells carrying commensal bacteria. *Science (New York, N.Y.)* **303**, 1662-1665 (2004).
80. Neish, a.S. Prokaryotic Regulation of Epithelial Responses by Inhibition of Ikappa B-alpha Ubiquitination. *Science* **289**, 1560-1563 (2000).

81. Clavel, T. & Haller, D. Bacteria- and host-derived mechanisms to control intestinal epithelial cell homeostasis: implications for chronic inflammation. *Inflammatory bowel diseases* **13**, 1153-1164 (2007).
82. Conte, M.P.*, et al.* Gut-associated bacterial microbiota in paediatric patients with inflammatory bowel disease. *Gut* **55**, 1760-1767 (2006).
83. Manichanh, C.*, et al.* Reduced diversity of faecal microbiota in Crohn's disease revealed by a metagenomic approach. *Gut* **55**, 205-211 (2006).
84. Gophna, U., Sommerfeld, K., Gophna, S., Doolittle, W.F. & Veldhuyzen van Zanten, S.J.O. Differences between tissue-associated intestinal microfloras of patients with Crohn's disease and ulcerative colitis. *Journal of clinical microbiology* **44**, 4136-4141 (2006).
85. Bibiloni, R. The bacteriology of biopsies differs between newly diagnosed, untreated, Crohn's disease and ulcerative colitis patients. *Journal of Medical Microbiology* **55**, 1141-1149 (2006).
86. Dicksved, J.*, et al.* Molecular analysis of the gut microbiota of identical twins with Crohn's disease. *The ISME journal* **2**, 716-727 (2008).
87. Maccaferri, S.*, et al.* Rifaximin modulates the colonic microbiota of patients with Crohn's disease: an in vitro approach using a continuous culture colonic model system. *The Journal of antimicrobial chemotherapy* **65**, 2556-2565 (2010).
88. Sokol, H.*, et al.* Faecalibacterium prausnitzii is an anti-inflammatory commensal bacterium identified by gut microbiota analysis of Crohn disease patients. *Proceedings of the National Academy of Sciences of the United States of America* **105**, 16731-16736 (2008).
89. Swidsinski, A., Loening-Baucke, V., Vaneechoutte, M. & Doerffel, Y. Active Crohn's disease and ulcerative colitis can be specifically diagnosed and monitored based on the biostructure of the fecal flora. *Inflammatory bowel diseases* **14**, 147-161 (2008).
90. Sokol, H.*, et al.* Low counts of Faecalibacterium prausnitzii in colitis microbiota. *Inflammatory bowel diseases* **15**, 1183-1189 (2009).
91. Willing, B.*, et al.* Twin studies reveal specific imbalances in the mucosa-associated microbiota of patients with ileal Crohn's disease. *Inflammatory bowel diseases* **15**, 653-660 (2009).
92. Kang, S.*, et al.* Dysbiosis of fecal microbiota in Crohn's disease patients as revealed by a custom phylogenetic microarray. *Inflammatory bowel diseases* **16**, 2034-2042 (2010).
93. Benjamin, J.L.*, et al.* Smokers with active Crohn's disease have a clinically relevant dysbiosis of the gastrointestinal microbiota. *Inflammatory bowel diseases* **18**, 1092-1100 (2012).
94. Uzoigwe, J.C., Khaitsa, M.L. & Gibbs, P.S. Epidemiological evidence for Mycobacterium avium subspecies paratuberculosis as a cause of Crohn's disease. *Epidemiology and infection* **135**, 1057-1068 (2007).
95. Biet, F.*, et al.* Serum Antibodies to Mycobacterium avium Subspecies paratuberculosis Combined with Anti-Saccharomyces cerevisiae Antibodies in Crohn's Disease Patients: Prevalence and Diagnostic Role. *Digestive diseases and sciences* (2011).
96. Boudeau, J., Glasser, A.-l., Masseret, E., Joly, B. & Darfeuille-michaud, A. Invasive Ability of an Escherichia coli Strain Isolated from the Ileal Mucosa of a Patient with Crohn's Disease. *Infection and immunity* **67**, 4499-4509 (1999).
97. Darfeuille-Michaud, A.*, et al.* High prevalence of adherent-invasive Escherichia coli associated with ileal mucosa in Crohn's disease. *Gastroenterology* **127**, 412-421 (2004).
98. Glasser, A.-L.*, et al.* Adherent Invasive Escherichia coli Strains from Patients with Crohn's Disease Survive and Replicate within Macrophages without Inducing Host Cell Death. *Infection and Immunity* **69**, 5529-5537 (2001).

99. Denizot, J.*, et al.* Adherent-invasive Escherichia coli induce claudin-2 expression and barrier defect in CEABAC10 mice and crohn's disease patients. *Inflammatory bowel diseases* **18**, 294-304 (2011).
100. Mow, W.S.*, et al.* Association of antibody responses to microbial antigens and complications of small bowel Crohn's disease. *Gastroenterology* **126**, 414-424 (2004).
101. Lodes, M.J.*, et al.* Bacterial flagellin is a dominant antigen in Crohn disease. *Journal of Clinical Investigation* **113**(2004).
102. Yoshimura, T.*, et al.* Immunomodulatory Action of Levofloxacin on Cytokine Production by Human Peripheral Blood Mononuclear Cells. *Chemotherapy* **42**, 459-464 (1996).
103. Selby, W.*, et al.* Two-year combination antibiotic therapy with clarithromycin, rifabutin, and clofazimine for Crohn's disease. *Gastroenterology* **132**, 2313-2319 (2007).
104. Borgaonkar, M.R., Macintosh, D.G. & Fardy, J.M. A Meta-analysis of Antimycobacterial Therapy for Crohn's Disease. *American Journal of Gastroenterology* **95**, 725-729 (2000).
105. Rahimi, R., Nikfar, S., Rezaie, A. & Abdollahi, M. A meta-analysis of broad-spectrum antibiotic therapy in patients with active Crohn's disease. *Clinical therapeutics* **28**, 1983-1988 (2006).
106. Huang, J., Liao, C., Wu, L., Cao, Y. & Gao, F. A meta-analysis of randomized controlled trials comparing antibacterial therapy with placebo in Crohn's disease. *Colorectal disease : the official journal of the Association of Coloproctology of Great Britain and Ireland* **13**, 617-626 (2011).
107. Johansson, M.E.V.*, et al.* The inner of the two Muc2 mucin-dependent mucus layers in colon is devoid of bacteria. *Proceedings of the National Academy of Sciences of the United States of America* **105**, 15064-15069 (2008).
108. Larsson, J.M.H., Karlsson, H., Sjövall, H. & Hansson, G.C. A complex, but uniform O-glycosylation of the human MUC2 mucin from colonic biopsies analyzed by nanoLC/MSn. *Glycobiology* **19**, 756-766 (2009).
109. Price, A.B. & Morson, B.C. The Surgical Pathology of Crohn's Disease and Ulcerative Colitis. *Human pathology* **6**, 7-29 (1975).
110. Myllarniemi, H. & Nickels, J. Scanning Electron Microscopy of Crohn's Disease and Ulcerative Colitis of the Colon. *Virchows Arch. A. Path. Anat. and Histol.* **385**, 343-350 (1980).
111. Buisine, M.-P.*, et al.* Abnormalities in Mucin Gene Expression in Crohn's Disease. *Inflammatory Bowel Diseases* **5**, 24-32 (1999).
112. Laukoetter, M.G., Nava, P. & Nusrat, A. Role of the intestinal barrier in inflammatory bowel disease. *World journal of gastroenterology : WJG* **14**, 401-407 (2008).
113. Heller, F.*, et al.* Interleukin-13 Is the Key Effector Th2 Cytokine in Ulcerative Colitis That Affects Epithelial Tight Junctions, Apoptosis, and Cell Restitution. *Gastroenterology* **129**, 550-564 (2005).
114. Li, Y.*, et al.* Exogenous Stimuli Maintain Intraepithelial Lymphocytes via Aryl Hydrocarbon Receptor Activation. *Cell* **147**, 629-640 (2011).
115. Kiss, E.a.*, et al.* Natural Aryl Hydrocarbon Receptor Ligands Control Organogenesis of Intestinal Lymphoid Follicles. *Science (New York, N.Y.)* **1561**(2011).
116. Owen, K.a., Abshire, M.Y., Tilghman, R.W., Casanova, J.E. & Bouton, A.H. FAK Regulates Intestinal Epithelial Cell Survival and Proliferation during Mucosal Wound Healing. *PloS one* **6**, e23123 (2011).
117. Marchiando, A.M.*, et al.* The epithelial barrier is maintained by in vivo tight junction expansion during pathologic intestinal epithelial shedding. *Gastroenterology* **140**, 1208-1218.e1201-1202 (2011).

118. Kreisel, D.*, et al.* Cutting edge: MHC class II expression by pulmonary nonhematopoietic cells plays a critical role in controlling local inflammatory responses. *Journal of immunology (Baltimore, Md. : 1950)* **185**, 3809-3813 (2010).
119. Solberg, I.*, et al.* Clinical course in Crohn's disease: results of a Norwegian population-based ten-year follow-up study. *Clinical Gastroenterology and Hepatology* **5**, 1430-1438 (2007).
120. Seiderer, J.*, et al.* Predictive Value of the CARD15 Variant 1007fs for the Diagnosis of Intestinal Stenoses and the Need for Surgery in Crohn ' s Disease in Clinical Practice : Results of a Prospective Study. *Inflammatory Bowel Diseases* **12**, 1114-1121 (2006).
121. Gurtner, G.C., Werner, S., Barrandon, Y. & Longaker, M.T. Wound repair and regeneration. *Nature* **453**, 314-321 (2008).
122. Rogler, G.*, et al.* Differential activation of cytokine secretion in primary human colonic fibroblast/myofibroblast cultures. *Scandinavian journal of gastroenterology* **36**, 389-398 (2001).
123. Bousvaros, A.*, et al.* Serum Basic Fibroblast Growth Factor in Pediatric Crohn's Disease Implications for Wound Healing. *Digestive Diseases and Sciences* **42**, 378-386 (1997).
124. Bousvaros, A.*, et al.* Elevated Serum Vascular Endothelial Growth Factor in Children and Young Adults with Crohn's Disease. *Digestive Diseases and Sciences* **44**, 424-430 (1999).
125. Kanazawa, S.*, et al.* VEGF, Basic-FGF, and TGF-β in Crohn' s Disease and Ulcerative Colitis: A Novel Mechanism of Chronic Intestinal Inflammation. *American Journal of Gastroenterology* **96**, 822-828 (2001).
126. Bulut, K.*, et al.* Vascular endothelial growth factor (VEGF 164) ameliorates intestinal epithelial injury in vitro in IEC-18 and Caco-2 monolayers via induction of TGF-β release from epithelial cells. *Scandinavian Journal of Gastroenterology* **41**, 687-692 (2006).
127. Clauss, M.*, et al.* Vascular Permeability Factor: A Tumor-derived Polypeptide that Induces Endothelial Cell and Monocyte Procoagulant Activity, and Promotes Monocyte Migration. *Journal of Experimental Medicine* **172**, 1535-1545 (1990).
128. Burke, J.P., Cunningham, M.F., Sweeney, C., Docherty, N.G. & O'Connell, P.R. N-cadherin is overexpressed in Crohn's stricture fibroblasts and promotes intestinal fibroblast migration. *Inflammatory bowel diseases* **17**, 1665-1673 (2011).
129. Leeb, S.N.*, et al.* Reduced Migration of Fibroblasts in Inflammatory Bowel Disease: Role of Inflammatory Mediators and Focal Adhesion Kinase. *Gastroenterology* **125**, 1341-1354 (2003).
130. Brannigan, A.E.*, et al.* Increased adhesion molecule expression in serosal fibroblasts isolated from patients with inflammatory bowel disease is secondary to inflammation. *Annals of surgery* **235**, 507-511 (2002).
131. Tao, Q., Ren, J. & Li, J. Vasoactive intestinal peptide inhibits adhesion molecule expression in activated human colon serosal fibroblasts by preventing NF-kappaB activation. *The Journal of surgical research* **140**, 84-89 (2007).
132. Koch, T.R., Carney, J.A. & Go, V.L.W. Distribution and Quantitation of Gut Neuropeptides in Normal Intestine and Inflammatory Bowel Diseases. *Digestive Diseases and Sciences* **32**, 369-376 (1987).
133. Zimmermann, E.M.*, et al.* IGF-I induces collagen and IGFBP-5 mRNA in rat intestinal smooth muscle. *American Journal of Physiology, Gastrointestinal and Liver Physiology* **273**, 875-882 (1997).
134. Zimmermann, E.M., Li, L., Hou, Y.T., Mohapatra, N.K. & Pucilowska, J.B. Insulin-like growth factor I and insulin-like growth factor binding protein 5 in Crohn's disease. *Am J Physiol Gastroinest Liver Physiol* **280**, G1022-1029 (2001).

135. Hao, J.*, et al.* Elevation of Expression of Smads 2, 3, and 4, Decorin and TGF-b in the Chronic Phase of Myocardial Infarct Scar Healing. *Journal of Molecular and Cell Cardiology* **31**, 667-678 (1999).
136. Flynn, R.S.*, et al.* Endogenous IGFBP-3 regulates excess collagen expression in intestinal smooth muscle cells of Crohn's disease strictures. *Inflammatory Bowel Diseases* **17**, 193-201 (2011).
137. Mulsow, J.J.W., Watson, R.W.G., Fitzpatrick, J.M. & O'Connell, P.R. Transforming Growth Factor-b Promotes Pro-fibrotic Behavior by Serosal Fibroblasts via PKC and ERK1/2 Mitogen Activated Protein Kinase Cell Signaling. *Annals of Surgery* **242**, 880-889 (2005).
138. Burke, J.P.*, et al.* Endoglin negatively regulates transforming growth factor beta1-induced profibrotic responses in intestinal fibroblasts. *The British journal of surgery* **97**, 892-901 (2010).
139. McKaig, B.C., McWilliams, D., Watson, S.a. & Mahida, Y.R. Expression and regulation of tissue inhibitor of metalloproteinase-1 and matrix metalloproteinases by intestinal myofibroblasts in inflammatory bowel disease. *The American journal of pathology* **162**, 1355-1360 (2003).
140. Ogura, Y.*, et al.* Expression of NOD2 in Paneth cells: a possible link to Crohn's ileitis. *Gut* **52**, 1591-1597 (2003).
141. Haapamäki, M.M.*, et al.* Gene expression of group II phospholipase A2 in intestine in ulcerative colitis. *Gut* **40**, 95-101 (1997).
142. Ghoos, Y. & Vantrappen, G. The cytochemical localization of lysozyme in Paneth cell granules. *The Histochemical journal* **3**, 175-178 (1971).
143. Harwig, S.S.*, et al.* Bactericidal properties of murine intestinal phospholipase A2. *The Journal of clinical investigation* **95**, 603-610 (1995).
144. Ayabe, T.*, et al.* Secretion of microbicidal alpha-defensins by intestinal Paneth cells in response to bacteria. *Nature immunology* **1**, 113-118 (2000).
145. Wehkamp, J., Koslowski, M., Wang, G. & Stange, E.F. Barrier dysfunction due to distinct defensin deficiencies in small intestinal and colonic Crohn's disease. *Mucosal immunology* **1 Suppl 1**, S67-74 (2008).
146. Voss, E.*, et al.* NOD2/CARD15 mediates induction of the antimicrobial peptide human beta-defensin-2. *The Journal of biological chemistry* **281**, 2005-2011 (2006).
147. Lala, S.*, et al.* Crohn's disease and the NOD2 gene: a role for paneth cells. *Gastroenterology* **125**, 47-57 (2003).
148. Wehkamp, J.*, et al.* Reduced Paneth cell alpha-defensins in ileal Crohn's disease. *Proceedings of the National Academy of Sciences of the United States of America* **102**, 18129-18134 (2005).
149. Petnicki-Ocwieja, T.*, et al.* Nod2 is required for the regulation of commensal microbiota in the intestine. *Proceedings of the National Academy of Sciences of the United States of America* **106**, 15813-15818 (2009).
150. Ciccia, F.*, et al.* Over-expression of paneth cell-derived anti-microbial peptides in the gut of patients with ankylosing spondylitis and subclinical intestinal inflammation. *Rheumatology (Oxford, England)* **49**, 2076-2083 (2010).
151. Lochner, M.*, et al.* In vivo equilibrium of proinflammatory IL-17+ and regulatory IL-10+ Foxp3+ RORgamma t+ T cells. *The Journal of experimental medicine* **205**, 1381-1393 (2008).
152. Bennett, C.L.*, et al.* The immune dysregulation, polyendocrinopathy, enteropathy, X-linked syndrome (IPEX) is caused by mutations of FOXP3. *Nat Genet* **27**, 20-21 (2001).
153. Wildin, R.S.*, et al.* X-linked neonatal diabetes mellitus, enteropathy and endocrinopathy syndrome is the human equivalent of mouse scurfy. *Nat Genet* **27**, 18-20 (2001).
154. Snapper, S.B.*, et al.* Wiskott-Aldrich Syndrome Protein-Deficient Mice Reveal a Role for WASP in T but Not B Cell Activation. *Immunity* **9**, 81-91 (1998).

155. Cretney, E.*, et al.* The transcription factors Blimp-1 and IRF4 jointly control the differentiation and function of effector regulatory T cells. *Nature immunology* **12**, 304-311 (2011).
156. Coombes, J.L.*, et al.* A functionally specialized population of mucosal CD103+ DCs induces Foxp3+ regulatory T cells via a TGF-beta and retinoic acid-dependent mechanism. *The Journal of experimental medicine* **204**, 1757-1764 (2007).
157. Rahman, M.K.*, et al.* The pathogen recognition receptor NOD2 regulates human FOXP3+ T cell survival. *Journal of immunology (Baltimore, Md. : 1950)* **184**, 7247-7256 (2010).
158. Ramon, H.E.*, et al.* The ubiquitin ligase adaptor Ndfip1 regulates T cell-mediated gastrointestinal inflammation and inflammatory bowel disease susceptibility. *Mucosal Immunology* **4**, 314-324 (2010).
159. Shembade, N.*, et al.* The E3 ligase Itch negatively regulates inflammatory signaling pathways by controlling the function of the ubiquitin-editing enzyme A20. *Nature Immunology* **9**, 254-262 (2008).
160. Venuprasad, K.*, et al.* The E3 ubiquitin ligase Itch regulates expression of transcription factor Foxp3 and airway inflammation by enhancing the function of transcription factor TIEG1. *Nature Immunology* **9**, 245-253 (2008).
161. Lohr, N.J.*, et al.* Human ITCH E3 Ubiquitin Ligase Deficiency Causes Syndromic Multisystem Autoimmune Disease. *The American Journal of Human Genetics* **86**, 447-453 (2010).
162. Bettelli, E.*, et al.* Reciprocal developmental pathways for the generation of pathogenic effector TH17 and regulatory T cells. *Nature* **441**, 235-238 (2006).
163. Ghoreschi, K.*, et al.* Generation of pathogenic T(H)17 cells in the absence of TGF-β signalling. *Nature* **467**, 967-971 (2010).
164. Do, J.-s., Visperas, A., Dong, C., Baldwin, W.M. & Min, B. Generation of Colitogenic Th17 CD4 T Cells Is Enhanced by IL-17+gamma-delta T Cells. *The Journal of Immunology* **186**, 4546-4550 (2011).
165. Park, S.-G.*, et al.* T regulatory cells maintain intestinal homeostasis by suppressing γ δ T cells. *Immunity* **33**, 791-803 (2010).
166. Chen, Y.*, et al.* Foxp3(+) regulatory T cells promote T helper 17 cell development in vivo through regulation of interleukin-2. *Immunity* **34**, 409-421 (2011).
167. Momozawa, Y.*, et al.* Resequencing of positional candidates identifies low frequency IL23R coding variants protecting against inflammatory bowel disease. *Nat Genet* **43**, 43-47 (2011).
168. Rivas, M.a.*, et al.* Deep resequencing of GWAS loci identifies independent rare variants associated with inflammatory bowel disease. *Nat Genet* **43**, 1066-1073 (2011).
169. Di Meglio, P.*, et al.* The IL23R R381Q gene variant protects against immune-mediated diseases by impairing IL-23-induced Th17 effector response in humans. *PloS one* **6**, e17160 (2011).
170. Ferreira, R.C.*, et al.* Association of IFIH1 and other autoimmunity risk alleles with selective IgA deficiency. *Nat Genet* **42**, 777-780 (2010).
171. Olson, T.S.*, et al.* Expanded B cell population blocks regulatory T cells and exacerbates ileitis in a murine model of Crohn disease. *The Journal of clinical investigation* **114**, 389-398 (2004).
172. Mizoguchi, A., Mizoguchi, E., Takedatsu, H., Blumberg, R.S. & Bhan, A.K. Chronic intestinal inflammatory condition Generates IL-10-Producing Regulatory B Cell Subset Characterized by CD1d Upregulation. *Immunity* **16**, 219-230 (2002).
173. Mitchison, N.A. T-cell–B-cell cooperation. *Nature reviews. Immunology* **308**, 308-312 (2004).

174. Prescott, N.J., *et al.* A nonsynonymous SNP in ATG16L1 predisposes to ileal Crohn's disease and is independent of CARD15 and IBD5. *Gastroenterology* **132**, 1665-1671 (2007).
175. Singh, S.B., Davis, A.S., Taylor, G.A. & Deretic, V. Human IRGM induces autophagy to eliminate intracellular mycobacteria. *Science* **313**, 1438-1441 (2006).
176. Steinman, R.M. & Cohn, Z.A. Identification of a novel cell type in peripheral lymphoid organs of mice I. Morphology, quantitation, tissue distibution. *The Journal of experimental medicine* **137**, 1142-1162 (1973).
177. Steinman, R.M. Dendritic cells: understanding immunogenicity. *European Journal of Immunology* **37 Suppl 1**, S53-60 (2007).
178. Naik, S.H. Demystifying the development of dendritic cell subtypes, a little. *Immunol Cell Biol* **86**, 439-452 (2008).
179. Hume, D.A. Macrophages as APC and the dendritic cell myth. *J Immunol* **181**, 5829-5835 (2008).
180. van Furth, R., Raeburn, J.A. & van Zwet, T.L. Characteristics of human mononuclear phagocytes. *Blood* **54**, 485-500 (1979).
181. Geissmann, F., *et al.* Development of monocytes, macrophages, and dendritic cells. *Science (New York, N.Y.)* **327**, 656-661 (2010).
182. Yona, S. & Jung, S. Monocytes: subsets, origins, fates and functions. *Current opinion in hematology* **17**, 53-59 (2010).
183. Steinman, R.M. & Witmer, M.D. Lymphoid dendritic cells are potent stimulators of the primary mixed leukocyte reaction in mice Immunology. *Proceedings of the National Academy of Sciences of the United States of America* **75**, 5132-5136 (1978).
184. Sallusto, B.F. & Lanzavecchia, A. Efficient presentation of soluble antigen by cultured human dendritic cells is maintained by granulocyte/macrophage colony-stimulating factor plus interleukin 4 and downregulated by tumor necrosis factor alpha. *The Journal of experimental medicine* **179**, 1109-1118 (1994).
185. De Smedt, T., *et al.* Regulation of Dendritic Cell Numbers and Maturation by Lipopolysaccharide In Vivo. *Journal of Experimental Medicine* **184**, 1413-1424 (1996).
186. Garrett, W.S., *et al.* Developmental control of endocytosis in dendritic cells by Cdc42. *Cell* **102**, 325-334 (2000).
187. West, M.a., Prescott, a.R., Eskelinen, E.L., Ridley, a.J. & Watts, C. Rac is required for constitutive macropinocytosis by dendritic cells but does not control its downregulation. *Current biology : CB* **10**, 839-848 (2000).
188. Arnold-Schild, D., *et al.* Cutting edge: receptor-mediated endocytosis of heat shock proteins by professional antigen-presenting cells. *Journal of immunology (Baltimore, Md. : 1950)* **162**, 3757-3760 (1999).
189. Schmid, D., Pypaert, M. & Münz, C. MHC class II antigen loading compartments continuously receive input from autophagosomes. *Immunity* **26**, 79-92 (2007).
190. Cooney, R., *et al.* NOD2 stimulation induces autophagy in dendritic cells influencing bacterial handling and antigen presentation. *Nature medicine* **16**, 90-97 (2010).
191. Dongre, A.R., *et al.* In vivo MHC class II presentation of cytosolic proteins revealed by rapid automated tandem mass spectrometry and functional analyses. *European Journal of Immunology* **31**, 1485-1494 (2001).
192. Chicz, R.M., *et al.* Specificity and Promiscuity among Naturally Processed Peptides Bound to HLA-DR Alleles. *Journal of Experimental Medicine* **178**, 27-47 (1993).
193. Dengjel, J., *et al.* Autophagy promotes MHC class II presentation of peptides from intracellular source proteins. *Proceedings of the National Academy of Sciences of the United States of America* **102**, 7922-7927 (2005).
194. Tsai, A.G. & Lieber, M.R. Mechanisms of chromosomal rearrangement in the human genome. *BMC genomics* **11 Suppl 1**, S1 (2010).
195. Takeda, K. & Akira, S. TLR signaling pathways. *Seminars in Immunology* **16**, 3-9 (2004).

196. Medzhitov, R., Preston-hurlburt, P. & Jr, C.A.J. letters to nature A human homologue of the Drosophila Toll protein signals activation of adaptive immunity. *Nature* **388**, 6-9 (1997).
197. Lien, E.*, et al.* Toll-like Receptor 2 Functions as a Pattern Recognition Receptor for Diverse Bacterial Products. *The Journal of biological chemistry* **274**, 33419-33425 (1999).
198. Takeuchi, O.*, et al.* Cutting edge: role of Toll-like receptor 1 in mediating immune response to microbial lipoproteins. *Journal of immunology (Baltimore, Md. : 1950)* **169**, 10-14 (2002).
199. Takeuchi, O.*, et al.* Discrimination of bacterial lipoproteins by Toll-like receptor 6. *International immunology* **13**, 933-940 (2001).
200. Hayashi, F.*, et al.* The innate immune response to bacterial flagellin is mediated by Toll-like receptor 5. *Nature* **410**, 1099-1103 (2001).
201. Poltorak, A.*, et al.* Defective LPS Signaling in C3H/HeJ and C57BL/10ScCr Mice: Mutations in Tlr4 Gene. *Science* **282**, 2085-2088 (1998).
202. Heil, F.*, et al.* Species-specific recognition of single-stranded RNA via toll-like receptor 7 and 8. *Science (New York, N.Y.)* **303**, 1526-1529 (2004).
203. Bauer, S.*, et al.* Human TLR9 confers responsiveness to bacterial DNA via species-specific CpG motif recognition. *Proceedings of the National Academy of Sciences of the United States of America* **98**, 9237-9242 (2001).
204. Medzhitov, R.*, et al.* MyD88 is an adaptor protein in the hToll/IL-1 receptor family signaling pathways. *Molecular cell* **2**, 253-258 (1998).
205. Kawai, T., Adachi, O., Ogawa, T., Takeda, K. & Akira, S. Unresponsiveness of MyD88-deficient mice to endotoxin. *Immunity* **11**, 115-122 (1999).
206. Muzio, M. IRAK (Pelle) Family Member IRAK-2 and MyD88 as Proximal Mediators of IL-1 Signaling. *Science* **278**, 1612-1615 (1997).
207. Muzio, M., Natoli, G., Saccani, S., Levrero, M. & Mantovani, A. The Human Toll Signaling Pathway: Divergence of Nuclear Factor kB and JNK/SAPK activation upstream of Tumor Necrosis Factor Receptor–associated Factor 6 (TRAF6). *Journal of Experimental Medicine* **187**, 2097-2101 (1998).
208. Church, L.D., Cook, G.P. & McDermott, M.F. Primer: inflammasomes and interleukin 1beta in inflammatory disorders. *Nature clinical practice. Rheumatology* **4**, 34-42 (2008).
209. Roy, N.*, et al.* The gene for neuronal apoptosis inhibitory protein is partially deleted in individuals with spinal muscular atrophy. *Cell* **80**, 167-178 (1995).
210. Chamaillard, M., Girardin, S.E., Viala, J. & Philpott, D.J. Nods, Nalps and Naip: intracellular regulators of bacterial-induced inflammation. *Cellular Microbiology* **5**, 581-592 (2003).
211. Shaw, M.H., Reimer, T., Kim, Y.-g. & Nuñez, G. NOD-like Receptors (NLRs): Bona Fide Intracellular Microbila Sensors. *Current opinion in immunology* **20**, 377-382 (2008).
212. Martinon, F., Petrilli, V., Mayor, A., Tardivel, A. & Tschopp, J. Gout-associated uric acid crystals activate the NALP3 inflammasome. *Nature* **440**, 237-241 (2006).
213. Martinon, F., Mayor, A. & Tschopp, J. The inflammasomes: guardians of the body. *Annu Rev Immunol* **27**, 229-265 (2009).
214. Ferwerda, G.*, et al.* Engagement of NOD2 has a dual effect on proIL-1beta mRNA transcription and secretion of bioactive IL-1beta. *Eur J Immunol* **38**, 184-191 (2008).
215. Hsu, L.C.*, et al.* A NOD2-NALP1 complex mediates caspase-1-dependent IL-1beta secretion in response to Bacillus anthracis infection and muramyl dipeptide. *Proc Natl Acad Sci U S A* **105**, 7803-7808 (2008).
216. Pan, Q.*, et al.* MDP-induced interleukin-1beta processing requires Nod2 and CIAS1/NALP3. *J Leukoc Biol* **82**, 177-183 (2007).
217. Bruey, J.M.*, et al.* Bcl-2 and Bcl-XL regulate proinflammatory caspase-1 activation by interaction with NALP1. *Cell* **129**, 45-56 (2007).

218. Martinon, F., Agostini, L., Meylan, E. & Tschopp, J. Identification of bacterial muramyl dipeptide as activator of the NALP3/cryopyrin inflammasome. *Curr Biol* **14**, 1929-1934 (2004).
219. Nakahira, K.*, et al.* Autophagy proteins regulate innate immune responses by inhibiting the release of mitochondrial DNA mediated by the NALP3 inflammasome. *Nat Immunol* (2010).
220. Saitoh, T.*, et al.* Loss of the autophagy protein Atg16L1 enhances endotoxin-induced IL-1beta production. *Nature* **456**, 264-268 (2008).
221. Suzuki, T. & Nunez, G. A role for Nod-like receptors in autophagy induced by Shigella infection. *Autophagy* **4**, 73-75 (2008).
222. Zhou, R., Yazdi, A.S., Menu, P. & Tschopp, J. A role for mitochondria in NLRP3 inflammasome activation. *Nature* (2010).
223. Otte, J.-M., Rosenberg, I.M. & Podolsky, D.K. Intestinal myofibroblasts in innate immune responses of the intestine. *Gastroenterology* **124**, 1866-1878 (2003).
224. Girardin, S.E.*, et al.* Nod2 is a general sensor of peptidoglycan through muramyl dipeptide (MDP) detection. *J Biol Chem* **278**, 8869-8872 (2003).
225. Inohara, N.*, et al.* Host recognition of bacterial muramyl dipeptide mediated through NOD2. Implications for Crohn's disease. *J Biol Chem* **278**, 5509-5512 (2003).
226. Marina-Garcia, N.*, et al.* Clathrin- and dynamin-dependent endocytic pathway regulates muramyl dipeptide internalization and NOD2 activation. *J Immunol* **182**, 4321-4327 (2009).
227. Lee, J.*, et al.* pH-dependent internalization of muramyl peptides from early endosomes enables Nod1 and Nod2 signaling. *The Journal of biological chemistry* **284**, 23818-23829 (2009).
228. Abbott, D.W., Wilkins, A., Asara, J.M. & Cantley, L.C. The Crohn's disease protein, NOD2, requires RIP2 in order to induce ubiquitinylation of a novel site on NEMO. *Curr Biol* **14**, 2217-2227 (2004).
229. Inohara, Chamaillard, McDonald, C. & Nunez, G. NOD-LRR proteins: role in host-microbial interactions and inflammatory disease. *Annu Rev Biochem* **74**, 355-383 (2005).
230. Kobayashi, K.S.*, et al.* Nod2-dependent regulation of innate and adaptive immunity in the intestinal tract. *Science* **307**, 731-734 (2005).
231. Pauleau, A.L. & Murray, P.J. Role of nod2 in the response of macrophages to toll-like receptor agonists. *Mol Cell Biol* **23**, 7531-7539 (2003).
232. Travassos, L.H.*, et al.* Nod1 and Nod2 direct autophagy by recruiting ATG16L1 to the plasma membrane at the site of bacterial entry. *Nature immunology* **11**, 55-62 (2010).
233. McDonald, C.*, et al.* A role for Erbin in the regulation of Nod2-dependent NF-kappaB signaling. *The Journal of biological chemistry* **280**, 40301-40309 (2005).
234. Kufer, T.a., Kremmer, E., Banks, D.J. & Philpott, D.J. Role for erbin in bacterial activation of Nod2. *Infection and immunity* **74**, 3115-3124 (2006).
235. Eitel, J.*, et al.* Beta-PIX and Rac1 GTPase mediate trafficking and negative regulation of NOD2. *Journal of immunology (Baltimore, Md. : 1950)* **181**, 2664-2671 (2008).
236. Bielig, H.*, et al.* A function for AAMP in Nod2-mediated NF-kappaB activation. *Molecular immunology* **46**, 2647-2654 (2009).
237. Rosenstiel, P.*, et al.* A short isoform of NOD2/CARD15, NOD2-S, is an endogenous inhibitor of NOD2/receptor-interacting protein kinase 2-induced signaling pathways. *Proceedings of the National Academy of Sciences of the United States of America* **103**, 3280-3285 (2006).
238. Rosenstiel, P.*, et al.* Functional characterization of two novel 5' untranslated exons reveals a complex regulation of NOD2 protein expression. *BMC genomics* **8**, 472 (2007).
239. Yamamoto-Furusho, J.K., Barnich, N., Xavier, R., Hisamatsu, T. & Podolsky, D.K. Centaurin beta1 down-regulates nucleotide-binding oligomerization domains 1- and

2-dependent NF-kappaB activation. *The Journal of biological chemistry* **281**, 36060-36070 (2006).
240. Park, J.-H.*, et al.* RICK/RIP2 mediates innate immune responses induced through Nod1 and Nod2 but not TLRs. *Journal of immunology (Baltimore, Md. : 1950)* **178**, 2380-2386 (2007).
241. Bertrand, M.J.M.*, et al.* Cellular inhibitors of apoptosis cIAP1 and cIAP2 are required for innate immunity signaling by the pattern recognition receptors NOD1 and NOD2. *Immunity* **30**, 789-801 (2009).
242. Tigno-Aranjuez, J.T., Asara, J.M. & Abbott, D.W. Inhibition of RIP2's tyrosine kinase activity limits NOD2-driven cytokine responses. *Genes & Development* **24**, 2666-2677 (2010).
243. Hasegawa, M.*, et al.* A critical role of RICK/RIP2 polyubiquitination in Nod-induced NF-kappaB activation. *The EMBO journal* **27**, 373-383 (2008).
244. Yang, Y.*, et al.* NOD2 pathway activation by MDP or Mycobacterium tuberculosis infection involves the stable polyubiquitination of Rip2. *The Journal of biological chemistry* **282**, 36223-36229 (2007).
245. Bertrand, M.J.M.*, et al.* cIAP1 and cIAP2 facilitate cancer cell survival by functioning as E3 ligases that promote RIP1 ubiquitination. *Molecular cell* **30**, 689-700 (2008).
246. Newton, K.*, et al.* Ubiquitin chain editing revealed by polyubiquitin linkage-specific antibodies. *Cell* **134**, 668-678 (2008).
247. Hitotsumatsu, O.*, et al.* The ubiquitin-editing enzyme A20 restricts nucleotide-binding oligomerization domain containing 2-triggered signals. *Immunity* **28**, 381-390 (2008).
248. Chen, C.-M., Gong, Y., Zhang, M. & Chen, J.-J. Reciprocal cross-talk between Nod2 and TAK1 signaling pathways. *The Journal of biological chemistry* **279**, 25876-25882 (2004).
249. Wang, C.*, et al.* TAK1 is a ubiquitin-dependent kinase of MKK and IKK. *Nature* **412**, 346-351 (2001).
250. Takaesu, G.*, et al.* Interleukin-1 (IL-1) Receptor-Associated Kinase Leads to Activation of TAK1 by Inducing TAB2 Translocation in the IL-1 Signaling Pathway. *Molecular and Cellular Biology* **21**, 2475-2484 (2001).
251. Ninomiya-tsuji, J.*, et al.* The kinase TAK1 can activate the NIK-IkB as well as the MAP kinase cascade in the IL-1 signalling pathway. *Nature* **398**, 252-256 (1999).
252. Wald, D., Commane, M., Stark, G.R. & Li, X. IRAK and TAK1 are required for IL-18-mediated signaling. *European journal of immunology* **31**, 3747-3754 (2001).
253. Mizukami, J.*, et al.* Receptor Activator of NF-κB Ligand (RANKL) Activates TAK1 Mitogen-Activated Protein Kinase Kinase Kinase through a Signaling Complex Containing RANK, TAB2, and TRAF6. *Molecular and Cellular Biology* **22**, 992-1000 (2002).
254. Yamaguchi, K.*, et al.* Identification of a member of the MAPKKK family as a potential mediator of TGF-beta signal transduction. *Science (New York, N.Y.)* **270**, 2008-2011 (1995).
255. Hara, H.*, et al.* The adaptor protein CARD9 is essential for the activation of myeloid cells through ITAM-associated and Toll-like receptors. *Nature immunology* **8**, 619-629 (2007).
256. LeibundGut-Landmann, S.*, et al.* Syk- and CARD9-dependent coupling of innate immunity to the induction of T helper cells that produce interleukin 17. *Nature immunology* **8**, 630-638 (2007).
257. Cuthbert, A.P.*, et al.* The contribution of NOD2 gene mutations to the risk and site of disease in inflammatory bowel disease. *Gastroenterology* **122**, 867-874 (2002).
258. Lesage, S.*, et al.* CARD15/NOD2 mutational analysis and genotype-phenotype correlation in 612 patients with inflammatory bowel disease. *American journal of human genetics* **70**, 845-857 (2002).

259. Sugimura, K.*, et al.* A novel NOD2/CARD15 haplotype conferring risk for Crohn disease in Ashkenazi Jews. *American journal of human genetics* **72**, 509-518 (2003).
260. Hugot, J.P.*, et al.* Prevalence of CARD15/NOD2 mutations in Caucasian healthy people. *The American journal of gastroenterology* **102**, 1259-1267 (2007).
261. Yazdanyar, S. & Nordestgaard, B.G. NOD2/CARD15 genotype and common gastrointestinal diseases in 43,600 individuals. *Journal of internal medicine* **267**, 228-236 (2010).
262. Dassopoulos, T.*, et al.* NOD2 mutations and anti-Saccharomyces cerevisiae antibodies are risk factors for Crohn's disease in African Americans. *The American journal of gastroenterology* **105**, 378-386 (2010).
263. Kugathasan, S.*, et al.* Comparative phenotypic and CARD15 mutational analysis among African American, Hispanic and White Children with Crohn's Disease. *Inflammatory Bowel Diseases* **11**, 631-638 (2005).
264. Inoue, N. Lack of common NOD2 variants in Japanese patients with Crohn's disease. *Gastroenterology* **123**, 86-91 (2002).
265. Yamazaki, K., Takazoe, M., Tanaka, T., Kazumori, T. & Nakamura, Y. Absence of mutation in the NOD2/CARD15 gene among 483 Japanese patients with Crohn's disease. *Journal of Human Genetics* **47**, 469-472 (2002).
266. Leong, R.W.L.*, et al.* NOD2/CARD15 gene polymorphisms and Crohn's disease in the Chinese population. *Alimentary Pharmacology and Therapeutics* **17**, 1465-1470 (2003).
267. Mahurkar, S.*, et al.* Common variants in NOD2 and IL23R are not associated with inflammatory bowel disease in Indians. *Journal of gastroenterology and hepatology* **26**, 694-699 (2011).
268. Croucher, P.J.P.*, et al.* Haplotype structure and association to Crohn's disease of CARD15 mutations in two ethnically divergent populations. *European journal of human genetics : EJHG* **11**, 6-16 (2003).
269. Lee, G.H., Kim, C.G., Kim, J.S., Jung, H.C. & Song, I.S. Frequency Analysis of NOD2 Gene Mutations in Korean Patients with Crohn's Disease. *The Korean Journal of Gastroenterology* **45**, 162-168 (2005).
270. Chua, K.H.*, et al.* Identification of NOD2/CARD15 mutations in Malaysian patients with Crohn's disease. *Journal of Digestive Diseases* **10**, 124-130 (2009).
271. Ozen, S.C.*, et al.* NOD2/CARD15, NOD1/CARD4, and ICAM-1 gene polymorphisms in Turkish patients with inflammatory bowel disease. *Journal of gastroenterology* **41**, 304-310 (2006).
272. Zouiten-Mekki, L.*, et al.* CARD15/NOD2 in a Tunisian Population with Crohn's Disease. *Digestive Diseases and Sciences* **50**, 130-135 (2005).
273. Holler, E.*, et al.* Both donor and recipient NOD2/CARD15 mutations associate with transplant-related mortality and GvHD following allogeneic stem cell transplantation. *Blood* **104**, 889-894 (2004).
274. Appenrodt, B.*, et al.* Nucleotide-binding oligomerization domain containing 2 (NOD2) variants are genetic risk factors for death and spontaneous bacterial peritonitis in liver cirrhosis. *Hepatology* **51**, 1327-1333 (2010).
275. Bruns, T.*, et al.* NOD2 gene variants are a risk factor for culture-positive spontaneous bacterial peritonitis and monomicrobial bacterascites in cirrhosis. *Liver International* **32**, 223-230 (2012).
276. Nischalke, H.D.*, et al.* Toll-like receptor (TLR) 2 promoter and intron 2 polymorphisms are associated with increased risk for spontaneous bacterial peritonitis in liver cirrhosis. *Journal of hepatology* **55**, 1010-1016 (2011).
277. Fishbein, T.*, et al.* NOD2-expressing bone marrow-derived cells appear to regulate epithelial innate immunity of the transplanted human small intestine. *Gut* **57**, 323-330 (2008).

278. Ningappa, M., *et al.* NOD2 gene polymorphism rs2066844 associates with need for combined liver-intestine transplantation in children with short-gut syndrome. *The American journal of gastroenterology* **106**, 157-165 (2011).
279. Courivaud, C., *et al.* No evidence of association between NOD2/CARD15 gene polymorphism and atherosclerotic events after renal transplantation. *Transplantation* **81**, 1212-1215 (2006).
280. Krüger, B., *et al.* Impact of NOD2/CARD15 haplotypes on the outcome after kidney transplantation. *Transplant international : official journal of the European Society for Organ Transplantation* **20**, 600-607 (2007).
281. Zhang, F.-R., *et al.* Genomewide association study of leprosy. *The New England Journal of Medicine* **361**, 2609-2618 (2009).
282. Berrington, W.R., *et al.* Common polymorphisms in the NOD2 gene region are associated with leprosy and its reactive states. *The Journal of infectious diseases* **201**, 1422-1435 (2010).
283. Stockton, J.C., *et al.* Polymorphism in NOD2, Crohn's disease, and susceptibility to pulmonary tuberculosis. *FEMS immunology and medical microbiology* **41**, 157-160 (2004).
284. Möller, M., *et al.* Host susceptibility to tuberculosis: CARD15 polymorphisms in a South African population. *Molecular and cellular probes* **21**, 148-151 (2007).
285. Austin, C.M., Ma, X. & Graviss, E.a. Common nonsynonymous polymorphisms in the NOD2 gene are associated with resistance or susceptibility to tuberculosis disease in African Americans. *The Journal of infectious diseases* **197**, 1713-1716 (2008).
286. Blau, E.B. Familial granulomatous arthritis, iritis, and rash. *The Journal of pediatrics* **107**, 689-693 (1985).
287. Jabs, D.A., Houk, L.J., Bias, W.B. & Arnett, F.C. Familial Granulomatous Synovitis, Uveitis and Cranial Neuropathies. *The American Journal of Medicine* **78**, 801-804 (1985).
288. Miceli-Richard, C., *et al.* CARD15 mutations in Blau syndrome. *Nat Genet* **29**, 19-20 (2001).
289. Kurokawa, T., Kikuchi, T., Ohta, K., Imai, H. & Yoshimura, N. Ocular Manifestations in Blau Syndrome Associated with a CARD15/Nod2 Mutation. *Ophthalmology* **110**, 2040-2044 (2003).
290. van Duist, M.M., *et al.* A new CARD15 mutation in Blau syndrome. *European journal of human genetics : EJHG* **13**, 742-747 (2005).
291. Kanazawa, N., *et al.* Early-onset sarcoidosis and CARD15 mutations with constitutive nuclear factor-kappaB activation: common genetic etiology with Blau syndrome. *Blood* **105**, 1195-1197 (2005).
292. Okada, S., *et al.* Cardiac infiltration in early-onset sarcoidosis associated with a novel heterozygous mutation, G481D, in CARD15. *Rheumatology (Oxford, England)* **48**, 706-707 (2009).
293. Schurmann, M., *et al.* CARD15 gene mutations in sarcoidosis. *European Respiratory Journal* **22**, 748-754 (2003).
294. Ho, L.-P., *et al.* CARD 15 gene mutations in sarcoidosis. *Thorax* **60**, 354-355 (2005).
295. Martin, T.M., *et al.* Uveitis in Patients With Sarcoidosis Is Not Associated With Mutations in NOD2 (CARD15). *American Journal of Ophthalmology* **136**, 933-935 (2003).
296. Jin, M.S., *et al.* Crystal structure of the TLR1-TLR2 heterodimer induced by binding of a tri-acylated lipopeptide. *Cell* **130**, 1071-1082 (2007).
297. Ozinsky, a., *et al.* The repertoire for pattern recognition of pathogens by the innate immune system is defined by cooperation between toll-like receptors. *Proceedings of the National Academy of Sciences of the United States of America* **97**, 13766-13771 (2000).
298. Hoebe, K., *et al.* CD36 is a sensor of diacylglycerides. *Nature* **433**, 523-527 (2005).

299. Burns, K.*, et al.* MyD88, an Adapter Protein Involved in Interleukin-1 Signaling. *The Journal of biological chemistry* **273**, 12203-12209 (1998).
300. Gray, P.*, et al.* MyD88 adapter-like (Mal) is phosphorylated by Bruton's tyrosine kinase during TLR2 and TLR4 signal transduction. *The Journal of biological chemistry* **281**, 10489-10495 (2006).
301. Mansell, A.*, et al.* Suppressor of cytokine signaling 1 negatively regulates Toll-like receptor signaling by mediating Mal degradation. *Nature immunology* **7**, 148-155 (2006).
302. Miggin, S.M.*, et al.* NF-kappaB activation by the Toll-IL-1 receptor domain protein MyD88 adapter-like is regulated by caspase-1. *Proceedings of the National Academy of Sciences of the United States of America* **104**, 3372-3377 (2007).
303. Kobayashi, K.*, et al.* IRAK-M Is a Negative Regulator of Toll-like Receptor Signaling. *Cell* **110**, 191-202 (2002).
304. Deng, L.*, et al.* Activation of the IkB Kinase Complex by TRAF6 Requires a Dimeric Ubiquitin-Conjugating Enzyme Complex and a Unique Polyubiquitin Chain. *Cell* **103**, 351-361 (2000).
305. Dai, P.*, et al.* Modulation of TLR Signaling by Multiple MyD88-Interacting Partners Including Leucine-Rich Repeat Fli-I-Interacting Proteins. *Journal of Immunology* **182**, 3450-3460 (2009).
306. Gerold, G.*, et al.* A Toll-like receptor 2-integrin beta3 complex senses bacterial lipopeptides via vitronectin. *Nature immunology* **9**, 761-768 (2008).
307. Palazzo, M.*, et al.* Cross-talk among Toll-like receptors and their ligands. *International immunology* **20**, 709-718 (2008).
308. Sabbatucci, M., Purificato, C., Fantuzzi, L. & Gessani, S. Toll-like receptor cross-talk in human monocytes regulates CC-chemokine production, antigen uptake and immune cell recruitment. *Immunobiology* **216**, 1135-1142 (2011).
309. van Heel, D.a.*, et al.* Synergistic enhancement of Toll-like receptor responses by NOD1 activation. *European journal of immunology* **35**, 2471-2476 (2005).
310. Xaplanteri, P., Lagoumintzis, G., Dimitracopoulos, G. & Paliogianni, F. Synergistic regulation of Pseudomonas aeruginosa -induced cytokine production in human monocytes by mannose receptor and TLR2. *European Journal of Immunology* **39**, 730-740 (2009).
311. Conforti-Andreoni, C.*, et al.* Synergism of NOD2 and NLRP3 activators promotes a unique transcriptional profile in murine dendritic cells. *Journal of leukocyte biology* **88**, 1207-1216 (2010).
312. Mitchell, D.*, et al.* Dual stimulation of MyD88-dependent Toll-like receptors induces synergistically enhanced production of inflammatory cytokines in murine bone marrow-derived dendritic cells. *The Journal of infectious diseases* **202**, 318-329 (2010).
313. Ghorpade, D.S., Kaveri, S.V., Bayry, J. & Balaji, K.N. Cooperative regulation of NOTCH1 protein-phosphatidylinositol 3-kinase (PI3K) signaling by NOD1, NOD2, and TLR2 receptors renders enhanced refractoriness to transforming growth factor-beta (TGF-beta)- or cytotoxic T-lymphocyte antigen 4 (CTLA-4)-mediated *The Journal of biological chemistry* **286**, 31347-31360 (2011).
314. Petterson, T.*, et al.* Effects of NOD-like receptors in human B lymphocytes and crosstalk between NOD1/NOD2 and Toll-like receptors. *Journal of leukocyte biology* **89**, 177-187 (2011).
315. Kishimoto, T.*, et al.* Peptidoglycan and lipopolysaccharide synergistically enhance bone resorption and osteoclastogenesis. *Journal of Periodontal Research* **epub**(2012).
316. Tuvim, M.J., Gilbert, B.E., Dickey, B.F. & Evans, S.E. Synergistic TLR2/6 and TLR9 Activation Protects Mice against Lethal Influenza Pneumonia. *PLoS ONE* **7**, e30596 (2012).

317. Demento, S.L.*, et al.* Inflammasome-activating nanoparticles as modular systems for optimizing vaccine efficacy. *Vaccine* **27**, 3013-3021 (2009).
318. Balachandran, P.*, et al.* The ubiquitin ligase Cbl-b limits Pseudomonas aeruginosa exotoxin T-mediated virulence. *J Clin Invest* **117**, 419-427 (2007).
319. Bjorkoy, G.*, et al.* p62/SQSTM1 forms protein aggregates degraded by autophagy and has a protective effect on huntingtin-induced cell death. *J Cell Biol* **171**, 603-614 (2005).
320. Kirkin, V., McEwan, D.G., Novak, I. & Dikic, I. A role for ubiquitin in selective autophagy. *Mol Cell* **34**, 259-269 (2009).
321. Alonso, S., Pethe, K., Russell, D.G. & Purdy, G.E. Lysosomal killing of Mycobacterium mediated by ubiquitin-derived peptides is enhanced by autophagy. *Proc Natl Acad Sci U S A* **104**, 6031-6036 (2007).
322. Delgado, M.A., Elmaoued, R.A., Davis, A.S., Kyei, G. & Deretic, V. Toll-like receptors control autophagy. *EMBO J* **27**, 1110-1121 (2008).
323. Barrett, J.C.*, et al.* Genome-wide association defines more than 30 distinct susceptibility loci for Crohn's disease. *Nat Genet* **40**, 955-962 (2008).
324. Kaser, A.*, et al.* XBP1 links ER stress to intestinal inflammation and confers genetic risk for human inflammatory bowel disease. *Cell* **134**, 743-756 (2008).
325. Lenk, S.E., Dunn, W.a., Trausch, J.S., Ciechanover, a. & Schwartz, a.L. Ubiquitin-activating enzyme, E1, is associated with maturation of autophagic vacuoles. *The Journal of cell biology* **118**, 301-308 (1992).
326. Bodemann, B.O.*, et al.* RalB and the exocyst mediate the cellular starvation response by direct activation of autophagosome assembly. *Cell* **144**, 253-267 (2011).
327. Hosokawa, N.*, et al.* Nutrient-dependent mTORC1 Association with the ULK1–Atg13–FIP200 Complex Required for Autophagy. *Molecular Biology of the Cell* **20**, 1981-1991 (2009).
328. Inoki, K., Li, Y., Zhu, T., Wu, J. & Guan, K.-L. TSC2 is phosphorylated and inhibited by Akt and suppresses mTOR signalling. *Nature cell biology* **4**, 648-657 (2002).
329. Stevens, C.*, et al.* Peptide combinatorial libraries identify TSC2 as a death-associated protein kinase (DAPK) death domain-binding protein and reveal a stimulatory role for DAPK in mTORC1 signaling. *The Journal of biological chemistry* **284**, 334-344 (2009).
330. Kim, J., Kundu, M., Viollet, B. & Guan, K.-L. AMPK and mTOR regulate autophagy through direct phosphorylation of Ulk1. *Nature cell biology* **13**, 132-141 (2011).
331. Hosokawa, N.*, et al.* Atg101, a novel mammalian autophagy protein interacting with Atg13. *Autophagy* **5**, 973-979 (2009).
332. Tang, D.*, et al.* High-mobility group box 1 is essential for mitochondrial quality control. *Cell metabolism* **13**, 701-711 (2011).
333. Zalckvar, E.*, et al.* DAP-kinase-mediated phosphorylation on the BH3 domain of beclin 1 promotes dissociation of beclin 1 from Bcl-XL and induction of autophagy. *EMBO reports* **10**, 285-292 (2009).
334. Suzuki, K.*, et al.* The pre-autophagosomal structure organized by concerted functions of APG genes is essential for autophagosome formation. *EMBO Journal* **20**, 5971-5981 (2001).
335. Mizushima, N.*, et al.* A protein conjugation system essential for autophagy. *Nature* **395**, 395-398 (1998).
336. Schmid, D., Dengjel, J., Schoor, O., Stevanovic, S. & Munz, C. Autophagy in innate and adaptive immunity against intracellular pathogens. *J Mol Med* **84**, 194-202 (2006).
337. Kabeya, Y.*, et al.* LC3, a mammalian homologue of yeast Apg8p, is localized in autophagosome membranes after processing. *EMBO J* **19**, 5720-5728 (2000).
338. Levine, B. & Deretic, V. Unveiling the roles of autophagy in innate and adaptive immunity. *Nature reviews. Immunology* **7**, 767-777 (2007).

339. Pua, H.H., Dzhagalov, I., Chuck, M., Mizushima, N. & He, Y.-W. A critical role for the autophagy gene Atg5 in T cell survival and proliferation. *The Journal of experimental medicine* **204**, 25-31 (2007).
340. Sanjuan, M.a*., et al.* Toll-like receptor signalling in macrophages links the autophagy pathway to phagocytosis. *Nature* **450**, 1253-1257 (2007).
341. Shui, W*., et al.* Membrane proteomics of phagosomes suggests a connection to autophagy. *Proceedings of the National Academy of Sciences* **105**, 16952-16957 (2008).
342. Nimmerjahn, F*., et al.* Major histocompatibility complex class II-restricted presentation of a cytosolic antigen by autophagy. *European journal of immunology* **33**, 1250-1259 (2003).
343. Li, Y*., et al.* Tumor-derived autophagosome vaccine: mechanism of cross-presentation and therapeutic efficacy. *Clinical cancer research : an official journal of the American Association for Cancer Research* **17**, 7047-7057 (2011).
344. Feng, J.T., Shang, S. & Beretta, L. Proteomics for the early detection and treatment of hepatocellular carcinoma. *Oncogene* **25**, 3810-3817 (2006).
345. Alex, P., Gucek, M. & Li, X. Applications of proteomics in the study of inflammatory bowel diseases: Current status and future directions with available technologies. *Inflammatory bowel diseases* **15**, 616-629 (2009).
346. Ong, S.-E. Stable Isotope Labeling by Amino Acids in Cell Culture, SILAC, as a Simple and Accurate Approach to Expression Proteomics. *Molecular & Cellular Proteomics* **1**, 376-386 (2002).
347. Desouza, L*., et al.* Search for Cancer Markers from Endometrial Tissues Using Differentially Labeled Tags iTRAQ and cICAT with Multidimensional Liquid Chromatography and Tandem Mass Spectrometry. *Journal of Proteome Research* **4**, 377-386 (2005).
348. Dayon, L*., et al.* Relative quantification of proteins in human cerebrospinal fluids by MS/MS using 6-plex isobaric tags. *Analytical chemistry* **80**, 2921-2931 (2008).
349. Wang, G., Wu, W.W., Zeng, W., Chou, C.-l. & Shen, R.-f. Label-Free Protein Quantification Using LC-Coupled Ion Trap or FT Mass Spectrometry: Reproducibility, Linearity, and Application with Complex Proteomes research articles. *Journal of proteome research* **5**, 1214-1223 (2006).
350. Domon, B. & Aebersold, R. Options and considerations when selecting a quantitative proteomics strategy. *Nature biotechnology* **28**, 710-721 (2010).
351. Sabidó, E., Selevsek, N. & Aebersold, R. Mass spectrometry-based proteomics for systems biology. *Current opinion in biotechnology*, 1-7 (2011).
352. Perkins, D.N., Pappin, D.J.C., Creasy, D.M. & Cottrell, J.S. Probability-based protein identification by searching sequence databases using mass spectrometry data Proteomics and 2-DE. *Electrophoresis* **20**, 3551-3567 (1999).
353. Hahn, K., DeBiasio, R. & Taylor, D.L. Patterns of elevated free calcium and calmodulin activation in living cells. *Nature* **359**, 736-738 (1992).
354. Namba, Y., Ito, M., Zu, Y., Shigesada, K. & Maruyama, K. Human T cell L-plastin bundles actin filaments in a calcium-dependent manner. *Journal of biochemistry* **112**, 503-507 (1992).
355. Petrilli, V*., et al.* Activation of the NALP3 inflammasome is triggered by low intracellular potassium concentration. *Cell Death Differ* **14**, 1583-1589 (2007).
356. Segura, M., Gottschalk, M. & Olivier, M. Encapsulated Streptococcus suis Inhibits Activation of Signaling Pathways Involved in Phagocytosis. *Infection and Immunity* **72**, 5322-5330 (2004).
357. Wu, G.Y., Deisseroth, K. & Tsien, R.W. Activity-dependent CREB phosphorylation: convergence of a fast, sensitive calmodulin kinase pathway and a slow, less sensitive mitogen-activated protein kinase pathway. *Proceedings of the National Academy of Sciences of the United States of America* **98**, 2808-2813 (2001).

358. Rock, K.L.*, et al.* Inhibitors of the proteasome block the degradation of most cell proteins and the generation of peptides presented on MHC class I molecules. *Cell* **78**, 761-771 (1994).
359. Grant, E.P., Michalek, M.T., Goldberg, A. & Rock, K.L. Rate of Antigen Degradation by the Ubiquitin-Proteasome Pathway Influences MHC Class I Presentation'. *Journal of immunology (Baltimore, Md. : 1950)* **155**, 3750-3758 (1995).
360. Booth, J.W., Kim, M.-K., Jankowski, A., Schreiber, A.D. & Grinstein, S. Contrasting requirements for ubiquitylation during Fc receptor-mediated endocytosis and phagocytosis. *The EMBO journal* **21**, 251-258 (2002).
361. Katkere, B., Rosa, S., Caballero, A., Repasky, E.a. & Drake, J.R. Physiological-range temperature changes modulate cognate antigen processing and presentation mediated by lipid raft-restricted ubiquitinated B cell receptor molecules. *Journal of immunology (Baltimore, Md. : 1950)* **185**, 5032-5039 (2010).
362. Walseng, E.*, et al.* Ubiquitination regulates MHC class II-peptide complex retention and degradation in dendritic cells. *Proceedings of the National Academy of Sciences of the United States of America* **107**, 20465-20470 (2010).
363. Perkins, D.J., Qureshi, N. & Vogel, S.N. A Toll-Like Receptor-Responsive Kinase, Protein Kinase R, Is Inactivated in Endotoxin Tolerance through Differential K63/K48 Ubiquitination. *MBio* **1**, e00239-00210 (2010).
364. Scherer, D.C., Brockman, J.A., Chen, Z., Maniatis, T. & Ballard, D.W. Signal-induced degradation of IkBa requires site-specific ubiquitination. *Proceedings of the National Academy of Sciences of the United States of America* **92**, 11259-11263 (1995).
365. Thurston, T.L.M., Ryzhakov, G., Bloor, S., von Muhlinen, N. & Randow, F. The TBK1 adaptor and autophagy receptor NDP52 restricts the proliferation of ubiquitin-coated bacteria. *Nature immunology* **10**, 1215-1221 (2009).
366. Zheng, Y.T.*, et al.* The adaptor protein p62/SQSTM1 targets invading bacteria to the autophagy pathway. *Journal of immunology (Baltimore, Md. : 1950)* **183**, 5909-5916 (2009).
367. Matsudaira, P.T. & Burgess, D.R. IDENTIFICATION AND ORGANIZATION OF THE COMPONENTS IN THE ISOLATED MICROVILLUS CYTOSKELETON. *Journal of Cell Biology* **83**, 667-673 (1979).
368. Bretscher, a. & Weber, K. Fimbrin, a new microfilament-associated protein present in microvilli and other cell surface structures. *The Journal of cell biology* **86**, 335-340 (1980).
369. Foran, E., McWilliam, P., Kelleher, D., Croke, D.T. & Long, A. The leukocyte protein L-plastin induces proliferation, invasion and loss of E-cadherin expression in colon cancer cells. *International journal of cancer. Journal international du cancer* **118**, 2098-2104 (2006).
370. Klemke, M.*, et al.* Phosphorylation of ectopically expressed L-plastin enhances invasiveness of human melanoma cells. *Int J Cancer* **120**, 2590-2599 (2007).
371. Janji, B.*, et al.* The actin filament cross-linker L-plastin confers resistance to TNF-alpha in MCF-7 breast cancer cells in a phosphorylation-dependent manner. *Journal of cellular and molecular medicine* **14**, 1264-1275 (2010).
372. Pazdrak, K., Young, T.W., Straub, C., Stafford, S. & Kurosky, A. Priming of Eosinophils by GM-CSF Is Mediated by Protein Kinase C β II-Phosphorylated L-Plastin. *Journal of immunology (Baltimore, Md. : 1950)* **186**, 6485-6496 (2011).
373. Morley, S.C.*, et al.* The actin-bundling protein L-plastin dissociates CCR7 proximal signaling from CCR7-induced motility. *Journal of immunology (Baltimore, Md. : 1950)* **184**, 3628-3638 (2010).
374. Chen, H.*, et al.* Role for plastin in host defense distinguishes integrin signaling from cell adhesion and spreading. *Immunity* **19**, 95-104 (2003).
375. Rosales, C., O'Brien, V., Kornberg, L. & Juliano, R. Signal transduction by cell adhesion receptors. *Biochimica et Biophysica Acta* **1242**, 77-98 (1995).

376. Langereis, J.D.*, et al.* A 2D-DIGE Approach To Identify Proteins Involved in Inside-Out Control of Integrins research articles. *Journal of Proteome Research* **8**, 3824-3833 (2009).
377. Wabnitz, G.H.*, et al.* Sustained LFA-1 cluster formation in the immune synapse requires the combined activities of L-plastin and calmodulin. *European journal of immunology* **40**, 2437-2449 (2010).
378. Wang, C.*, et al.* Actin-Bundling Protein L-Plastin Regulates T Cell Activation. *Journal of immunology (Baltimore, Md. : 1950)* **185**, 7487-7497 (2010).
379. Monks, C.R.F., Freiberg, B.A., Kupfer, H., Sciaky, N. & Kupfer, A. Three-dimensional segregation of supramolecular activation clusters in T cells. *Nature* **395**, 82-86 (1998).
380. Marrero, M.B., Venema, V.J., Ju, H., Eaton, D.C. & Venema, R.C. Regulation of angiotensin II-induced JAK2 tyrosine phosphorylation: roles of SHP-1 and SHP-2 activation system. *American journal of physiology, Cell physiology* **275**, C1216-1223 (1998).
381. Banville, D., Stocco, R. & Shen, S.-H. Human protein tyrosine phosphatase 1C (PTPN6) gene structure: alternate promoter usage and exon skipping generate multiple transcripts. *Genomics* **27**, 165-173 (1995).
382. Beauchemin, N.*, et al.* Association of biliary glycoprotein with protein tyrosine phosphatase SHP-1 in malignant colon epithelial cells. *Oncogene* **14**, 783-790 (1997).
383. Huber, M.*, et al.* The carboxyl-terminal region of biliary glycoprotein controls its tyrosine phosphorylation and association with protein-tyrosine phosphatases SHP-1 and SHP-2 in epithelial cells. *The Journal of biological chemistry* **274**, 335-344 (1999).
384. Uchida, T.*, et al.* Insulin stimulates the phosphorylation of Tyr538 and the catalytic activity of PTP1C, a protein tyrosine phosphatase with Src homology-2 domains. *The Journal of biological chemistry* **269**, 12220-12228 (1994).
385. Ganju, R.K., Brubaker, S.a., Chernock, R.D., Avraham, S. & Groopman, J.E. Beta-chemokine receptor CCR5 signals through SHP1, SHP2, and Syk. *The Journal of biological chemistry* **275**, 17263-17268 (2000).
386. Zhou, D., Collins, C.a., Wu, P. & Brown, E.J. Protein tyrosine phosphatase SHP-1 positively regulates TLR-induced IL-12p40 production in macrophages through inhibition of phosphatidylinositol 3-kinase. *Journal of leukocyte biology* **87**, 845-855 (2010).
387. Lorenz, U.*, et al.* Lck-Dependent Tyrosyl Phosphorylation of the Phosphotyrosine Phosphatase SH-PTP1 in Murine T Cells. *Molecular and Cellular Biology* **14**, 1824-1834 (1994).
388. Alvarez, S.E., Seguin, L.R., Villarreal, R.S., Nahmias, C. & Ciuffo, G.M. Involvement of c-Src tyrosine kinase in SHP-1 phosphatase activation by Ang II AT2 receptors in rat fetal tissues. *Journal of cellular biochemistry* **105**, 703-711 (2008).
389. Ramachandran, I.R.*, et al.* The phosphatase SRC homology region 2 domain-containing phosphatase-1 is an intrinsic central regulator of dendritic cell function. *Journal of immunology (Baltimore, Md. : 1950)* **186**, 3934-3945 (2011).
390. An, H.*, et al.* Phosphatase SHP-1 promotes TLR- and RIG-I-activated production of type I interferon by inhibiting the kinase IRAK1. *Nature immunology* **9**, 542-550 (2008).
391. Lee, S.-M., Kim, E.-J., Suk, K. & Lee, W.-H. CD300F blocks both MyD88 and TRIF-mediated TLR signaling through activation of Src homology region 2 domain-containing phosphatase 1. *Journal of immunology (Baltimore, Md. : 1950)* **186**, 6296-6303 (2011).
392. Slevogt, H.*, et al.* CEACAM1 inhibits Toll-like receptor 2-triggered antibacterial responses of human pulmonary epithelial cells. *Nature immunology* **9**, 1270-1278 (2008).

393. Croker, B.a., *et al.* Neutrophils require SHP1 to regulate IL-1β production and prevent inflammatory skin disease. *Journal of immunology (Baltimore, Md. : 1950)* **186**, 1131-1139 (2011).
394. Roach, T.I., *et al.* The protein tyrosine phosphatase SHP-1 regulates integrin-mediated adhesion of macrophages. *Current biology : CB* **8**, 1035-1038 (1998).
395. Liang, B., *et al.* Activation Gene-3 Engagement of MHC Class II 1. *Journal of immunology (Baltimore, Md. : 1950)* **180**, 5916-5926 (2008).
396. Scaffidi, P., Misteli, T. & Bianchi, M.E. Release of chromatin protein HMGB1 by necrotic cells triggers inflammation. *Nature* **418**, 191-195 (2002).
397. Hofmann, M.a., *et al.* RAGE mediates a novel proinflammatory axis: a central cell surface receptor for S100/calgranulin polypeptides. *Cell* **97**, 889-901 (1999).
398. Orlova, V.V., *et al.* A novel pathway of HMGB1-mediated inflammatory cell recruitment that requires Mac-1-integrin. *The EMBO journal* **26**, 1129-1139 (2007).
399. Andersson, U., *et al.* High Mobility Group 1 Protein (HMG-1) Stimulates Proinflammatory Cytokine Synthesis in Human Monocytes. *Journal of Experimental Medicine* **192**, 565-570 (2000).
400. Oh, Y.J., *et al.* HMGB1 is phosphorylated by classical protein kinase C and is secreted by a calcium-dependent mechanism. *Journal of immunology (Baltimore, Md. : 1950)* **182**, 5800-5809 (2009).
401. Dumitriu, I.E., Bianchi, M.E., Bacci, M., Manfredi, A.a. & Rovere-Querini, P. The secretion of HMGB1 is required for the migration of maturing dendritic cells. *Journal of leukocyte biology* **81**, 84-91 (2007).
402. Tang, D., *et al.* Endogenous HMGB1 regulates autophagy. *The Journal of cell biology* **190**, 881-892 (2010).
403. Deiss, L.P., Feinstein, E., Berissi, H., Cohen, O. & Kimchi, a. Identification of a novel serine/threonine kinase and a novel 15-kD protein as potential mediators of the gamma interferon-induced cell death. *Genes & Development* **9**, 15-30 (1995).
404. Lin, Y., Hupp, T.R. & Stevens, C. Death-associated protein kinase (DAPK) and signal transduction: additional roles beyond cell death. *The FEBS journal* **277**, 48-57 (2010).
405. Jang, C.-W., *et al.* TGF-beta induces apoptosis through Smad-mediated expression of DAP-kinase. *Nature cell biology* **4**, 51-58 (2002).
406. Widau, R.C., Jin, Y., Dixon, S.a., Wadzinski, B.E. & Gallagher, P.J. Protein phosphatase 2A (PP2A) holoenzymes regulate death-associated protein kinase (DAPK) in ceramide-induced anoikis. *The Journal of biological chemistry* **285**, 13827-13838 (2010).
407. Anjum, R., Roux, P.P., Ballif, B.a., Gygi, S.P. & Blenis, J. The tumor suppressor DAP kinase is a target of RSK-mediated survival signaling. *Current biology : CB* **15**, 1762-1767 (2005).
408. Shohat, G., *et al.* The pro-apoptotic function of death-associated protein kinase is controlled by a unique inhibitory autophosphorylation-based mechanism. *The Journal of biological chemistry* **276**, 47460-47467 (2001).
409. Llambi, F., *et al.* The dependence receptor UNC5H2 mediates apoptosis through DAP-kinase. *The EMBO journal* **24**, 1192-1201 (2005).
410. Jin, Y., Blue, E.K. & Gallagher, P.J. Control of death-associated protein kinase (DAPK) activity by phosphorylation and proteasomal degradation. *The Journal of biological chemistry* **281**, 39033-39040 (2006).
411. Wei, Y., Pattingre, S., Sinha, S., Bassik, M. & Levine, B. JNK1-mediated phosphorylation of Bcl-2 regulates starvation-induced autophagy. *Molecular cell* **30**, 678-688 (2008).
412. Gozuacik, D. & Kimchi, A. DAPk Protein Family and Cancer. *Autophagy* **2**, 74-79 (2006).

413. Tian, J.-H., Das, S. & Sheng, Z.-H. Ca2+-dependent phosphorylation of syntaxin-1A by the death-associated protein (DAP) kinase regulates its interaction with Munc18. *The Journal of biological chemistry* **278**, 26265-26274 (2003).
414. Pelkmans, L.*, et al.* Genome-wide analysis of human kinases in clathrin- and caveolae/raft-mediated endocytosis. *Nature* **436**, 78-86 (2005).
415. Hu, S.*, et al.* Translational inhibition of colonic epithelial heat shock proteins by IFN-gamma and TNF-alpha in intestinal inflammation. *Gastroenterology* **133**, 1893-1904 (2007).
416. Kato, K.*, et al.* Role of HSP27 in tumor necrosis factor-α-stimulated interleukin-6 synthesis in osteoblasts. *International journal of molecular medicine* **28**, 887-893 (2011).
417. Paul, C.*, et al.* Dynamic processes that reflect anti-apoptotic strategies set up by HspB1 (Hsp27). *Experimental cell research* **316**, 1535-1552 (2010).
418. Guay, J.*, et al.* Regulation of actin filament dynamics by p38 map kinase-mediated phosphorylation of heat shock protein 27. *Journal of cell science* **110 (Pt 3**, 357-368 (1997).
419. Shiryaev, A., Dumitriu, G. & Moens, U. Distinct roles of MK2 and MK5 in cAMP/PKA- and stress/p38MAPK-induced heat shock protein 27 phosphorylation. *Journal of molecular signaling* **6**, 4 (2011).
420. Waetzig, G.H., Rosenstiel, P., Nikolaus, S., Seegert, D. & Schreiber, S. Differential p38 Mitogen-activated protein kinase target phosphorylation in responders and nonresponders to infliximab. *Gastroenterology* **125**, 633-634 (2003).
421. Bhattacharyya, S., Dudeja, P.K. & Tobacman, J.K. ROS, Hsp27, and IKKbeta mediate dextran sodium sulfate (DSS) activation of IkappaBa, NFkappaB, and IL-8. *Inflammatory bowel diseases* **15**, 673-683 (2009).
422. Benndorf, R.*, et al.* Phosphorylation and Supramolecular Organization of Murine Small Heat Shock Protein HSP25 Abolish Its Actin Polymerization-inhibiting Activity. *Journal of Biological Chemistry* **269**, 20780-20784 (1994).
423. Rogalla, T.*, et al.* Regulation of Hsp27 oligomerization, chaperone function, and protective activity against oxidative stress/tumor necrosis factor alpha by phosphorylation. *The Journal of biological chemistry* **274**, 18947-18956 (1999).
424. Lee, J.-W.*, et al.* HSP27 regulates cell adhesion and invasion via modulation of focal adhesion kinase and MMP-2 expression. *European journal of cell biology* **87**, 377-387 (2008).
425. Jones, T.J.*, et al.* Primary cilia regulates the directional migration and barrier integrity of endothelial cells through the modulation of hsp27 dependent actin cytoskeletal organization. *Journal of cellular physiology* **227**, 70-76 (2012).
426. Lavoie, J.N., Gingras-Breton, G., Tanguay, R.M. & Landry, J. Induction of Chinese hamster HSP27 gene expression in mouse cells confers resistance to heat shock. HSP27 stabilization of the microfilament organization. *The Journal of biological chemistry* **268**, 3420-3429 (1993).
427. Lavoie, J.N., Hickey, E., Weber, L.a. & Landry, J. Modulation of actin microfilament dynamics and fluid phase pinocytosis by phosphorylation of heat shock protein 27. *The Journal of biological chemistry* **268**, 24210-24214 (1993).
428. Rousseau, S., Houle, F., Landry, J. & Huot, J. p38 MAP kinase activation by vascular endothelial growth factor mediates actin reorganization and cell migration in human endothelial cells. *Oncogene* **15**, 2169-2177 (1997).
429. Chen, R.*, et al.* Unfolded Protein Response Suppresses Cisplatin-Induced Apoptosis via Autophagy Regulation in Human Hepatocellular Carcinoma Cells. *Folia Biologica (Praha)* **57**, 87-95 (2011).
430. Wortzel, I. & Seger, R. The ERK Cascade: Distinct Functions within Various Subcellular Organelles. *Genes & cancer* **2**, 195-209 (2011).
431. Dhanasekaran, N. & Reddy, E.P. Signaling by dual specificity kinases. *Oncogene* **17**, 1447-1455 (1998).

432. Gollmer, K.*, et al.* CCL21 mediates CD4+ T-cell costimulation via a DOCK2/Rac-dependent pathway. *Blood* **114**, 580-588 (2009).
433. Meng, D.*, et al.* MEK1 binds directly to betaarrestin1, influencing both its phosphorylation by ERK and the timing of its isoprenaline-stimulated internalization. *The Journal of biological chemistry* **284**, 11425-11435 (2009).
434. Namgoong, G.M.*, et al.* The Prolyl Isomerase Pin1 Induces LC-3 Expression and Mediates Tamoxifen Resistance in Breast Cancer. *Journal of Biological Chemistry* **285**, 23829 -23841 (2010).
435. Suzuki, T., Yoshinaga, N. & Tanabe, S. IL-6 regulates claudin-2 expression and tight junction permeability in intestinal epithelium. *The Journal of biological chemistry* **286**, 31263-31271 (2011).
436. Batycka, M.*, et al.* Ultra-fast tandem mass spectrometry scanning combined with monolithic column liquid chromatography increases throughput in proteomic analysis. *Rapid Commun Mass Spectrom* **20**, 2074-2080 (2006).
437. Lotze, M.T. & Tracey, K.J. High-mobility group box 1 protein (HMGB1): nuclear weapon in the immune arsenal. *Nature reviews. Immunology* **5**, 331-342 (2005).
438. Hsu, Y.M.*, et al.* The adaptor protein CARD9 is required for innate immune responses to intracellular pathogens. *Nature Immunology* **8**, 198-205 (2007).
439. Wang, Y.*, et al.* Association of beta-arrestin and TRAF6 negatively regulates Toll-like receptor-interleukin 1 receptor signaling. *Nature Immunology* **7**, 139-147 (2006).
440. Chen, W. Dishevelled 2 Recruits -Arrestin 2 to Mediate Wnt5A-Stimulated Endocytosis of Frizzled 4. *Science* **301**, 1391-1394 (2003).
441. Chen, W.*, et al.* Beta-arrestin 2 mediates endocytosis of type III TGF-beta receptor and down-regulation of its signaling. *Science* **301**, 1394-1397 (2003).
442. Gao, H.*, et al.* Identification of beta-arrestin2 as a G protein-coupled receptor-stimulated regulator of NF-kappaB pathways. *Molecular cell* **14**, 303-317 (2004).
443. Witherow, D.S., Garrison, T.R., Miller, W.E. & Lefkowitz, R.J. beta-Arrestin inhibits NF-kappaB activity by means of its interaction with the NF-kappaB inhibitor IkappaBalpha. *Proceedings of the National Academy of Sciences of the United States of America* **101**, 8603-8607 (2004).
444. Chen, K.*, et al.* Cooperation between NOD2 and Toll-like receptor 2 ligands in the up-regulation of mouse mFPR2, a G-protein-coupled Abeta42 peptide receptor, in microglial cells. *Journal of leukocyte biology* **83**, 1467-1475 (2008).
445. Shi, G.X., Harrison, K., Han, S.B., Moratz, C. & Kehrl, J.H. Toll-like receptor signaling alters the expression of regulator of G protein signaling proteins in dendritic cells: implications for G protein-coupled receptor signaling. *Journal of Immunology* **172**, 5175-5184 (2004).
446. Roseth, A.G., Fagerhol, M.K., Aadland, E. & Schjonsby, H. Assessment of the neutrophil dominating protein calprotectin in feces. A methodologic study. *Scandinavian journal of gastroenterology* **27**, 793-798 (1992).
447. Leukert, N.*, et al.* Calcium-dependent tetramer formation of S100A8 and S100A9 is essential for biological activity. *Journal of molecular biology* **359**, 961-972 (2006).
448. Rammes, A.*, et al.* Myeloid-related protein (MRP) 8 and MRP14, calcium-binding proteins of the S100 family, are secreted by activated monocytes via a novel, tubulin-dependent pathway. *The Journal of biological chemistry* **272**, 9496-9502 (1997).
449. Vogl, T.*, et al.* Mrp8 and Mrp14 are endogenous activators of Toll-like receptor 4, promoting lethal, endotoxin-induced shock. *Nature medicine* **13**, 1042-1049 (2007).
450. Rice, G.I.*, et al.* Mutations involved in Aicardi-Goutières syndrome implicate SAMHD1 as regulator of the innate immune response. *Nat Genet* **41**, 829-832 (2009).
451. Laguette, N.*, et al.* SAMHD1 is the dendritic- and myeloid-cell-specific HIV-1 restriction factor counteracted by Vpx. *Nature*, 1-5 (2011).

452. Cicchetti, P., Ridley, a.J., Zheng, Y., Cerione, R.a. & Baltimore, D. 3BP-1, an SH3 domain binding protein, has GAP activity for Rac and inhibits growth factor-induced membrane ruffling in fibroblasts. *The EMBO journal* **14**, 3127-3135 (1995).
453. Parrini, M.C.*, et al.* SH3BP1, an Exocyst-Associated RhoGAP, Inactivates Rac1 at the Front to Drive Cell Motility. *Molecular cell* **42**, 650-661 (2011).
454. Zhou, D., Mooseker, M.S. & Galan, J.E. An invasion-associated Salmonella protein modulates the actin-bundling activity of plastin. *Proc Natl Acad Sci U S A* **96**, 10176-10181 (1999).
455. Blom, N., Sicheritz-Pontén, T., Gupta, R., Gammeltoft, S. & Brunak, S. Prediction of post-translational glycosylation and phosphorylation of proteins from the amino acid sequence. *Proteomics* **4**, 1633-1649 (2004).
456. Messier, J.M., Shaw, L.M., Chafel, M., Matsudaira, P. & Mercurio, a.M. Fimbrin localized to an insoluble cytoskeletal fraction is constitutively phosphorylated on its headpiece domain in adherent macrophages. *Cell motility and the cytoskeleton* **25**, 223-233 (1993).
457. Janji, B., Giganti, A., Corte, V.D. & Catillon, M. Phosphorylation on Ser5 increases the F-actin-binding activity of L-plastin and promotes its targeting to sites of actin assembly in cells. *Journal of cell science* **119**, 1947-1960 (2006).
458. Nagl, M.*, et al.* Phagocytosis and Killing of Bacteria by Professional Phagocytes and Dendritic Cells. *Clinical and vaccine immunology* **9**, 1165-1168 (2002).
459. Savina, A. & Amigorena, S. Phagocytosis and antigen presentation in dendritic cells. *Immunological reviews* **219**, 143-156 (2007).
460. Elsen, S.*, et al.* Cryptic O2- -generating NADPH oxidase in dendritic cells. *Journal of cell science* **117**, 2215-2226 (2004).
461. Vulcano, M.*, et al.* Toll Receptor-Mediated Regulation of NADPH Oxidase in Dendritic Cells. *The Journal of Immunology* **173**, 5749-5756 (2004).
462. Newman, S.L. & Holly, A. Candida albicans Is Phagocytosed, Killed, and Processed for Antigen Presentation by Human Dendritic Cells. *Infection and immunity* **69**, 6812-6822 (2001).
463. Jones, S.L. & Brown, E.J. FcgammaRII-mediated adhesion and phagocytosis induce L-plastin phosphorylation in human neutrophils. *The Journal of biological chemistry* **271**, 14623-14630 (1996).
464. Jones, S.L., Wang, J., Turck, C.W. & Brown, E.J. A role for the actin-bundling protein L-plastin in the regulation of leukocyte integrin function. *Proceedings of the National Academy of Sciences of the United States of America* **95**, 9331-9336 (1998).
465. Nathan, C.F. Respiratory burst in adherent human neutrophils: triggering by colony-stimulating factors CSF-GM and CSF-G. *Blood* **73**, 301-306 (1989).
466. Nathan, C.*, et al.* Cytokine-induced respiratory burst of human neutrophils: dependence on extracellular matrix proteins and CD11/CD18 integrins. *The Journal of cell biology* **109**, 1341-1349 (1989).
467. Shappell, S.B.*, et al.* Mac-1 (CDllb/CD18) MEDIATES ADHERENCE-DEPENDENT HYDROGEN PEROXIDE PRODUCTION BY HUMAN AND CANINE NEUTROPHILS. *The Journal of Immunology* **144**, 2702-2711 (1990).
468. Yano, T.*, et al.* Autophagic control of listeria through intracellular innate immune recognition in drosophila. *Nat Immunol* **9**, 908-916 (2008).
469. Gresham, H.D.*, et al.* Survival of Staphylococcus aureus Inside Neutrophils Contributes to Infection. *Journal of immunology (Baltimore, Md. : 1950)* **164**, 3713-3722 (2000).
470. Martinon, F., Chen, X., Lee, A.-H. & Glimcher, L.H. TLR activation of the transcription factor XBP1 regulates innate immune responses in macrophages. *Nature immunology* **11**, 411-418 (2010).
471. Tang, Z. & Saltzman, A. Understanding human dendritic cell biology through gene profiling. *Inflammation Research* **53**, 424-441 (2004).

472. Ahn, J.H., *et al.* Identification of the genes differentially expressed in human dendritic cell subsets by cDNA subtraction and microarray analysis. *Blood* **100**, 1742-1754 (2002).
473. Del Cornò, M., *et al.* CC chemokine ligand 2 down-modulation by selected Toll-like receptor agonist combinations contributes to T helper 1 polarization in human dendritic cells. *Blood* **114**, 796-806 (2009).
474. Flores-villanueva, P.O., *et al.* A functional promoter polymorphism in monocyte chemoattractant protein–1 is associated with increased susceptibility to pulmonary tuberculosis. *Journal of Experimental Medicine* **202**, 1649-1658 (2005).
475. Kim, Y.-G., *et al.* The Nod2 sensor promotes intestinal pathogen eradication via the chemokine CCL2-dependent recruitment of inflammatory monocytes. *Immunity* **34**, 769-780 (2011).
476. Bevilacqua, M.P., Amrani, D., Mosesson, M.W. & Bianco, C. Receptors for cold-insoluble globulin (plasma fibronectin) on human monocytes. *Journal of Experimental Medicine* **153**, 42-60 (1981).
477. Tamkun, J.W., *et al.* Structure of integrin, a glycoprotein involved in the transmembrane linkage between fibronectin and actin. *Cell* **46**, 271-282 (1986).
478. Yi, T., Cleveland, J.L. & Ihle, J.N. Protein Tyrosine Phosphatase Containing SH2 Domains: Characterization, Preferential Expression in Hematopoietic Cells, and Localization to Human Chromosome 12p12-p13. *Molecular and Cellular Biology* **12**, 836-846 (1992).
479. Khaled, A.R., Butfiloski, E.J., Sobel, E.S. & Schiffenbauer, J. Functional consequences of the SHP-1 defect in motheaten viable mice: role of NF-kappa B. *Cellular immunology* **185**, 49-58 (1998).
480. Forget, G., *et al.* Regulation of the Leishmania-induced innate inflammatory response by the protein tyrosine phosphatase SHP-1. *European journal of immunology* **35**, 1906-1917 (2005).
481. Lee, S.-M., Kim, E.-J., Suk, K. & Lee, W.-H. Synthetic peptides containing ITIM-like sequences of IREM-1 inhibit BAFF-mediated regulation of interleukin-8 expression and phagocytosis through SHP-1 and/or PI3K. *Immunology* **134**, 224-233 (2011).
482. Youn, J.H. & Shin, J.-S. Nucleocytoplasmic shuttling of HMGB1 is regulated by phosphorylation that redirects it toward secretion. *Journal of immunology (Baltimore, Md. : 1950)* **177**, 7889-7897 (2006).
483. Wisniewski, J.R., Schulze, E. & Sapetto, B. DNA binding and nuclear translocation of insect high-mobility-group protein-1 (HMG1) proteins are inhibited by phosphorylation. *European journal of biochemistry* **225**, 687-693 (1994).
484. Cohen, O., *et al.* DAP-kinase Participates in TNF-a– and Fas-induced Apoptosis and Its Function Requires the Death Domain. *Journal of Cell Biology* **146**, 141-148 (1999).
485. Yamamoto, M., Hioki, T., Ishii, T., Nakajima-iijima, S. & Uchino, S. DAP kinase activity is critical for C2-ceramide-induced apoptosis in PC12 cells. *European journal of biochemistry* **269**, 139-147 (2002).
486. Pelled, D., *et al.* Death-associated Protein (DAP) Kinase Plays a Central Role in Ceramide-induced Apoptosis in Cultured Hippocampal Neurons. *Journal of Biological Chemistry* **277**, 1957-1961 (2002).
487. Raveh, T., Droguett, G., Horwitz, M.S., DePinho, R.a. & Kimchi, a. DAP kinase activates a p19ARF/p53-mediated apoptotic checkpoint to suppress oncogenic transformation. *Nature cell biology* **3**, 1-7 (2001).
488. Bialik, S., Bresnick, a.R. & Kimchi, A. DAP-kinase-mediated morphological changes are localization dependent and involve myosin-II phosphorylation. *Cell Death and Differentiation* **11**, 631-644 (2004).
489. Kuo, J.-C., Lin, J.-r., Staddon, J.M., Hosoya, H. & Chen, R.-H. Uncoordinated regulation of stress fibers and focal adhesions by DAP kinase. *Journal of Cell Science* **116**, 4777-4790 (2003).

490. Kuo, J.-c., Wang, W.-j., Yao, C.-c., Wu, P.-r. & Chen, R.-h. The tumor suppressor DAPK inhibits cell motility by blocking the integrin-mediated polarity pathway. *Journal of Cell Biology* **172**, 619-631 (2006).
491. Inbal, B., Bialik, S., Sabanay, I., Shani, G. & Kimchi, A. DAP kinase and DRP-1 mediate membrane blebbing and the formation of autophagic vesicles during programmed cell death. *The Journal of cell biology* **157**, 455-468 (2002).
492. Shani, G.*, et al.* Death-Associated Protein Kinase Phosphorylates ZIP Kinase, Forming a Unique Kinase Hierarchy To Activate Its Cell Death Functions. *Molecular and Cellular Biology* **24**, 8611-8626 (2004).
493. Chuang, Y.-T., Fang, L.-W., Lin-Feng, M.-H., Chen, R.-H. & Lai, M.-Z. The Tumor Suppressor Death-Associated Protein Kinase Targets to TCR-Stimulated NF-kB Activation. *Journal of Immunology* **180**, 3238-3249 (2008).
494. Chen, C.-h.*, et al.* Bidirectional signals transduced by DAPK–ERK interaction promote the apoptotic effect of DAPK. *EMBO Journal* **24**, 294-304 (2005).
495. Wang, W.-J.*, et al.* The tumor suppressor DAPK is reciprocally regulated by tyrosine kinase Src and phosphatase LAR. *Molecular cell* **27**, 701-716 (2007).
496. Paul, P.*, et al.* A Genome-wide Multidimensional RNAi Screen Reveals Pathways Controlling MHC Class II Antigen Presentation. *Cell* **145**, 268-283 (2011).
497. Jin, Y.*, et al.* Identification of a new form of death-associated protein kinase that promotes cell survival. *The Journal of biological chemistry* **276**, 39667-39678 (2001).
498. Jin, Y., Blue, E.K., Dixon, S., Shao, Z. & Gallagher, P.J. A death-associated protein kinase (DAPK)-interacting protein, DIP-1, is an E3 ubiquitin ligase that promotes tumor necrosis factor-induced apoptosis and regulates the cellular levels of DAPK. *The Journal of biological chemistry* **277**, 46980-46986 (2002).
499. Chuang, Y.-T.*, et al.* Tumor suppressor death-associated protein kinase is required for full IL-1 β production. *Blood* **117**, 960-970 (2011).
500. Hsu, L.C.*, et al.* A NOD2-NALP1 complex mediates caspase-1-dependent IL-1beta secretion in response to Bacillus anthracis infection and muramyl dipeptide. *Proceedings of the National Academy of Sciences of the United States of America* **105**, 7803-7808 (2008).
501. Martinon, F., Agostini, L., Meylan, E. & Tschopp, J. Identification of bacterial muramyl dipeptide as activator of the NALP3/cryopyrin inflammasome. *Current biology : CB* **14**, 1929-1934 (2004).
502. Lee, T.H.*, et al.* Death-Associated Protein Kinase 1 Phosphorylates Pin1 and Inhibits Its Prolyl Isomerase Activity and Cellular Function. *Molecular Cell* **42**, 147-159 (2011).
503. Zhang, L., Nephew, K.P. & Gallagher, P.J. Regulation of death-associated protein kinase. Stabilization by HSP90 heterocomplexes. *The Journal of biological chemistry* **282**, 11795-11804 (2007).
504. Lee, Y.-R.*, et al.* The Cullin 3 substrate adaptor KLHL20 mediates DAPK ubiquitination to control interferon responses. *The EMBO journal* **29**, 1748-1761 (2010).
505. Dejardin, E. The alternative NF-kappaB pathway from biochemistry to biology: pitfalls and promises for future drug development. *Biochem Pharmacol* **72**, 1161-1179 (2006).

8. Appendix

8.1. Mass spectrometry data tables

Accession	Mascot Score	Protein identified	Fraction identified in (D=dephosphorylated, P=phosphorylated)
P04745	210	AMY1	D7
P19961	163	AMY2B	D6
P26641	153	EEF1G	D7
P13639	145	EEF2	D7
P13796	139	LCP1	p4
P35241	118	RDX	D7
Q15185	113	TEBP	p1
Q32MZ4	108	LRRFIP1	D2
Q01518	107	CAP1	D10
P15311	106	EZR	D7
P50552	103	VASP	D10
P25789	100	PSMA4	p9
Q8N257	98	HIST32BB	p6
O43765	93	SGTA	p2
P24534	90	EEF1B2	D2
P23528	89	CFL1	p6
Q13765	88	NACA	p1
P28062	85	PSMB8	p9
P01037	84	CST1	D8
O14814	84	AML2	D11
P15311	83	EZR	p6
P63244	78	GNB2L1	p9
P08670	77	VIM	p2
P59666	75	DEFA3	D11
Q14651	74	PLS1	p4
P11216	73	PYGB	p7
P29350	73	PTPN6 or SHP-1	p8
P11021	70	HSPA5 or GRP78	p3
P04792	69	HSPB1	p5
Q9Y3L3	68	SH3BP1	p6
Q9P258	67	RCC2	p9
Q96HN2	66	AHCYL2	p6
P05109	66	S100A8	p9
Q8TD55	66	PLEKHO2	D3
P49407	64	ARRB1	D6
P13639	64	EEF2	D10
Q92688	63	ANP32B or APRIL	p6
P26583	63	HMGB2	p11
P14317	62	HCLS1	p5
P46736	61	BRCC3	D5
P67809	60	YBX1	p3
P06454	60	PTMA	p5

Accession	Mascot Score	Protein identified	Fraction identified in (D=dephosphorylated, P=phosphorylated)
P29350	59	PTPN6 or SHP-1	p9
P83916	59	CBX1	D3
P13010	59	XRCC5	D5
Q01518	59	CAP1	D11
O95352	58	ATG7	p6
P00488	58	F13A1	p6
O75351	57	VPS4B	p7
Q32MZ4	57	LRRFIP1	D1
P23588	56	EIF4B	p4
P01036	56	CST4	D8
P14314	55	PRKCSH	D1
P25787	54	PSMA2	D8
Q9H009	53	NACA2	p1
Q02750	52	MAP2K1 or MEK1	p6
Q9Y3Z3	52	SMAHD1	p8
P06454	52	PTMA	D1
P11217	51	PYGM	p7
Q9HCD6	50	TANC2	p3
Q06210	50	GFPT1	p7
P01903	49	HLA-DRA	p3
P0C0S5	45	H2AFZ	p6
P19338	44	NCL	p5
P68363	43	TUBA1B	D6
P13639	42	EEF2	D8
P62753	41	RPS6	p5
Q9UQ80	40	PA2G4	D6
Q9NVA2	40	SEPT11	D7
Q6ZU15	40	SEPT14	D7
P46060	39	RANGAP1	p6
P04792	39	HSPB1	p6
P35579	38	MYH9	p5
Q92882	37	OSTF1	p6
Q9BTM1	36	H2AFJ	p5
Q16181	36	SEPT7	p11
P40306	35	PSMB10	p6
Q9UFC0	35	LRWD1	D5
P36382	35	GJA5	D6
P55854	34	SUMO3	D4
Q86UE8	34	TLK2	D11
Q9NT68	31	ODZ2	p12
P04792	31	HSPB1	D6
P21333	25	FLNA	p11

Table 1: Proteins identified by MS on single stimulation of DCs with MDP. The table depicts the Uniprot accession number, MASCOT score, the protein identified and whether the protein was preferentially phosphorylated or dephosphorylated on stimulation and which fraction they were found in.

Gene	Accession Number	Ratio: 127/126	IPA Fold change	Dual stimulation Mascot Score	Single Fraction	MDP only Mascot score	Change in Phosphorylation status?
VASP	P50552	0.741	-1.350	78	D10	103	
HMGB2	P26583	0.793	-1.261	39	P11	63	Opposite
HCLS1	P14317	0.817	-1.224	37	P5	62	Opposite
LASP1	Q14847	0.822	-1.217	75	D6	88	
PYGB	P11216	0.842	-1.188	39	P7	73	Opposite
SEPT7	Q16181	0.842	-1.188	247	P11	36	Opposite
PYGB	P11216	0.842	-1.188	39	P7	47	Opposite
PA2G4	Q9UQ80	0.843	-1.186	40	D6	40	
PA2G4	Q9UQ80	0.843	-1.186	40	D6	46	
GFPT1	Q06210	0.851	-1.175	59	P7	50	Opposite
PRKCSH	P14314	0.883	-1.133	29	D1	55	
SEPT11	Q9NVA2	0.889	-1.125		D7	40	
NCL	P19338	0.890	-1.124	208	P5	44	Opposite
MSN	P26038	0.893	-1.120	382	P6	110	Opposite
PSMB4	P28070	0.895	-1.117	46	D5	141	
EZR	P15311	0.899	-1.112		D7	106	
EZR	P15311	0.899	-1.112		P6	83	Opposite
EZR	P15311	0.899	-1.112		P6	107	Opposite
EZR	P15311	0.899	-1.112		P7	84	Opposite
NACA	Q13765	0.911	-1.098	71	P1	88	Opposite
XRCC6	P12956	0.912	-1.096	30	D7	47	
PTPN6 or SHP-1	P29350	0.913	-1.095	139	P8	73	Opposite
PTPN6 or SHP-1	P29350	0.913	-1.095	139	P9	59	Opposite
PSMA4	P25789	0.942	-1.062	32	P9	100	Opposite
F13A1	P00488	0.942	-1.062	494	P6	58	Opposite
	P00488	0.942	-1.062	494	D5	37	
GMIP	Q9P107	0.943	-1.060	45	D5	58	
DEK	P35659	0.944	-1.059	76	P6	26	Opposite
EIF4B	P23588	0.948	-1.055	80	P4	56	Opposite
HSPA5 or GRP78	P11021	0.950	-1.053	48	P3	70	Opposite
HMGB1	P09429	0.994	-1.006	49	D7	140	Opposite
PLEKHO2	Q8TD55	1.009	1.009	257	D3	66	Opposite
S100A8	P05109	1.019	1.019	64	P9	66	
MYH9	P35579	1.035	1.035	854	P5	38	
RCC2	Q9P258	1.053	1.053	76	P9	67	
HNRNPC	P07910	1.055	1.055	299	D5	37	Opposite
LMNA	P02545	1.056	1.056	158	D7	124	Opposite
ABR	Q12979	1.059	1.059	117	P6	37	
PSMB3	P49720	1.090	1.090	304	P6	109	
PALD	Q8WX93	1.091	1.091	129	D6	45	Opposite
SAMHD1	Q9Y3Z3	1.095	1.095	209	P8	52	
CTPS	P17812	1.097	1.097	20	P6	79	
FAM129B	Q96TA1	1.100	1.100	163	P5	49	
TUBA1A	Q71U36	1.106	1.106	695	P6	135	
FLNA	P21333	1.114	1.114	25	P11	25	
TUBA1B	P68363	1.115	1.115	673	D6	43	Opposite
CBX1	P83916	1.127	1.127		D3	59	Opposite
CAP1	Q01518	1.136	1.136	154	D10	107	Opposite
CAP1	Q01518	1.136	1.136	154	D11	59	Opposite
OSTF1	Q92882	1.161	1.161	262	P6	37	
OSTF1	Q92882	1.161	1.161	262	P5	85	
OSTF1	Q92882	1.161	1.161	262	P6	76	
OSTF1	Q92882	1.161	1.161	262	P7	71	
SH3BP1	Q9Y3L3	1.231	1.231	217	P6	68	
EVL	Q9UI08	1.255	1.255	186	P6	57	
EIF5	P55010	1.312	1.312	47	D5	36	Opposite
VPS4B	O75351	1.340	1.340	47	P7	57	

Table 2: Not significantly phosphorylated or dephosphorylated proteins on either MDP alone or MDP/PAM stimulated DCs.

Protein	Accession Number	1.008	IPA Fold change
SNX1	Q13596	1.354	1.354
NRBP1	Q9UHY1	1.356	1.356
ANKRD18B	A2A2Z9	1.367	1.367
LRRC47	Q8N1G4	1.371	1.371
DOK2	O60496	1.382	1.382
ACSS2	Q9NR19	1.398	1.398
RPS16	P62249	1.400	1.400
TMX1	Q9H3N1	1.401	1.401
RPS6KA4	O75676	1.406	1.406
FAM175B	Q15018	1.417	1.417
CBX3	Q13185	1.423	1.423
DYNC1H1	Q14204	1.442	1.442
RPS6KA1	Q15418	1.448	1.448
AP3D1	O14617	1.449	1.449
UBE2Z	Q9H832	1.450	1.450
USP9Y	O00507	1.451	1.451
VPS16	Q9H269	1.453	1.453
ELMO2	Q96JJ3	1.457	1.457
UBE2E1	P51965	1.458	1.458
RPLP2	P05387	1.474	1.474
DDX17	Q92841	1.486	1.486
KCTD12	Q96CX2	1.494	1.494
RRAGC	Q9HB90	1.497	1.497
HLA-DRB1	Q9TQE0	1.515	1.515
Histone H4	P62805	1.523	1.523
SQRDL	Q9Y6N5	1.528	1.528
TLN1	Q9Y490	1.538	1.538
CORO7	P57737	1.539	1.539
EXOC2	Q96KP1	1.549	1.549
SNX2	O60749	1.590	1.590
PAN2	Q504Q3	1.593	1.593
EEF1AL3	Q5VTE0	1.601	1.601
CD209	Q9NNX6	1.625	1.625
RTN1	Q16799	1.631	1.631
HLA-B	Q9TNN7	1.633	1.633
MYO9B	Q13459	1.637	1.637
AMPD3	Q01432	1.646	1.646
FHOD1	Q9Y613	1.650	1.650
USP39	Q53GS9	1.667	1.667
NAP1L1	P55209	1.672	1.672
MAPRE1	Q15691	1.744	1.744
CD74	P04233	1.789	1.789
MICAL1	Q8TDZ2	1.803	1.803
SNX6	Q9UNH7	1.860	1.860
PIK3AP1	Q6ZUJ8	1.882	1.882
ARHGAP10	A1A4S6	1.948	1.948
SEC31A	O94979	1.971	1.971
SIN3A	Q96ST3	1.981	1.981
POLR3C	Q9BUI4	2.124	2.124
DAPK1	P53355	2.190	2.190
EHBP1L1	Q8N3D4	2.564	2.564
TNPO3	Q9Y5L0	2.641	2.641
NOP56	O00567	3.126	3.126
IQGAP2	Q13576	3.328	3.328

Protein	Accession Number	127/126	IPA Fold change
GBF1	Q92538	0.271	-3.690
UPF1	Q92900	0.280	-3.571
FCHO2	Q0JRZ9	0.309	-3.236
ARHGAP25	P42331	0.331	-3.021
FNBP1	Q96RU3	0.393	-2.545
KRT9	P35527	0.407	-2.457
SPAG9	O60271	0.414	-2.415
KRT1	P04264	0.419	-2.387
DRAP1	Q14919	0.448	-2.232
KRT10	P13645	0.454	-2.203
HNRPLL	Q8WVV9	0.455	-2.198
FAM120A	Q9NZB2	0.470	-2.128
PAK2	Q13177	0.478	-2.092
RABGAP1	Q9Y3P9	0.487	-2.053
MPDU1	O75352	0.493	-2.028
ARHGAP9	Q9BRR9	0.521	-1.919
DNPEP	Q9ULA0	0.526	-1.901
DNMT1	P26358	0.561	-1.783
ANXA6	P08133	0.575	-1.739
PKM2	P14618	0.578	-1.730
FGD2	Q7Z6J4	0.579	-1.727
SF3B1	O75533	0.589	-1.698
RPN1	P04843	0.600	-1.667
PGAM4	Q8N0Y7	0.603	-1.658
HSP70.1/HSP70.2	P08107	0.603	-1.658
PAK1	Q13153	0.609	-1.642
ARHGEF1	Q92888	0.620	-1.613
MPHOSPH8	Q99549	0.637	-1.570
UNC13D	Q70J99	0.639	-1.565
NONO	Q15233	0.649	-1.541
PSMD7	P51665	0.657	-1.522
ALKBH5	Q6P6C2	0.658	-1.520
GIT2	Q14161	0.666	-1.502
STK4	Q13043	0.669	-1.495
IQGAP1	P46940	0.671	-1.490
TOP2B	Q02880	0.674	-1.484
PSMB9	P28065	0.691	-1.447
CAND1	Q86VP6	0.691	-1.447
DSCR3	O14972	0.694	-1.441
RPRD1B	Q9NQG5	0.696	-1.437
KPNA3	O00505	0.698	-1.433
DIAPH1	O60610	0.704	-1.420
MTMR14	Q8NCE2	0.718	-1.393
SNRPD3	P62318	0.725	-1.379
SNX9	Q9Y5X1	0.727	-1.376
PSMA3	P25788	0.729	-1.372
HIST1H2BJ	P06899	0.732	-1.366
ARHGAP26	Q9UNA1	0.736	-1.359
ERO1L	Q96HE7	0.740	-1.351

Table 3: Significantly phosphorylated (left group) and dephosphorylated (right group) proteins identified by MS from MDP/PAM stimulated DCs but were not found on MDP alone.

Dephosphorylated proteins

Protein symbol	Uniprot Accession number	Fold Change	127/126
26S proteasome non-ATPase regulatory subunit 6	Q15008	-1.344086	0.744
Cnt-b2	Q15057	-1.3315579	0.751
Histone H2B type 2-F	Q5QNW6	-1.3297872	0.752
Gemin5	Q8TEQ6	-1.3280212	0.753
PDI	P07237	-1.3175231	0.759
RAI	P13489	-1.3175231	0.759
MAP7 domain-containing protein 1	Q3KQU3	-1.3140604	0.761
hnRNP M	P52272	-1.305483	0.766
Protein flightless-1 homolog	Q13045	-1.3020833	0.768
ACE	P12821	-1.3020833	0.768
LANP-L	Q9BTT0	-1.3003901	0.769
PKA C-alpha	P17612	-1.2970169	0.771
GALGP	P16150	-1.2919897	0.774
hnRNP D0	Q14103	-1.2903226	0.775
TBP-1	P17980	-1.2804097	0.781
apoB-48R	Q0VD83	-1.2787724	0.782
CRHSP-24	Q9Y2V2	-1.2771392	0.783
Hsp90 co-chaperone Cdc37	Q16543	-1.2738854	0.785
ArhGAP15	Q53QZ3	-1.2626263	0.792
p115	P98171	-1.2594458	0.794
CK II alpha	P68400	-1.2562814	0.796
IKK-beta	O14920	-1.2531328	0.798
Protein PRRC1	Q96M27	-1.2437811	0.804
Annexin A1	P04083	-1.242236	0.805
Rho GTPase-activating protein 1	Q07960	-1.2406948	0.806
SLP76	Q13094	-1.2376238	0.808
TGF-beta-activated kinase 1 (TAK1)	O43318	-1.2360939	0.809
Tight junction protein ZO-2	Q9UDY2	-1.2330456	0.811
PTPG1	Q05209	-1.2300123	0.813
p47	P08567	-1.2269939	0.815
Myosin-Va	Q9Y4I1	-1.2239902	0.817
Serine/arginine-rich splicing factor 7	Q16629	-1.2210012	0.819
Glycogen phosphorylase, liver form	P06737	-1.2195122	0.82
DRG-2	P55039	-1.2048193	0.83
Protein TFAR19	O14737	-1.2019231	0.832
60S ribosomal protein L4	P36578	-1.1961722	0.836
Coronin-1B	Q9BR76	-1.1961722	0.836
PROS-30	P25786	-1.1947431	0.837
G3BP-2	Q9UN86	-1.1947431	0.837
Torsin-1A-interacting protein 1	Q5JTV8	-1.1947431	0.837
DENN domain-containing protein 4B	O75064	-1.1890606	0.841
PDHE1-A type I	P08559	-1.1820331	0.846
SS-B	P05455	-1.1792453	0.848
CBP-I	P08758	-1.1709602	0.854
GRF-1	Q9NRY4	-1.1709602	0.854
PI4K-alpha	P42356	-1.1682243	0.856
IGAAD	Q01105	-1.1682243	0.856
BCKD-kinase	O14874	-1.1682243	0.856
NPM	P06748	-1.1668611	0.857
C1qBP	Q07021	-1.1641444	0.859
Beta-actin	P60709	-1.1614402	0.861
Proteasome subunit p42	P62333	-1.1614402	0.861
SR-alpha	P08240	-1.1547344	0.866
ASF-1	Q07955	-1.1520737	0.868
Protein FAM110B	Q8TC76	-1.146789	0.872
BRCA1-A complex subunit BRE	Q9NXR7	-1.1454754	0.873
NC2-beta	Q01658	-1.1441648	0.874
Proteasome subunit p58	O43242	-1.1441648	0.874
Alpha-actinin-4	O43707	-1.1415525	0.876
Transcription factor BTF3 homolog 4	Q96K17	-1.1402509	0.877
AMPKb	Q9Y478	-1.1376564	0.879
ER protein 70	P13667	-1.1337868	0.882
CPSF 73 kDa subunit	Q9UKF6	-1.1337868	0.882
CPI-17	Q96A00	-1.1325028	0.883
eIF-2-gamma A	Q2VIR3	-1.1312217	0.884
HSP 86	P07900	-1.1299435	0.885
Histone H1.1	Q02539	-1.1273957	0.887
Signal transducer and activator of transcription 5A	P42229	-1.1261261	0.888
CPSF 25 kDa subunit	O43809	-1.1235955	0.89

GRP-94	P14625	-1.1223345	0.891
Transaldolase	P37837	-1.1223345	0.891
hVps24	Q9Y3E7	-1.1223345	0.891
MacGAP	Q8N392	-1.1223345	0.891
Protein SOLO	Q8TER5	-1.1223345	0.891
UKHC	P33176	-1.1210762	0.892
Calnexin	P27824	-1.1210762	0.892
MDDase	P53602	-1.1210762	0.892
Qip1	O00629	-1.1198208	0.893
H3-K4-HMTase SETD7	Q8WTS6	-1.1185682	0.894
G3BP-1	Q13283	-1.1173184	0.895
Proteasome subunit Z	Q99436	-1.1160714	0.896
STAT6	P42226	-1.1135857	0.898
Putative protein FAM10A5	Q8NFI4	-1.1135857	0.898
BAP-135	P78347	-1.1123471	0.899
Plexin-B1	O43157	-1.1098779	0.901
15-LOX	P16050	-1.1061947	0.904
ATP-binding cassette 50	Q8NE71	-1.1049724	0.905
Ifi-16	Q16666	-1.1037528	0.906
eIF3a	Q14152	-1.1037528	0.906
TRIP-12	Q14669	-1.1037528	0.906
Uncharacterized protein C22orf9	Q6ICG6	-1.1037528	0.906
APG3-like	Q9NT62	-1.0952903	0.913
Heat shock 70 kDa protein 8	P11142	-1.0905125	0.917
Protein dopey-2	Q9Y3R5	-1.0869565	0.92
Ubiquitin carboxyl-terminal hydrolase 10	Q14694	-1.0857763	0.921
hnRNP U	Q00839	-1.0845987	0.922
hVPS4	Q9UN37	-1.0845987	0.922
Exocyst complex component Sec8	Q96A65	-1.0822511	0.924
CBF5 homolog	O60832	-1.0810811	0.925
Autoantigen p542	Q9UKM9	-1.0741139	0.931
DFS 70	O75475	-1.0718114	0.933
E1B-AP5	Q9BUJ2	-1.0718114	0.933
PKB	P31749	-1.0706638	0.934
Protein BAP2	Q9UQB8	-1.0706638	0.934
CHD-4	Q14839	-1.0706638	0.934
RNase Z 2	Q9BQ52	-1.0649627	0.939
L-CA	P08575	-1.0638298	0.94
Deptor	Q8TB45	-1.0626993	0.941
AOE37-2	Q13162	-1.0582011	0.945
MAP-1S	Q66K74	-1.0515247	0.951
ARL-6-interacting protein 5	O75915	-1.0471204	0.955
hTM5	P06753	-1.0460251	0.956
TBC1 domain family member 5	Q92609	-1.0449321	0.957
Protein arginine N-methyltransferase 5	O14744	-1.0438413	0.958
Angiotensin-converting enzyme	P46779	-1.0438413	0.958
HSP 90	P08238	-1.0416667	0.96
DRG-1	Q9Y295	-1.0416667	0.96
Putative tropomyosin alpha-3 chain-like protein	A6NL28	-1.0384216	0.963
TM30p1	P67936	-1.0351967	0.966
Proteasome subunit alpha type-5	P28066	-1.0330579	0.968
P-Rex1	Q8TCU6	-1.0309278	0.97
Proteasome subunit alpha type-7	O14818	-1.0298661	0.971
ERp60	P27797	-1.0277492	0.973
DRBP76	Q12906	-1.026694	0.974
R-PTP-epsilon	P23469	-1.026694	0.974
PACS-1	Q6VY07	-1.026694	0.974
eIF3e	P60228	-1.025641	0.975
Protein HP1-BP74	Q5SSJ5	-1.0235415	0.977
PLC-beta-2	Q00722	-1.0235415	0.977
60S acidic ribosomal protein P0	P05388	-1.0183299	0.982
Myotubularin	Q13496	-1.0162602	0.984
EF-1-delta	P29692	-1.0141988	0.986
Proteasome subunit beta type-1	P20618	-1.0131712	0.987
Protein mago nashi homolog 2	Q96A72	-1.0111223	0.989
CaM-kinase phosphatase	P49593	-1.010101	0.99
CK II alpha'	P19784	-1.010101	0.99
Lysp100b	P23497	-1.010101	0.99
Cofilin-2	Q9Y281	-1.0090817	0.991
Zizimin-3	Q96BY6	-1.0050251	0.995
Transcriptional activator protein Pur-alpha	Q00577	-1.003009	0.997

Phosphorylated proteins

Protein symbol	Uniprot Accession number	Fold Change	127/126
Coiled-coil domain-containing protein 162	A2VCL2	1.001	1.001
DEAD box protein 21	Q9NR30	1.001	1.001
RING finger protein 114	Q9Y508	1.003	1.003
Rho guanine nucleotide exchange factor 16	Q5VV41	1.007	1.007
MAP kinase 14	Q16539	1.01	1.01
Nogo protein	Q9NQC3	1.012	1.012
SAF-A2	Q1KMD3	1.013	1.013
Interleukin enhancer-binding factor 2	Q12905	1.013	1.013
hnRNP E1	Q15365	1.022	1.022
Heat shock protein 105 kDa	Q92598	1.023	1.023
Tubulin beta-6 chain	Q9BUF5	1.023	1.023
Tubulin beta chain	P07437	1.024	1.024
Int3	Q68E01	1.024	1.024
U5-200KD	O75643	1.025	1.025
ADP-ribosylation factor 3	P61204	1.026	1.026
RICH-1	Q68EM7	1.027	1.027
HDGF	P51858	1.029	1.029
E-Syt1	Q9BSJ8	1.041	1.041
KCIP-1	P61981	1.041	1.041
eIF-4G 1	Q04637	1.041	1.041
Tubulin 5 beta	P04350	1.045	1.045
Cardiac zipper protein	Q5JR59	1.052	1.052
Protein phosphatase 1 regulatory subunit 7	Q15435	1.055	1.055
Serrate RNA effector molecule homolog	Q9BXP5	1.057	1.057
Tubulin beta-8 chain	Q3ZCM7	1.059	1.059
NgBR	Q96E22	1.059	1.059
PROS-27	P60900	1.063	1.063
DNA-PKcs	P78527	1.063	1.063
Protein A1S9	P22314	1.064	1.064
Protein ICB-1	Q5TEJ8	1.065	1.065
E3 ubiquitin-protein ligase CBL	P22681	1.065	1.065
Nuclear ubiquitous casein and cyclin-dependent kinases substrate	Q9H1E3	1.065	1.065
Sra-1	Q7L576	1.066	1.066
Tubulin beta-2B chain	Q9BVA1	1.071	1.071
MNF	P85037	1.071	1.071
RING finger protein 213	Q63HN8	1.072	1.072
Matrin-3	P43243	1.076	1.076
NMT 1	P30419	1.079	1.079
NRD convertase	O43847	1.081	1.081
Proteasome subunit beta type-6	P28072	1.083	1.083
TER ATPase	P55072	1.084	1.084
Dedicator of cytokinesis protein 2	Q92608	1.084	1.084
Protein FAM129A	Q9BZQ8	1.088	1.088
HD protein	P42858	1.092	1.092
Serine/threonine-protein kinase 10	O94804	1.096	1.096
Formin-like protein 1	O95466	1.097	1.097
hCARD9	Q9H257	1.098	1.098
VIAF-1	Q9H2J4	1.102	1.102
PAP	Q13442	1.102	1.102
Tubulin beta-2C chain	P68371	1.103	1.103
Annexin A2	P07355	1.103	1.103
AP-2 complex subunit mu	Q96CW1	1.104	1.104
MAPKAP kinase 2	P49137	1.105	1.105
Dedicator of cytokinesis protein 8	Q8NF50	1.109	1.109
PAP-alpha	P51003	1.114	1.114
AP-2 complex subunit sigma	P53680	1.116	1.116
Protein TFG	Q92734	1.116	1.116
EAP	P35268	1.118	1.118
PDHE1-B	P11177	1.12	1.12
GEF-H1	Q92974	1.124	1.124
DDBa	Q16531	1.128	1.128
TSE1	P10644	1.128	1.128
Abi-1	Q8IZP0	1.132	1.132
N4BP1	O75113	1.133	1.133
THUMP domain-containing protein 1	Q9NXG2	1.135	1.135
Gamma-adducin	Q9UEY8	1.14	1.14
Protein 197/15a	Q53EL6	1.141	1.141
Hermansky-Pudlak syndrome 3 protein	Q969F9	1.142	1.142
Sam68	Q07666	1.145	1.145
Putative basic leucine zipper and W2 domain-containing protein 1-like 1	P0C7T9	1.147	1.147

Imp7	O95373	1.149	1.149
eIF-2-alpha	P05198	1.15	1.15
Myotubularin-related protein 10	Q9NXD2	1.153	1.153
hNIPA	Q86WB0	1.159	1.159
AMPK subunit gamma-1	P54619	1.16	1.16
hnRNP K	P61978	1.162	1.162
Macropain subunit C7-I	P49721	1.162	1.162
Sugen kinase 223	Q86YV5	1.162	1.162
KCIP-1	P63104	1.166	1.166
pp52	P33241	1.17	1.17
TP	P19971	1.172	1.172
Protein HS1	P27348	1.173	1.173
PP6C	O00743	1.174	1.174
SGN7b	Q9H9Q2	1.175	1.175
H2A.1	P0C0S8	1.185	1.185
CBP80	Q09161	1.193	1.193
ATP synthase subunit alpha, mitochondrial	P25705	1.196	1.196
Sorting nexin-5	Q9Y5X3	1.196	1.196
100 kDa coated vesicle protein C	O94973	1.199	1.199
ATP-citrate synthase	P53396	1.204	1.204
Myosin-If	O00160	1.205	1.205
Myosin-Ie	Q12965	1.205	1.205
PCN	Q15149	1.211	1.211
60S acidic ribosomal protein P1	P05386	1.213	1.213
Hematopoietic protein 1	P55160	1.215	1.215
PSP2	Q96PK6	1.215	1.215
TAP	O60763	1.218	1.218
Cnt-d2	Q96P48	1.224	1.224
AP105B	P63010	1.229	1.229
GDI-2	P50395	1.229	1.229
SAF-B2	Q14151	1.23	1.23
WD repeat-containing protein 15	Q9BZH6	1.232	1.232
PP-1G	P36873	1.234	1.234
SGN5	Q92905	1.235	1.235
PP-1B	P62140	1.24	1.24
Gag polyprotein	Q9HDB9	1.242	1.242
AEG-1	Q86UE4	1.246	1.246
CAS	O60716	1.249	1.249
LC17	P60660	1.249	1.249
PMCA1	P20020	1.251	1.251
MLL septin-like fusion protein	Q9UHD8	1.252	1.252
UPF0668 protein C10orf76	Q5T2E6	1.253	1.253
Maspardin	Q9NZD8	1.254	1.254
Beta-1-adaptin	Q10567	1.257	1.257
AFP	Q12899	1.26	1.26
NCF-2	P19878	1.263	1.263
Alpha-COP	P53621	1.268	1.268
S6K-alpha-3	P51812	1.269	1.269
DAL-1	Q9Y2J2	1.269	1.269
ILK-1	Q13418	1.276	1.276
Bap31	P51572	1.279	1.279
eIF-4G 3	O43432	1.285	1.285
IQ motif and SEC7 domain-containing protein 1	Q6DN90	1.287	1.287
HIP-55	Q9UJU6	1.291	1.291
MST-3	Q9Y6E0	1.307	1.307
YjeF_N2	Q96F86	1.312	1.312
DEAD box protein 5	P17844	1.329	1.329
SIP-145	Q92835	1.329	1.329

Table 4: Non-significantly dephosphorylated (top set) and phosphorylated (bottom set) proteins identified by MS from MDP/PAM stimulated DCs but were not found on MDP alone.

8.2. Gentamicin killing assay

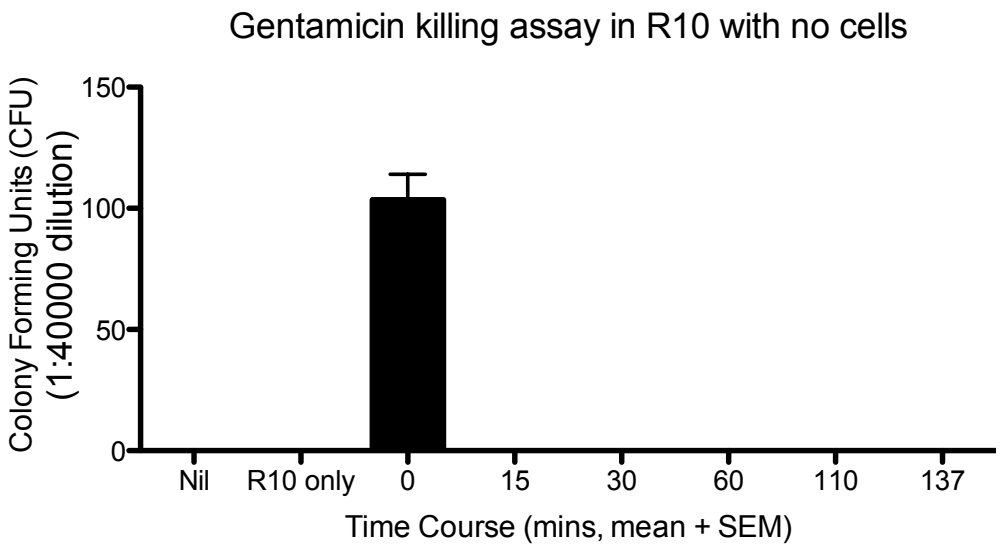


Figure 1: Gentamicin killing assay

9. Papers published during DPhil

Cooney R, Baker J, Brain O, Danis B, Pichulick T, Allan P, Ferguson DJP, Campbell BJ, Jewell D, Simmons A. NOD2 stimulation induces autophagy in dendritic cells influencing bacterial handling and antigen presentation. Nature Medicine (2010) **16** (1), 90-97. doi: 10.1038/nm.2069. Epub 2009 Dec 6.
http://dx.doi.org/10.1038/nm.2069

Brain O, Allan P, Simmons A. NOD2-mediated autophagy and Crohn disease. Autophagy **6**, 412-414 (2010)
http://dx.doi.org/10.4161/auto.6.3.11389

The paper [Cooney R, Baker J, Brain O, Danis B, Pichulick T, Allan P, Ferguson DJP, Campbell BJ, Jewell D, Simmons A. NOD2 stimulation induces autophagy in dendritic cells influencing bacterial handling and antigen presentation. Nature Medicine (2010) **16** (1), 90-97. doi: 10.1038/nm.2069. Epub 2009 Dec 6.] originally presented here cannot be made freely available via ORA because of copyright. The paper pdf was sourced at:

http://www.nature.com/nm/journal/v16/n1/full/nm.2069.html

The paper [Brain O, Allan P, Simmons A. NOD2-mediated autophagy and Crohn disease. Autophagy (2010) **6**, 412-414] originally presented here cannot be made freely available via ORA because of copyright. The paper pdf was sourced at:

http://www.landesbioscience.com/journals/autophagy/article/11389/